Inelastic Buckling Behavior of Concrete Reinforcing Bars under Monotonic Uniaxial Compressive Loading

by

Alexa Marie Mieses, B.S.C.E.

Thesis

Presented to the Faculty of the Graduate School of

The University of Texas at Austin

in Partial Fulfillment

of the Requirements

for the Degree of

Master of Science in Engineering

The University of Texas at Austin

August 2002

Inelastic Buckling Behavior of Concrete Reinforcing Bars under Monotonic Uniaxial Compressive Loading

APPROVED BY
SUPERVISING COMMITTEE:

Oguzhan Bayrak, supervisor

Michael E. Kreger

Dedication

For my husband, J. Orlando Rivera,

and my parents, Juan D. Mieses and Lydia E. de Jesús.

Acknowledgements

I would like to thank the Structural Engineering faculty and staff of The University of Texas at Austin for letting me be part of their prestigious program and contribute to their recognized work. Thanks to my research advisor, Dr. Oguzhan Bayrak, for his guidance and direction in the laboratory work and writing of this thesis throughout this research project. I also wish to thank my second reader, Dr. Michael E. Kreger, for his support and assistance.

Thank you to the technical FSEL staff, Mike Bell, Dennis Fillip, Ray Madonna, and Blake Stasney, for their help and guidance during my experimental work. Thanks also to the administration of the FSEL laboratory: Regina Forward, Wanda Kitts, Barbara Lafferty, and Hortensia Peoples.

Thanks to professor Dr. Eric B. Williamson and my special friend Juan Felipe Beltrán who helped me understand some analytical parts of my project, even though they weren't involved with my project. Thank you to the students who took time to help me during my tests with their strength, knowledge, and friendly support, especially Gabriela Arce, Alfredo Castro, Jenny Tanner, Jorge Varela, Baris Binici, Matthew Memberg, Larry Memberg, Lisa Novak, Joe Spadea, Nat Ativitavas, and Sungjin Bae.

Thank you especially to my husband, J. Orlando Rivera, for his unconditional support and for his help in finishing my thesis and the experiments required for it. Thanks most of all to my husband and my parents for believing in me all the way through.

August 2002

Abstract

Inelastic Buckling Behavior of Concrete Reinforcing Bars under Monotonic Uniaxial Compressive Loading

by

Alexa Marie Mieses, MSE

The University of Texas at Austin, 2002

SUPERVISOR: Oguzhan Bayrak

The main objective of this research is to expand the experimental information available on the buckling behavior of longitudinal reinforcement. Compression tests on well-instrumented bars are performed and axial and lateral deformations are reported herein. To establish a constitutive relationship for reinforcing bars under axial compression, an experimental study on 108-#8 and 54-#10 reinforcing bar specimens having unsupported length to bar diameter ratios (*L/d*) ranging between 4 and 12 and mid-span eccentricity to bar diameter ratio (*e/d*) between 0.0 and 0.5 was conducted. In addition, #8 and #10 bars with different material properties were tested to investigate the influence of strain hardening response on the post-buckling behavior of reinforcing bars. Finally, the results obtained are comparatively studied, and the effects of *e/d* ratio, *L/d* ratio, and material properties on reinforcing bar behavior are evaluated.

Table of Contents

List of Tables

List of Figures

CHAPTER 1
Introduction

1.1 General Overview

The capability of concrete framed structures to withstand strong ground motions during earthquakes or any other dynamic type loading depends primarily in the ability of the structure to develop reasonable ductility. This relates to the capacity of the structure to redistribute loads and to the ability of plastic hinges to absorb and dissipate energy without significant strength loss. As a result, building codes take a “strong column-weak beam” approach in which members are designed in order to form plastic hinges in the beams rather than in the columns. However, it has been observed in recent earthquakes and investigations (Bayrak and Sheikh 2001) that the formation of plastic hinges in columns is still possible and inevitable as seen in Figures 1.1 and 1.2. Therefore, the possibility of hinging in columns should be taken into consideration in design to ensure the stability of the structure as well as vertical load carrying capacity of the columns.

When plastic hinges form in columns, buckling of the longitudinal reinforcement is often observed. This has been explained in a previous study due to the inadequacy of tie spacing requirements when ductility is required (Bayrak and Sheikh 2001). Since buckling of the longitudinal reinforcement is not considered in conventional sectional analysis of concrete column members, the load-carrying capacity and the ductility of the columns at large inelastic deformations are generally over predicted.

Figure 1.1 Buckling of freeway support column's reinforcement under the Simi Valley Freeway at the north end of the San Fernando Valley during the Northridge earthquake in California 1994 (photo: Ta-Liang Teng), from: http://www.scecdc.scec.org/slidesho.html

Several research papers were studied to establish the availability of analytical models for longitudinal bar buckling in columns. The studies presented by Bresler and Gilbert (1961), Scribner (1986), Russo (1988), Papia et al. (1988), Mau and El-Mabsout (1989), and Monti and Nuti (1992) were investigated. Based on the literature survey conducted, it was determined that previous studies failed to include the effect of the interaction between the concrete core and the reinforcing cage. Recently, Bayrak and Sheikh (2001) developed an innovative plastic hinge analysis technique in which the interaction between the reinforcing cage and the concrete core and the buckling of reinforcing bars are incorporated

into the sectional analysis to predict the ultimate deformation capacity of column members. Bayrak and Sheikh (2001) reported that there is a limited amount of experimental data of reinforcing bars tested under compression. Therefore, further testing is required in order to develop a reasonable database to incorporate in analytical techniques.

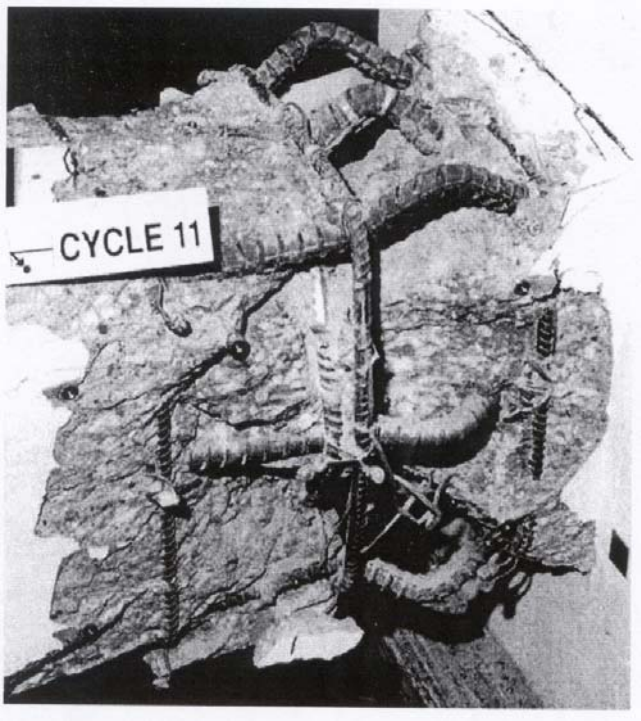

Figure 1.2 Longitudinal bar buckling in specimen RS-12HT tested by Bayrak and Sheikh (2001)

1.2 BACKGROUND FOR RESEARCH

When a reinforced concrete column is loaded axially in compression to failure, the concrete cover spalls after reaching a limiting strain value leaving the reinforcement exposed. This results in reduction of the cross sectional area

causing additional straining of the transverse reinforcement and of the core. The pressure applied by the core to the longitudinal reinforcement and the inadequacy of hoop spacing may result in buckling of the longitudinal reinforcement. For this to be avoided, columns should be designed and detailed to provide a reasonable level of ductility when subjected to cyclic flexure and constant axial load. In this way, the maximum displacement capacity of frame concrete structures can be determined with a reasonable level of confidence. In addition, the capacity of the columns should be determined by taking into consideration the possibility of buckling of longitudinal reinforcement and the interaction of the concrete core with the reinforcing cage.

The behavior of plastic hinges needs to be studied carefully in order to understand the overall behavior of reinforced concrete framed structures. The plastic hinge analysis technique developed by Bayrak and Sheikh (2001) aims to determine reasonable estimates of the maximum useful deformation capacities of plastic hinges that the members will undergo under strong ground motions.

Although Bayrak and Sheikh (2001) outlined the governing equations that need to be used in the plastic hinge analysis, they did not recommend any closed-form expression that can be employed in sectional analyses to simulate buckling of longitudinal bars. This was mainly due to the lack of a comprehensive database of reinforcing bar buckling. In order to address this problem, testing is required to enlarge the database of axial stress-strain relationships under compressive loading required for sectional analysis. As identified by the previous researchers mentioned in Chapter 2, this behavior depends on the size of the bars, the hoop spacing, and the material properties of the reinforcing steel.

1.3 OBJECTIVE OF RESEARCH

The ultimate objective of the research, for which the present study is part of, is to contribute to the development of an analytical technique that predicts the immediate and long-term behavior of reinforced concrete columns, including repaired and upgraded columns. However, the present study focuses on enlarging the database of longitudinal bars tested under compressive loads.

One of the goals of the research project is to develop a unified model that predicts the behavior of reinforcing bars under compression given the geometric and material properties. By developing a constitutive relationship for the reinforcing bars under compression, conventional sectional analyses can be extended to incorporate the buckling of longitudinal reinforcement phenomenon into the analyses. The model should be verified by using experimental data from reinforced concrete column tests. This model will enable an engineer to evaluate the pre and post buckling behavior of reinforcing bars under compression given the material properties and geometric nature of the problem and hence evaluate the impact of the rebar buckling on the deformation capacity of a reinforced concrete plastic hinge. This part of the investigation will require further experimental research to enlarge the available database of axial stress-strain relationships under compressive loading. Therefore, the present study will concentrate only on the study of inelastic buckling of longitudinal steel reinforcement.

Bayrak and Sheikh tested 56 #6 reinforcing bars with a clear length-to-bar diameter ratio (L/d) ranging from 4 to 10 and with initial eccentricity at midspan-to-bar diameter ratio (e/d) ranging from 0.0 to 0.3. A series of tests performed during this research include reinforcing steel bars with an L/d range of 4 to 12, an e/d range of 0.0 to 0.5, of varying material properties and bar size. This will

expand the required database on longitudinal bar buckling by 162 specimens. In addition, the specimens tested during this study are instrumented extensively to involve lateral deformation measurements. It is interesting to note that Bayrak and Sheikh (2001) did not measure lateral deformations of their test specimens.

1.4 SCOPE AND OBJECTIVES OF THE THESIS

The main objective of this thesis is to expand the experimental information available on the buckling behavior of longitudinal reinforcement (axial and lateral) by experimentally investigating buckling behavior of reinforcing bars. Compression tests on well-instrumented bars are performed and axial and lateral deformations are reported. The experimental setup follows that developed by Bayrak and Sheikh (2001), which simulates realistically the force and geometric boundary conditions of reinforcing bars in concrete members.

To establish a constitutive relationship for reinforcing bars under axial compression, an experimental study on 108-#8 and 54-#10 reinforcing bar specimens having unsupported length to bar diameter ratios (L/d) ranging between 4 and 12 and mid-span eccentricity to bar diameter ratio (e/d) between 0.0 and 0.5 was conducted. In addition, #8 and #10 bars with different material properties were tested to investigate the influence of strain hardening response on the post-buckling behavior of reinforcing bars. Finally, the results obtained are comparatively studied, and the effects of e/d ratio, L/d ratio, and material properties on reinforcing bar behavior are evaluated.

CHAPTER 2
Background Information on Longitudinal Bar Buckling

2.1 INTRODUCTION

Reinforced concrete frames may undergo significant deformations when subjected to ground motions or any other type of cyclic loading. These deformations may result in buckling of the longitudinal reinforcement at zones where plastic hinges are expected. To avoid or minimize this, the members should be designed and detailed to provide a reasonable level of ductility. Currently, the inelastic behavior of longitudinal steel bars in compression members is not incorporated in conventional analysis procedures. Therefore, behavior of concrete members subjected to large inelastic curvatures and deformations is generally overestimated with respect to strength and ductility (Bayrak and Sheikh, 2001).

Bar size, material strength, spacing and configuration of the transverse reinforcement are among the most important factors affecting the inelastic behavior of reinforcing bars, as pointed out by previous researchers. The inelastic behavior of reinforcing bars in a concrete member is a complicated phenomenon that involves different factors and may result in complicated modeling. Different researchers have studied this behavior, and their work will be discussed in this chapter in order to describe the evolution of knowledge in buckling of longitudinal steel in reinforced concrete.

2.2 PREVIOUS RESEARCH

Following is a series of previous research performed to study the buckling of longitudinal bars in concrete columns starting with the earliest study published.

The results and conclusions from previous research will be examined in order to explain the basis for the current research.

2.2.1 Bresler and Gilbert (1961)

This is the first information available on the topic of tie-spacing requirements and buckling behavior of longitudinal reinforcing steel of compressed concrete members. Bresler and Gilbert described the mechanism of failure of reinforced concrete columns, the analytical tie spacing and tie sizing resulting from the study of buckling of longitudinal reinforcement, and experimental work done with tie size requirements. They reviewed the design guidelines given in ACI Building Code 318-56 concerning tie spacing requirements and proposed a new design criterion that required further experimental verification.

Based on a preliminary study, they proposed a hypothesis as for the mechanism of failure: the local strains in concrete cover increased as axial load increased until a limit strain value was reached. At the limit strain, the cover concrete cracked and spalled off. After spalling occurred, the cross-sectional area decreased, thus increasing the stress level in the remaining concrete core and the steel reinforcement. The longitudinal steel began to yield or buckled outward due to the additional stress. The loss of stiffness of the reinforcement would cause an additional increase in the stress concentration in the concrete core, which would result in a subdivision of the core into prisms because of the ties. The core maintained its integrity until it reached its ultimate strength and failed. The concrete in the core reached its ultimate strength rapidly after buckling of longitudinal reinforcement. In addition, it was indicated that the size and spacing of ties influenced the local state of stress in the concrete at the region next to the

ties, the strength of the concrete core, and the buckling strength of longitudinal reinforcement.

The authors stated that the state of stress at the interface of the concrete cover and the lateral ties was one of the primary reasons for cracking and spalling. Axial loading of the concrete member produced lateral expansion of the concrete. Ties controlled this movement as well as prevented the displacement of longitudinal reinforcement of the longitudinal bars. The described effect would cause distortion of the cross section, resulting in spalling of the unconfined concrete (the cover).

Bresler and Gilbert described two modes of failure of the concrete core: short compression members and long prisms. Short compression members i.e. (standard concrete cylinders) would fail in a "shear cone" failure due to axial loading and lateral restraint at the ends. Long prisms would fail along planes that were parallel to the longitudinal axis because of a large reduction of friction on the ends; furthermore, they would carry a smaller load before failure than the short compression elements. Large tie spacing would force the core to fail by longitudinal splitting; for this reason, Bresler and Gilbert recommended that lateral ties should be designed to be spaced so as to prevent this weaker mode of failure.

To select appropriate tie spacing, Bresler and Gilbert recommended considering the buckling behavior of longitudinal reinforcement between tie spacing once the concrete cover was lost. Factors affecting the critical buckling force were the bar diameter, tie spacing, buckling mode, and mechanical properties of the steel. The spacing of the ties should be so as to permit the development of buckling of longitudinal reinforcement when steel reached its yield stress. To determine the critical buckling stress, Bresler and Gilbert assumed that the lateral ties had sufficient rigidity so that the lateral displacement of

longitudinal bars at that point was insignificant. Bresler and Gilbert introduced the concept of tie spacing-to-bar diameter ratio (*l/D*) in the calculation of the critical buckling stress:

$$f_{cr} = C\pi^2 E_t \left(\frac{l}{r}\right)^2 \qquad \textbf{(2.1)}$$

where C was the end restraint coefficient of the longitudinal bar, E_t was the tangent modulus for critical stress f_{cr}, l was the unsupported length, and r was the radius of gyration of the reinforcing bar. By setting the critical stress equal to the yield stress, an equation for the *l/D* ratio was formulated to select appropriate tie spacing:

$$\frac{l}{D} = B\left(\frac{E_t}{f_y}\right)^{1/2} \qquad \textbf{(2.2)}$$

where $B=1/2\pi C^{1/2}$ and f_y was the yield stress of the longitudinal steel. The formulated equation depended on the mechanical properties of the material (E_t and f_y). Therefore, there was no possibility of having a constant *l/D* ratio; as the yield stress of the reinforcing bars increased, the required *l/D* ratio decreased.

For the assumption of sufficiently rigid ties to be valid, the size of ties selected should have a minimum size corresponding to a minimum stiffness in order to prevent premature buckling of longitudinal reinforcement. Bresler and Gilbert modeled a bar with length *2l* that was fixed at its ends, and had an elastic spring support at the middle. Using the Ritz method, they solved for the minimum stiffness required by the middle support to prevent lateral displacement at that point and developed an equation based on the relationship of the transverse and longitudinal steel diameters (*d/D*).

The test setup for the experimental program performed by Bresler and Gilbert consisted of four columns measuring 8″ x 8″ x 60″, reinforced with #5

deformed bars of f_y = 44.5 ksi and fu = 77.5 ksi for longitudinal reinforcement, #2 deformed bars of f_y = 52.1 ksi, and $^1/_{16}$″-diameter steel wire of f_y = 48.2 ksi for transverse reinforcement. Concrete with strengths (*f'c*) of 4 ksi and 6 ksi were used. Two columns were cast with each kind of concrete; one was reinforced with #2 bars outside the core and $^1/_{16}$″ steel wire inside, and the second was reinforced with #2 bars both inside and outside the core. Load was applied axially in 20-kip increments. Axial shortening was measured at each increment up to a strain of 1.5 milli strain (this strain was below the yield point of the longitudinal steel). After the tests were performed, it was observed that the load-deflection relationship was nearly linear within the strains measured with a slight decrease of stiffness in the upper values recorded. Failure path was as follows: no noticeable cracks up to ultimate load, then the column deformed inelastically while maintaining its ultimate load until cracking was visible, then the load began to drop, the cover spalled, the longitudinal steel buckled between ties, and the core exhibited "shear cone" failure. Secondary consequences of failure were: splitting of concrete at corner lap splices #2 ties without yielding and yielding and rupture of $^1/_{16}$″ steel wire. The ultimate load was not affected.

Bresler and Gilbert proposed the following design criteria and conclusions for lateral reinforcement after all tests and calculations were performed:

- Tie spacing should be less than a distance equal to the smallest dimension of the column in order to develop the maximum strength of the core.
- Tie spacing should be less than the value calculated using Equation 2.2 in order to prevent premature buckling of longitudinal reinforcement.
- The size of the ties should be based on an empirical equation, which was a function of tie and longitudinal bar geometries, to

prevent excessive deformation of the ties and reduction of the buckling stress capacity of the longitudinal reinforcement.

- The size of transverse reinforcement inside the core (cross-ties) could be reduced without affecting the ultimate load capacity of the column, which would facilitate the placement of concrete on-site.
- Smaller tie sizes could be used and closer tie spacing than specified in ACI 318-56 should be provided for high-strength longitudinal steel.

For the analytical part of the study, Bresler and Gilbert investigated the isolated longitudinal bar and neglected the effect of interaction between the longitudinal bar and the concrete core. They also did not consider possible imperfections in the system or possible buckling over several tie spacings, which might result in buckling of longitudinal bars before reaching their yield stress. It could also be concluded that, since axial deformation was not measured through the end of the test, results might not represent the entire load-deformation relationship for the column up to failure. It was stated that the different types of reinforcement arrangements did not affect the maximum load-carrying capacity; however, Bresler and Gilbert did not discuss the ductility resulting from the various rebar arrangements.

2.2.2 Scribner (1986)

Scribner focused his study on developing and testing the inelastic response of flexural concrete members. Scribner assumed that the buckling of the longitudinal bars could occur over a length larger than the spacing of transverse reinforcement. This assumption was based on the observations reported for previous research (Bresler and Gilbert, 1961). The length of these regions was

chosen to be equivalent to a length of approximately three times the spacing of transverse reinforcement. He developed an analytical model to represent the buckling of longitudinal reinforcement in concrete flexural members including the effect of longitudinal bar size, tie size, and beam dimensions. In addition, laboratory tests were performed on six cantilever beams with different beam sizes and reinforcement arrangements by applying reversed inelastic moments to verify the applicability of the analytical model.

In the analytical model, the longitudinal bar was assumed to buckle in a mode shape spanning three tie intervals, and was modeled as a fixed-fixed column supported by lateral springs at its third points. The selection of the model was based on previous observations of failure in which longitudinal reinforcement had buckled over regions where concrete cover had spalled, which was approximately the spacing of three ties. Throughout the derivation, an appropriate lateral stiffness and critical load to prevent buckling of longitudinal reinforcement were developed. In addition, a relationship between the longitudinal bar diameter and the tie diameter was established, which depended on the tangent modulus at a given strain, the unsupported lengths of the ties, and the longitudinal bars. It was concluded that a tie with half the diameter of the longitudinal reinforcement was required to prevent buckling for the configuration that was analyzed.

In the experimental program, six doubly reinforced cantilever beams with enlarged end-blocks were constructed. Specimens were grouped into three pairs; each pair had the same beam size, longitudinal reinforcing steel size and arrangement, and tie spacing. Within each pair, one beam had ties with a diameter less than half of that of the longitudinal reinforcement, and the second beam had ties with a diameter at least half as large as that of the longitudinal bars. In addition, the material properties of the concrete (i.e. f'_c) and the reinforcing steel

(i.e. f_y, f_u) were different for each pair. Table 2.1 provides the geometric and material properties of the specimens tested by Scribner.

Table 2.1 Specimen dimensions and material properties for the experimental program of Scribner (1986).

Specimen	Dimensions (in)				A_s	A'_s	A_v	f'_c (ksi)	f_y, f_u (ksi)		
	a	d	h	b					A_s	A'_s	A_v
1-A	36	10.1	12.1	8.1	3-#6	3-#5	#2 @ 2.5″	4290	63.6, 103	64.2, 106	56.0, 74.0
1-B	36	10.2	12	8.1	3-#6	3-#5	#3 @ 2.5″	3920	63.6, 103	64.2, 106	67.3, 102
2-A	50	11.6	14.1	10	3-#8	3-#7	#3 @ 3″	3860	69.4, 112	68.8, 116	67.3, 102
2-B	50	11.9	14.1	10.1	3-#8	3-#7	#4 @ 3″	4230	69.4, 112	68.8, 116	66.5, 101
3-A	60	11.6	14.1	10.1	3-#9	3-#8	#4 @ 3″	4010	62.8, 97.9	69.4, 112	67.3, 102
3-B	60	11.6	14.1	10.1	3-#9	3-#8	#5 @ 3″	4210	62.8, 97.9	69.4, 112	66.5, 101

Note: a = shear span, d = effective depth, h = beam height, b = beam width, A_s = tension longitudinal reinforcement, A'_s = compression longitudinal reinforcement, A_v = transverse reinforcement (ties), f'_c = compressive strength of concrete (from standard cylinder test), f_y = tensile yield strength of steel, f_u = ultimate tensile strength of steel.

During testing, several modes of failure were observed. Specimen 1-A failed when the shear capacity of the hinging zone was exceeded, and the longitudinal reinforcement did not buckle. Specimen 1-B failed due to buckling of the longitudinal reinforcement in the hinging zone over a length approximately equal to the spacing of the stirrups. Specimens 2-A and 2-B failed due to buckling of the longitudinal reinforcement in the hinging zones over a length of approximately three times the stirrup spacing. The buckled shape of the bars in specimens 2-A and 2-B demonstrated the appropriateness of the analytical model and the inability of large ties to prevent buckling of longitudinal reinforcement. Specimens 3-A and 3-B exhibited a different failure mechanism than the other specimens because the longitudinal reinforcement was not developed adequately

within the large end-blocks, and both members failed due to loss of anchorage of longitudinal reinforcement.

The data indicated that beams subjected to large flexural deformations had a greater possibility of experiencing buckling of longitudinal reinforcement than beams subjected to smaller displacements. In addition, the researchers reported that prediction of the flexural deformation capacity of a doubly reinforced beam was very difficult, if not impossible, mainly due to buckling of compression bars.

Scribner concluded that ties with a diameter approximately equal to ½ times the diameter of the longitudinal reinforcement would be required to prevent buckling of longitudinal reinforcement in beams subjected to cyclic inelastic flexure.

Conclusions from the experimental study performed by Scribner included two major observations: (1) the buckling shape assumed in the analytical model was observed in only one specimen, and (2) large ties prevented the type of buckling of the longitudinal bars suggested by their analytical study but did not prevent other types of buckling of longitudinal reinforcement. The latter was in agreement with the conclusion of Bresler and Gilbert, who stated that larger amount of transverse reinforcement did not affect the maximum capacity of the member.

Scribner proposed the following design recommendations: (1) lateral ties should have a diameter of at least half as large as the diameter of longitudinal reinforcement, and (2) ties larger than those recommended by the ACI 318-83 seismic provisions prevented only certain types of buckling of longitudinal reinforcement in members subjected to cyclic inelastic flexure. Using very large ties did not guarantee that longitudinal bars would not buckle under severe loading conditions.

2.2.3 Russo (1988)

Russo developed an analytical method to determine the critical buckling load of the longitudinal bars in reinforced concrete elements subjected to large compressive strains. The proposed model represented the longitudinal bar as a beam of infinite length on equally spaced intermediate elastic supports having equal stiffness, which represent the transverse reinforcement of a concrete column. To account for the bounding effect of the concrete core, the problem was considered as one of unilateral instability with a half-wave buckled shape. This half-wave shape was obtained by analyzing the deflection curves satisfying the assumed condition. The instability was assumed to occur over a length larger than the hoop spacing. The model made it possible to calculate the length of the element that became unstable and to calculate the critical load. Two cases were presented: even and odd numbers of hoops. The number of supports or amount of hoops present in the longitudinal bar would shift the center of the longitudinal bar from a support to a point located at the center of the hoop spacing.

The analytical problem was solved by formulating a differential equation for the deflection curve and imposing geometric and force boundary conditions. When the geometry, material properties, and stiffness of supports of a given bar were known, then the stiffness ratio could be calculated (stiffness ratio = stiffness of support / (the hoop spacing cubed x the hoop stiffness cubed)). The critical load was found by using an iterative process in which the length of instability was assumed, and the load was changed until the maximum value of the unstable length that satisfied the equations was found. The model was applied to a range of stiffness ratios between 0.04 and 10,000 in order to cover a large number of cases that were possible in an actual beam.

After evaluating the proposed analytical model, Russo compared the results with the experimental work performed by Vallenas, Bertero, and Popov

(1977). The experimental model consisted of a compressed reinforced concrete element of size 254-mm x 254-mm with 8 longitudinal bars with a diameter of 19.05-mm, 4.55-mm diameter stirrups spaced at 33.7-mm, and diamond shape internal hoops. When calculating the stiffness of the supports for the corner bars, one leg of the stirrup with a length equal to the spacing between corner bars was considered; it was assumed that all four corners buckled outward at the same time. Similarly, for intermediate bars, one leg was considered for the stiffness calculation of the supports, but the leg length was less than the spacing between corner-bars resulting in a larger stiffness.

Russo took into account the initial imperfection possible along the bar; the tangent modulus was used for regions where the initial curvature coincided with the curvature of the assumed buckled configuration. For the cases where the curvatures did not coincide, a reduced modulus was introduced. Finally, the critical stress calculated was 33% larger than the experimental value obtained by Vallenas et al. (1977). The assumed length to be affected by instability (5.8 times the tie spacing) was in good agreement with the experimental observations, in which this length was measured to be at least the spacing between six hoops.

Russo reached the following conclusions: (1) the models with even number of supports (stirrups) were weaker than the models with an odd number of supports; (2) buckling could occurr between two consecutive hoops only if the hoops were non-deformable; (3) the critical load and the length of the region affected by instability could be determined by using the diagrams that were developed with the analytical model; (4) the analytical model gave a good understanding of the physical phenomenon as seen in previous experiments by Vallenas et al. 1977.

The analytical work developed by Russo was restricted to the prediction of the critical buckling stress and the length of instability. Although it used the

overall length of the reinforcement and amount of stirrups, took into account initial imperfections, and considered different material properties, it was not aimed at evaluating the complete stress-strain relationships of bars under compression.

2.2.4 Papia, Russo, and Zingone (1988)

Papia et al. (1988) studied the failure of reinforced concrete elements under compression due to the instability of longitudinal reinforcement. They developed an analytical model that provided a general solution to the instability of longitudinal bars in concrete columns subjected to concentric loading. The model provided formulas to calculate the length of the region in which longitudinal bars would buckle and the critical load for buckling. The developed equations were applied to sections tested by previous researchers, and the results were compared in order to validate the model.

The longitudinal bar was represented as a column with length L and built-in ends. The column had intermediate unilateral elastic supports with spacing equal to the distance l between the transverse reinforcement. The intermediate supports had stiffness (α) that depended on the geometric and mechanical properties of the hoops. The equations developed were applicable for odd and even number of hoops. The transverse strain of the concrete core was assumed to be constant along the column, and the bar was considered to be straight because the authors deemed the effect of lateral pressure on the bar due to the confining concrete to be negligible.

A parameter γ was introduced in order to incorporate stiffness of intermediate supports (α) in the calculation of the critical load. The parameter γ depended on the stiffness and spacing of hoops, as well as on geometric and mechanical properties of the longitudinal bars. The modulus of elasticity (E)

considered for the longitudinal bars was the instantaneous value that corresponded to the critical strain (ε_{cr}) that produced buckling. The analytical model suggested by Papia et al. employed a reduced modulus technique (E_r) that depended on the elastic modulus of the steel (E_s) and the modulus at strain hardening (E_h). A length of instability (the length at which buckling took place) to spacing of hoops ratio (L/l) was introduced to establish the effect of the structural configuration. As γ increased, the L/l ratio decreased, and the critical load increased. The critical load determined by the proposed model depended on the parameter γ.

The developed analytical model of Papia et al. was compared to the experimental results obtained by Scott et al. (1982) and Sheikh and Uzumeri (1980). The comparison showed that the analytical model was valid, demonstrating that the failure of a compressed concrete element was always affected by the instability of the longitudinal bars, despite the size and spacing of the stirrups. It was also reported that the stirrups involved in the buckling of the longitudinal bars resulted in a local loss of confinement. As a result, the columns failed by crushing of the core. In addition, the calculated length of the region involved in buckling was quite consistent with the observations made during experiments.

Papia et al. recognized that taking into account only the degree of confinement and yield stress of the hoops when evaluating the maximum load was not completely accurate because these assumptions neglected the instability load of the longitudinal bars. The interaction between the confined concrete core and reinforcing cage, a phenomenon that was observed in all the previous research reported herein, was ignored in the formulation provided by Papia et al. In addition, they concentrated on predicting the critical buckling load of the longitudinal bars and did not attempt to evaluate the complete stress-strain behavior of longitudinal bars.

2.2.5 Papia and Russo (1989)

Papia and Russo related the failure of compressed concrete elements with the instability of the longitudinal steel reinforcement. They proposed an analytical procedure to be used to determine the ultimate strain of compressed concrete elements based on the limit stability condition of the bars, further developing the work of Papia et al. (1988) who developed a model to determine the critical load of the bar. The critical strain of the longitudinal reinforcement was assumed to correspond with the ultimate strain of the concrete element; this was obtained by assuming a variable elastic modulus in the strain-hardening region of the steel, adopted from the constitutive relationship proposed by Park and Paulay (1975). The effect of the slenderness of the longitudinal bars, hoop spacing, and hoop stiffness were the primary factors affecting the ultimate strain calculated from the proposed equation.

Papia and Russo also analytically studied the effect of steel properties in the ultimate strain calculation by varying the material properties. An approximate analytical expression was also proposed for the ultimate strain calculation to be used in practical ductility calculations. The results of the proposed equation and the approximate expressions were then compared to the experimental and analytical results obtained by other authors to confirm the validity of the proposed theoretical approach.

The ultimate compressive strain of confined concrete had a crucial effect on the ductility of the potential plastic hinge region developed in columns and piers under dynamic loads. Previous studies had shown deterioration of structural elements due to buckling of the compressed longitudinal bars (this was identified as ultimate state). Similar to Russo (1988), the analytical model of the longitudinal bar was characterized by a continuous beam element on elastic supports (representing hoops and concrete core together) buckling unilaterally.

The value for the instantaneous elastic modulus was determined from the average value of the tangent modulus in the range of strains expected, providing an accurate evaluation of the critical load. Because of the shape of the steel stress-strain diagram in the hardening region, an equation for the critical strain was developed in which the variation of the tangent modulus in the strain-hardening region was considered.

Papia and Russo established the relationship between the critical load and the stiffness parameters. A clear relationship between the tangent modulus and the reduced modulus was also identified. The proposed procedure of Papia and Russo was only applicable for strains in the reinforcement that resulted within the strain-hardening region of the stress-strain relationship. For this to be true, the range of values of the geometric and material characteristics of the structural element that made it possible to be in the strain-hardening region needed to be determined. Then, the element had to satisfy the following conditions: (1) slenderness value ($4l/d$) must be less than the maximum slenderness value ($2\pi(E_{ro}/f_y)^{1/2}$, E_{ro} = reduced modulus at onset of strain hardening, f_y = yielding of longitudinal reinforcement); and (2) the stiffness of the hoops must be so large that buckling of the longitudinal reinforcement could not occur before the strain of the longitudinal bars reached strain hardening. In order to meet this last condition, a minimum lateral stiffness was defined based on the minimum stiffness ratio of the longitudinal bar.

To account for the effect of material steel properties, Papia and Russo considered eight types of steel. For all types, the critical strain was calculated in relation to different lateral stiffnesses of hoops, including several cases of engineering interest. Once the material properties and slenderness of the bar were established, a maximum critical strain could be obtained.

An approximate expression was developed for the case in which the critical strain was equal to the ultimate strain in concrete. This expression took into account the maximum slenderness of the bar, the yield strength of the longitudinal steel, and the hardening capacity of the steel used. The proposed approximate expression was intended for practical applications in engineering practice.

Lastly, Papia and Russo compared the results of their theoretical and approximate equations with the experimental results of Sheikh and Uzumeri (1980) and Scott et al. (1982). Both experimental studies consisted of specimens with varying diameters and material properties for the longitudinal and transverse reinforcement. In addition, the results obtained using the empirical expressions developed by Kaar and Corley (1977) and Scott et al. (1982) were included for comparison purposes. The results showed that the procedure proposed by Papia and Russo determined the critical stress of the longitudinal bars with a better precision than their previous work, Papia et al. (1988), which led to a good approximation of the ultimate strain. Papia and Russo reported that the results provided by the Kaar and Corley (1977) expressions produced overly conservative values, while the Scott et al (1982) expression gave values closer to the experimental results but not conservative for all the specimens.

Papia and Russo concluded that the proposed analytical procedure made it possible to determine the ultimate strain of compressed reinforced concrete elements, which was assumed to coincide with the strain that produced buckling of the longitudinal reinforcement. Papia and Russo observed the following when comparing the results of the experimental work: (1) the assumptions made were valid, (2) the critical strain of the longitudinal bars was calculated with a reasonable degree of accuracy, and (3) the analytical relationships used to define the critical loading coefficient, the reduced modulus, and the consecutive law of

steel proposed by Park and Paulay (1975) were adequate. For the developed theoretical approach, the lateral stiffness provided by the hoops was identified as the major influence to the calculation of the maximum strain of the compressed element, as opposed to the resistance provided by the confinement. In addition, a maximum value of strain that depended exclusively on the slenderness parameters of the longitudinal reinforcement was identified. The approximate analytical expression used to calculate the ultimate strain proved to be explicit and particularly useful in practical applications.

Papia and Russo concentrated their study on the characterization of the ultimate state of failure and not on the complete behavior that led to failure. Their work focused on the determination of the critical stress and strain at failure that made it possible for the longitudinal reinforcement to reach strain hardening before the concrete reached its ultimate strain. It was useful for the research presented herein, because it considered the effects of the hoop spacing and the different material properties of steel in the final behavior of longitudinal reinforcement. However, it did not mention the effect of initial imperfections of the system.

2.2.6 Mau and El-Mabsout (1989)

Mau and El-Mabsout developed a beam-column element using the finite element analysis method to determine the inelastic post-buckling behavior of reinforcing bars in concrete columns. They identified the slenderness ratio of the bar, as well as the tie spacing, as primary factors affecting the buckling and post-buckling behavior of the longitudinal reinforcement. In this study, the elastic-plastic-strain hardening behavior of steel and the stress reversal occurring after buckling were incorporated to determine more precisely the maximum load-carrying capacity of the reinforcing steel.

The following assumptions were considered when developing the beam-column element model: (1) the cross section of the beam-column was circular; (2) the beam-column had no initial crookedness and was concentrically loaded at the end; (3) before and after buckling occurred, plane sections remain plane; (4) shear deformations were negligible; (5) the transverse displacement (w) was such that $(dw/dx)^2 << 1$, where x = the longitudinal, or axial coordinate; (6) the axial strain was small relative to unity; and (7) the material behavior was elastic-plastic-strain hardening with a distinct plastic yield plateau.

Based on the assumptions considered in the formulation, the authors defined the independent field of displacements, which included three (nodal) degrees of freedom at each of the two nodes. Then, the equilibrium condition equations were derived using the principle of virtual work, resulting in two equations for the beam-column element in two dimensions. An equation, that modeled the inelastic stress-strain law and also included a strain reversal rule was presented and imposed on the model. Numerical integration was emphasized to solve for forces and moments because of the complicated stress distribution over the circular cross section; the Simpson rule with 21 points across the section was used. Numerical integration was also used to solve for the equilibrium condition equations and for the two-point Gaussian quadrature formula over the length of the element.

When proceeding to solve a given problem with a specified boundary condition, the first step was to assume a vector of nodal displacements. Then, the nodal forces were calculated to check nodal equilibrium, and the Newton-Raphson method was used to iterate between the input nodal displacement and the equilibrium forces until the error between them was within the predetermined threshold error. The element was assumed to be loaded without premature

buckling, and the pre-buckling path was entirely linear and elastic. The only point of interest was the post-buckling path that began at yielding.

The developed numerical model was applied, and the results were compared to the experimental results reported by Mander et al. (1984) to validate the assumption of the model and to verify its accuracy. The experimental work consisted of medium-strength reinforcing steel bars with 16 mm diameter with spacing-to-diameter ratios (*S/D*) of 5.5, 6, 6.5, 10, and 15 and respective slenderness ratios (*L/r*) of 11, 12, 13, 20, and 30. Strains were measured over a gage length of 30 mm. The numerical model was applied using material properties for medium-strength as well as high-strength reinforcing steel.

Mau and El-Mabsout reported a case in which the material was assumed to be elastic-perfectly plastic for the medium strength reinforcing steel. Although this was not realistic for the behavior of reinforcing bars, it served as a basis for general comparison of the effect of varying length (*L/r*). The result from this assumption could be useful for the buckling of truly elastic-perfectly plastic short bars.

The case that considered the elastic-plastic-hardening behavior of the material for both medium and high strength steel was of interest because the results represented a more realistic behavior and, therefore, were used to compare analyses results with experimental results. The comparison between the calculated values for medium-strength and the measured results demonstrated good agreement. In general, it was observed that the load-carrying capacity rose after an initial drop for the shorter bars (smaller *L/r*); as the unsupported length of the bar decreased, the compressive stress-strain behavior moved closer to the tension stress-strain curve. It was reported that the hardening behavior had a significant effect on the overall load-carrying capacity. Mander et al (1984) reported that a *S/D* of 6 was an appropriate design limit for tie spacing because it more resembled

the tension stress-strain curve for strains lower than 0.02. Mau and El-Mabsout agreed with Mander et al. (1984) and defined a critical slenderness ratio, which was a value corresponding to *S/D* at which the stress stays close to that of the yield point until the axial strain reached 0.04. This point was characteristic of ductile behavior of the material because of its capability of sustaining a load for a wide range of deformations. The value for this critical slenderness ratio (*S/D*) was 8. For high strength steel, *S/D* = 7 corresponded to the 0.02 strain limit, and *S/D* = 10 corresponded to the critical slenderness ratio. These were based on the analytical model and were not compared to any experimental data. The difference between the *S/D* ratios from one type of steel to another confirmed what Bresler and Gilbert (1961) mentioned that the *S/D* ratio required to prevent premature buckling was lower with higher values of yield strength.

Mau and El-Mabsout also reported the transverse deflection of the bar under axial loading. In general, it was discussed that for smaller *L/r*, the displacement decreased after reaching a maximum point (yielding). The displacement started increasing again until reaching a second maximum point, and then continued decreasing. This second maximum point was defined as "second buckling" due to "straightening". It was observed that the axial load vs. transverse displacement on a normalized scale was identical for all slenderness ratios.

Mau and El-Mabsout drew the following conclusions: (1) the load-carrying capacity dropped after the buckling at the yielding load for the elastic-perfectly plastic case; (2) the post-buckling behavior was dominated by the formation of a plastic hinge early in the post buckling history; (3) the strain hardening behavior dominated the post-buckling path; (4) the post-buckling peak load may be higher than the yielding load; and (5) a critical slenderness ratio (L/r) could be defined by equating the peak load and the yielding load.

2.2.7 Mau (1990)

In this paper, the author reported an extended application to the beam-column finite element analysis model introduced earlier in Mau and El-Mabsout (1989). This time, the focus of the study was particularly on the effect of the tie spacing-to-diameter ratio (*S/D*) on the load carrying capacity of reinforcing steel. For these cases, a simplified model for the different stress-strain curves of high-strength steels was used to identify the effect on the inelastic post-buckling behavior, particularly, on the selection of an appropriate *S/D* for design. In addition, the peak loading calculated using the finite element model was compared to those calculated using the tangent modulus theory explained by Bresler and Gilbert (1961).

The load deflection curves were calculated for *S/D* values varying from 5 to 15 with increments of 1. The report presented the results for *S/D* of 5, 10, and 15. It was observed from the results that: for small *S/D* (i.e. 5), the axial load-deflection curve followed that of the tension curve until axial strains reached 0.04; at large *S/D* values (i.e. 15), the steel became unstable after reaching the yield load and showed a constant decrease in the capacity on the post-buckling region; and for intermediate values of *S/D* (i.e. 10), the steel buckled at yield load but regained a portion of the capacity (slightly larger than the yielding load) for strains of 0.02 before becoming unstable. Subsequently, it was recognized in the study that the load carrying capacity was dependent of the post-buckling behavior. Strain hardening provided increased stiffness after first yield, and the *S/D* value was a major factor in characterizing the effect of the strain-hardening region.

S/D = 7 was defined as the critical spacing-to-diameter ratio, consistent with the value previously reported for high-strength steels, (Mau and El-Mabsout, 1989). It was recognized in the report that this value may vary with the material properties. The author simplified the stress-strain curve for high strength steel

with two straight lines for the linear elastic and plateau and two lines for the strain-hardening portion. A total of 27 cases with a series of *S/D* values (5, 6, and 7) were studied. The 27 cases combined the different possibilities among the strain hardening ratio (equal to the ratio of the highest strain of the plateau region to the yielding strain), peak stress ratio (ratio of ultimate stress to yield stress), and the hardening modulus ratio (ratio of strain-hardening stiffness to elastic stiffness). It was concluded that *S/D* was more sensitive to the hardening modulus ratio and less sensitive to the peak stress ratio.

The following conclusions were drawn from the study: (1) for reinforcing steel with elastic-plastic-hardening behavior under monotonic loading, the finite element studies showed that the axial load carrying capacity was greatly improved beyond the yield load if the tie spacing was smaller than *S/D* = 7; (2) for *S/D* ratios below 7 and for sections with sufficiently stiff ties, the axial load-deflection history of the reinforcing steel followed closely the material stress-strain curve; (3) the yield plateau had a negligible effect on the load carrying capacity; (4) the tangent modulus theory could be used to predict the inelastic buckling load, as well as to calculate sufficient stiffness of the tie (Bresler and Gilbert, 1961); (5) for *S/D* ratios larger than 7, the actual load-deflection path could be unstable after the yielding load; and (6) the load-carrying capacity of the reinforcing steel could not be predicted accurately by the tangent modulus theory.

Similar to Mau and El-Mabsout (1989), Mau (1990) did not take into account the possibility of initial imperfections on the bars or the effect of non-concentric loading on the reinforcing steel.

2.2.8 Monti and Nuti (1992)

Monti and Nuti studied the inelastic behavior of reinforcing steel under monotonic and cyclic loading. They performed experiments on different bar sizes

of different length and developed an analytical model of rebars accounting for inelastic buckling behavior. Monti and Nuti stated that the proposed model had three major advantages over previous models developed: (1) it had a simpler formulation which avoided extensive calculations, making it applicable in reinforced concrete design; (2) it had a stress-strain type formulation that introduced nonlinear effects more easily; and (3) it depended on parameters that were easy to calibrate even for inelastic buckling.

The experimental program consisted of testing reinforcing bars with yield strength of 440 MPa under monotonic and cyclic loading. The varying parameters introduced for comparison were the tie spacing (S) and the bar diameter (D). The results were compared based on their tie spacing-to-bar diameter ratio (S/D) and the chosen values represented the most commonly used tie spacing (i.e. S/D = 5, 8, 11). The bar diameters tested had diameters of 16, 20, and 24 mm. The tests were displacement-controlled. The paper reported the experimental stress-strain curves of rebars in tension and compression.

The proposed analytical model incorporated cyclic behavior of reinforcing bars. A plasticity approach was used to derive the analytical model. The proposed model consisted of a finite stress-strain relationship for branches between two subsequent reversal points or loading branches in which the parameters were updated after each load reversal. These updating steps were done using four hardening rules: kinematic, isotropic, memory, and saturation. The last two rules accounted for the memory of the material to the plastic path followed and for the asymptotic character of hardening phenomena, respectively. Four parameters were needed to predict the cyclic behavior of reinforcing bars in the absence of buckling: yield stress, modulus of elasticity, hardening ratio, and a weighting coefficient. In the cases where buckling was critical more parameters were introduced and the model became more complicated. Material hardening models

were incorporated in the suggested analytical model to reproduce the behavior of nine rebar samples that were tested by the authors. An equation for the reduced modulus in the strain hardening region was developed.

The analytical model was compared to the experimental results, plus it was compared with the results obtained by previous analytical models (i.e. Filippou, Bertero, and Popov – 1983 and Menegotto and Pinto – 1973).

Monti and Nuti reported the following conclusions: (1) inelastic buckling of steel reinforcing bars occurred when the *L/D* ratio exceeded a critical value of 5, while Mau and El-Mabsout (1989) reported the critical *L/D* ratio to be 7 for high-strength steels. This softening behavior resulted in the modification of monotonic and cyclic behavior. (2) The proposed model properly replicated symmetrical and non-symmetrical cyclic strain histories. The model proved to be more accurate than the Menegotto-Pinto (1973) model for cases with no buckling after yielding, and it had comparable accuracy with respect to the Filippou-Bertero-Popov (1983) model. Monti and Nuti's proposed model was the most accurate for cases with no buckling after yielding.

The hysteretic analytical model proposed by Monti and Nuti was quite accurate in simulating the cyclic behavior of reinforcing bars that had no initial imperfections. However, the researchers did not address the actual physical problem encountered in a tied reinforced concrete column; the confined concrete core-reinforcing cage interaction and imperfections in the system were not considered.

2.2.9 Bayrak and Sheikh (2001)

Bayrak and Sheikh developed an analytical procedure and performed experimental research to predict the response of plastic hinges developed in concrete frames due to strong ground motions. Using a plastic hinge analysis

technique (which considered equilibrium, compatibility, and constitutive relations in a three-dimensional space), the analytical model was developed. The interaction between the concrete core and the reinforcement cage was considered in the analysis. Bayrak and Sheikh incorporated the behavior of longitudinal reinforcement under monotonic compression and developed stress-strain relationships by means of experimentation. The proposed analytical technique was compared with previous published models and also with results obtained from previous experiments of concrete columns.

The analysis of plastic hinges consisted of performing conventional sectional analysis before the longitudinal bars started to buckle. After the bars started to buckle, the axial strain was determined using experimental results (Bayrak 1999), and the tie stress was determined using experimental data from compressive tests of tied columns (Sheikh 1978), in which average tie strains for a given axial strain were given. For the calculation of the average strains for a given axial strain, a confined concrete expansion ratio was introduced, which depended on the varying material properties. Equilibrium equations were then used to determine the total transverse forces acting on the longitudinal bars. Proper boundary conditions and shape functions for the forces acting on the longitudinal bars were applied to calculate the outward deflection of the bars at the midspan between two ties. The deflection calculated was divided by the bar diameter in order to obtain an initial imperfection-to-bar diameter ratio (e/d). With this e/d ratio and the tie spacing-to-bar diameter ratio (L/d) the appropriate stress-strain relationship under compression for the longitudinal bars could be selected and used in the sectional analysis.

After the longitudinal bars began to buckle, four constitutive relationships were used: (1) a stress-strain relationship for unconfined concrete cover, (2) a stress-strain relationship for confined concrete core, (3) a stress-strain relationship

for longitudinal bars under tension, and (4) a stress-strain relationship for longitudinal bars with initial imperfections under compression.

The experimental program that was performed to establish the constitutive relationship for reinforcing bars under compressive loading consisted of 56 Grade 400 (U.S. Grade 60) reinforcing bars with designation 20M (20-mm diameter). Seven different *L/d* ratios (4 to 10 with increments of 1) were tested, and for each *L/d* ratio, four different *e/d* ratios (0.0 to 0.3 with increments of 0.1) were tested. Each combination of *L/d* and *e/d* ratios had two identical specimens in order to ensure reliability of the data. It was observed that for the same *L/d* ratio, the strength and ductility decreased with an increase on *e/d* ratio (initial imperfection). The critical *L/d* ratio, at which the load-carrying capacity was smaller than yielding, was reported to be 7. Mau and El-Mabsout (1989) reported this value to be 8 for medium-strength steel and 7 for high-strength steel, and Mander et al. (1984) reported it as 6. The yield strength for *L/d* ratios lower than the critical value could be achieved for $e/d = 0.1$. For structures that required high ductility, the critical L/d ratio should not be exceeded in regions were plastic hinging could occur. For structures that required moderate ductility, an *L/d* ratio lower than 8 was reported to be appropriate.

When incorporating the interaction between the concrete core and the reinforcing cage in the 3D analysis, a tied column with diamond-shape internal arrangement of the transverse reinforcement was used. Critical tie spacing was defined as the tie spacing that resulted in zero confining pressure at the center between two ties. As the actual tie spacing was reduced from the critical value, the midspan deflection of the longitudinal reinforcement between ties was also reduced. Therefore, the *e/d* ratio was also reduced, improving the behavior of the longitudinal bars under compression as described above. The analytical model proposed was also applicable for cases in which more than one tie spacing was

involved in the rupture by ignoring the ruptured ties and modifying the spacing in the equations.

The developed model was applied to predict the moment-curvature relationship of the four specimens tested by Sheikh and Khoury (1993). The use of the plastic hinge analysis technique resulted in fairly accurate predictions of the capacity, the ultimate curvature, and the maximum tip displacement of specimens tested by Sheikh and Khoury (1993).

In general, the analytical model developed by Bayrak and Sheikh resulted in good estimates of the cyclic behavior of concrete columns. The model incorporated all factors considered in previous research plus a 3D model of the concrete core-reinforcing cage interaction that caused the buckling of longitudinal reinforcement. However, the experimental program for the reinforcing bars was not sufficient to create a comprehensive database such that closed form expressions could be developed for the stress-strain behavior of reinforcing bars under compression. Testing of other bar sizes and other types of steel was required to complement this plastic hinge model.

2.3 SUMMARY AND CONCLUSIONS

Previous research involving longitudinal bar buckling in reinforced concrete members was studied in this chapter. Many of the researchers concentrated their study on evaluating how buckling of longitudinal reinforcement affected the critical load-carrying capacity. Most of the work consisted of developing analytical models to represent the instability phenomenon. What all the previous researchers had in common was the recognition of the effect of the longitudinal bar size, tie size and spacing, and the material properties of steel (based on tension tests) in the buckling of longitudinal reinforcement in concrete members.

Bresler and Gilbert (1961) studied the effect of tie spacing and buckling of longitudinal reinforcement in concrete elements affected by the bar size, lateral stiffness, and material properties, but did not incorporate either the interaction with the core or the possibility of buckling along more than one spacing. On the other hand, Bresler and Gilbert (1961) were the first to recognize the deficiency of building codes for detailing reinforcement where ductility was required and also in establishing the importance of closer tie spacing in the zones where ductile behavior was expected.

Most of the research focused on developing analytical models to represent the buckling of reinforcing bars. Scribner (1986) modeled the buckling of the reinforcing bar over three tie spacings in order to calculate the critical load for buckling. Russo (1988) developed a model for buckling over several tie spacings considering the stiffness provided by the transverse reinforcement in order to calculate the affected length and the critical load. Papia, Russo, and Zingone (1988), and Papia and Russo (1989) developed an analytical model for determining the critical strain of concrete based on the instability of the longitudinal bars. The analytical models of Mau and El-Mabsout (1989), Mau (1990), and Monti and Nuti (1992) were developed with the purpose of developing complete stress-strain behavior curves for reinforcing bars under compressive loads. Mau and El-Mabsout (1989) developed a finite element model to predict the buckling response under monotonic loading, while Monti and Nuti (1992) developed a model for buckling under cyclic loading.

The interaction between the concrete core and the reinforcement was not considered in the analytical models mentioned above. Some of them represented the presence of the concrete core by assuming the problem as one of unilateral displacement. Bayrak and Sheikh (2001), on the other hand, developed an analytical model that takes into consideration the tie spacing, bar sizes, material

properties, initial imperfections, stress-strain relationships of compressed longitudinal bars, and the forces introduced by the concrete core to the longitudinal bars due to core-cage interaction.

Various experimental tests have been performed through the years in order to validate analytical formulations. Bresler and Gilbert (1961) tested columns to prove that the spacing required by the building code was not appropriate. Scribner (1986) tested cantilever beams to demonstrate that displacements caused by flexure may also cause buckling of reinforcement even when axial loads were not present. Monti and Nuti (1992) tested reinforcing bars under monotonic compressive loading to develop stress-strain relationships for different bar sizes and lengths. Bayrak and Sheikh (2001) tested reinforcing bars of different lengths and initial imperfections to develop stress-strain relationships; also, they tested concrete columns in order to verify the applicability of the compressive stress-strain curves that were obtained for the bars with sectional analysis.

General conclusions may be reached based on previous research reported in the literature. Bresler and Gilbert (1961) and Scribner (1986) recognized that large ties did not guarantee the prevention of all types of buckling of longitudinal reinforcement nor did they affect the load-carrying capacity. Russo (1988) and Papia et al. (1988) concluded that buckling of longitudinal bars might involve more than one hoop spacing. Papia et al. (1988), Mau and El-Mabsout (1989), Monti and Nuti (1992), and Bayrak and Sheikh (2001) observed that as the spacing-to bar diameter ratio (L/d) decreased, the critical load to cause buckling increased. In addition, for those tests in which the complete stress-strain behavior was developed, a critical L/d ratio was recognized: for Mander et al. (1984) the critical ratio was 6, for Mau and El-Mabsout (1989) it was 8 for medium-strength steel and 7 for high-strength steel, for Monti and Nuti (1992) it was 5, and for Bayrak and Sheikh (2001) it was 7. In all of the tests and in all the analyses, it was

established that the strain hardening portion of the tensile behavior governed the post-buckling behavior of bars, and for most of the tests and analyses, a relationship for a reduced modulus in this region was used. For higher values of yield strength, a lower value of *L/d* ratio was required for buckling, e.g. Bresler and Gilbert (1961) and Mau and El-Mabsout (1989).

As studied earlier, the work by Bayrak and Sheikh (2001) was considered a fairly complete study in modeling the reinforcing bar buckling in concrete columns. A careful examination of the results of Monti and Nuti (1992) and Bayrak and Sheikh (2001) revealed the fact that there was a small amount of experimental data available. Hence, the results were not enough to represent the compressive behavior of all commonly used bars. A larger database of stress-strain behavior curves under compression was required to develop a constitutive relationship for simulating the behavior of reinforcing bars in compression. Bars with varying material properties that were commonly used must be tested so that such a constitutive relationship can be developed. As in previous research, these new specimens needed to be tested for different lengths, accounting for initial imperfections that may be introduced by the concrete core pressure in the initial stages of buckling. Such testing was carried out for this research project and will be reported in the following chapters.

CHAPTER 3
Experimental Program

3.1 INTRODUCTION

As presented in Chapter 2, a number of studies have been conducted to determine the complete stress-strain behavior of steel reinforcing bars under compression, i.e. Mau and El-Mabsout (1989), Mau (1990), Monti and Nuti (1992), and Bayrak and Sheikh (2001). As recognized by previous researchers, considering the interaction between concrete and steel reinforcement better represented the real stress-strain behavior of longitudinal bars under dynamic loadings during column hinging. It was also demonstrated by Bayrak and Sheikh (2001) that the results obtained by testing reinforcing bars under monotonic compressive loading can be used to predict the behavior of concrete columns. Therefore, only reinforcing bars were tested for this project by applying monotonic uniaxial compressive loading.

The experimental program of the present study followed the experimental procedures performed by Bayrak and Sheikh (2001); its purpose was to expand the database required in plastic-hinge analyses. In addition, the previous results performed on Grade 400 20M (#6) reinforcing bars (Bayrak and Sheikh, 2001) were incorporated in order to compare the results provided by different bar sizes and material properties. Once the experimental work is described and the tensile and compressive stress-strain relationships of the reinforcing steel are presented, then the results are compared based on length, size, material properties, and initial imperfections.

The experimental program consisted of tests of Grade 60 steel reinforcing bars of sizes #8 and #10 under monotonic uniaxial tension and compression. The

compression test specimens varied depending on their geometric parameters, i.e. bar size, length, and initial eccentricity at midspan. The #8 bars selected were U.S. domestic Grade 60 steel and the #10 reinforcing bars were of weldable steel material with the same yield strength.

3.2 TENSION TEST SPECIMEN PREPARATION AND PROCEDURE

For the tension test, three (3) specimens were selected for each of the bar sizes to be studied. Preparation of specimens was performed in accordance with ASTM A370-97a. The test specimens measured 8-inches for the gage length, at least two bar diameters between the gage mark and the testing machine grip, plus at least 10-inches on each end to fill the grips with some excess to extend beyond the end of each grip.

The bars were instrumented with long elongation strain gages to measure axial strains. The gauges were placed between the ribs of the bars by barely grinding the surface between the ribs. To capture large strain values in the strain-hardening region, four gages were placed within the center of the specimens. The average of the readings was used to represent the final stress-strain curves. The average was acceptable to use, because all four readings from the strain gages were approximately the same, as expected for a pure tension test. The loads, and hence stresses were measured by using three load cells that were integrally installed in the test machine: a Satec System Universal Testing Machine with 600 kip capacity. The measurements were recorded by a Data Acquisition system: HP 75000 Series B, and were converted to engineering units by a custom data acquisition program.

The average of three tests was used to obtain a typical tension stress-strain curve for each bar size. These curves were used to study the behavior of the bars under compression.

3.3 COMPRESSION TEST

3.3.1 Selection of specimens

As observed in previous studies, the compressive behavior of reinforcing steel depended on its unsupported length to bar diameter ratio (*L/d*), as well as its initial imperfections at midspan with respect to the bar size (*e/d*). Therefore, for the monotonic compression tests that were performed, a range of nine unsupported length-to-bar diameter ratios (*L/d* = 4, 5, 6, 7, 8, 9, 10, 11, and 12) and six initial eccentricities-to-bar diameter ratios (*e/d* = 0.0, 0.1,0.2, 0.3, 0.4, and 0.5) were used for each bar size, resulting in 108 specimens of #8 bars and 54 specimens of #10 bars. For the #8 bar tests, two specimens of each *e/d* – *L/d* combination were tested, and for the #10 bar tests, only one specimen was tested per combination.

The specimen designation (i.e. 8L10e0.0) indicated the following: the first character (i.e. 8) indicated the bar size of the specimen tested, either #8 or #10. The second and third character, i.e. L10, indicated the *L/d* ratio of the specimen. The last two characters indicated the *e/d* ratio of the specimen (i.e. e0.0). The specimens also had a number, which identified the test performed. The tests were grouped by the same *L/d* ratio with different initial eccentricities (i.e. *L/d* = 12, *e/d* = 0.0, 0.1, 0.2, 0.3, 0.4, 0.5). The tests were performed starting with the largest *L/d* ratio group because less force was required to buckle longer bars. Table 3.1 and 3.2 show the experimental program for #8 and #10 bar tests, respectively.

Table 3.1 Experimental program for #8 bars, diameter (d) = 1.00-in

Specimen	*L* in	*e* in	*L/d*	*e/d*	Specimen	*L* in	*e* in	*L/d*	*e/d*	Specimen	*L* in	*e* in	*L/d*	*e/d*
#1-8L4e0.0	4	0.0	4	0.0	#37-8L7e0.0	7	0.0	7	0.0	#73-8L10e0.0	10	0.0	10	0.0
#2-8L4e0.0	4	0.0	4	0.0	#38-8L7e0.0	7	0.0	7	0.0	#74-8L10e0.0	10	0.0	10	0.0
#3-8L4e0.1	4	0.1	4	0.1	#39-8L7e0.1	7	0.1	7	0.1	#75-8L10e0.1	10	0.1	10	0.1
#4-8L4e0.1	4	0.1	4	0.1	#40-8L7e0.1	7	0.1	7	0.1	#76-8L10e0.1	10	0.1	10	0.1
#5-8L4e0.2	4	0.2	4	0.2	#41-8L7e0.2	7	0.2	7	0.2	#77-8L10e0.2	10	0.2	10	0.2
#6-8L4e0.2	4	0.2	4	0.2	#42-8L7e0.2	7	0.2	7	0.2	#78-8L10e0.2	10	0.2	10	0.2
#7-8L4e0.3	4	0.3	4	0.3	#43-8L7e0.3	7	0.3	7	0.3	#79-8L10e0.3	10	0.3	10	0.3
#8-8L4e0.3	4	0.3	4	0.3	#44-8L7e0.3	7	0.3	7	0.3	#80-8L10e0.3	10	0.3	10	0.3
#9-8L4e0.4	4	0.4	4	0.4	#45-8L7e0.4	7	0.4	7	0.4	#81-8L10e0.4	10	0.4	10	0.4
#10-8L4e0.4	4	0.4	4	0.4	#46-8L7e0.4	7	0.4	7	0.4	#82-8L10e0.4	10	0.4	10	0.4
#11-8L4e0.5	4	0.5	4	0.5	#47-8L7e0.5	7	0.5	7	0.5	#83-8L10e0.5	10	0.5	10	0.5
#12-8L4e0.5	4	0.5	4	0.5	#48-8L7e0.5	7	0.5	7	0.5	#84-8L10e0.5	10	0.5	10	0.5
#13-8L5e0.0	5	0.0	5	0.0	#49-8L8e0.0	8	0.0	8	0.0	#85-8L11e0.0	11	0.0	11	0.0
#14-8L5e0.0	5	0.0	5	0.0	#50-8L8e0.0	8	0.0	8	0.0	#86-8L11e0.0	11	0.0	11	0.0
#15-8L5e0.1	5	0.1	5	0.1	#51-8L8e0.1	8	0.1	8	0.1	#87-8L11e0.1	11	0.1	11	0.1
#16-8L5e0.1	5	0.1	5	0.1	#52-8L8e0.1	8	0.1	8	0.1	#88-8L11e0.1	11	0.1	11	0.1
#17-8L5e0.2	5	0.2	5	0.2	#53-8L8e0.2	8	0.2	8	0.2	#89-8L11e0.2	11	0.2	11	0.2
#18-8L5e0.2	5	0.2	5	0.2	#54-8L8e0.2	8	0.2	8	0.2	#90-8L11e0.2	11	0.2	11	0.2
#19-8L5e0.3	5	0.3	5	0.3	#55-8L8e0.3	8	0.3	8	0.3	#91-8L11e0.3	11	0.3	11	0.3
#20-8L5e0.3	5	0.3	5	0.3	#56-8L8e0.3	8	0.3	8	0.3	#92-8L11e0.3	11	0.3	11	0.3
#21-8L5e0.4	5	0.4	5	0.4	#57-8L8e0.4	8	0.4	8	0.4	#93-8L11e0.4	11	0.4	11	0.4
#22-8L5e0.4	5	0.4	5	0.4	#58-8L8e0.4	8	0.4	8	0.4	#94-8L11e0.4	11	0.4	11	0.4
#23-8L5e0.5	5	0.5	5	0.5	#59-8L8e0.5	8	0.5	8	0.5	#95-8L11e0.5	11	0.5	11	0.5
#24-8L5e0.5	5	0.5	5	0.5	#60-8L8e0.5	8	0.5	8	0.5	#96-8L11e0.5	11	0.5	11	0.5
#25-8L6e0.0	6	0.0	6	0.0	#61-8L9e0.0	9	0.0	9	0.0	#97-8L12e0.0	12	0.0	12	0.0
#26-8L6e0.0	6	0.0	6	0.0	#62-8L9e0.0	9	0.0	9	0.0	#98-8L12e0.0	12	0.0	12	0.0
#27-8L6e0.1	6	0.1	6	0.1	#63-8L9e0.1	9	0.1	9	0.1	#99-8L12e0.1	12	0.1	12	0.1
#28-8L6e0.1	6	0.1	6	0.1	#64-8L9e0.1	9	0.1	9	0.1	#100-8L12e0.1	12	0.1	12	0.1
#29-8L6e0.2	6	0.2	6	0.2	#65-8L9e0.2	9	0.2	9	0.2	#101-8L12e0.2	12	0.2	12	0.2
#30-8L6e0.2	6	0.2	6	0.2	#66-8L9e0.2	9	0.2	9	0.2	#102-8L12e0.2	12	0.2	12	0.2
#31-8L6e0.3	6	0.3	6	0.3	#67-8L9e0.3	9	0.3	9	0.3	#103-8L12e0.3	12	0.3	12	0.3
#32-8L6e0.3	6	0.3	6	0.3	#68-8L9e0.3	9	0.3	9	0.3	#104-8L12e0.3	12	0.3	12	0.3
#33-8L6e0.4	6	0.4	6	0.4	#69-8L9e0.4	9	0.4	9	0.4	#105-8L12e0.4	12	0.4	12	0.4
#34-8L6e0.4	6	0.4	6	0.4	#70-8L9e0.4	9	0.4	9	0.4	#106-8L12e0.4	12	0.4	12	0.4
#35-8L6e0.5	6	0.5	6	0.5	#71-8L9e0.5	9	0.5	9	0.5	#107-8L12e0.5	12	0.5	12	0.5
#36-8L6e0.5	6	0.5	6	0.5	#72-8L9e0.5	9	0.5	9	0.5	#108-8L12e0.5	12	0.5	12	0.5

Table 3.2 Experimental program for #10 bars, diameter (d) = 1.27-in

Specimen	*L*, in	*e*, in	*L/d*	*e/d*	Specimen	*L*, in	*e*, in	*L/d*	*e/d*
#1-10L4e0.0	5.08	0.0	4	0.0	#28-10L8e0.3	10.16	0.381	8	0.3
#2-10L4e0.1	5.08	0.127	4	0.1	#29-10L8e0.4	10.16	0.508	8	0.4
#3-10L4e0.2	5.08	0.254	4	0.2	#30-10L8e0.5	10.16	0.635	8	0.5
#4-10L4e0.3	5.08	0.381	4	0.3	#31-10L9e0.0	11.43	0.0	9	0.0
#5-10L4e0.4	5.08	0.508	4	0.4	#32-10L9e0.1	11.43	0.127	9	0.1
#6-10L4e0.5	5.08	0.635	4	0.5	#33-10L9e0.2	11.43	0.254	9	0.2
#7-10L5e0.0	6.35	0.0	5	0.0	#34-10L9e0.3	11.43	0.381	9	0.3
#8-10L5e0.1	6.35	0.127	5	0.1	#35-10L9e0.4	11.43	0.508	9	0.4
#9-10L5e0.2	6.35	0.254	5	0.2	#36-10L9e0.5	11.43	0.635	9	0.5
#10-10L5e0.3	6.35	0.381	5	0.3	#37-10L10e0.0	12.7	0.0	10	0.0
#11-10L5e0.4	6.35	0.508	5	0.4	#38-10L10e0.1	12.7	0.127	10	0.1
#12-10L5e0.5	6.35	0.635	5	0.5	#39-10L10e0.2	12.7	0.254	10	0.2
#13-10L6e0.0	7.62	0.0	6	0.0	#40-10L10e0.3	12.7	0.381	10	0.3
#14-10L6e0.1	7.62	0.127	6	0.1	#41-10L10e0.4	12.7	0.508	10	0.4
#15-10L6e0.2	7.62	0.254	6	0.2	#42-10L10e0.5	12.7	0.635	10	0.5
#16-10L6e0.3	7.62	0.381	6	0.3	#43-10L11e0.0	13.97	0.0	11	0.0
#17-10L6e0.4	7.62	0.508	6	0.4	#44-10L11e0.1	13.97	0.127	11	0.1
#18-10L6e0.5	7.62	0.635	6	0.5	#45-10L11e0.2	13.97	0.254	11	0.2
#19-10L7e0.0	8.89	0.0	7	0.0	#46-10L11e0.3	13.97	0.381	11	0.3
#20-10L7e0.1	8.89	0.127	7	0.1	#47-10L11e0.4	13.97	0.508	11	0.4
#21-10L7e0.2	8.89	0.254	7	0.2	#48-10L11e0.5	13.97	0.635	11	0.5
#22-10L7e0.3	8.89	0.381	7	0.3	#49-10L12e0.0	15.24	0.0	12	0.0
#23-10L7e0.4	8.89	0.508	7	0.4	#50-10L12e0.1	15.24	0.127	12	0.1
#24-10L7e0.5	8.89	0.635	7	0.5	#51-10L12e0.2	15.24	0.254	12	0.2
#25-10L8e0.0	10.16	0.0	8	0.0	#52-10L12e0.3	15.24	0.381	12	0.3
#26-10L8e0.1	10.16	0.127	8	0.1	#53-10L12e0.4	15.24	0.508	12	0.4
#27-10L8e0.2	10.16	0.254	8	0.2	#54-10L12e0.5	15.24	0.635	12	0.5

3.3.2 Preparation of specimens

The #8 bar specimens were cut using a chop saw and the #10 bar specimens, using a water cooled band saw; therefore, the #8 bars experienced a heating/slow cooling process that might affect the capacity of the end regions. The final length (L_T) was equal to the corresponding length of a specimen for a

given *L/d* ratio (*L = L/d*d*) plus an additional 8 inches that allowed the specimens to fit into the test setup supports.

The initial eccentricity (*e = e/d*d*) was introduced by pushing at the middle length of the specimen using a steel T-shaped section with a welded rod on the tip of the web and triangular steel stiffeners at both faces of the section. Two rectangular blocks were fixed by four screws each to a 1" steel plate to support the bar in a horizontal position. The plate was previously drilled to locate the blocks in the correct position in order to allow the bars to span the corresponding length for a given *L/d* ratio and to bend them into the correct shape. Figure 3.1 shows a sketch of the setup used for the introduction of initial eccentricity to the specimens, and Figure 3.2 shows a picture of the built setup.

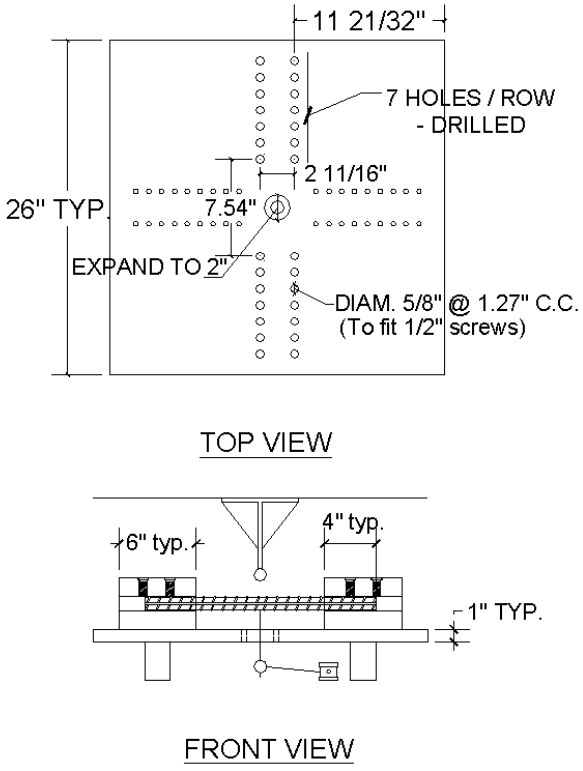

Figure 3.1 Sketch of the specimen preparation setup

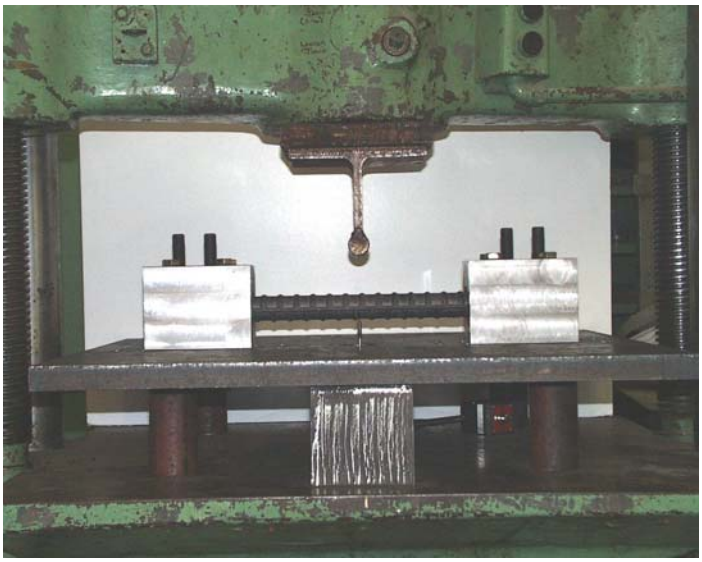

Figure 3.2 Picture of specimen preparation setup

The deflection introduced at midspan was monitored using a dial gage with 0.001 precision, which was located underneath the specimen and the steel plate. To achieve the desired eccentricity, a series of loading and unloading steps were followed. The bar was loaded in bending until the desired eccentricity was reached and then unloaded. The amount of recovered deflection was then recorded. This procedure was repeated until the deflection matched the desired eccentricity. The actual eccentricities accomplished are listed in Appendix A. The machine that was used in this test was a Southwark Emery universal test machine with 60-kip capacity. When the eccentricity obtained reached a value larger than approximately 0.004″, the specimen was discarded, and a new specimen was prepared. This criterion was established because of the closeness of the range of eccentricities selected for the experimental program.

3.3.3 Test setup, instrumentation, and procedure

A custom-made setup was assembled for the monotonic compression test of the reinforcing steel. It consisted of two 1-inch thick steel plates with two 6-inch deep high-strength steel blocks on each plate. The blocks were intended to represent rigid supports. Each block had 16 set screws (2 screws every 45° angle staggered up or down at each increment) to hold the bar in position and was attached to the base plates with high strength bolts. The specimen was anchored 4 inches into each support, allowing a contact surface with the blocks of 2 inches. The upper plate had a threaded rod welded to its center to hold it in place. In addition, two screws were used to attach it to the machine. Because the lower part of the machine did not have holes to attach the plate, the lower plate was set in place using four clamps. The plates were tight in their position after aligning the blocks in order to ensure alignment of the specimens. Figure 3.3 shows a sketch of the compression test setup.

The test setup was built to work in the same testing machine that was used for the tension tests. The load reading was obtained from the load cell of the testing machine. The voltage measurements were converted to engineering units by the Data Acquisition system and recorded using a program based on Microsoft Excel 2000, similar to the tension tests. The strain measurements were not taken using strain gages, because the grinding that was necessary to prepare the specimen for strain gauge installation would have negatively affected the results by disturbing the cross-sectional area of the bars. Furthermore, strain gage measurements are not representative of the overall displacement of the bar because of the deflection mode shape, which causes changes in strains and stresses along the bar (tension and compression zones are at same cross-sectional location). During testing, vertical and lateral deformations were monitored using linear potentiometers, as shown in Figure 3.3. Two linear potentiometers were

used for the vertical displacement readings and one was used for the lateral displacement readings.

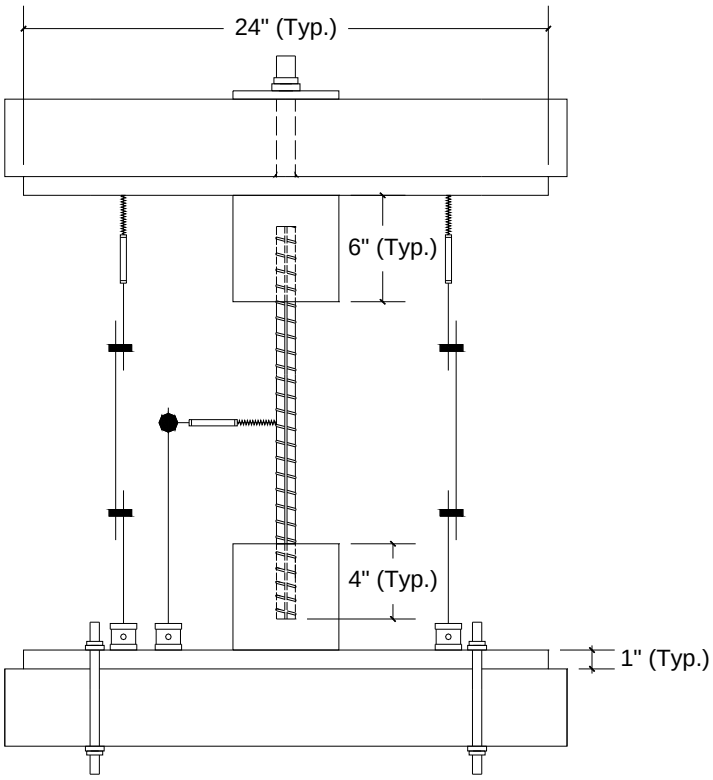

Figure 3.3 Sketch of the compression test setup

Before selecting the final testing procedure, several trial tests were performed on #8 bars with L/d = 12. From the results provided by these trials, the test speed and acquisition intervals were selected. The final testing procedure was as follows:

(1) Locate the bars in the blocks putting a small amount of load (approximately 0.5 to 1.0 kip) in the specimen to ensure that the bar did not slip during the test.

(2) Tighten setscrews on each block with a pneumatic torque-wrench to ensure that each screw had the same amount of torque and to ensure that the bar was centered inside the block.

(3) Verify that all instrumentation was located in place and readings were taken correctly.

(4) Start the machine and the scanner, then load the bar at a medium-rate (approximately level 8 of the machine used) until the linear slope changes.

(5) Decrease the load rate to low-rate (approximately level 12 of the machine used) to capture the strains in the initial stage of post-buckling.

(6) After reaching a vertical displacement of approximately 0.3 inch, increase load to the medium-rate used before until the vertical reading is no longer available (i.e. reaching the limit of the instrumentation) or the specimen fails.

The machine used did not allow a displacement-controlled test and hence the load control feature of the test machine was used. All test data were recorded at one-second intervals continuously for the duration of the test. Figures 3.4 and 3.5 show the test setup for a #8 bar before and after testing, respectively.

Figure 3.4 Test setup with a #8 bar specimen with L/d =10, e = 0.5 before test

Figure 3.5 Test setup with a #8 bar specimen with L/d =10, e = 0.5 after test

CHAPTER 4
Test Results

4.1 TENSION TESTS

As mentioned in Chapter 3, three specimens were tested in tension for each bar size studied herein. The average of the three tests was taken as the representative stress-strain behavior curve for the reinforcing bars. Figure 4.1 and 4.2 show the test results from the three tests and the average curve for #8 and #10 bars, respectively.

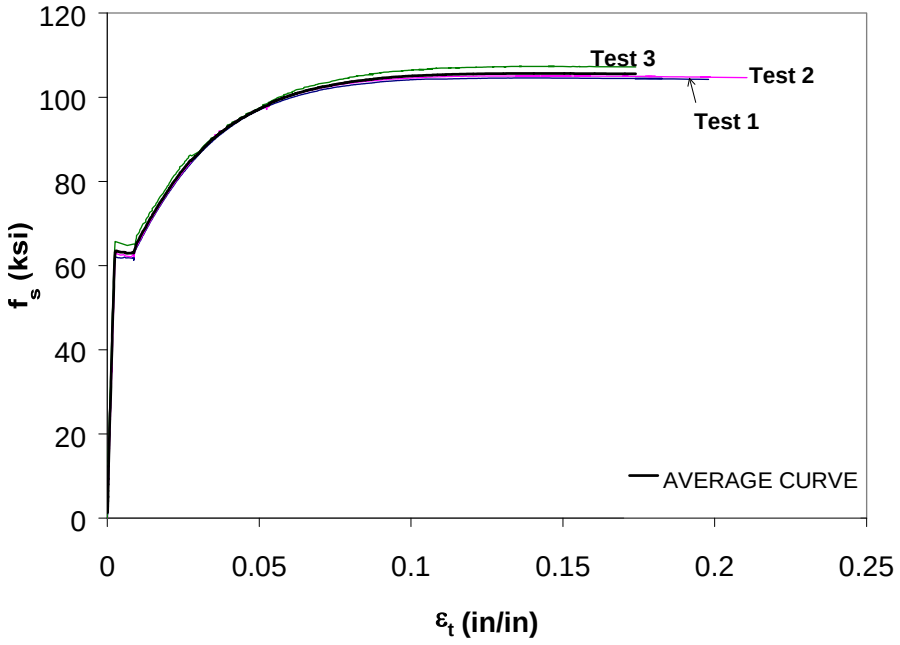

Figure 4.1 Tensile stress-strain curves of #8 reinforcing bars

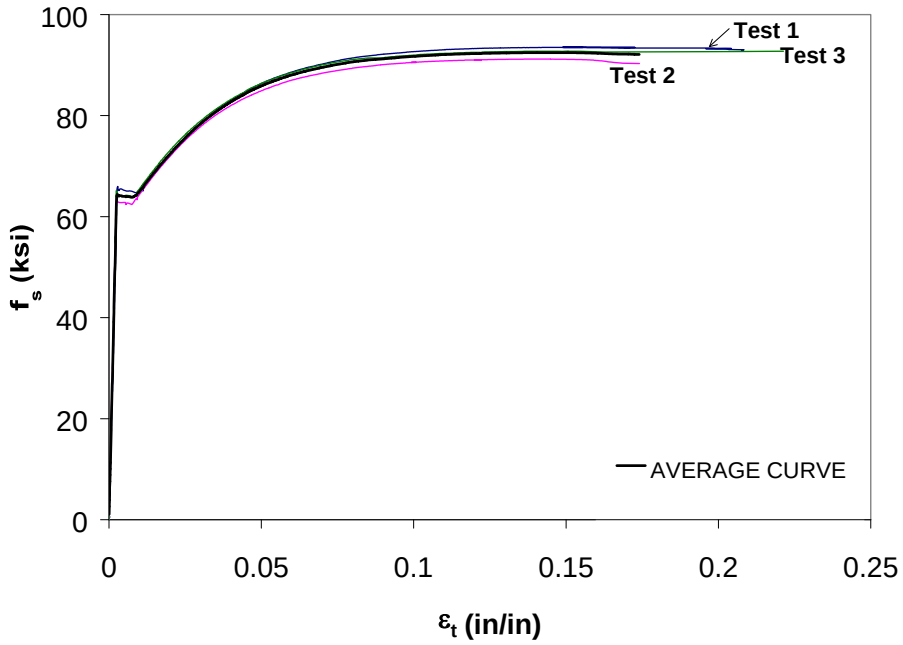

Figure 4.2 Tensile stress-strain curves of #10 reinforcing bars

The results obtained from the tension tests of the #8 and #10 bars were compared to those obtained by Bayrak and Sheikh (2001) for the Grade 400 20 mm in diameter bars, that corresponds to a #6 bar. Bayrak and Sheikh (2001) also tested three specimens to obtain an average stress-strain curve. This comparison helps understand the difference in material behavior for a given bar size with respect to the strength, ductility, and strain hardening behavior. Figure 4.3 shows the stress-strain behavior obtained for the three types of bar (#6, #8, and #10).

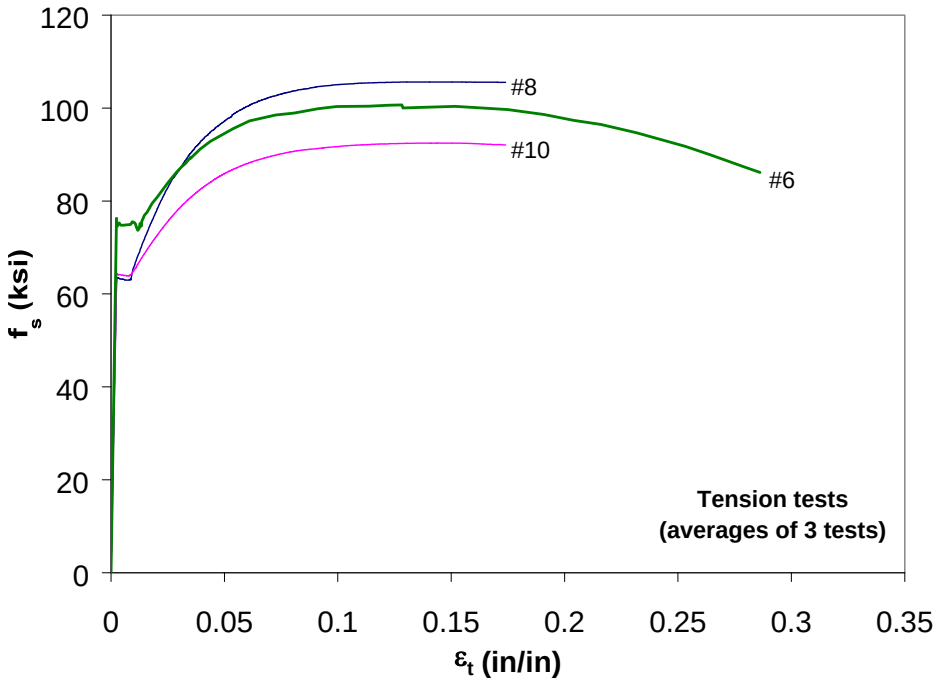

Figure 4.3 Stress-strain curves for three different reinforcing bar sizes, #8, #10, and #6 (Bayrak and Sheikh 2001).

The stress-strain curves for the #8 and #10 bars are not complete up to fracture (Figure 4.3). Measurements are given up to the capacity of the long-elongation strain gages used, but there is enough data to reach strains beyond those at ultimate strength. The #8 and #10 bars had approximately the same yielding strength, while the #6 bars had 20% larger yield strength. The #8 bar has larger ultimate strength than the #10 bars, and the #6 lies in between those. All the bars showed different strain hardening behavior. As has been mentioned before in literature, smaller bars tend to harden more than larger bars in the process of fabrication, therefore, smaller bars will have more strain hardening than larger bars. This trend is demonstrated herein with the #8 and #10 Grade 60 steel (f_{yt} =

60-ksi) US-fabricated reinforced bars. The #6 bars are of different grade of steel, Grade 400, which has a yielding strength of 400 MPa that is 58-ksi, but slightly different fabrication (produced in Canada). Table 4.1 gives the mechanical properties obtained from Figure 4.3.

Table 4.1 Mechanical Properties of #6, #8, and #10 reinforcing bars.

Bar designation	ε_{yt}	f_{yt} **(ksi)**	f_{ut} **(ksi)**	f_{ut}/f_{yt}
#6	0.0026	76.2	100.7	1.32
#8	0.0022	63.4	105.6	1.67
#10	0.0022	64.4	92.5	1.44

4.2 COMPRESSION TESTS

The results are represented graphically as axial stress vs. axial strain and load vs. lateral deformation relationships. As mentioned in chapter 3, two specimens were tested per *L/d-e/d* combination for #8 bars, and single specimens for #10 bars. For #8 specimens, the average curve resulting from the two tests is reported. To calculate the average of the two tests, a program was written in MSExcel-Visual Basic; see Appendix B for the computer program developed to average various experimental curves. The graphic results obtained for all specimens in every *L/d-e/d* combination are presented in Appendix C.

In the following sections, the effects of *L/d* ratio, *e/d* ratio, and bar size on specimen behavior are discussed and the results are reported. The variables used in the graphs and the starting points of measurements reported, shown further on, are illustrated with the model in Figure 4.4.

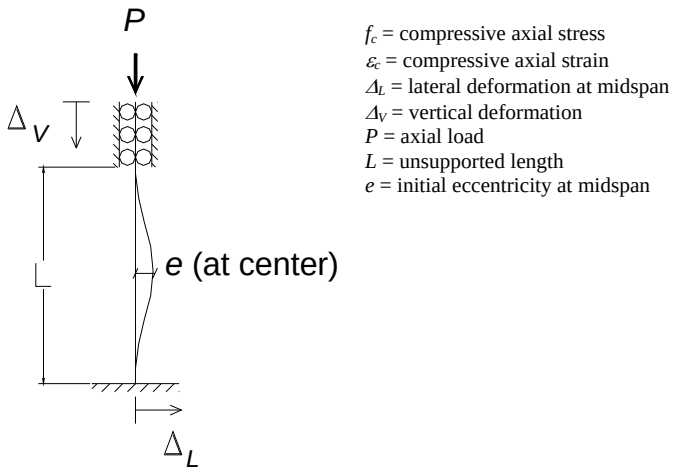

Figure 4.4 A typical test specimen and measurements

4.2.1 Effect of *e/d* ratio

In order to compare the effect of initial imperfection at midspan in the compressive axial behavior of reinforcing bars, all *e/d* ratios for the same *L/d* ratio were plotted on the same graph for the axial stress-strain and load vs. lateral deformation at midspan relationships. The results obtained for the #8 reinforcing bars are discussed first (Figures 4.5 to 4.22). Then, the results obtained for #10 reinforcing bars are presented in Figures 4.23 to 4.40.

In Figure 4.5, 4.6 and Table 4.2, it can be observed that for an *L/d* ratio of 4 the compressive strength of #8 reinforcing bars decreases with increase in *e/d* ratio. For values of compressive strains less than 0.027, the load carried by the bar with *e/d* ratio of 0.0 was larger than that of the tension curve, and after that point the load carried by the bars tested in compression was less than that carried in the tension test. The capacities of the bars with *e/d* ratio of 0.1 and 0.2 followed the same path up to a strain of 0.043, beyond that point the load carried by the bar with *e/d* = 0.1 increased. Similarly, the curves with *e/d* ratios of 0.4 and 0.5 followed very similar paths with little difference. Table 4.2 shows the numerical values corresponding to the yield strength in compression (f_{yc}) (which is the

largest stress measured in the linear elastic range), the increased capacity in the post-buckling inelastic region (f_{uc}), and the ratio of the increased capacity after buckling and the yield strength in compression. The tensile yield strength was reached for an *e/d* ratio of 0.0 and was lower for all other *e/d* ratios. The ratio f_{uc}/f_{yc} for compression tests where *e/d* was smaller then or equal to 0.3, was very similar to that observed in the tension test (f_{ut}/f_{yt} = 1.67). In general, there was no decrease of capacity after buckling of the bars, the capacity remained approximately constant after reaching f_{uc} for all *e/d* ratios with *L/d* = 4.

Table 4.2 Mechanical Properties of #8 reinforcing bars with L/d = 4.

e/d	f_{yc} **(ksi)**	f_{uc} **(ksi)**	f_{uc}/f_{yc}	P_{max} **(kip) @** Δ_L^* **(in)**
0.0	63.6	96.3	1.52	75.8 @ 0.39″
0.1	54.1	92.2	1.70	72.5 @ 0.64″
0.2	51.2	88.2	1.72	69.4 @ 0.49″
0.3	50.2	82.3	1.64	64.8 @ 0.87″
0.4	51.4	74.4	1.45	58.4 @ 0.98″
0.5	47.2	72.2	1.53	56.8 @ 0.94″
Tension test:	f_{yt} = 63.4 ksi f_{ut} = 105.6 ksi f_{ut}/f_{yt} = 1.67			

*Δ_L = the displacement corresponding to P_{max}

Figure 4.6 illustrates the load vs. lateral deformations at midspan for #8 reinforcing bars with *L/d* = 4. The maximum compressive force (P_{max}) decreased with increasing *e/d* ratio (Table 4.2), which means that as the initial imperfection was increased the capacity decreased. For the amount of lateral deflection recorded (up to 1”) the capacity of the reinforcing bars did not decrease. For some of the bars the last data point corresponded with fracture, which indicated that the #8 bars with *L/d* = 4 can sustain large inelastic deformations without losing strength. This behavior is also observed in Figure 4.5.

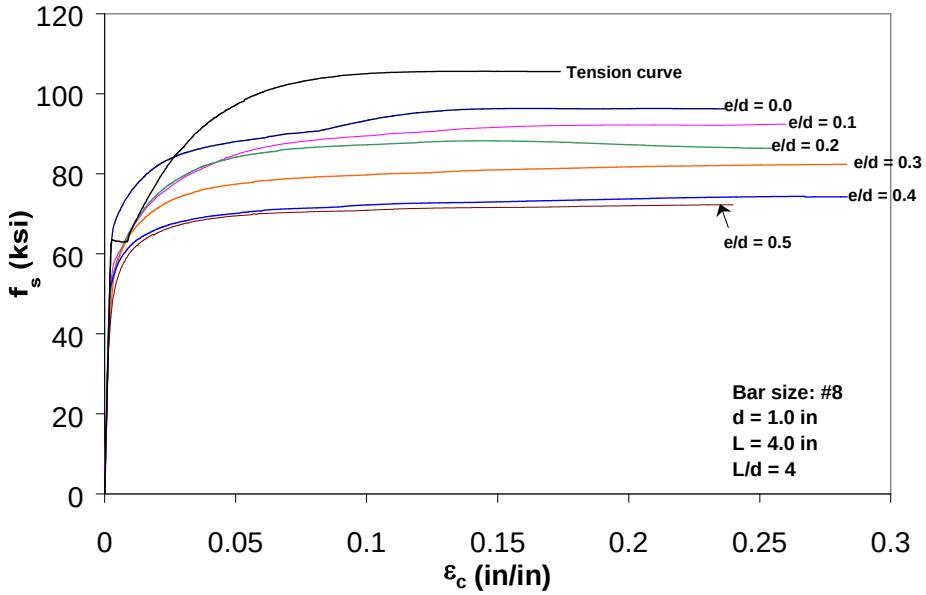

Figure 4.5 Axial stress-strain curves for #8 reinforcing bars with L/d = 4.

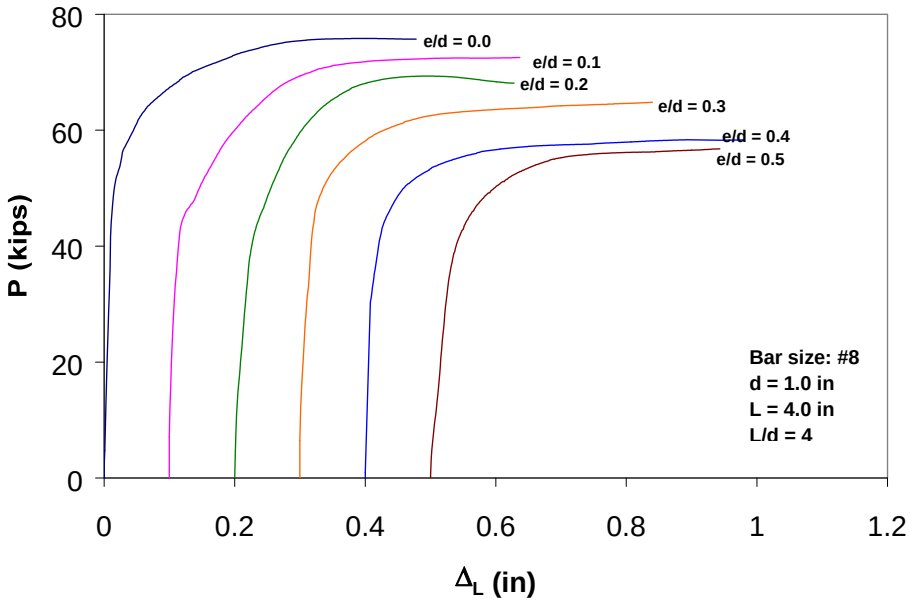

Figure 4.6 Axial load vs. lateral deformation curves of #8 bars with L/d =4.

Figure 4.7 illustrates the results for the axial compressive behavior of #8 reinforcing bars with *L/d* ratio of 5. As can be seen in this figure, the axial capacity decreases with an increase in *e/d* ratio. In the curve for *e/d* = 0.0, a slight plastic plateau after yielding like for the tension test, but with lower capacity, can be observed. The behavior of the bars with *e/d* ratio of 0.1 and 0.2 were similar up to a strain level of about 0.045, beyond that point the capacity of specimens with *e/d* = 0.1 increased. In general, there was not much difference between the load-carrying capacity and post-buckling behavior for the reinforcing bars with *L/d* = 5 and *e/d* = 0.0, 0.1, and 0.2. This was mainly attributed to experimental scatter. The values in Table 4.3 demonstrate that the yield strength under compressive loading is lower than the tensile yield strength for all *e/d* ratios with *L/d* = 5. The increases of capacity after post-buckling for the specimens with *e/d* = 0.1 and 0.2 were 55% and 56%, respectively. These values are very close to the percentage increase in stress due to strain hardening for #8 reinforcing bars under tension (f_{ut}/f_{yt} = 1.67). However, the tensile capacity is about 27% higher than the compressive capacity. In general, the load carrying capacity of the bars with *L/d* = 5 decreases with increased *e/d* ratio. Although the specimens displayed reasonably stable stress-strain response, the capacity decreased somewhat after reaching the maximum value in the post-buckling path.

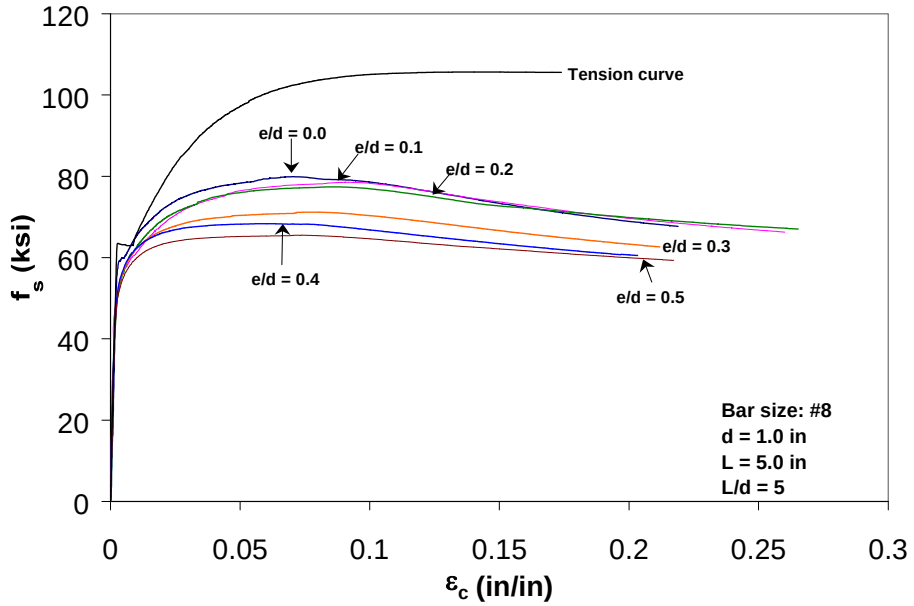

Figure 4.7 Axial stress-strain curves for #8 reinforcing bars with L/d = 5.

Table 4.3 Mechanical Properties of #8 reinforcing bars with L/d = 5.

e/d	f_{yc} **(ksi)**	f_{uc} **(ksi)**	f_{uc}/f_{yc}	P_{max} **(kip) @** Δ_L^* **(in)**
0.0	58.8	79.9	1.36	62.7 @ 0.32″
0.1	50.6	78.5	1.55	62.4 @ 0.43″
0.2	49.6	77.4	1.56	61.3 @ 0.53″
0.3	50.1	71.2	1.42	55.8 @ 0.59″
0.4	49.5	68.4	1.38	53.7 @ 0.60″
0.5	48.7	65.5	1.35	51.5 @ 0.76″
Tension test:	f_{yt} = 63.4 ksi f_{ut} = 105.6 ksi f_{ut}/f_{yt} = 1.67			

*Δ_L = the displacement corresponding to P_{max}

Figure 4.8 illustrates the load vs. lateral deformation at midspan for #8 reinforcing bars with L/d = 5. As can be observed in this figure, the maximum force, P_{max}, decreases with increasing e/d ratio (Table 4.3). Strain corresponding

to maximum load, P_{max}, increases with increasing *e/d* ratio. It is interesting to observe that for reinforcing bars with *e/d* ratios of 0.0 and 0.1, the stress-strain curve in compression looks similar to the tensile stress-strain curve. Mau and El-Mabsout (1989) reported that for reinforcing bars with smaller slenderness ratios "first buckling" (or first peak) load was followed by a capacity decrease, and a "second buckling" (or second peak) load was observed before capacity dropped once again. This phenomenon was referred to as "straightening" by Mau and El-Mabsout (1989), in which the "second buckling" occurred at a higher load than the yield load due to stiffening of the reinforcing bar caused by strain hardening. When the behavior of #8 reinforcing bars with *L/d* = 5 and *e/d* = 0.0 is examined (Figure 4.8) occurrence of "first buckling" and "second buckling" loads can be observed.

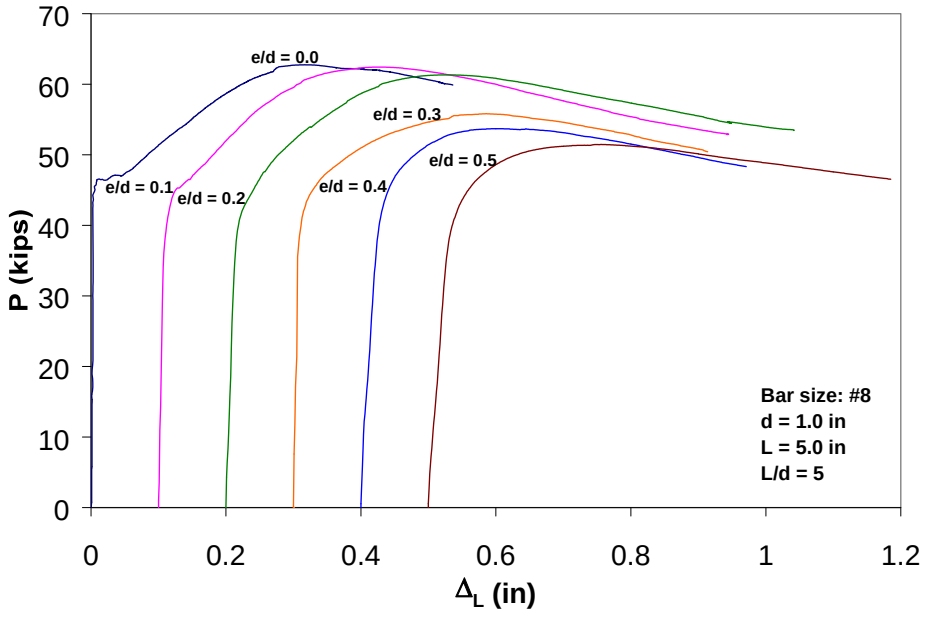

Figure 4.8 Axial load vs. lateral deformation curves of #8 bars with L/d =5

The compressive behavior of #8 reinforcing bars with *L/d* ratio of 6 shows similar trends to that of bars with *L/d* = 5 (Figure 4.9). With increasing *e/d* values, the maximum load carrying capacity of the specimen decreased. For initially straight specimens, a yield plateau was observed followed by a strain hardening region. The path followed by the bars with *e/d* ratio of 0.0 and 0.1 overlap at a strain of 0.024. The decrease in yield stress with increasing *e/d* ratios is more noticeable for specimens with *L/d* = 6 in comparison to those of specimens with *L/d* = 5 and *L/d* = 4 (Tables 4.2, 4.3, and 4.4). The load carrying capacity of specimens with *e/d* = 0.0 is about the same (3% lower) as the load carrying capacity of a specimen tested in tension. Otherwise, the capacity decreases with increasing *e/d* ratios. It is important to recognize that post-buckling capacities of specimens with *L/d* = 6 are about 17 to 30 % larger than the corresponding capacities at yield. All specimens with *L/d* = 6 are able to deform inelastically up to an axial strain of 0.06 without losing strength.

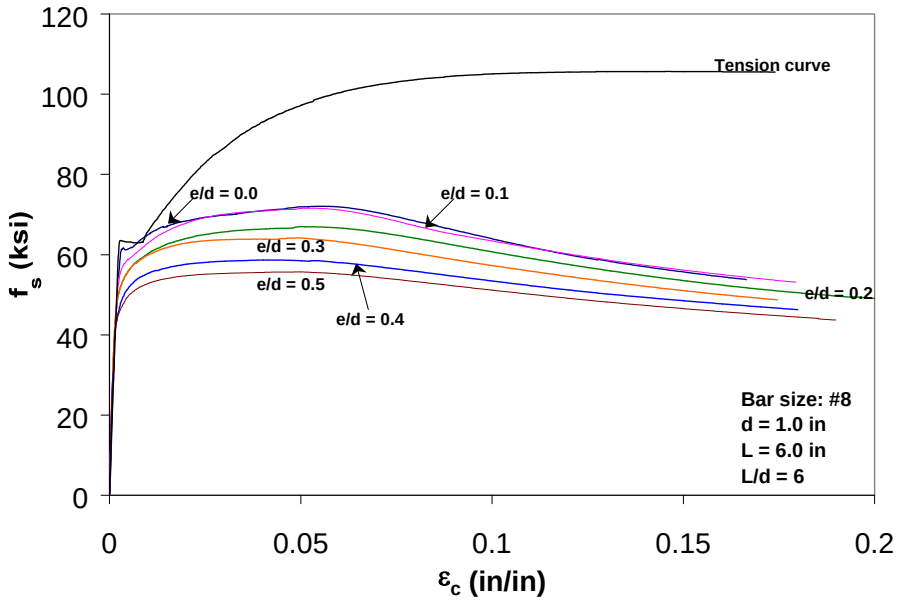

Figure 4.9 Axial stress-strain curves for #8 reinforcing bars with L/d = 6.

Table 4.4 Mechanical Properties of #8 reinforcing bars with L/d = 6.

e/d	f_{yc} **(ksi)**	f_{uc} **(ksi)**	f_{uc}/f_{yc}	P_{max} **(kip) @** Δ_L^* **(in)**
0.0	61.7	72.1	1.17	55.9 @ 0.35″
0.1	55.1	71.6	1.30	56.2 @ 0.35″
0.2	50.7	67.0	1.32	52.6 @ 0.47″
0.3	50.6	64.2	1.27	50.3 @ 0.54″
0.4	44.9	58.7	1.31	46.1 @ 0.62″
0.5	43.6	55.7	1.28	43.8 @ 0.73″
Tension test:	f_{yt} = 63.4 ksi f_{ut} = 105.6 ksi f_{ut}/f_{yt} = 1.67			

*Δ_L = the displacement corresponding to P_{max}

The axial load vs. lateral deformation behavior of specimens with L/d = 5 and e/d = 0.0 is similar to that of specimens with L/d = 6 and e/d = 0.0 (Figures 4.8 and 4.10). At large lateral deformations (0.8″-1.0″) the axial load vs. lateral deformation behavior of all specimens, regardless of the initial imperfections, becomes practically identical. The peak load P_{max} occurs at a larger lateral deflection as the e/d ratio increases. It is interesting to recognize that the general trend observed in the axial force vs. lateral deformation behavior of the test specimens was previously encountered by Timoshenko (1961).

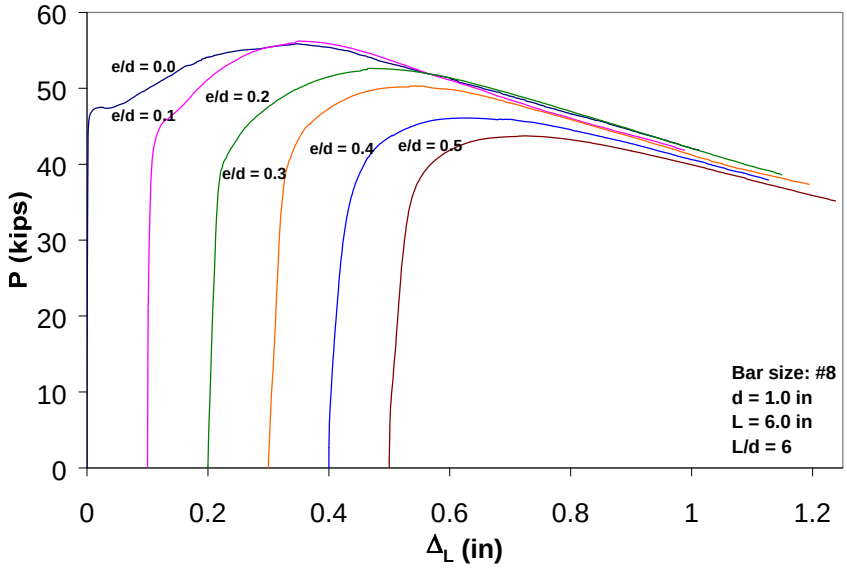

Figure 4.10 Axial load vs. lateral deformation curves of #8 bars with L/d =6.

Once again, for #8 reinforcing bars with *L/d* = 7, the load carrying capacity decreased with increasing initial imperfection. As can be seen in Figure 4.11, the response of bars with *e/d* = 0.0 and 0.1 are very similar. This similarity is attributed to experimental scatter. The stress-strain response of specimens with *e/d* = 0.2 merged with that of *e/d* = 0.1 at a strain of 0.0751. The compressive stress-strain relationships obtained for reinforcing bars with *e/d* ratios of 0.3, 0.4, and 0.5 yield considerably different results (Figure 4.11). The stress-strain curves for all reinforcing bars with *L/d* = 7 converged to the same post-buckling path of instability to reach a level of stress of approximately 40 ksi. For an *L/d* ratio of 7, none of the *e/d* cases reached the tensile yield strength at a strain of 0.0022, as observed in specimens tested in tension. The differences in yield strength are between 8 to 34% (Table 4.5) and the yield stress in compression occurred at lower strain values than 0.0022 as the *e/d* ratio increased. Only bars with *e/d* = 0.0 and 0.1 reached the tensile yield strength (63.4 ksi) at larger strains. The post-buckling capacity increased by about 11 to 19% from that at yield for bars with

e/d ratios of 0.0, 0.1, and 0.2. For other *e/d* ratios, it increased by about 27 to 23%. The curves for reinforcing bars with *e/d* of 0.0, 0.1, and 0.3 showed stable responses for strains up to 0.038, and for bars with *e/d* of 0.3, 0.4, and 0.5 up to a strain of about 0.044. For specimens with *L/d = 7*, the range of strains over which stresses were sustained without any significant loss were lower than observed for specimens with *L/d* = 6.

Table 4.5 Mechanical Properties of #8 reinforcing bars with L/d = 7.

e/d	f_{yc} **(ksi)**	f_{uc} **(ksi)**	f_{uc}/f_{yc}	P_{max} **(kip) @** Δ_L^* **(in)**
0.0	58.4	65.1	1.11	50.7 @ 0.33″
0.1	56.8	65.5	1.15	52.3 @ 0.36″
0.2	53.1	63.4	1.19	49.8 @ 0.44″
0.3	45.4	57.8	1.27	45.4 @ 0.56″
0.4	43.8	54.3	1.24	42.7 @ 0.69″
0.5	41.9	51.7	1.23	40.6 @ 0.72″
Tension test:	f_{yt} = 63.4 ksi f_{ut} = 105.6 ksi f_{ut}/f_{yt} = 1.67			

*Δ_L = the displacement corresponding to P_{max}

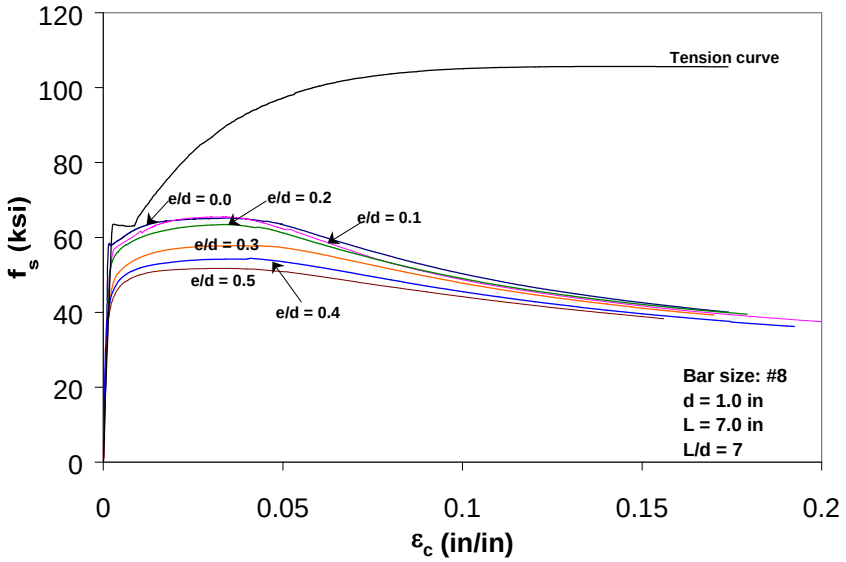

Figure 4.11 Axial stress-strain curves for #8 reinforcing bars with L/d = 7.

Axial load vs. lateral deformation relationships for #8 reinforcing bars with L/d = 7 are presented in Figure 4.12. The peak load of the specimen with e/d = 0.0 was slightly lower than that of the specimen with e/d = 0.1. This is attributed to experimental scatter. Otherwise, the capacities decreased as the e/d ratios increased, and the peak load, P_{max}, occurred at larger lateral deflections with increasing e/d ratio (Table 4.5). The "second buckling" phenomenon was observed for specimens with L/d = 7 with e/d = 0.0 and 0.1. Similar to the stress-strain curves in compression, the path followed by all specimens with L/d = 7 in the axial load vs. lateral displacement curves for all e/d ratios converged to the same post-buckling path (Figure 4.12).

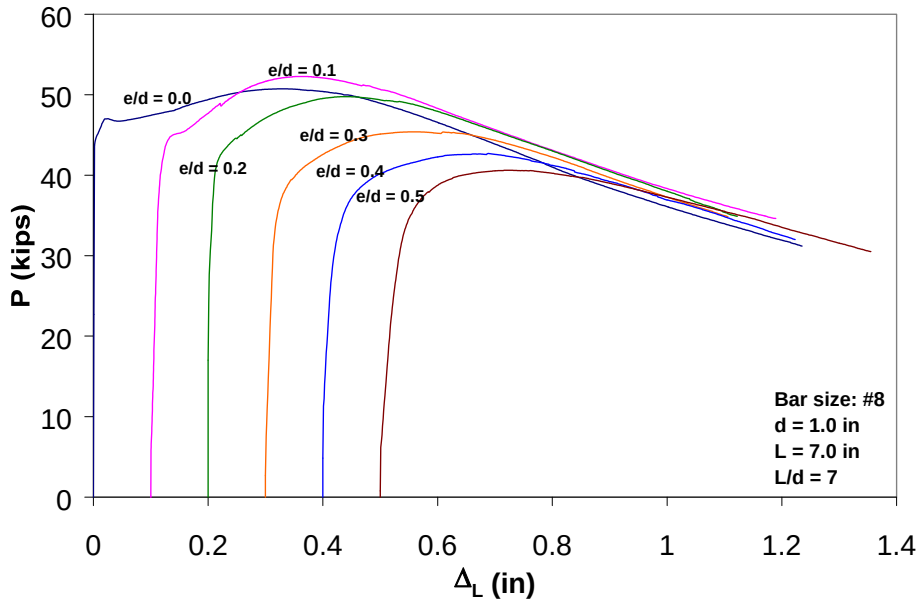

Figure 4.12 Axial load vs. lateral deformation curves of #8 bars with L/d =7.

Figure 4.13 illustrates the axial stress-strain behavior in compression for #8 reinforcing bars with L/d = 8 where the reduced capacities with increased e/d

ratios were observed once again. For this set of specimens the difference in load carrying capacity for various *e/d* ratios is more pronounced. The post-buckling paths of reinforcing bars with *e/d* ratios 0.0 and 0.1 merged at a strain of approximately 0.073, while those of the bars with *e/d* ratios 0.2 and 0.3 merged at a strain of approximately 0.071, and those of the bars with *e/d* ratios 0.4 and 0.5 merged at approximately 0.087. All stress-strain curves for specimens with *L/d* = 8 converged to the same post-buckling path with a stress level of approximately 32 ksi (lower than that of the bars with *L/d* = 7) (Figures 4.11 and 4.13). For reinforcing bars with *L/d* = 8, decreases in yield stress were observed for all in all *e/d* values. These stresses were about 5 to 31% lower than the tensile yield stress. The post-buckling capacity of #8 reinforcing bars increased by about 6 to 18% from that at yield (Figure 4.13). No significant decrease in the post-buckling stress-strain responses of the test specimens with *L/d* =8 was observed prior to an axial strain of about 0.027.

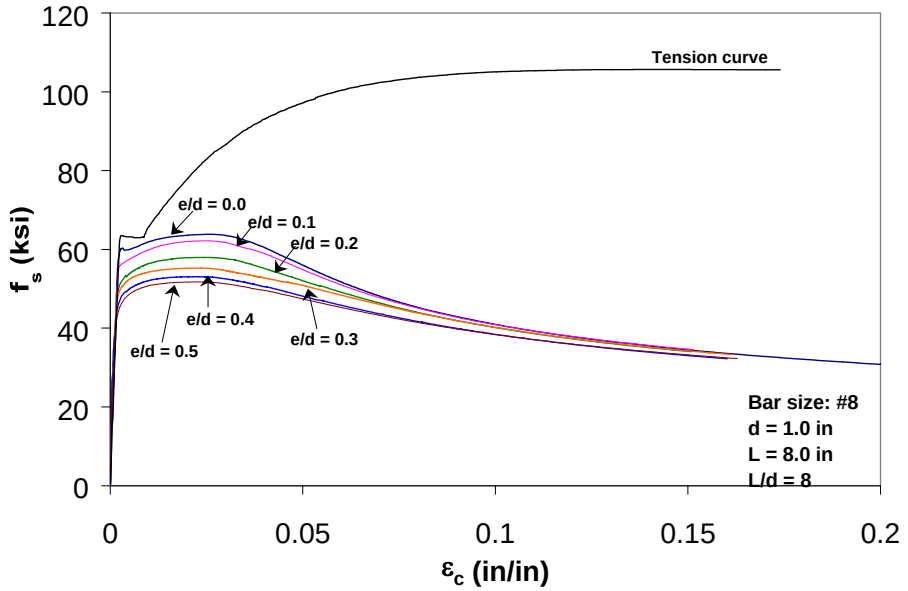

Figure 4.13 Axial stress-strain curves for #8 reinforcing bars with L/d = 8.

Figure 4.14 shows the load vs. lateral deformation curves obtained for all #8 reinforcing bars with *L/d* = 8. In this figure, it can be seen that the load carrying capacities decrease as the *e/d* ratios increase. The lateral deflections at which the peak loads occurred in the specimens with *L/d* = 8 are similar to those for *L/d* = 7 (see Table 4.5 and 4.6). The "second buckling" phenomenon is observed in reinforcing bars with *L/d* = 8 and *e/d* = 0.0. It is interesting to observe the convergence of all the axial force-lateral deformation responses of the specimens at large (0.6″-0.8″) lateral deformations. As can be seen in Figure 4.14, the effect of the initial midspan eccentricity on the post-buckling response of the test specimens decreases with increasing lateral deformations. The convergence of the curves shown in Figure 4.14 at large lateral deflections is more noticeable for this set of curves.

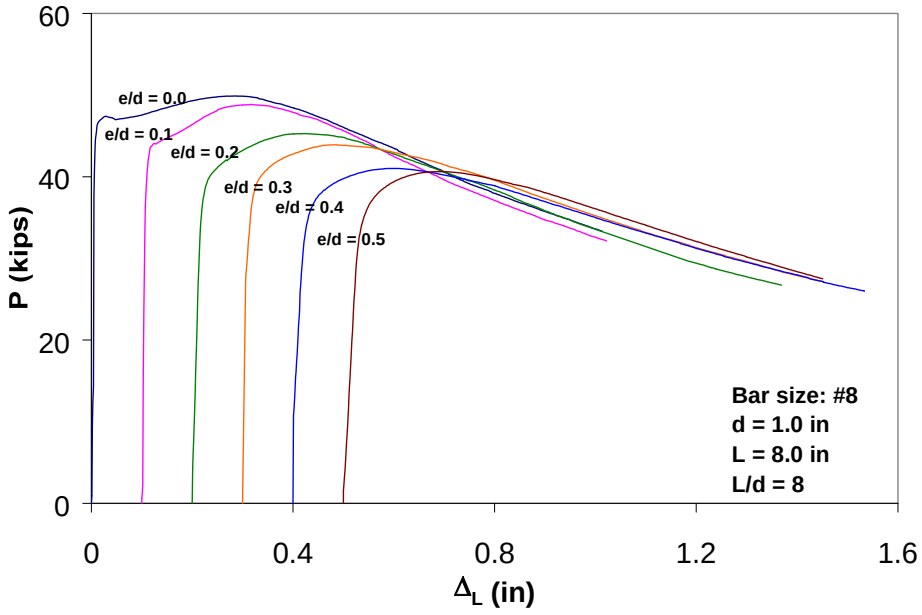

Figure 4.14 Axial load vs. lateral deformation curves of #8 bars with L/d =8.

Table 4.6 Mechanical Properties of #8 reinforcing bars with L/d = 8.

e/d	f_{yc} (ksi)	f_{uc} (ksi)	f_{uc}/f_{yc}	P_{max} (kip) @ Δ_L^* (in)
0.0	60.3	63.8	1.06	49.9 @ 0.29″
0.1	55.6	62.2	1.03	48.8 @ 0.32″
0.2	50.4	58.0	1.15	45.3 @ 0.43″
0.3	49.0	55.3	1.13	43.9 @ 0.49″
0.4	46.0	53.1	1.15	41.0 @ 0.60″
0.5	43.7	51.7	1.18	40.6 @ 0.69″
Tension test:	f_{yt} = 63.4 ksi f_{ut} = 105.6 ksi f_{ut}/f_{yt} = 1.67			

*Δ_L = the displacement corresponding to P_{max}

For a given strain, reduction of strength with an increase in *e/d* ratio can be observed in the axial stress-strain curves of #8 reinforcing bars with *L/d* = 9 (Figure 4.15 and Table 4.7). As can be observed in Figure 4.15, the differences observed in axial stress-strain curves for various *e/d* ratios are discernable. The stress-strain curves converged to a stress of approximately 26 ksi at large inelastic deformations. This stress value is approximately 20% lower than that for *L/d* = 8. The decrease in compressive yield strength can be observed in Figure 4.15 and Table 4.7. For rebar specimens with *e/d* = 0.0 the yield strength was merely lower by 4.5% than the tensile yield strength. The decrease in yield stress was between 16 to 41% for other *e/d* ratios. Post-buckling capacity of the #8 reinforcing bars with *L/d* = 9 increased by about 2%, 7%, 10%, 14%, 16%, and 18% with respect to the corresponding yield stress for *e/d* ratios of 0.0 to 0.5 respectively (Figure 4.15 and Table 4.7). The increase in capacity due to strain hardening for reinforcing bars with *L/d* = 9 and *e/d* = 0.0 is noticeably lower than the increases observed for previous cases of *L/d* ratios. In general, the maximum stress

achieved by specimens with L/d = 9 remained virtually unchanged up to strains of about 0.021 for all e/d ratios.

Table 4.7 Mechanical Properties of #8 reinforcing bars with L/d = 9.

e/d	f_{yc} (ksi)	f_{uc} (ksi)	f_{uc}/f_{yc}	P_{max} (kip) @ Δ_L^* (in)
0.0	60.5	61.6	1.02	49.5 @ 0.01″
0.1	53.4	57.4	1.07	45.0 @ 0.32″
0.2	49.7	54.8	1.10	43.3 @ 0.42″
0.3	45.0	51.4	1.14	40.8 @ 0.48″
0.4	41.1	47.8	1.16	37.6 @ 0.57″
0.5	37.5	44.3	1.18	34.8 @ 0.74″
Tension test:	f_{yt} = 63.4 ksi f_{ut} = 105.6 ksi f_{ut}/f_{yt} = 1.67			

*Δ_L = the displacement corresponding to P_{max}

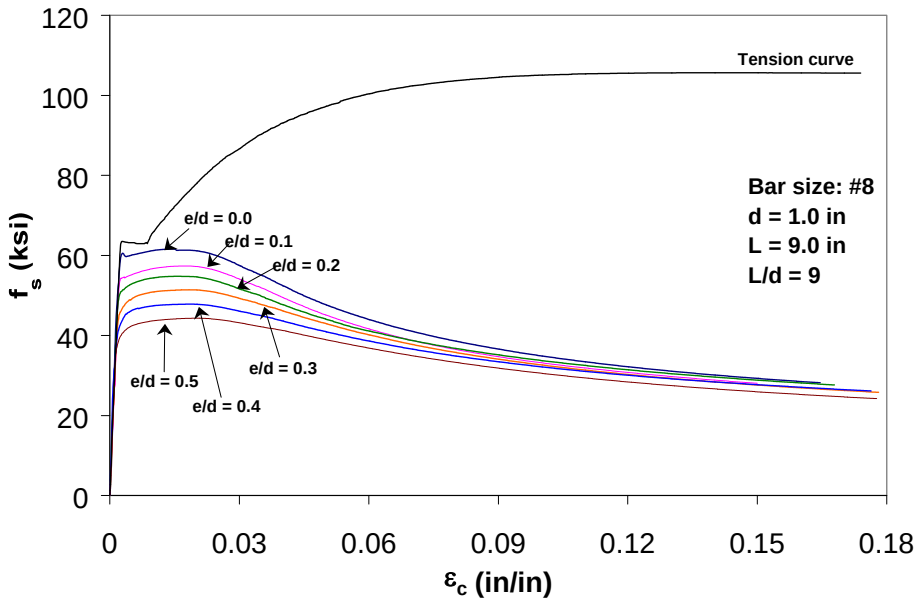

Figure 4.15 Axial stress-strain curves for #8 reinforcing bars with L/d = 9.

The axial load vs. lateral deformation behavior observed for reinforcing bars with L/d = 9 is similar to that discussed before for previous L/d cases (Figure 4.16). The lateral deflections at which the peak loads occurred are similar to those for L/d = 8 (Tables 4.6 and 4.7). For specimens with e/d = 0.0, the maximum load, P_{max}, occurred at "first buckling" load rather than the "second buckling" load. All axial load vs. lateral deformation curves converged at approximately 1″. At this point, it is interesting to observe that as L/d ratios increased from 4 (lowest tested in this study) to 9, axial load vs. lateral deformation response of the test specimens with varying degree of initial imperfections became markedly different than each other. Conversely, as the unsupported length of the bars increase and hence the inelastic buckling case under consideration moves closer to the elastic buckling range, initial imperfections influenced specimen behavior in a pronounced manner.

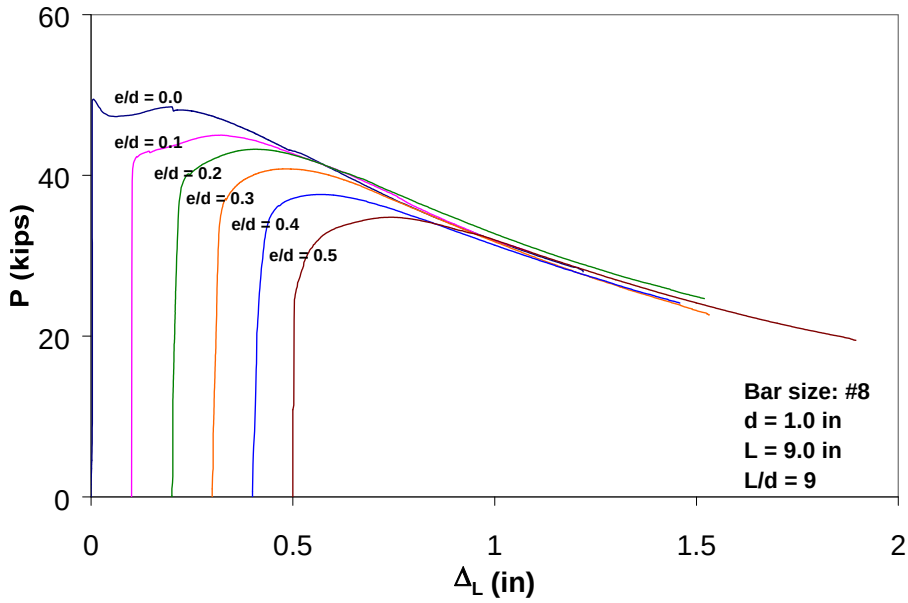

Figure 4.16 Axial load vs. lateral deformation curves of #8 bars with L/d =9.

Number 8 reinforcing bars with *L/d* = 10 showed noticeable instability under compression at lower strain values than the previously studied *L/d* cases (Figure 4.17 and Table 4.8). For reinforcing bars with *e/d* = 0.0, the load carrying capacity could not be recovered after yielding in compression, even though the yield strength in compression was only 3.6% lower than the tensile yield strength (Table 4.8). For specimens with *L/d* = 10 and *e/d* = 0.0, it can be observed that the capacity was maintained up to $\varepsilon_c \approx 0.015$ after a sudden drop at yield strain. This is attributed to strain hardening. For all other *e/d* cases, post-buckling capacities increased by about 1, 5, 11, 14, and 13% with respect to the yield stress for *e/d* ratios of 0.1, 0.2, 0.3, 0.4, and 0.5, respectively. In general, all bars with *L/d* = 10 maintained the maximum stress in the post-buckling path for strains of about 0.015. All stress-strain curves with *L/d* = 10 converged down to a stress of approximately 24 ksi, approximately 8% lower than that for *L/d* = 9 (Figures 4.15 and 4.17). The yield strength under compression was lower than that in tension by about 14 to 41% for reinforcing bars with various *e/d* ratios (Table 4.8).

Table 4.8 Mechanical Properties of #8 reinforcing bars with L/d = 10.

e/d	f_{yc} **(ksi)**	f_{uc} **(ksi)**	f_{uc}/f_{yc}	P_{max} **(kip @** Δ_L^* **(in)**
0.0	61.1	59.0	0.97	46.9 @ 0.00″
0.1	54.4	54.8	1.01	43.0 @ 0.32″
0.2	48.6	51.2	1.05	40.1 @ 0.43″
0.3	43.1	47.7	1.11	37.5 @ 0.48″
0.4	40.5	46.2	1.14	36.2 @ 0.58″
0.5	37.4	42.2	1.13	33.1 @ 0.70″
Tension test:		f_{yt} = 63.4 ksi f_{ut} = 105.6 ksi f_{ut}/f_{yt} = 1.67		

*Δ_L = the displacement corresponding to P_{max}

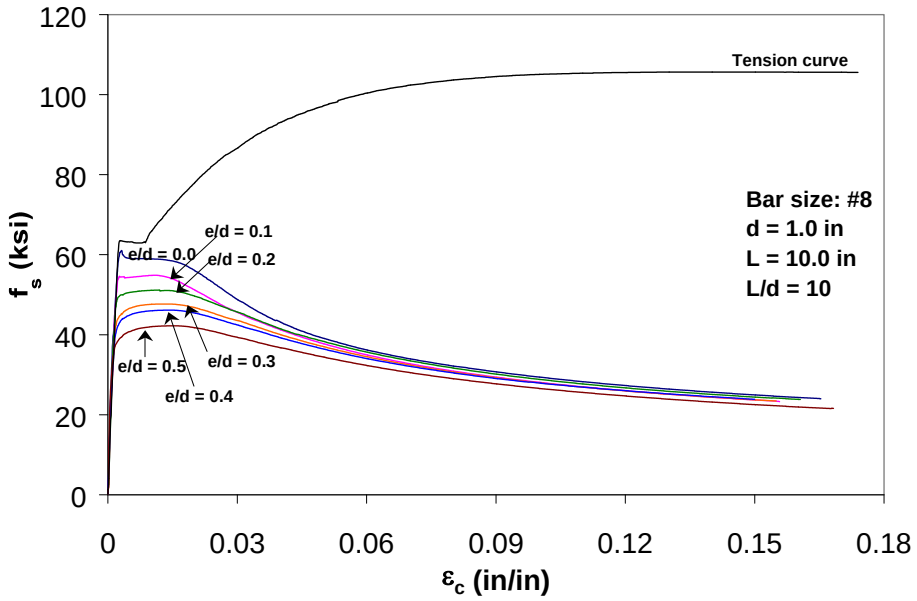

Figure 4.17 Axial stress-strain curves for #8 reinforcing bars with L/d = 10.

As can be seen in Figure 4.18, the peak load for the specimen with *e/d* = 0.0 occurred at the "first buckling" load. For this case, there was no increase in capacity after "first buckling" resulting in considerable instability after reaching P_{max}. For all other *e/d* ratios, the capacity increased to reach the peak load after the loss of the initial linear stiffness. The P_{max} values occurred at the same deflections as for specimens with *L/d* = 9, except for *e/d* = 0.0 (Tables 4.7 and 4.8). The axial load vs. lateral deformation curves converged at around a lateral deformation of 1″. This is very similar to the corresponding lateral deformation measured for specimens with *L/d* = 9 (Δ_L = 1″).

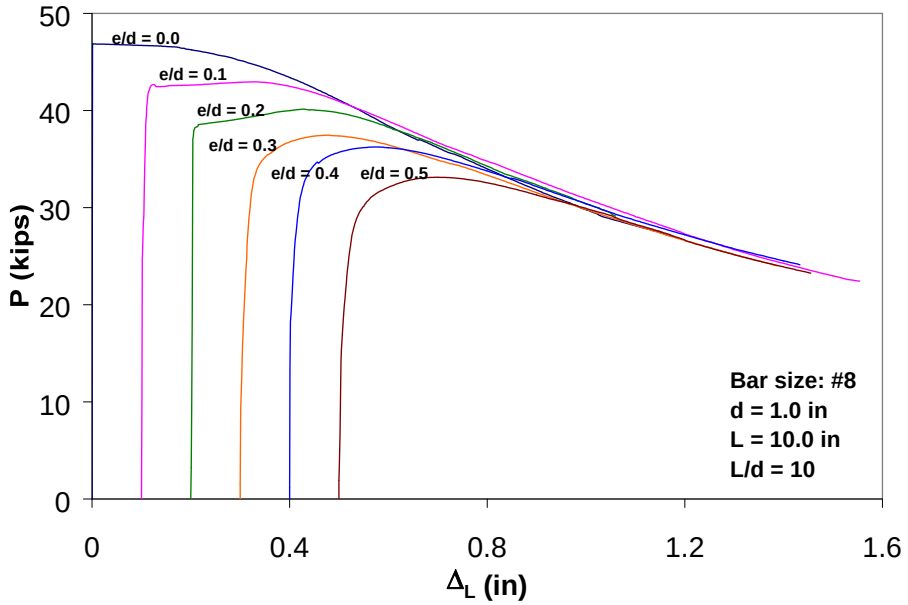

Figure 4.18 Axial load vs. lateral deformation curves of #8 bars with L/d =10.

Instability after yielding is observed in a pronounced manner for #8 reinforcing bars with *L/d* = 11 and *e/d* = 0.0 and 0.1. This time, the capacity rapidly decreased after yielding in compression resulting in an unstable post-buckling path (Figure 4.19). The yield strengths under compression for *e/d* = 0.0 and 0.1 were 8.8 and 15% lower than the tensile yield stress (f_{yt} = 63.4 ksi), respectively. For the rebars with other *e/d* ratios, the strength slightly increased after yielding in compression in the post-buckling path by about 1, 11, 15, and 17% for specimens with *e/d* = 0.2, 0.3, 0.4, and 0.5 (Table 4.9). The increased strength was sustained for strains up to about 0.012 for rebars with *e/d* = 0.2 and 0.3. For reinforcing bars with *e/d* = 0.4 and 0.5, the maximum strength was sustained up to strains of about 0.015. This observation is very similar to that for specimens with *L/d* = 10 (Figures 4.17 and 4.19). The yield stress in compression for bars with *e/d* = 0.2, 0.3, 0.4, and 0.5 was lower than the tensile yield stress by

about 27, 36, 41 and 48%, respectively. Finally, stress-strain curves with L/d = 11 converged to a stress of about 20 ksi at large strains ($\varepsilon_c \approx 0.12$). This stress level is approximately 17% lower than that for reinforcing bars with L/d = 10.

Table 4.9 Mechanical Properties of #8 reinforcing bars with L/d = 11.

e/d	f_{yc} (ksi)	f_{uc} (ksi)	f_{uc}/f_{yc}	P_{max} (kip @ Δ_L^* (in)
0.0	57.8	---	---	44.9 @ 0.00″
0.1	54.1	---	---	42.5 @ 0.12″
0.2	46.6	47.2	1.01	37.3 @ 0.37″
0.3	40.8	45.4	1.11	35.6 @ 0.55″
0.4	37.1	42.7	1.15	33.7 @ 0.57″
0.5	32.9	38.8	1.17	30.4 @ 0.69″
Tension test:	f_{yt} = 63.4 ksi f_{ut} = 105.6 ksi f_{ut}/f_{yt} = 1.67			

*Δ_L = the displacement corresponding to P_{max}

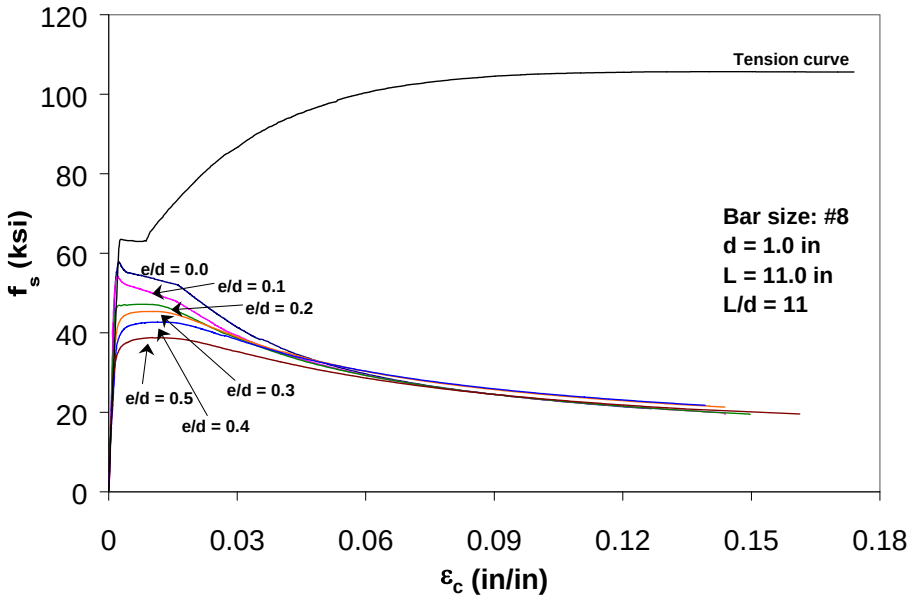

Figure 4.19 Axial stress-strain curves for #8 reinforcing bars with L/d = 11.

Figure 4.20 illustrates that #8 reinforcing bars with *L/d* = 11 and *e/d* = 0.0 and 0.1 had no increase in the load carrying capacity after "first buckling", did not display ductile behavior, and after "first buckling" the load-carrying capacity decreased steadily. For all the test specimens with *L/d* = 11, the path followed after reaching P_{max} was unstable regardless of the initial eccentricity. For specimens with *e/d* ratios ranging from 0.2 to 0.5, the capacity increased slightly after the linear elastic portion. The maximum load, P_{max}, occurred at somewhat lower lateral deflections for specimens with *e/d* = 0.1, 0.2, and 0.3 than specimens with comparable *e/d* ratios and *L/d* = 10. However, specimens with *L/d* = 10 and *e/d* = 0.4 or 0.5 reached their maximum load carrying capacities at strains similar to those experienced by specimens with *L/d* = 10 and comparable *e/d* ratios. As can be seen in Figure 4.20, all curves converge to the "same" unstable descending path. Specimens with *e/d* = 0.1 showed slightly lower stress values than the other specimens (Figure 4.20) and this is attributed to experimental scatter.

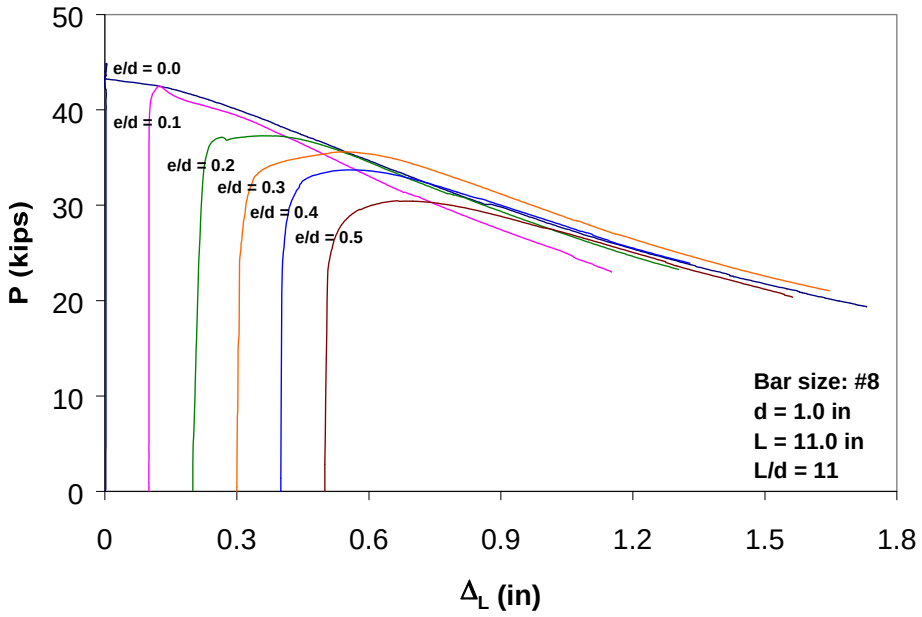

Figure 4.20 Axial load vs. lateral deformation curves of #8 bars with L/d =11.

Figure 4.21 illustrates axial stress-strain responses for specimens with *L/d* = 12. As can be seen in this figure, all specimens with *L/d* = 12 displayed very unstable post-buckling paths. The yield stresses in compression for specimens with *L/d* = 12, *e/d* = 0.0 and 0.1 were 7% and 16% lower than the tensile yield stress. Reinforcing bars with *e/d* = 0.2 had a 1% increase in load-carrying capacity at a strain of 0.007. The yield stress in compression for specimens with *L/d* = 12 and *e/d* = 0.2 was 27% less than tensile yield stress. The specimens with *e/d* = 0.3, 0.4, and 0.5 reached their maximum stress level after yielding in compression at a strain of about 0.0096, which was 36% less than the corresponding values for specimens with *L/d* = 10 and 11. The yield stress in compression for specimens with *e/d* = 0.3, 0.4, and 0.5 was 35, 43, and 48% lower than the tensile yield stress, respectively. The increase in strength after the initial yielding for these cases was about 4, 8, and 10%, respectively (Table 4.10). The axial stress-strain curves converge to a stress level of approximately 17.5 ksi at the end of the post-buckling path.

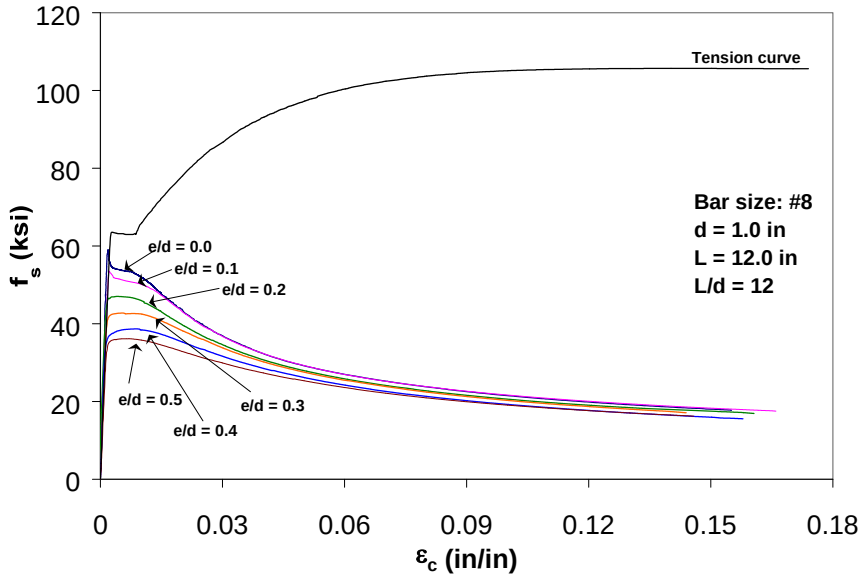

Figure 4.21 Axial stress-strain curves for #8 reinforcing bars with L/d = 12.

Table 4.10 Mechanical Properties of #8 reinforcing bars, L/d = 12.

e/d	f_{yc} **(ksi)**	f_{uc} **(ksi)**	f_{uc}/f_{yc}	P_{max} **(kip) @** Δ_L^* **(in)**
0.0	59.0	---	---	39.4 @ 0.00″
0.1	53.5	---	---	43.0 @ 0.10″
0.2	46.5	47.0	1.01	35.3 @ 0.36″
0.3	41.1	42.7	1.04	33.2 @ 0.47″
0.4	35.8	38.7	1.08	30.4 @ 0.57″
0.5	32.8	36.1	1.10	27.3 @ 0.68″
Tension test:	f_{yt} = 63.4 ksi f_{ut} = 105.6 ksi f_{ut}/f_{yt} = 1.67			

*Δ_L = the displacement corresponding to P_{max}

The axial load vs. lateral deformation relationships of #8 reinforcing bars with *L/d* = 12 and *e/d* = 0.0 are shown in Figure 4.22. As can be observed in this figure, specimens with *L/d* = 12 displayed unstable responses and they were not able to maintain the maximum load at yield. It is interesting to note that the family of curves presented in Figure 4.22 shows more scatter than the previous curves. This is mainly attributed to experimental scatter. However, it is still possible to state that the post-buckling responses of all specimens with *L/d* = 12 are in a reasonably narrow band at large deformations. For all reinforcing bars with *L/d* = 12 the maximum load, P_{max}, occurs at approximately the same lateral deflection as those specimens with *L/d* = 11 (Figures 4.20 and 4.22).

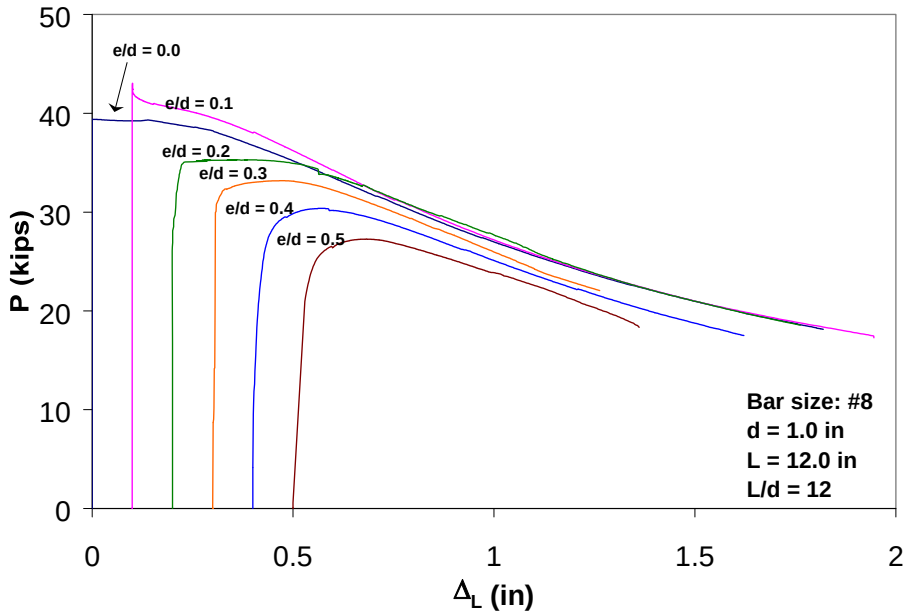

Figure 4.22 Axial load vs. lateral deformation curves of #8 bars with L/d =12.

Having completed the first phase of the experimental program, where #8 reinforcing bars with *L/d* ratios ranging from 4 to 12 and *e/d* ratios ranging from 0.0 to 0.5 were tested, the following conclusions were reached:

- For a given *L/d* ratio, as the *L/d* ratio increased, the behavior of the test specimens deteriorated and they showed less ductility and energy dissipation capacity.
- For a given *L/d* ratio, as the *e/d* ratio increased, the behavior of the test specimens depended highly on the strain hardening response of a representative reinforcing bar tested in tension. Hence, it was decided that in order to make recommendations on the maximum unsupported length of longitudinal bars in the potential plastic hinge regions of reinforced concrete columns, reinforcing bars displaying various f_{ut}/f_{yt} ratios needed to be tested.

The f_{ut}/f_{yt} ratio of specimens tested by Bayrak and Sheikh (2001) was 1.32 and that of the reinforcing bars tested during the first phase of the study was 1.67. Prior to making any design recommendations, it was decided that #10 bars with a different f_{ut}/f_{yt} ratio needed to be tested. In this way, not only the size of the specimen was to be changed but also material properties were going to change as well. In this way, an extensive database could be formed and design recommendations and analytical models could be based on this rather extensive database.

Figure 4.23 illustrates the results obtained for #10 bars with L/d = 4. Regardless of the e/d ratio, specimens displayed very stable responses and the load-carrying capacity did not decrease, although the buckled bars showed as much as 1.2″ of lateral deformation. The axial stress-strain curve obtained for the bar with e/d = 0.0 showed similar behavior to the tensile stress-strain curve. The yield stress in compression for this L/d-e/d combination was 0.2% lower than the tensile yield stress, and the yield plateau was significantly shorter than the tensile yield plateau. For the reinforcing bars with e/d = 0.1, 0.2, and 0.3, the stress-strain response followed the tensile stress-strain curve up to strains of about 0.018, 0.022, and 0.015, respectively. For reinforcing bars with e/d = 0.1, 0.2, 0.3, 0.4, and 0.5, the yield stress in compression was about 8.8, 15, 16, 30, and 31% lower than the tensile yield stress, respectively. For specimens with e/d = 0.0, 0.1, and 0.2, the increase in capacity in the post-buckling region was similar to that in tension. For specimens with e/d = 0.4 and 0.5, the capacity increases in the post-buckling region were 60% and 53% (Table 4.11).

Table 4.11 Mechanical Properties of #10 reinforcing bars, L/d = 4.

e/d	f_{yc} (ksi)	f_{uc} (ksi)	f_{uc}/f_{yc}	P_{max} (kip) @ Δ_L^* (in)
0.0	64.3	93.7	1.46	118.6 @ 0.45″
0.1	58.7	83.8	1.43	106.7 @ 0.74″
0.2	54.5	81.1	1.49	102.7 @ 0.55″
0.3	54.4	75.7	1.39	95.9 @ 0.81″
0.4	45.2	72.2	1.60	91.3 @ 1.22″
0.5	44.6	68.4	1.53	86.6 @ 1.26″
Tension test:	f_{yt} = 64.4 ksi f_{ut} = 92.5 ksi f_{ut}/f_{yt} = 1.44			

*Δ_L = the displacement corresponding to P_{max}

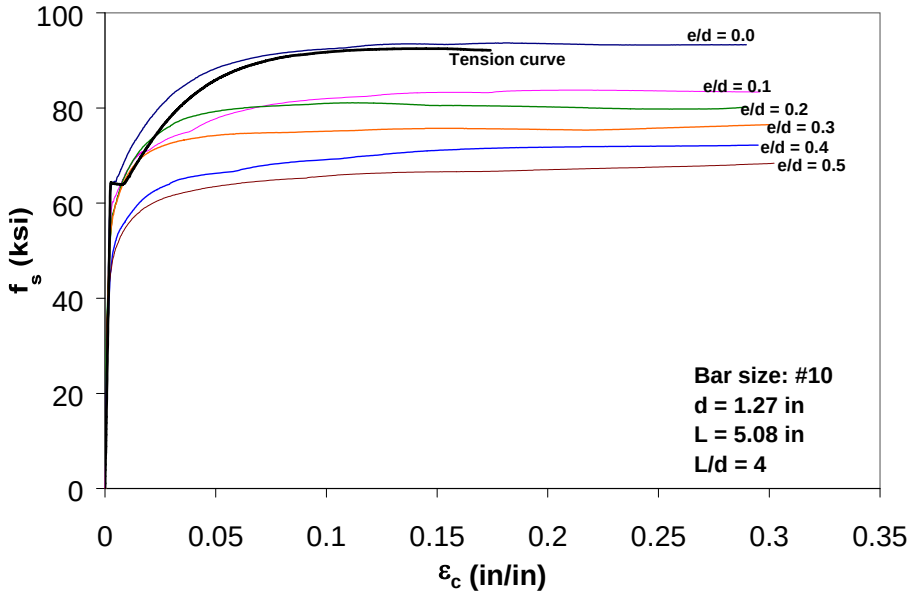

Figure 4.23 Axial stress-strain curves for #10 reinforcing bars with L/d = 4.

Similar to #8 reinforcing bars with *L/d* = 4, #10 reinforcing bars with *L/d* = 4 had very stable axial load vs. lateral deformation responses, where the axial load increased with increasing lateral deformations regardless of the initial

eccentricity (Figure 4.24). The maximum compressive force (P_{max}) (within the recorded data range) decreased with increasing *e/d* ratio (Table 4.11). For some of the bars the last data point was marked by fracture, which indicated that #10 bars with *L/d* = 4 could sustain large inelastic deformations without strength loss.

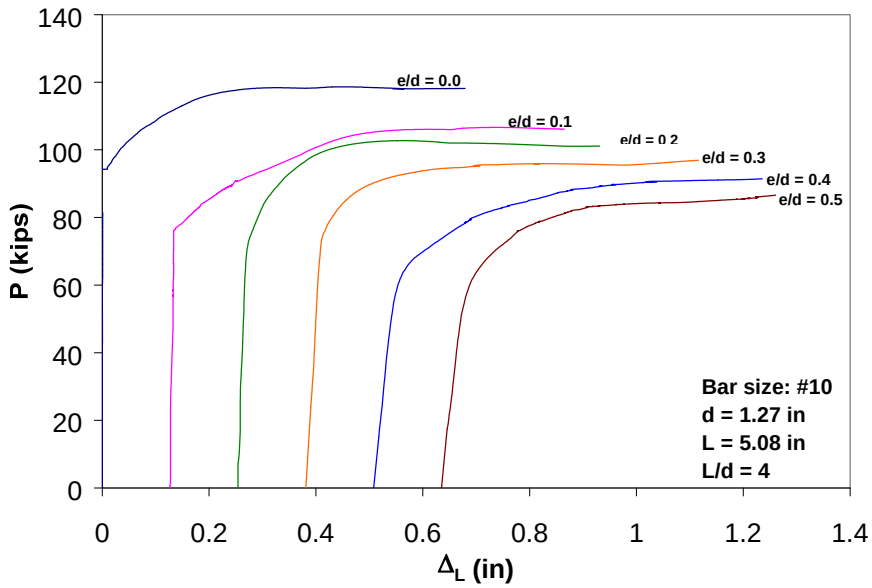

Figure 4.24 Axial load vs. lateral deformation curves of #10 bars with L/d = 4.

Axial stress-strain response of initially straight #10 reinforcing bars with *L/d* = 5 was very stable, but at large axial strains ($\varepsilon_c > \varepsilon_{t\text{-}sh}$), axial stress carried in compression was not as high as that carried in tension (Figure 4.25). For this *L/d-e/d* combination, the yield stress in compression was 1.1% larger than the tensile yield stress and the specimen with *L/d* = 5 and *e/d* = 0.0 was able to deform without any strength loss up to an axial strain of about 0.075. For axial strains smaller than 0.016, the axial stress-strain behavior of the specimen with *L/d* = 5 and *e/d* = 0.1 was similar to the tensile stress-strain response. Specimens with *e/d*

= 0.0 and 0.1 were able to deform up to a strain of about 0.068 without losing strength. Specimens with higher *e/d* ratios were able to deform without strength loss up to strains of about 0.075. The tensile yield stress was reached by the specimen with *e/d* = 0.0 at the expected tensile yield strain of 0.0022. The axial compressive stresses were about 8, 17, 24, 30, and 38% less than the tensile yield stress for specimens with *e/d* ratios of 0.1, 0.2, 0.3, 0.4, and 0.5, respectively (Table 4.12). As can be observed in Table 4.12, the ultimate strength of specimens tested in tension was 4.4% higher than the yield stress. However, the ultimate strengths of the bars tested in compression were 22% to 35% higher than the corresponding compressive stresses.

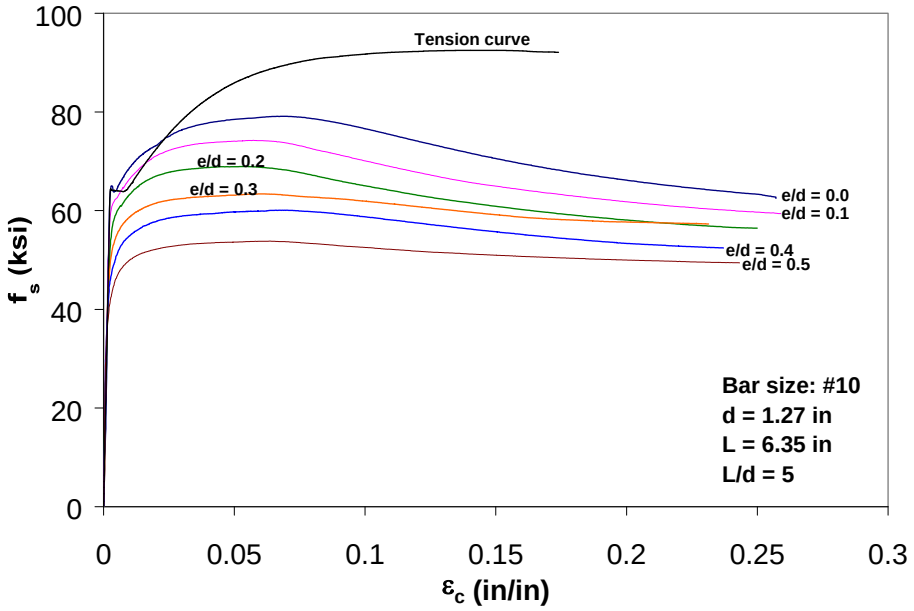

Figure 4.25 Axial stress-strain curves for #10 reinforcing bars with L/d = 5.

Table 4.12 Mechanical Properties of #10 reinforcing bars, L/d = 5.

e/d	f_{yc} **(ksi)**	f_{uc} **(ksi)**	f_{uc}/f_{yc}	P_{max} **(kip) @** Δ_L^* **(in)**
0.0	65.0	79.1	1.22	99.6 @ 0.29″
0.1	59.2	74.2	1.25	94.1 @ 0.38″
0.2	53.1	68.9	1.30	87.3 @ 0.49″
0.3	48.9	63.4	1.30	80.3 @ 0.68″
0.4	44.8	60.1	1.34	76.1 @ 0.87″
0.5	39.9	53.8	1.35	68.2 @ 1.00″
Tension test:	f_{yt} = 64.4 ksi f_{ut} = 92.5 ksi f_{ut}/f_{yt} = 1.44			

*Δ_L = the displacement corresponding to P_{max}

Figure 4.26 illustrates the axial load vs. lateral deformation behavior of #10 reinforcing bars with *L/d* = 5. As can be observed in Table 4.12 and Figure 4.26, the maximum compressive force, P_{max}, decreased with increasing *e/d* ratio. For a given *e/d* ratio, the load carrying capacity decreased with increasing lateral deformations. It is interesting to note that the maximum loads carried by specimens with L/d = 5 occurred at smaller lateral deformations than those experienced by specimens with L/d = 4 (Figures 4.24 and 4.26). With increasing *e/d* ratio, the amount of lateral displacement required to reach the maximum compressive load increased. For #10 rebars with *L/d* = 5, the "second buckling" phenomenon was not observed. However, for #8 reinforcing bars with *L/d* =5 "second buckling" was observed (Figure 4.8).

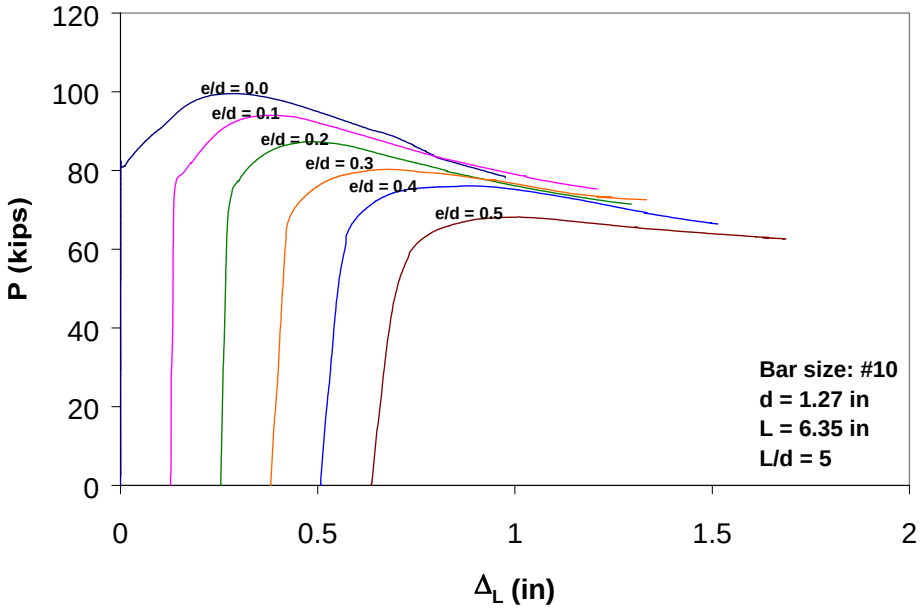

Figure 4.26 Axial load vs. lateral deformation curves of #10 bars with L/d = 5.

As can be seen in Figure 4.27, #10 rebar with *L/d* = 6 and *e/d* = 0.0 had a stress-strain behavior that was very similar to the tensile stress-strain behavior for strains smaller than 0.019. The improvement of the load-carrying capacity in the post-buckling branch due to strain hardening was about 11 to 42 % for specimens with *L/d* = 6 (Table 4.13). All specimens with *L/d* = 6 displayed very stable stress-strain responses and there was no capacity loss observed prior to axial strains smaller than 0.04. Yield stresses of reinforcing bars tested in compression were 8, 20, 24, 31, and 46% lower than the tensile yield stress for specimens with *e/d* ratios of 0.1 to 0.5.

Table 4.13 Mechanical Properties of #10 reinforcing bars, L/d = 6.

E/d	f_{yc} (ksi)	f_{uc} (ksi)	f_{uc}/f_{yc}	P_{max} (kip) @ Δ_L^* (in)
0.0	66.7	74.3	1.11	94.1 @ 0.26″
0.1	59.4	69.7	1.17	88.3 @ 0.41″
0.2	51.5	64.6	1.26	81.8 @ 0.58″
0.3	48.7	59.4	1.22	75.4 @ 0.67″
0.4	44.2	53.7	1.21	68.0 @ 0.76″
0.5	344.8	49.4	1.42	62.6 @ 0.92″
Tension test:	f_{yt} = 64.4 ksi f_{ut} = 92.5 ksi f_{ut}/f_{yt} = 1.44			

*Δ_L = the displacement corresponding to P_{max}

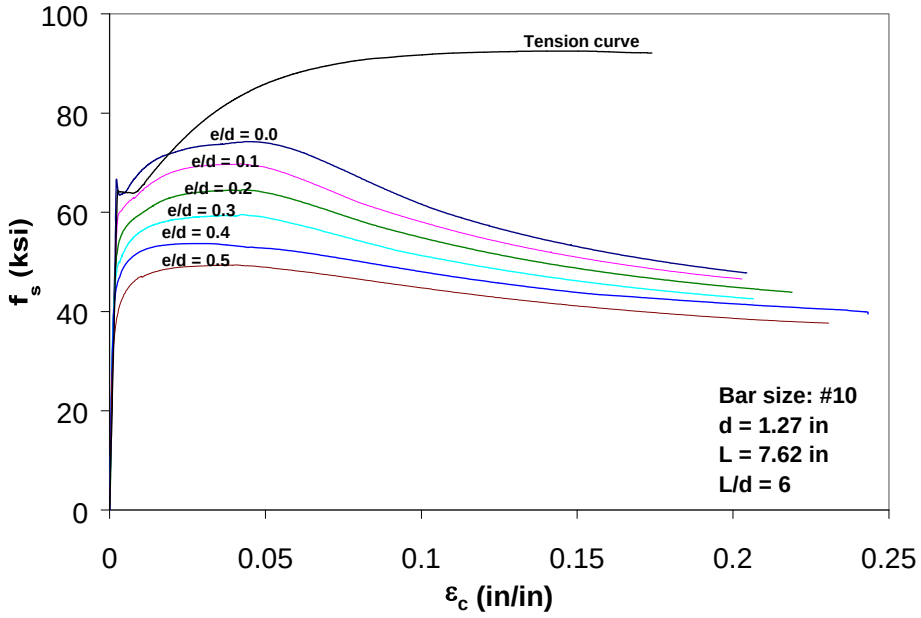

Figure 4.27 Axial stress-strain curves for #10 reinforcing bars with L/d = 6.

The peak loads for the reinforcing bars with *L/d* = 6 were recorded at lateral deformations similar to those for *L/d* = 5 (Tables 4.12 and 4.13). The peak load occurred at larger lateral deflections as the initial eccentricity increased. The

reinforcing bar with *e/d* = 0.0 had a bifurcation type behavior. The rebar carried the increasing load up to the "first" peak without buckling, then the load dropped to the bifurcation point with zero lateral deflection, and then the capacity started increasing and the "second" peak was reached while the rebar was buckling laterally (Figure 4.28). The post-buckling paths of the #10 reinforcing bars with *L/d* = 6 converged to the same curve at large lateral deformations.

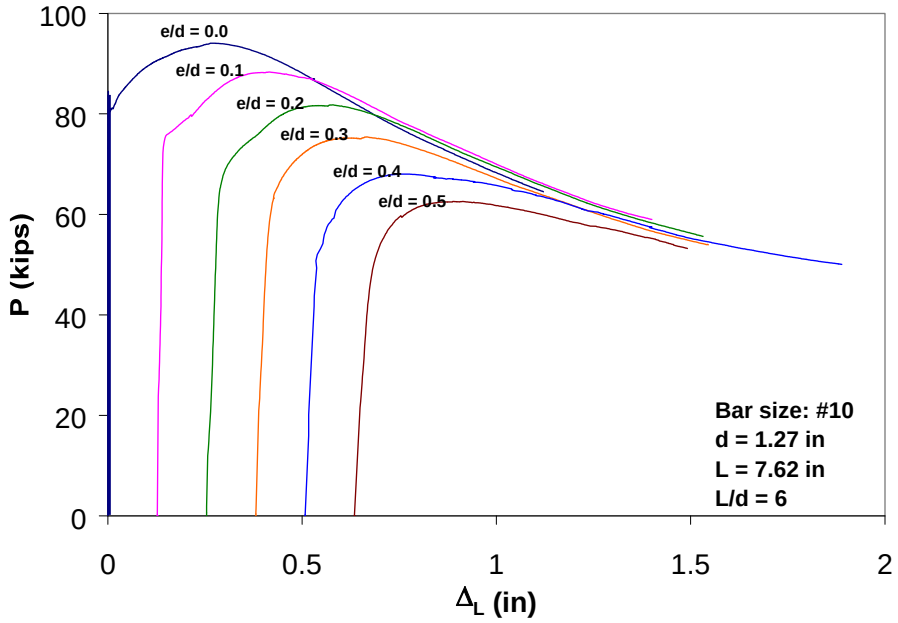

Figure 4.28 Axial load vs. lateral deformation curves of #10 bars with L/d = 6.

An examination of the family of curves presented in Figure 4.29 reveals the fact that axial compressive behavior of #10 reinforcing bars with *L/d* = 7 show instability over a wider range of axial strains than those of the #10 bars with *L/d* = 4, 5, and 6. At large axial strains, the curves for all *e/d* ratios converge to a stress level of about 30 ksi. Initially straight bars had stress-strain behavior similar to the behavior in tension up to a strain of 0.01. The ultimate strength of the initially straight bar tested in compression was 2% higher than the compressive yield

stress. For the other *e/d* ratios, the yield stress in compression was lower than that in tension by about 10, 20, 30, 37, and 46% for *e/d* ratios of 0.1, 0.2, 0.3, 0.4, and 0.5. The post-buckling capacities increased by about 9 to 28% with respect to the corresponding yield stress for *e/d* ratios of 0.1 to 0.5 (Table 4.14).

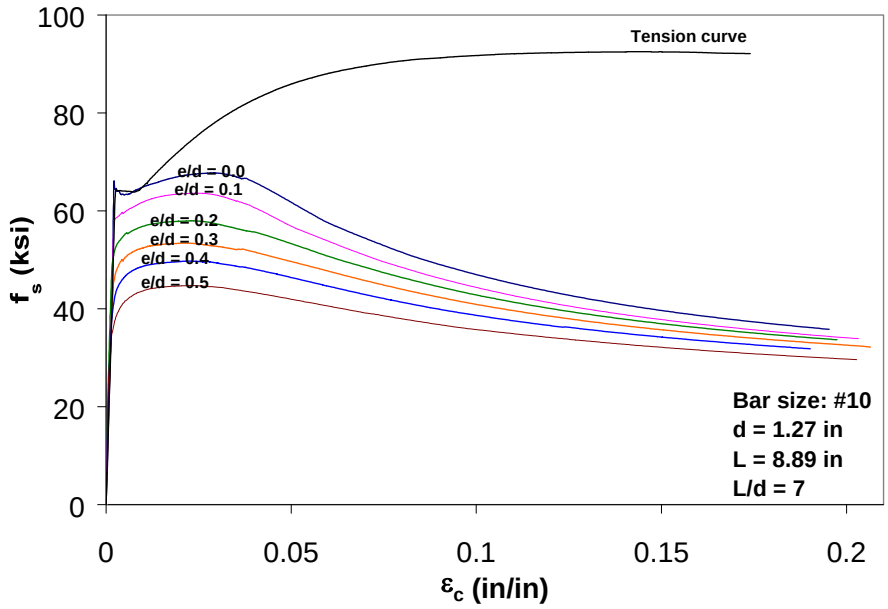

Figure 4.29 Axial stress-strain curves for #10 reinforcing bars with L/d = 7.

Table 4.14 Mechanical Properties of #10 reinforcing bars, L/d = 7.

e/d	f_{yc} **(ksi)**	f_{uc} **(ksi)**	f_{uc}/f_{yc}	P_{max} **(kip) @** Δ_L^* **(in)**
0.0	66.2	67.7	1.02	85.8 @ 0.24″
0.1	58.1	63.6	1.09	80.6 @ 0.34″
0.2	51.7	58.0	1.12	73.4 @ 0.48″
0.3	45.0	53.4	1.19	67.7 @ 0.60″
0.4	40.8	49.7	1.22	63.0 @ 0.71″
0.5	34.9	44.8	1.28	56.7 @ 0.86″
Tension test:	f_{yt} = 64.4 ksi f_{ut} = 92.5 ksi f_{ut}/f_{yt} = 1.44			

*Δ_L = the displacement corresponding to P_{max}

The maximum compressive loads reached by the #10 bars with *L/d* = 7 were about 8-kips less than those obtained for specimens with *L/d* = 6 and occurred at lower lateral displacement values (Figure 4.30 and Table 4.14). For the specimen with *L/d* = 7 and *e/d* = 0.0, two peak loads (i.e. buckling loads) were encountered. The path followed by the axial load vs. lateral displacement curves for all *e/d* ratios try converged to the same post-buckling path with increasing lateral deformations.

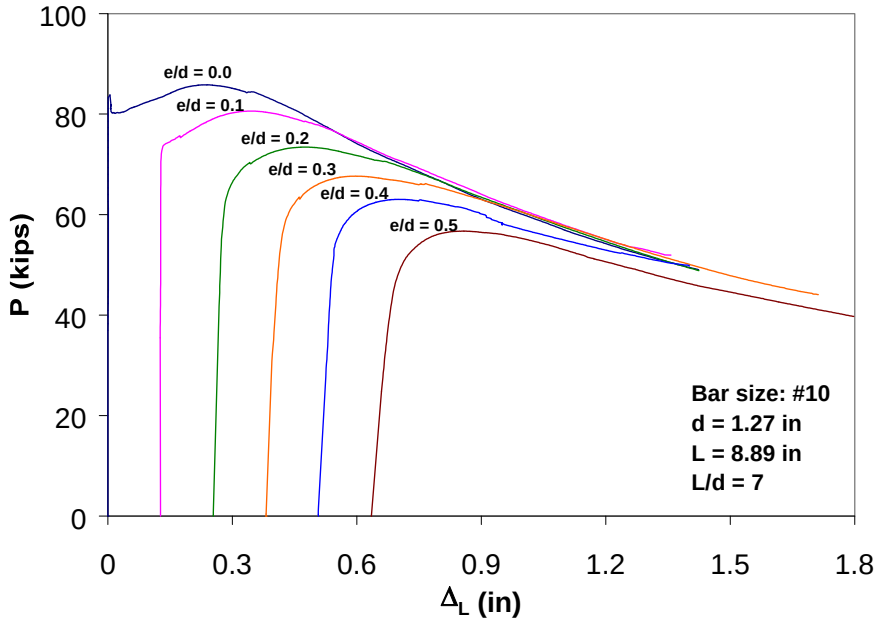

Figure 4.30 Axial load vs. lateral deformation curves of #10 bars with L/d = 7.

Figure 4.31 illustrates the axial stress-strain behavior in compression for #10 reinforcing bars with *L/d* = 8. For the initially straight bar, the compressive yield stress was similar to the tensile yield stress (0.6% difference). However after this stress was reached, the bar became unstable and capacity was lost rapidly. Previously, for #8 bars with *L/d* = 8 and *e/d* = 0.0 the specimens recovered some of the capacity and hence the behavior was more ductile. The #10 bar with *e/d* =

0.1 displayed axial stress-strain behavior in which maximum stress was maintained up to a strain of 0.022. The rebars with *e/d* ratios = 0.2, 0.3 and 0.4 maintained the maximum axial stress levels up to a strain of about 0.018. The specimen with *e/d* = 0.5 did not show any decrease in strength up to an axial strain of 0.022. All stress-strain curves converged to the same post-buckling stress of approximately 26 ksi at large axial deformations. The bars with *e/d* ratios of 0.1 to 0.5 showed decreasing yield stress values that were 7 to 48% lower than the tensile yield stress. The post-buckling capacity of the #10 reinforcing bars with *L/d* = 8 increased by about 3, 9, 14, 10, and 27% with respect to the yield stress for *e/d* ratios of 0.1, 0.2, 0.3, 0.4, and 0.5 respectively (Table 4.15).

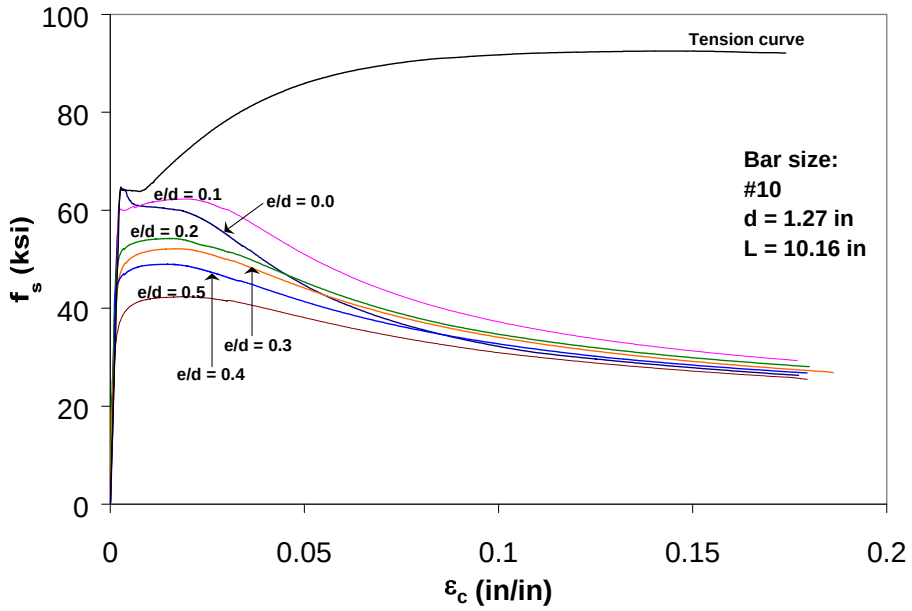

Figure 4.31 Axial stress-strain curves for #10 reinforcing bars with L/d = 8.

Table 4.15 Mechanical Properties of #10 reinforcing bars, L/d = 8.

e/d	f_{yc} (ksi)	f_{uc} (ksi)	f_{uc}/f_{yc}	P_{max} (kip) @ Δ_L^* (in)
0.0	64.8	---	---	82.0 @ 0.00″
0.1	60.3	62.3	1.03	78.9 @ 0.34″
0.2	49.8	54.2	1.09	68.7 @ 0.46″
0.3	45.9	52.1	1.14	66.1 @ 0.59″
0.4	44.7	49.0	1.10	62.1 @ 0.69″
0.5	33.4	42.4	1.27	53.7 @ 0.88″
Tension test:	f_{yt} = 64.4 ksi f_{ut} = 92.5 ksi f_{ut}/f_{yt} = 1.44			

*Δ_L = the displacement corresponding to P_{max}

Figure 4.32 shows the load vs. lateral deformation relationships of the #10 reinforcing bars with L/d = 8. The lateral deflections at which the peak loads occurred were similar to those of specimens with L/d = 7 (Tables 4.14 and 4.15). As can be seen in this figure, the specimen that was initially straight had a higher peak stress than the other specimens. However, the post-buckling response of this specimen showed lower stresses than the other specimens at large inelastic deformations. The convergence of the axial load vs. lateral deformation curves at large lateral displacements can be observed in Figure 4.32.

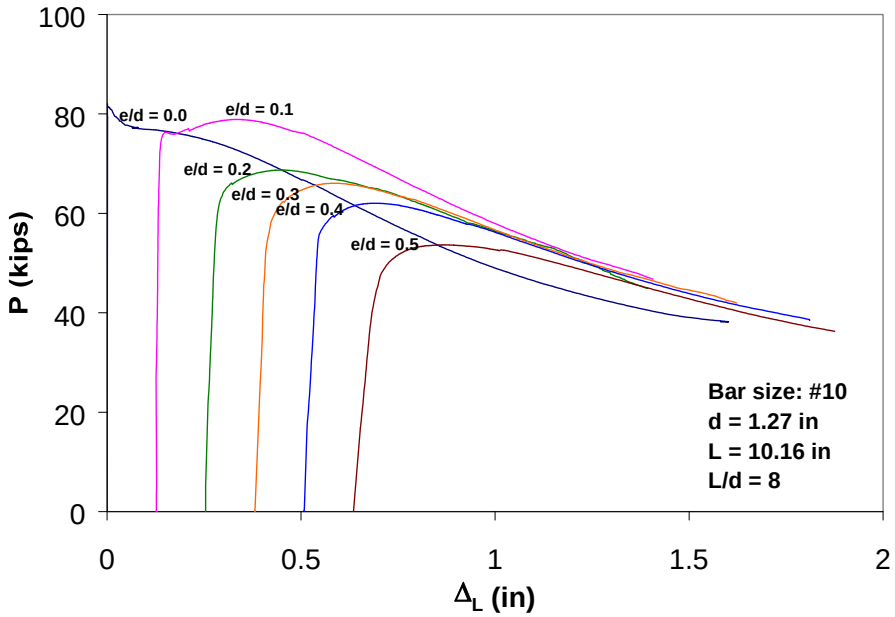

Figure 4.32 Axial load vs. lateral deformation curves of #10 bars with L/d = 8.

The stress-strain curves of #10 bars with *L/d* = 9 tested under monotonic compression are presented in Figure 4.33. A careful examination of this figure illustrates that the initially straight specimen was able to reach the tensile yield point. However, the capacity dropped quickly thereafter and the post-buckling path is unstable (Figure 4.33). At an axial strain of 0.009, the stress-strain curves of the initially straight bar and bars with *e/d* = 0.1 crossed and after this point the behavior of these bars was fairly similar. For the bar with *e/d* = 0.1, the yield stress was about 7% lower than the yield stress in tension and the capacity did not increase after yielding. The maximum stress in the post-buckling branch was 2% less than the yield stress. The specimens with *e/d* = 0.2 to 0.5 had compressive yield stress values lower than the tensile yield stress by about 24 to 45% (Table 4.16). For these cases, the maximum capacity in the post-buckling region

increased by about 7 to 17% with respect to corresponding yield stresses. All stress-strain curves converged to a stress level of approximately 23 ksi (Figure 4.33).

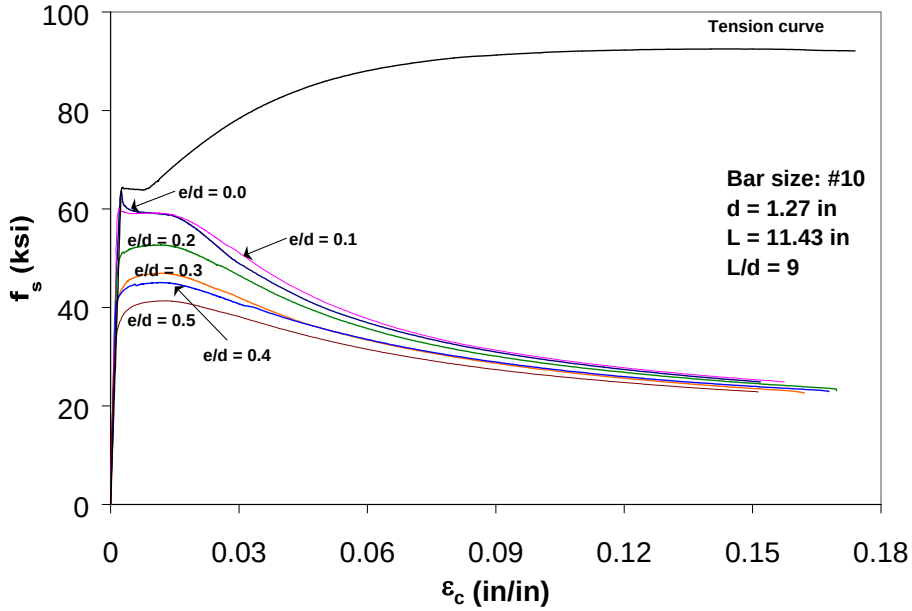

Figure 4.33 Axial stress-strain curves for #10 reinforcing bars with L/d = 9.

Table 4.16 Mechanical Properties of #10 reinforcing bars, L/d = 9.

e/d	f_{yc} (ksi)	f_{uc} (ksi)	f_{uc}/f_{yc}	P_{max} (kip) @ Δ_L^* (in)
0.0	63.7	---	---	80.7 @ 0.00″
0.1	60.2	59.2	0.98	76.3 @ 0.14″
0.2	49.1	52.7	1.07	66.7 @ 0.47″
0.3	42.6	46.9	1.10	59.5 @ 0.60″
0.4	40.9	45.1	1.10	57.1 @ 0.71″
0.5	35.4	41.3	1.17	52.4 @ 0.85″
Tension test:	f_{yt} = 64.4 ksi f_{ut} = 92.5 ksi f_{ut}/f_{yt} = 1.44			

*Δ_L = the displacement corresponding to P_{max}

Axial load vs. lateral deformation behavior of #10 bars with *L/d* = 9 is presented in Figure 4.34. The behavior of #10 bars with *L/d* = 9 (Figure 4.34) and #8 bars with *L/d* = 9 (Figure 4.33) was very similar. The axial load vs. lateral deformation behavior for #10 bars with *e/d* = 0.0 resulted in lower load-carrying capacity than the other *e/d* cases after buckling (Figure 4.34). The maximum compressive loads for all *e/d* cases were about 2 kips less than the loads obtained for #10 bars with *L/d* = 8, except for #10 bars with *e/d* = 0.3 and 0.4 for which the loads were about 5 kips (Tables 4.15 and 4.16). For #10 bars with *L/d* = 8 and 9, the maximum capacities under compression occurred at approximately the same lateral displacements. The region where all the curves converge to a single curve is very well defined and starts at approximately 1.0″ (Figure 4.34).

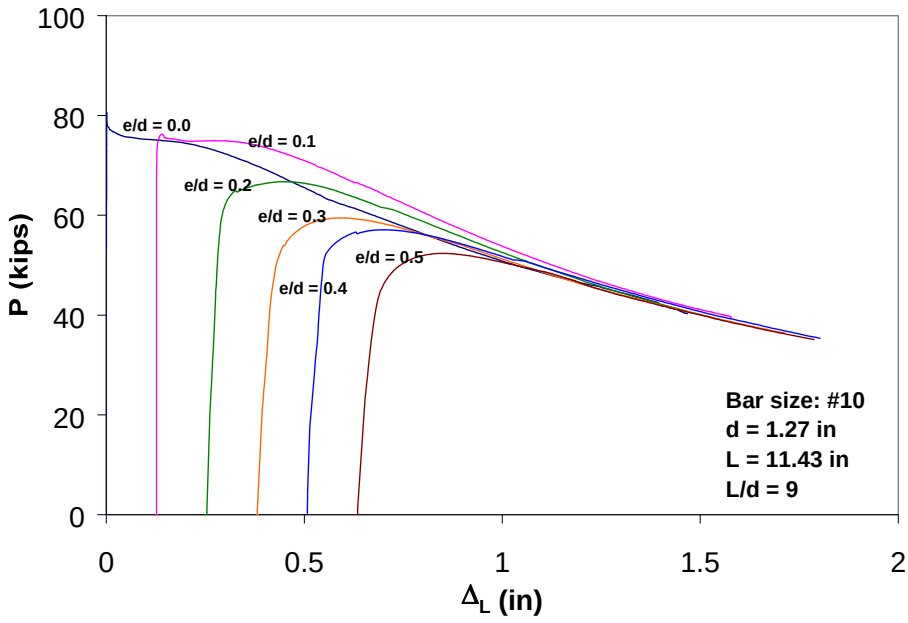

Figure 4.34 Axial load vs. lateral deformation curves of #10 bars with L/d = 9.

Stress-strain relationships of #10 reinforcing bars with *L/d* = 10 are presented in Figure 4.35. As can be seen in this figure, this group of test specimens experienced noticeable instability at lower strains resulting in a severe decrease in load-carrying capacity. The bar with *e/d* = 0.0 reached the tensile yield point, but the load-carrying capacity was lost after yielding (Table 4.17). The yield stress for the specimen with *e/d* = 0.1 was 13% lower than the tensile yield stress. The specimens with other *e/d* ratios experienced a slight increase in stress after reaching the yield point. This increase ranged from 5 to 16% (Table 4.17). The yield stress in compression was about 25 to 52% lower than that in tension. The stress-strain curves converged to the same level of stress (18.6 ksi) at large inelastic deformations. This stress level is approximately 20% lower than that for #8 bars with the same *L/d* ratio.

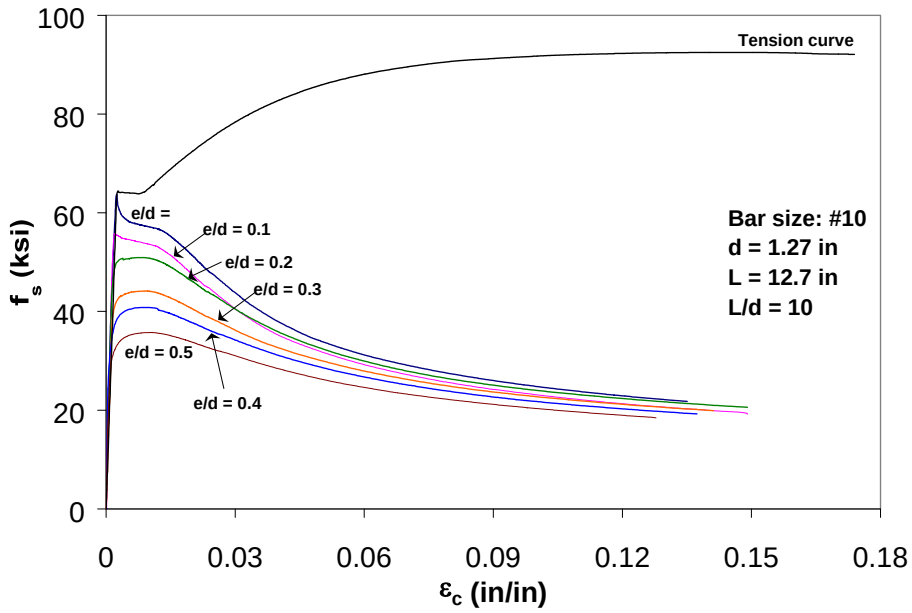

Figure 4.35 Axial stress-strain curves for #10 reinforcing bars with L/d = 10.

Table 4.17 Mechanical Properties of #10 reinforcing bars, L/d = 10.

e/d	f_{yc} **(ksi)**	f_{uc} **(ksi)**	f_{uc}/f_{yc}	P_{max} **(kip) @** Δ_L^* **(in)**
0.0	63.7	---	---	80.7 @ 0.01″
0.1	55.9	---	---	70.8 @ 0.13″
0.2	48.4	50.9	1.05	64.5 @ 0.42″
0.3	39.8	44.1	1.11	55.9 @ 0.56″
0.4	36.2	40.8	1.13	51.7 @ 0.71″
0.5	30.8	35.7	1.16	45.3 @ 0.85″
Tension test:	f_{yt} = 64.4 ksi f_{ut} = 92.5 ksi f_{ut}/f_{yt} = 1.44			

*Δ_L = the displacement corresponding to P_{max}

Figure 4.36 illustrates the axial load vs. lateral displacement relationships recorded for #10 reinforcing bars with *L/d* = 10. The maximum compression loads for all *e/d* cases occurred at lateral deformation levels comparable to those experienced by #10 bars with *L/d* = 8 and 9 (Tables 4.15, 4.16, and 4.17). For most *e/d* cases, the capacity increased after the loss of initial linear stiffness until the peak load was reached. Number 10 reinforcing bars with *L/d* = 10 and *e/d* = 0.0 and 0.1 had a linear-elastic response until the peak load was reached; load-carrying capacities were lost thereafter due to instability. All the curves converged to the same post-buckling path at around a lateral deformation of 1.0″ (similar to #10 bars with *L/d* = 9).

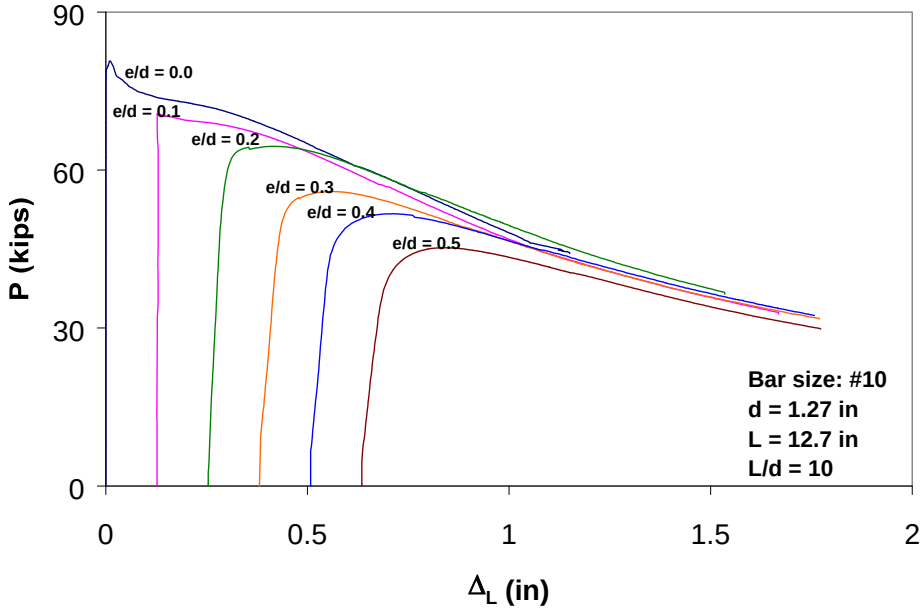

Figure 4.36 Axial load vs. lateral deformation curves of #10 bars with L/d = 10.

For #10 bars with *L/d* = 11 and *e/d* = 0.0 and 0.1, the strength was lost after yielding in compression making the post-buckling path unstable (Figure 4.37). The yield stress for #10 bars with *e/d* = 0.0 and 0.1 was lower than the tensile yield stress by about 4.8 and 12%, respectively (Table 4.18). For #10 bars with *e/d* = 0.2 to 0.5, the capacities increased slightly after yielding in compression (Figure 4.37). The yield stresses for these cases were lower than the tensile yield stress by about 29 to 48%. The maximum axial stress in the post-buckling response of bars with *e/d* = 0.2, 0.3, 0.4, and 0.5 increased from the corresponding yield stress by about 8, 6, 10, and 11% (Table 4.18). Eventually, capacities were lost due to buckling. The stress-strain curves for bars with *L/d* = 11 converged to a stress of 17.7 ksi. This stress level was 5% lower than that of #10 bars with *L/d* = 10.

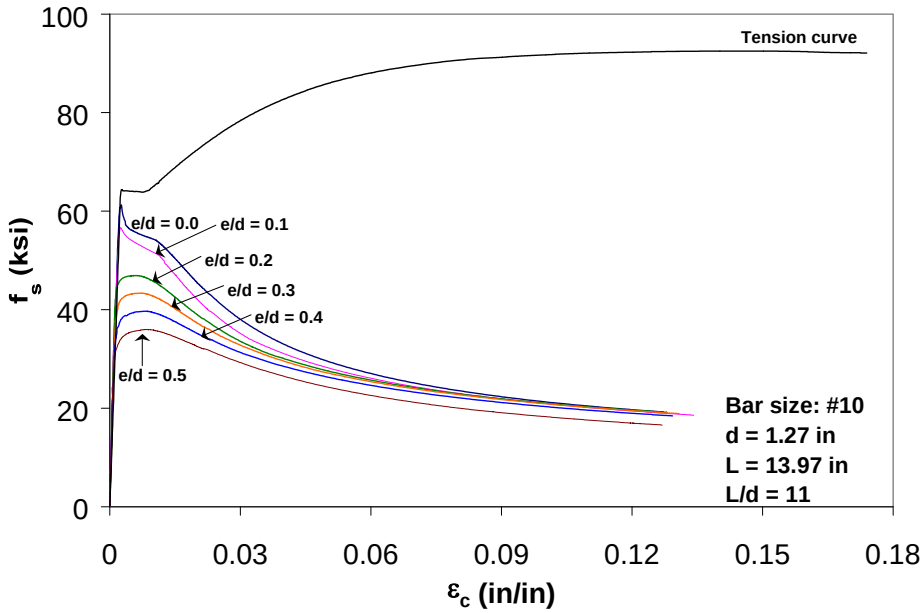

Figure 4.37 Axial stress-strain curves for #10 reinforcing bars with L/d = 11.

Table 4.18 Mechanical Properties of #10 reinforcing bars, L/d = 11.

e/d	f_{yc} **(ksi)**	f_{uc} **(ksi)**	f_{uc}/f_{yc}	P_{max} **(kip) @** Δ_L^* **(in)**
0.0	61.3	---	---	77.6 @ 0.02″
0.1	56.7	---	---	71.8 @ 0.15″
0.2	44.7	46.9	1.05	59.4 @ 0.40″
0.3	40.7	43.3	1.07	54.9 @ 0.56″
0.4	36.2	39.7	1.10	50.3 @ 0.69″
0.5	31.6	35.9	1.14	45.6 @ 0.86″
Tension test:	f_{yt} = 64.4 ksi f_{ut} = 92.5 ksi f_{ut}/f_{yt} = 1.44			

*Δ_L = the displacement corresponding to P_{max}

For the cases with *e/d* = 0.0 and 0.1 there was no increase in capacity after "first buckling" (Figure 4.38). The P_{max} values for the bars with *L/d* = 11 and 10 occurred at similar lateral deflections. The maximum loads carried by #10 bars

with *L/d* = 11 were in average 2 kips lower than those carried by #10 bars with *L/d* = 10 (Tables 4.17 and 4.18). All curves converged to the same post-buckling path at a lateral deformation of about 1″.

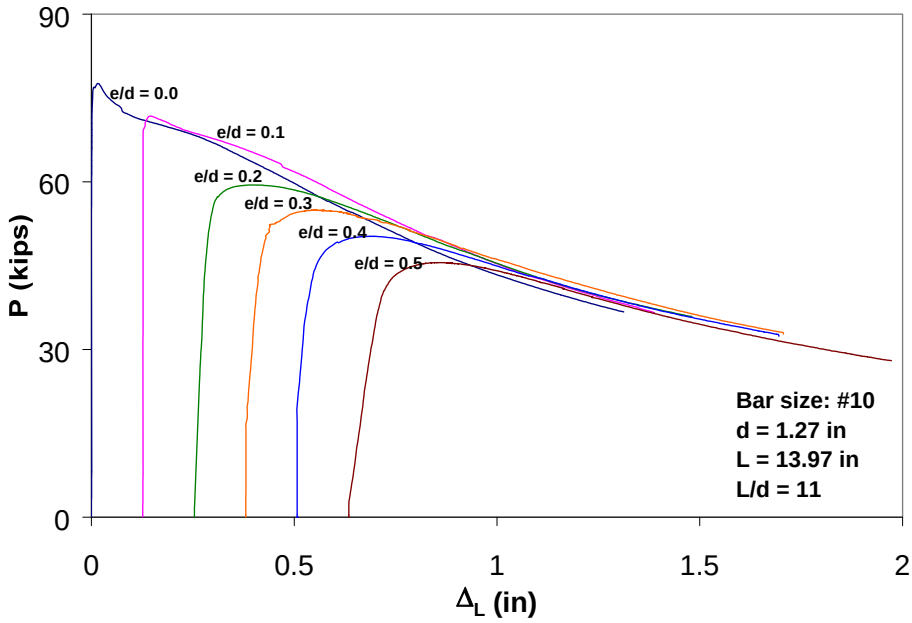

Figure 4.38 Axial load vs. lateral deformation curves of #10 bars with L/d = 11.

Figure 4.39 illustrates stress-strain behavior of #10 reinforcing bars with *L/d* = 12. As can be seen in this figure, all the axial stress-strain curves showed significant instability. The maximum capacities were lost soon after yielding, which indicated that for cases with such large unsupported lengths, reinforcing bars do not display any ductility. The specimen with *e/d* = 0.0 had a yield stress 4% higher than the tensile yield stress, but showed significant instability after that point. For the specimen with *e/d* = 0.1, the yield stress was 8% lower than that in tension. For all other *e/d* cases yield stresses were lower than that in tension by about 29 to 48%. After yielding, the stress in the specimens with *e/d* ratios of 0.2, 0.3, 0.4, and 0.5 increased by about 8, 6, 10, and 11%, respectively (Table 4.19).

These increases occurred between axial strains of 0.0022 and 0.006. For strains larger than 0.006 axial stresses dropped rapidly (Figure 4.39). All curves converged to a stress of about 16.4 ksi at the end of the post-buckling path.

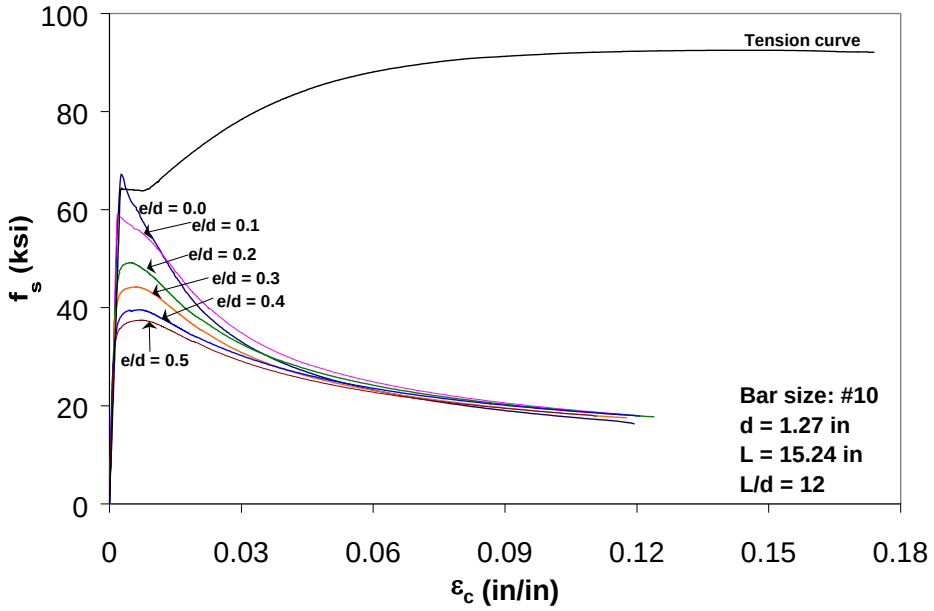

Figure 4.39 Axial stress-strain curves for #10 reinforcing bars with L/d = 12.

Table 4.19 Mechanical Properties of #10 reinforcing bars, L/d = 12.

e/d	f_{yc} (ksi)	f_{uc} (ksi)	f_{uc}/f_{yc}	P_{max} (kip) @ Δ_L^* (in)
0.0	67.2	---	---	85.1 @ 0.00″
0.1	59.0	---	---	74.8 @ 0.13″
0.2	45.7	49.1	1.08	62.3 @ 0.36″
0.3	41.5	44.2	1.06	56.0 @ 0.57″
0.4	35.9	39.5	1.10	50.1 @ 0.72″
0.5	33.7	37.4	1.11	47.4 @ 0.86″
Tension test:	f_{yt} = 64.4 ksi f_{ut} = 92.5 ksi f_{ut}/f_{yt} = 1.44			

*Δ_L = the displacement corresponding to P_{max}

The axial load vs. lateral deformation relationships obtained for #10 bars with *L/d* = 12 are presented in Figure 4.40. As can be seen in this figure, after reaching the maximum load, lateral deformations increased rapidly and significant instability was experienced by #10 bars with *L/d* = 12. The peak load for all *e/d* cases occurred at approximately the same lateral displacements as for the previous *L/d* case discussed (*L/d* =11). The maximum loads were smaller than those measured for the previous *L/d* case by about 7, 3, 2, and 1 kip for *e/d* ratios of 0.0, 0.1, 0.2, and 0.3 (Table 4.19).

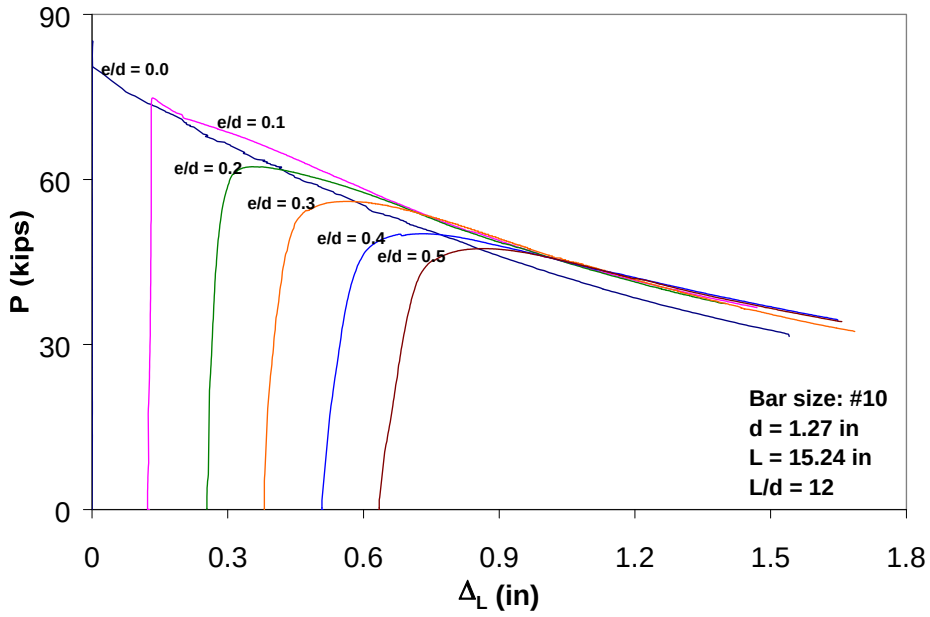

Figure 4.40 Axial load vs. lateral deformation curves of #10 bars with L/d = 12.

4.2.2 Effect of *L/d* ratio

To discuss how the *L/d* ratio affects the post-buckling behavior of concrete reinforcing bars, the data presented previously in Section 4.2.1 will be rearranged herein by combining the cases with the same *e/d* ratios in the same axial stress-strain plot. Figures 4.41 and 4.42 illustrate the axial stress-strain response for all #8 specimens and #10 specimens, respectively.

For #8 reinforcing bars, it is observed that load-carrying capacity and ductility decrease as the clear span between supports increases (Figure 4.41). For initially straight bars (*e/d* = 0.0), the yield strength is achieved for *L/d* ratios up to 6 at strains within the yield plateau for a bar tested in tension. For an *e/d* ratio of 0.1, the yield strength is achieved for an *L/d* ratio of 4 at strains within the yield plateau. For *L/d* ratios of 5 and 6, the yield strength is achieved at strains comparable to those at the beginning of strain hardening in tension. For *e/d* ratios of 0.2 and 0.3, the yield strength is achieved by *L/d* = 4 at a strain between the yield plateau and strain hardening in tension, and by *L/d* = 5 and 6 at strains corresponding with the beginning of strain hardening in tension. For larger magnitudes of initial eccentricities at midspan, the yield strength is not be achieved. Only reinforcing bars with *L/d* = 4 and 5 sustain the load for a larger range of strains at a level of loading equal to the yield strength. In general, for all *e/d* ratios, the bars with an *L/d* ratio less than 6 have the ability to achieve large inelastic deformations with minimal or no decrease in load-carrying capacity. Therefore, the behavior can be classified ductile even though the capacities in the post-buckling branch for these bars are lower than that in the strain hardening region in tension. For some of the *e/d* cases (*e/d* = 0.0, 0.1, 0.2, and 0.3), specimens with an *L/d* ratio of 7 reach the yield strength at larger strain values ($\varepsilon_c \approx 0.015$). In these cases, the specimens sustain tensile stresses around the tensile yield stress for strain levels of 0.05. This can be classified as moderate level of

ductility. Larger *L/d* ratios have significant instability problems once the maximum load is reached. These specimens do not sustain the load in a stable manner, and load-carrying capacity drops gradually with increasing strains.

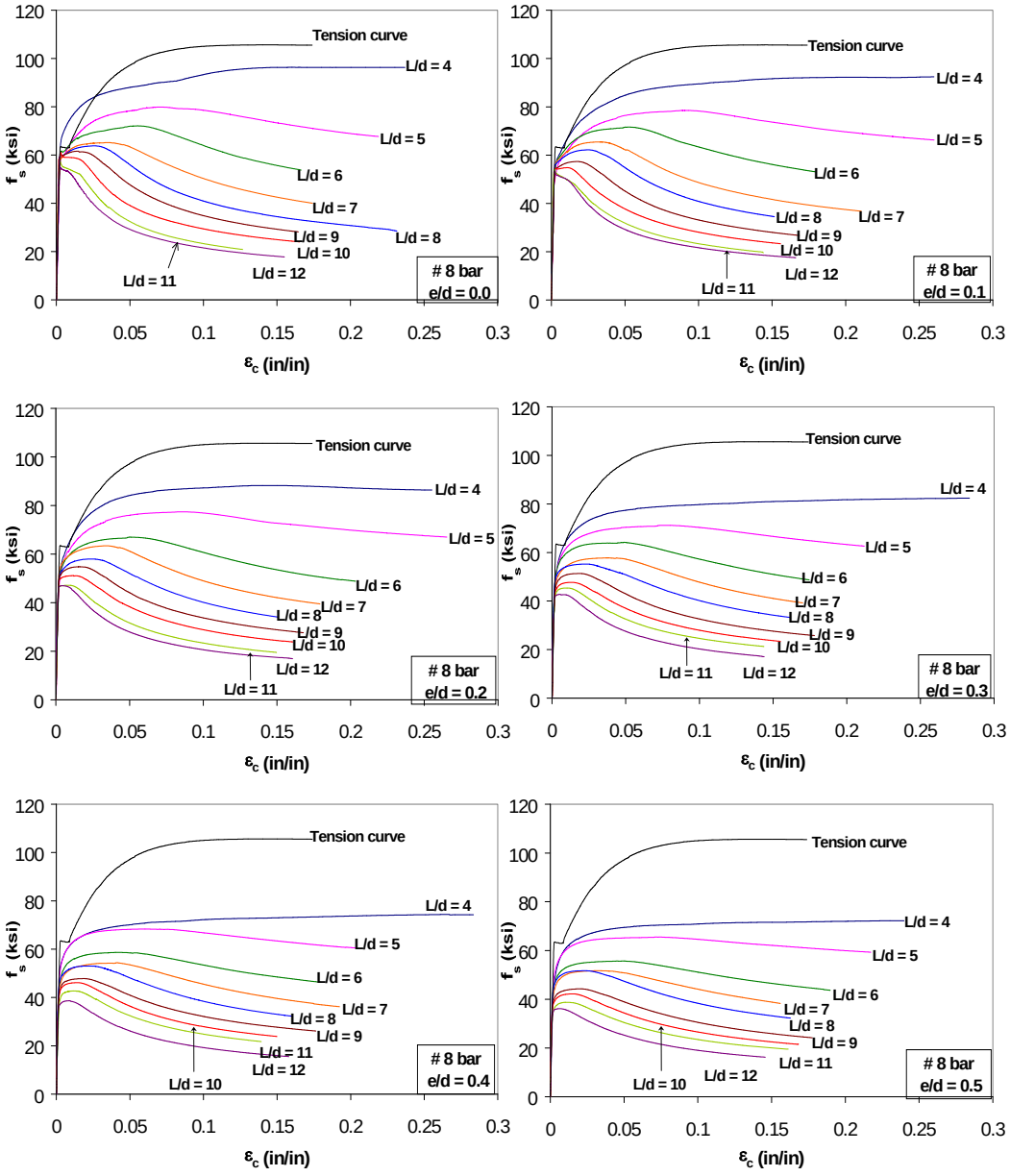

Figure 4.41 Axial stress-strain curves of #8 bars with different e/d ratios.

As can be seen in Figure 4.42, similar observations can be made for #10 reinforcing bars tested under compression. In this section, the differences observed between #8 and #10 bars are discussed. For #10 bars with e/d = 0.0 and L/d = 4, a capacity greater than that in tension is observed. Initially straight bars with L/d ratios of 5 and 6 reach the yield strength almost exactly at the same strain as in tension. It is interesting to note that the ductility observed in similar cases for the #8 bars is lower. For an e/d ratio of 0.1, the yield strength is achieved for L/d ratios of 4, 5, and 6 at strains within the yield plateau of the tension test. Although this observation is similar to that in #8 bars, it is interesting to note that #10 bars show lesser ductility than their #8 companions. For specimens with e/d = 0.2, a substantial amount of ductility is observed for cases where L/d = 4 and 5. These specimens display stress levels higher than the yield stress observed in the tension test. In addition, after reaching the maximum stress these specimens are able to maintain most (if not all) of their load-carrying capacity for large inelastic deformations. Number 10 bars with L/d = 6 barely reach the tensile yield stress, but this occurs at a strain of approximately 0.02. Number 10 bars with e/d = 0.2 and L/d ratios greater than or equal to 7 display lower ductility and do not maintain their load-carrying capacity with increasing axial deformations. For specimens with e/d = 0.3, the yield strength is achieved only by #10 bars with L/d = 4. The stress-strain curve for the #10 bar with e/d = 0.3 and L/d = 4 follow a similar path at the initial stages of the strain hardening region for the specimen tested in tension. This combination of length to initial eccentricity results in a reasonably stable behavior in compression. For larger magnitudes of initial eccentricities at midspan, the yield strength in tension is achieved only by specimens with L/d = 4, though at larger strains (around 0.03 to 0.07). For specimens with L/d = 4, there is no drop in load-carrying capacity after yielding.

In general, for all *e/d* ratios the #10 bars showed lower ductility than for #8 bars. However, as can be observed in Figure 4.42, for *L/d* ratios less than 6 the behavior is ductile and stable and the capacity can be sustained for larger strains even though the capacities in the post-buckling branch for these bars are lower than that in the strain-hardening region for the tensile response. For an *L/d* ratio of 7 with *e/d* = 0.0, although the yield strength is achieved at a similar strain as that in tension, the post-buckling behavior is not stable.

In general, for a given *e/d* ratio, an increase in *L/d* ratio results in a decrease in strength and ductility of reinforcing bars under compressive loading. To ensure ductile behavior, a critical *L/d* ratio of 7 can be defined for initially straight #8 bars and *L/d* = 6 for #10 bars with *e/d* = 0.0. Bayrak and Sheikh (2001) reported this critical *L/d* ratio as 7 and Mau and El-Mabsout (1989) reported the same value for reinforcing bars with high strength steel.

For #8 bars with *L/d* ratios lower than 6 and #10 bars with *L/d* ratios lower than 5, ductile and stable behavior is observed. The limit of *L/d* = 6 is the same as that recommended by Mander et al. (1984) and by Bayrak and Sheikh (2001) for cases where ductility is expected. The limit of *L/d* = 5, on the other hand, is comparable to the value suggested by Monti and Nuti (1992).

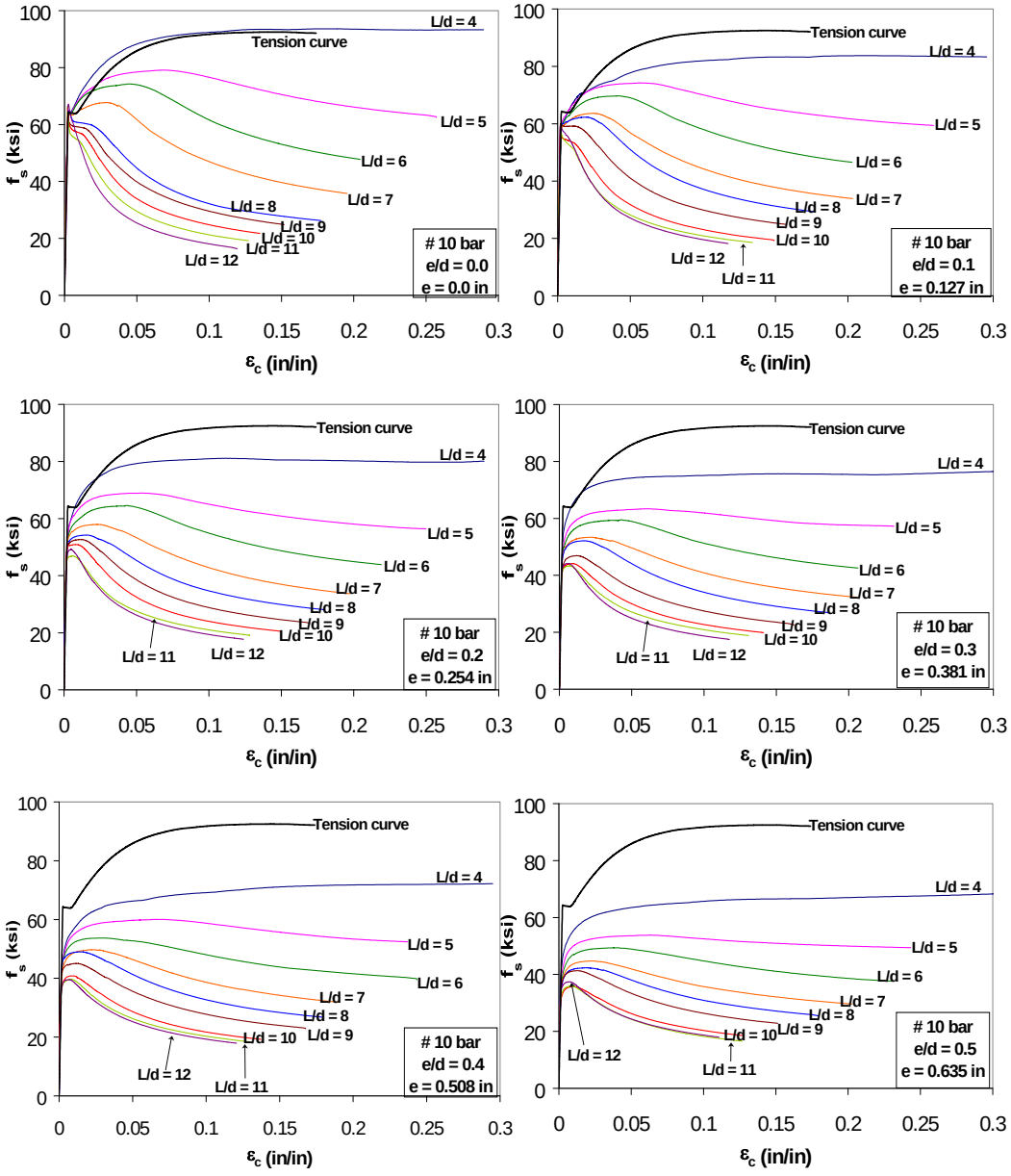

Figure 4.42 Axial stress-strain curves of #10 bars with different e/d ratios.

4.2.3 Effect of bar size and material strength

The post-buckling path of reinforcing bars varies with their clear span length and their initial imperfections. Their behavior also depends on the size of the reinforcing bars and on the material properties of the steel. In this section, the results obtained for the #8 and #10 bars are rearranged and compared. To extend the comparison, the data published by Bayrak and Sheikh (2001) for #6 (20M) reinforcing bars is incorporated.

Figure 4.43 illustrates the normalized stress-strain curves for #8 and #10 bars tested in this study and that for #6 bars tested by Bayrak and Sheikh (2001). The data is normalized in order to illustrate differences in ratios of ultimate strength to yield. It is believed that this influences the post-buckling behavior of reinforcing bars significantly.

The axial stress-strain curves obtained from the compression tests for different bar sizes are also normalized. All stresses are normalized by the yield stress (f_y) and all strains are normalized by the yield strain (ε_y). The results for the different bar sizes with same L/d ratio are presented in the same figure to facilitate comparison (Figures 4.44 to 4.52). Each figure consists of six plots and each of these plots show the behavior of the three bar sizes (that have three different material properties) with the same e/d ratio. Because Bayrak and Sheikh (2001) did not test reinforcing bars with L/d = 11, L/d = 12, e/d = 0.4, and e/d = 0.5, information about #6 bars with these geometric properties is not included in Figures 4.44 to 4.52.

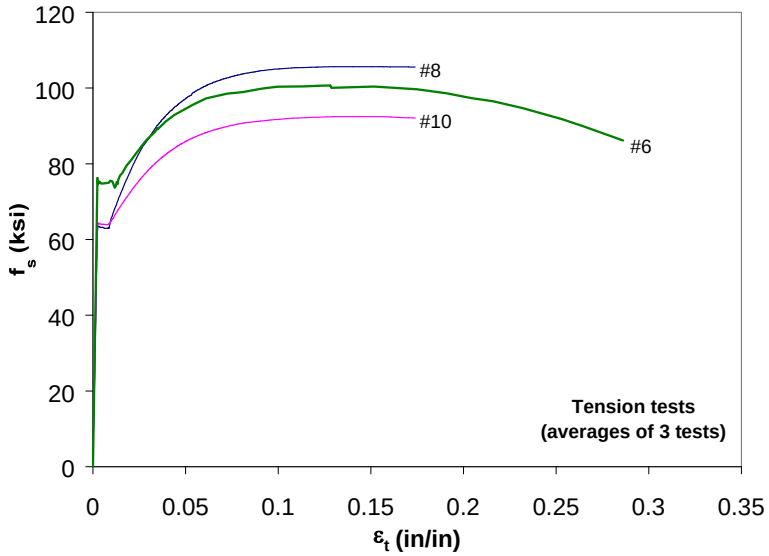

(a)

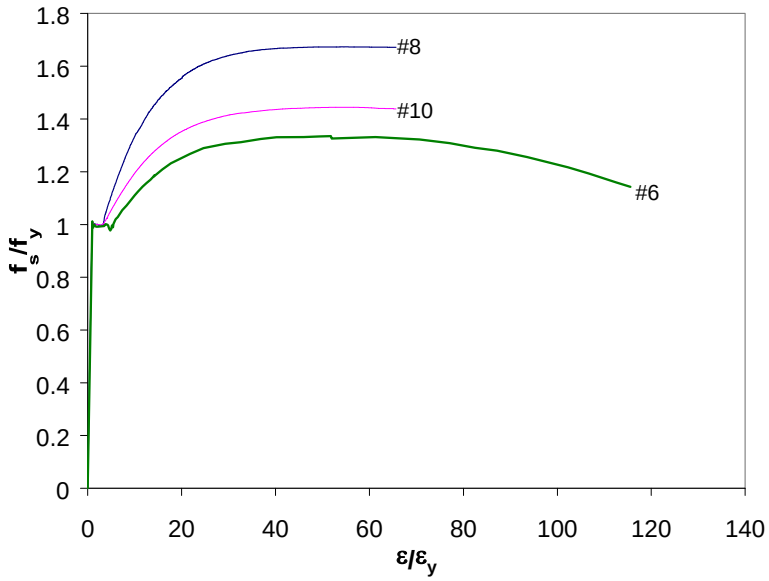

(b)

Figure 4.43 Stress-strain curves for reinforcing bars tested in tension:

(a) actual and (b) normalized

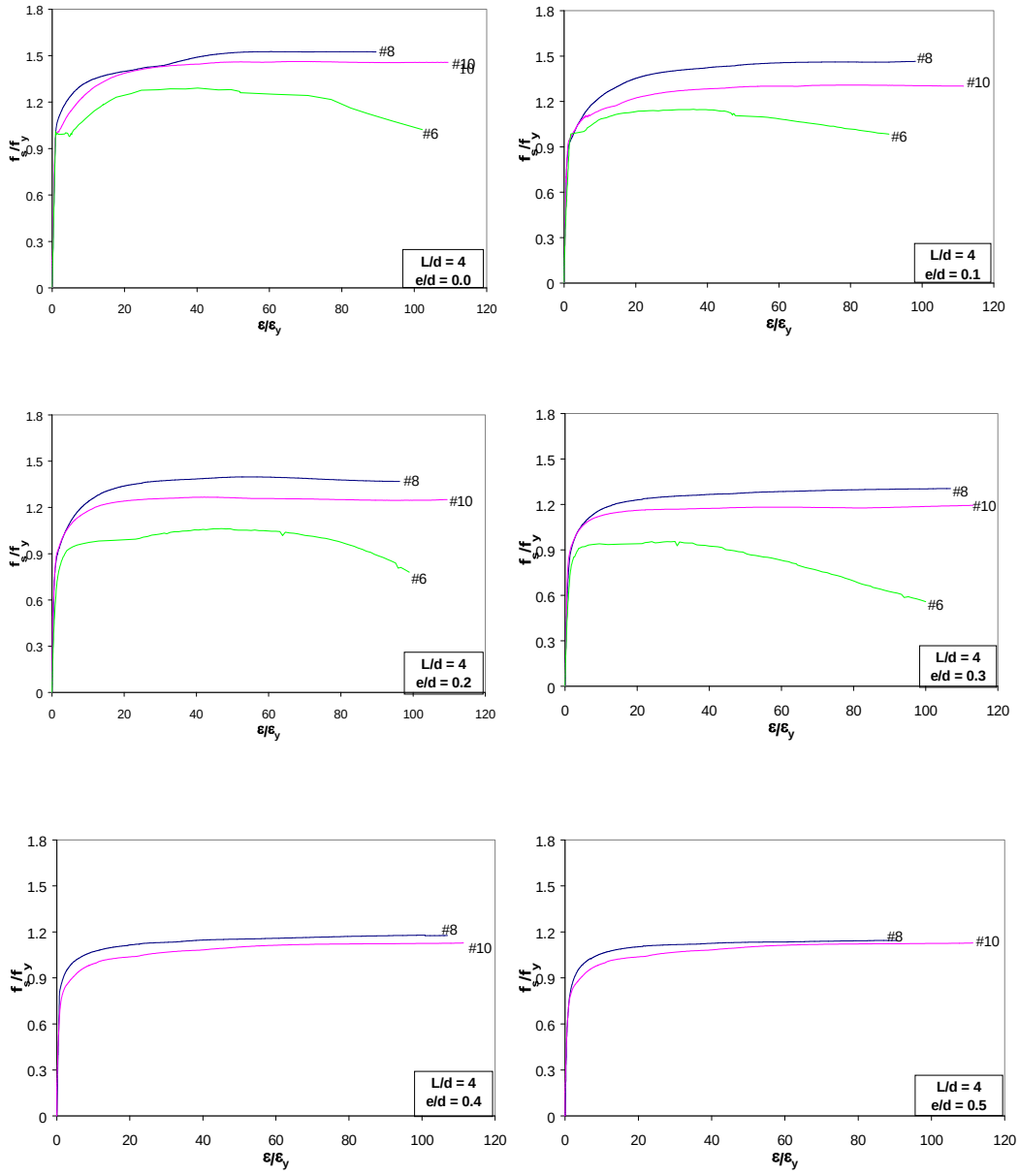

Figure 4.44 Axial stress-strain curves of reinforcing bars with L/d = 4

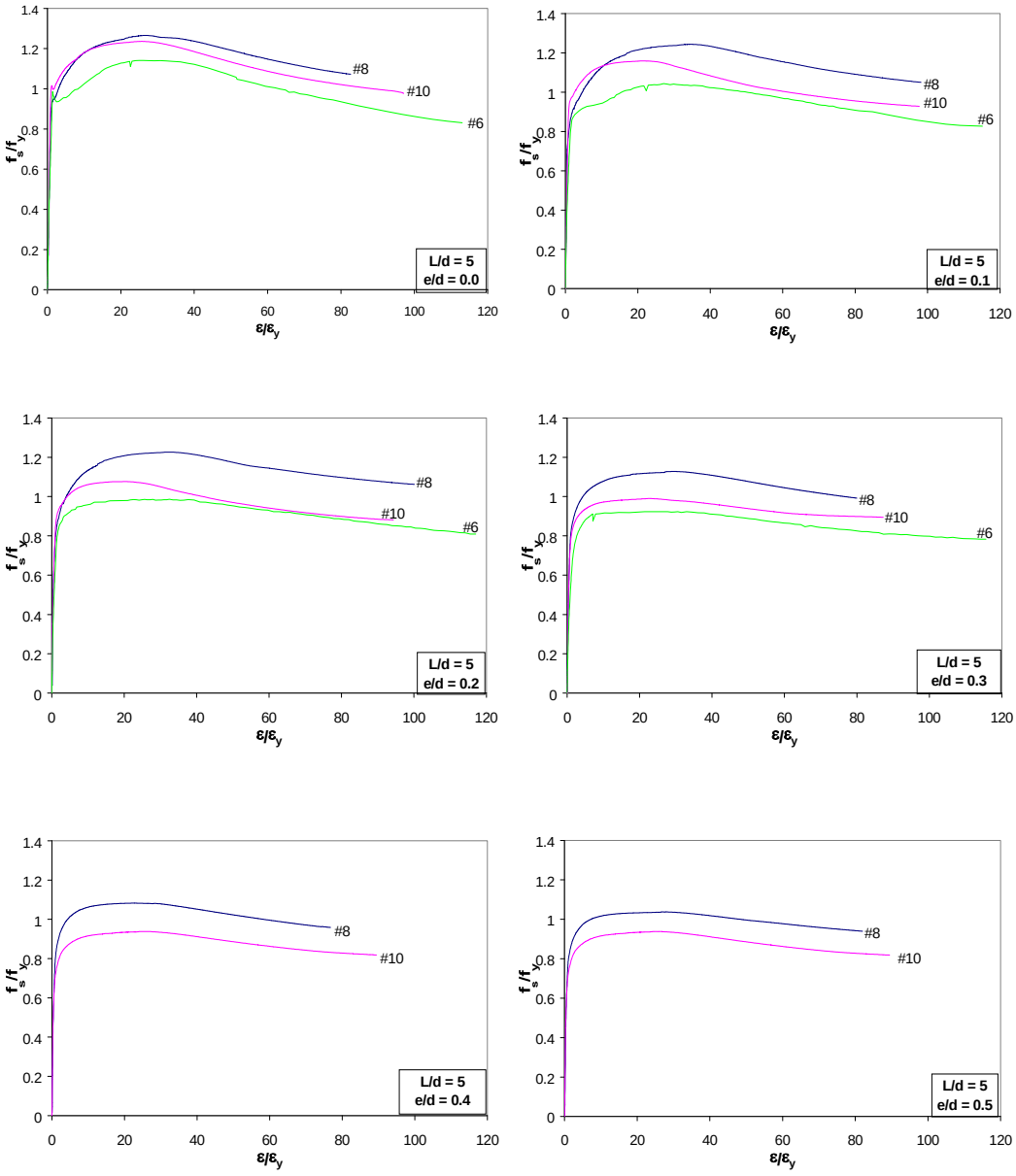

Figure 4.45 Normalized axial stress-strain curves for reinforcing bars with L/d=5

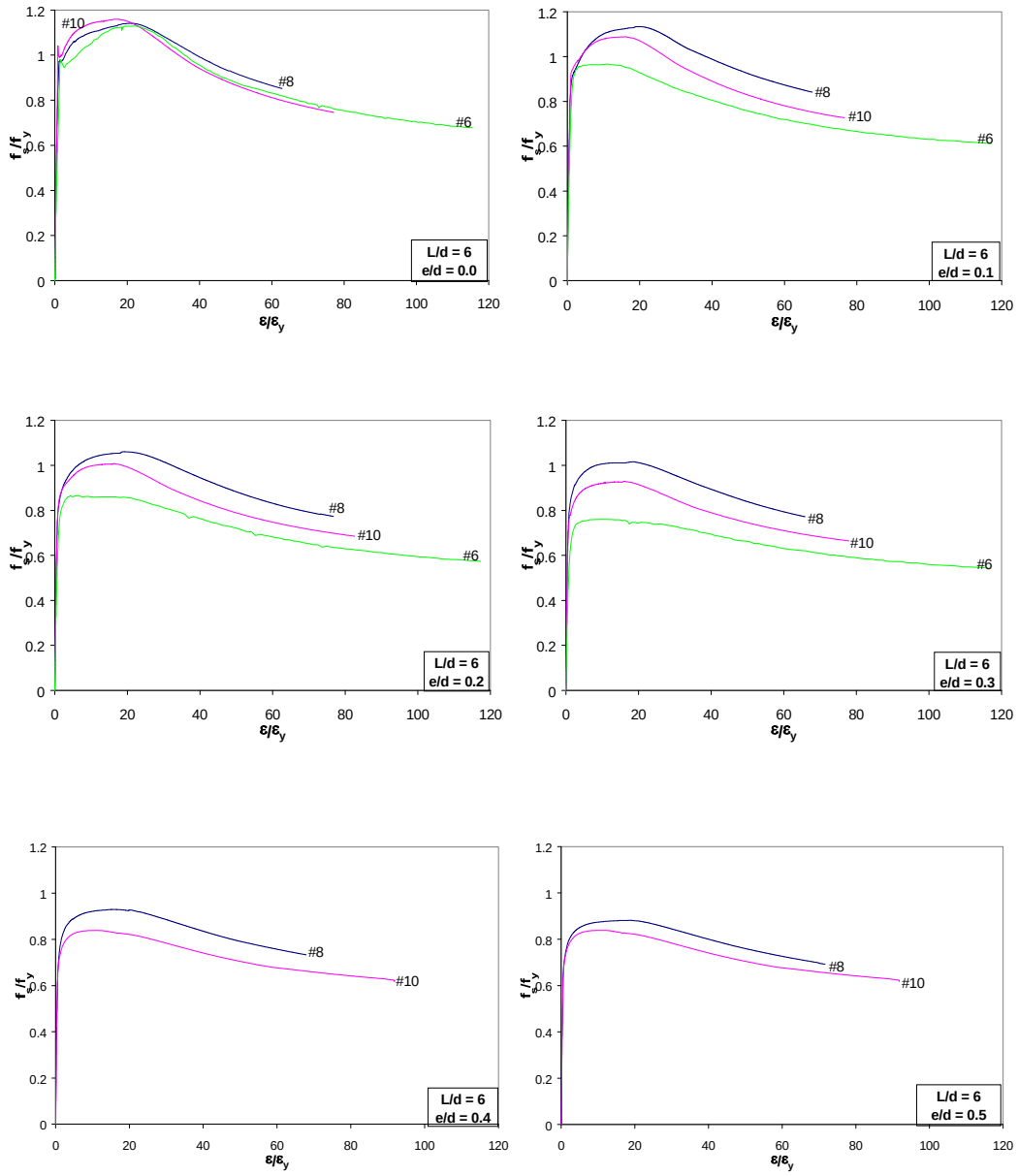

Figure 4.46 Normalized axial stress-strain curves of reinforcing bars with L/d=6

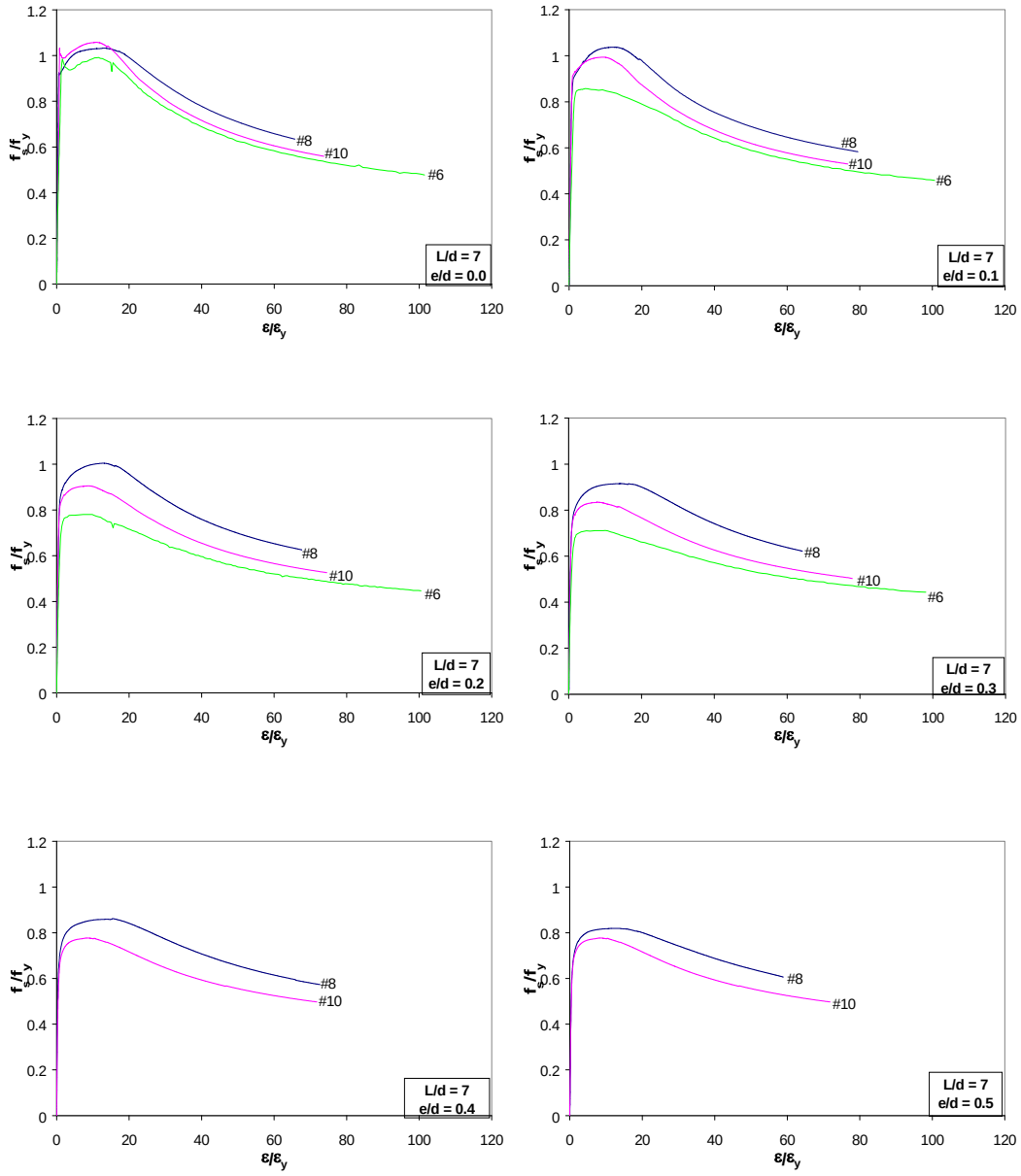

Figure 4.47 Normalized axial stress-strain curves of reinforcing bars with L/d=7

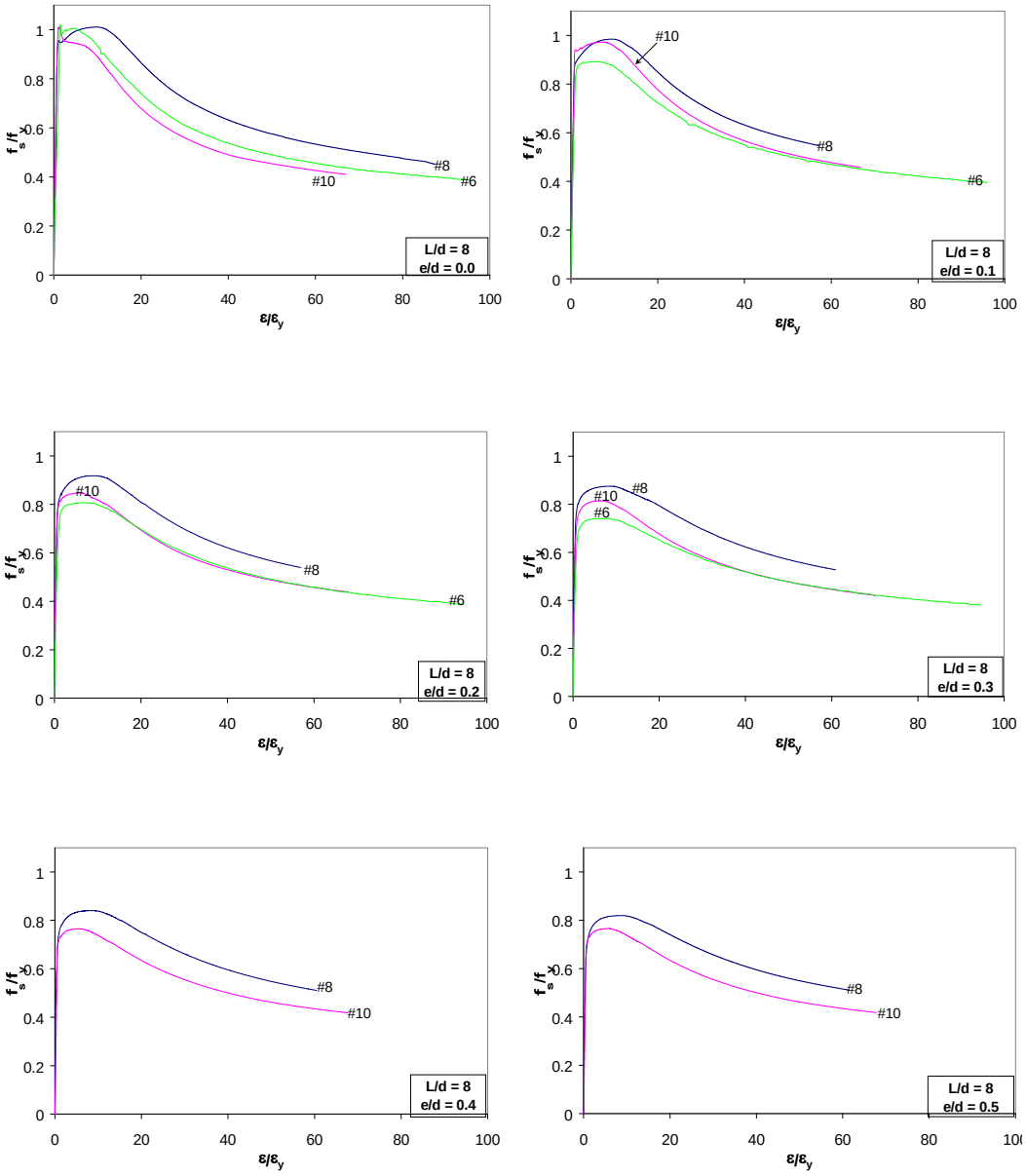

Figure 4.48 Normalized axial stress-strain curves of reinforcing bars with L/d=8

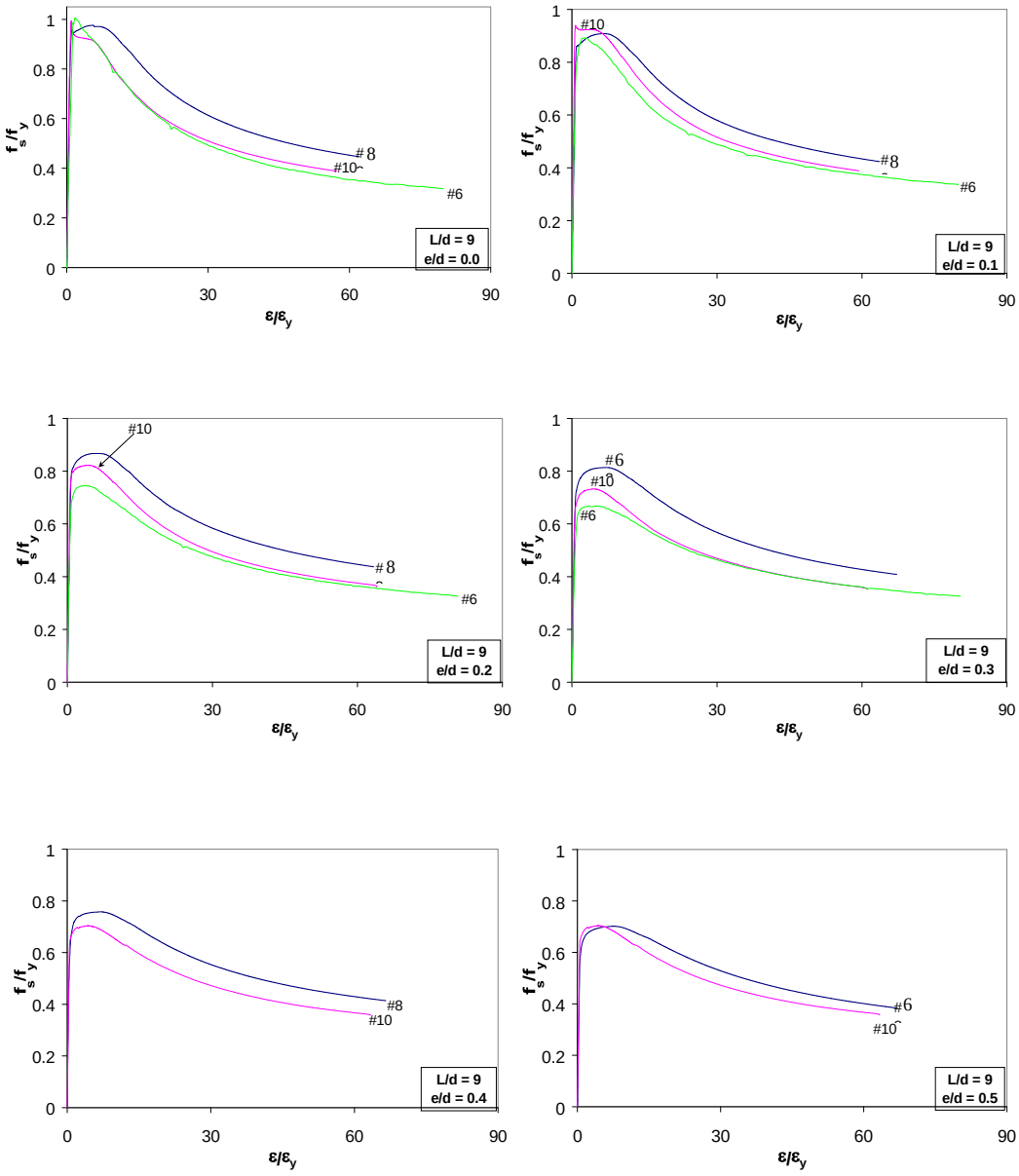

Figure 4.49 Normalized axial stress-strain curves of reinforcing bars with L/d=9

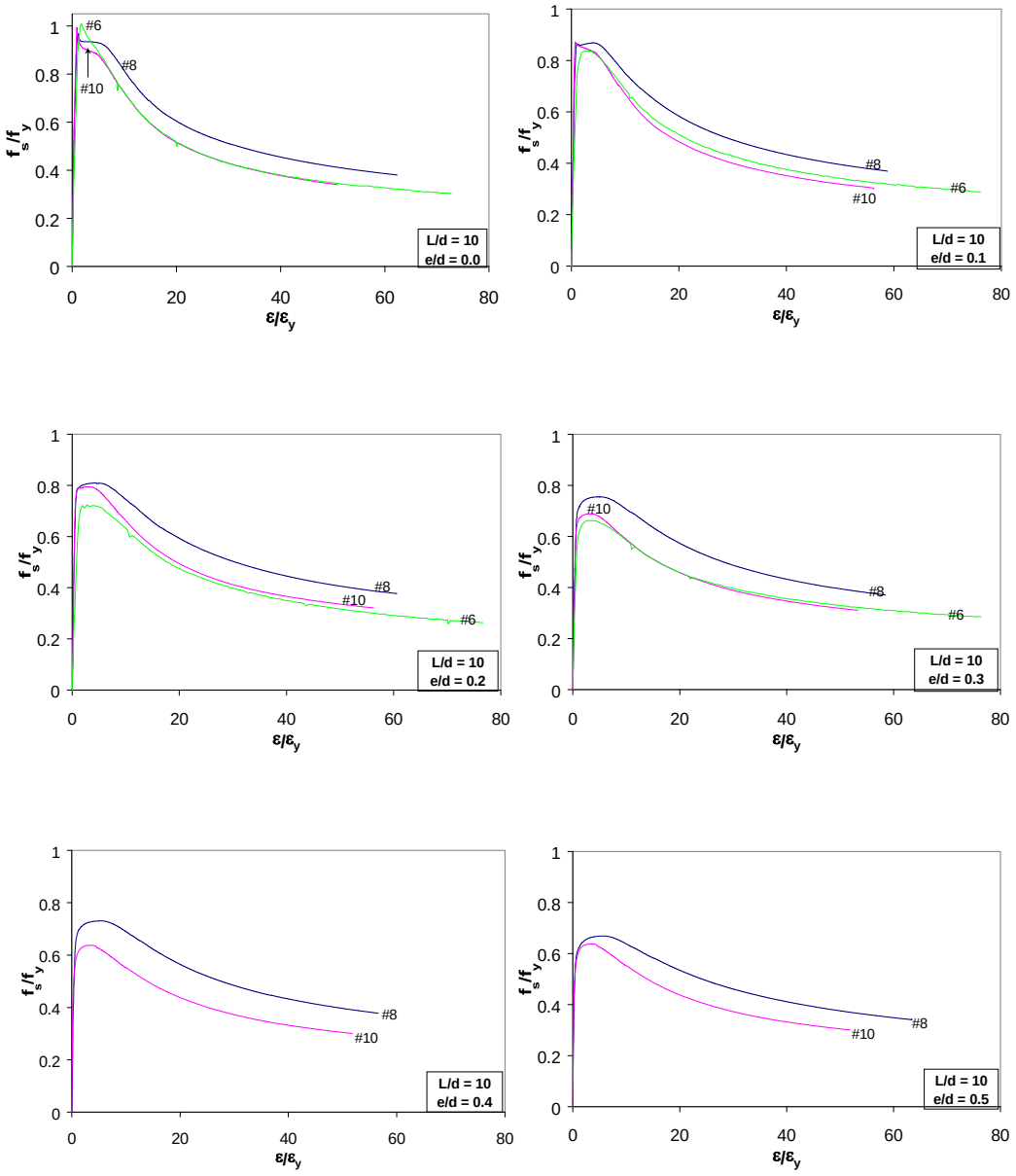

Figure 4.50 Normalized axial stress-strain curves of reinforcing bars with L/d=10

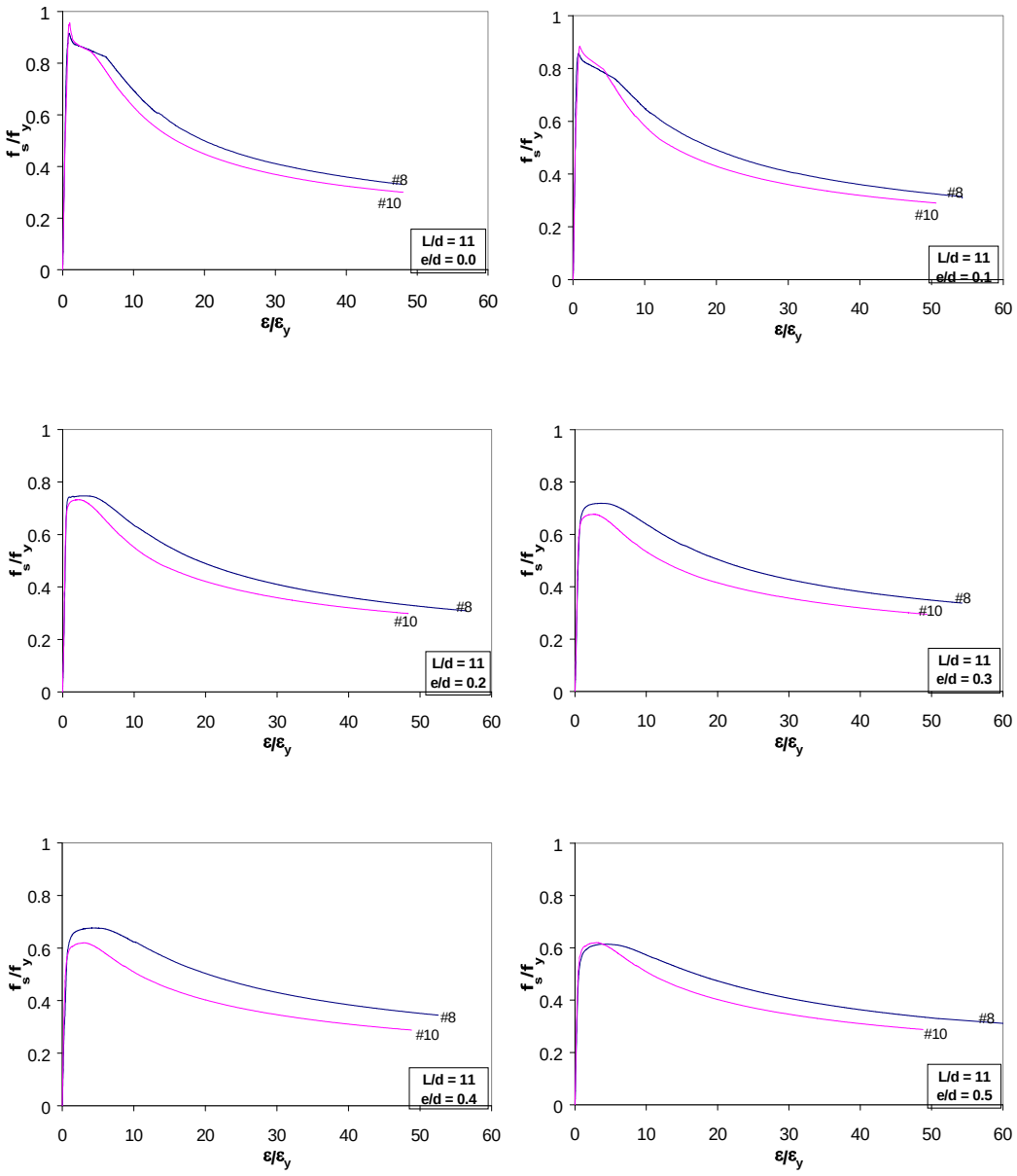

Figure 4.51 Normalized axial stress-strain curves of reinforcing bars with L/d=11

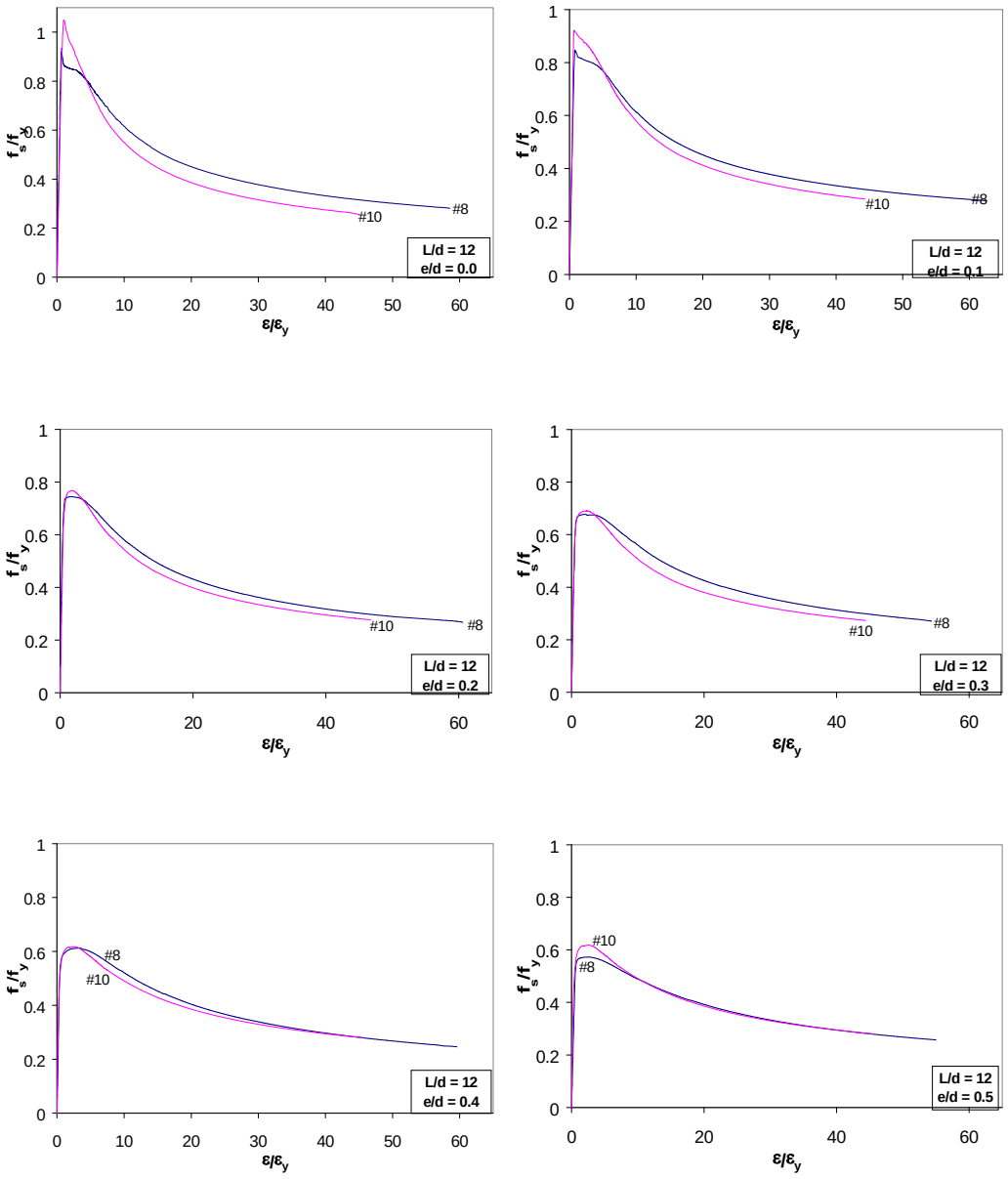

Figure 4.52 Normalized axial stress-strain curves of reinforcing bars with L/d=12

For L/d = 4, all bars displayed stable behavior for all e/d ratios. As can be observed in Figure 4.44, test specimens were able to sustain loads under considerably large inelastic deformations (up to $100\varepsilon_y$). Behavior of specimens with L/d = 5 are illustrated in Figure 4.45. It is interesting to note that for almost all cases presented in Figures 4.44 to 4.52 #8 bars showed larger normalized stresses in the post-buckling response than #10 bars. Similarly, #10 bars had greater normalized stresses in the descending branch of their response than #6 bars. As can be observed in Figure 4.43, #8, #10, and #6 bars have ultimate strength to yield strength ratios of 1.67, 1.44, and 1.32, respectively. Hence, it is possible to conclude that reinforcing bars that have a significantly high ultimate strength to yield strength ratio have a more stable post-buckling response and display higher normalized stresses. A close examination of Figures 4.44 to 4.52 reveals the following points:

- As the L/d ratio increases, the differences observed in the post-buckling response of #8, #10, and #6 bars decreases regardless of the e/d ratio.
- It is possible to conclude that strain hardening properties of reinforcing bars play an important role in determining the post-buckling response of specimens where inelastic buckling dominates the response. With increasing L/d ratio, and hence moving away from inelastic buckling towards elastic buckling, the influence of strain hardening properties on post-buckling response diminishes (Figures 4.44 to 4.52).
- For a given L/d ratio, an increase in e/d ratios results in insignificant differences between the relative position of the post-buckling responses of #8, #10, and #6 specimens.

As can be observed in Figures 4.44 to 4.52, the *L/d* ratio required to prevent premature buckling cannot be specified as a constant value, because it depends on the mechanical properties of the steel. With an increase in steel strength, the critical *L/d* ratio decreases as explained by Bresler and Gilbert (1961). It is important to note that Mau and El-Mabsout (1989), in their analytical study, identified that high strength steel has a critical *L/d* ratio of 7, and medium strength steel has one of 8. Experimental results reported in this Chapter support observations reported by Bresler and Gilbert (1961), Mau and El-Mabsout (1989), and Bayrak and Sheikh (2001).

CHAPTER 5
Summary, Conclusions and Recommendations

5.1 SUMMARY

Since buckling of longitudinal bars is generally not considered in conventional analytical procedures to determine the response of concrete column sections, behavior at large inelastic curvatures is generally over predicted with respect to strength and ductility. An extensive literature survey was undertaken to determine the availability of rational analytical models for longitudinal bar buckling in tied concrete columns. Research conducted by Bresler and Gilbert (1961), Mander et al. (1984), Scribner (1986), Russo (1988), Papia et al. (1988), Papia and Russo (1989), Mau and El-Mabsout (1989), Mau (1990), Monti and Nuti (1992), and Bayrak and Sheikh (2001) were studied herein. Different analytical approaches to predict the buckling behavior of longitudinal reinforcement were encountered in the literature, but most techniques did not represent all factors involved in the complex phenomenon of longitudinal bar buckling in concrete columns. Bayrak and Sheikh (2001) developed a plastic hinge analysis technique to predict the deformation capacities of concrete members under cyclic loading taking into consideration the bar buckling behavior and the interaction between the concrete core and the reinforcing cage. However, they did not develop a closed-form constitutive relationship due to the lack of an extensive database. They reported that in order to develop a constitutive model, reinforcing bars with different material properties needed to be tested. With this motivation an extensive literature survey was conducted to identify all of the experimental data available in the literature. The literature survey revealed the

fact that the only available data consisted of four bars tested by Mander et al. (1984), nine bars tested by Monti and Nuti (1992), and 56 bars tested by Bayrak and Sheikh (2001). It was concluded that the available data did not cover a wide range of bar sizes, length, or type.

The effect of unsupported length to bar diameter ratio (*L/d*), initial mid-span eccentricity to bar diameter ratio (*e/d*), and various material properties on the behavior of reinforcing bars subjected to compressive loads were studied. One hundred eight #8 bars and fifty four #10 bars were tested under monotonic compressive loading. The results for the different bar sizes (#8 and #10 bars) were compared to those reported by Bayrak and Sheikh (2001) for #6 bars.

5.2 CONCLUSIONS

The following conclusions can be reached based on the experimental study conducted:

1. For a given *L/d* ratio, an increase in the initial eccentricity (i.e. *e/d* ratio) resulted in a decrease in the load-carrying capacity and ductility.
2. For a given *e/d* ratio and bar size, the maximum axial load (P_{max}) occurred at approximately the same lateral deformation.
3. For reinforcing bars with $L/d = 4$, regardless of the *e/d* ratio, the load-carrying capacity was maintained while specimens experienced large inelastic deformations.
4. The increase in strength after yielding was lower as the *L/d* ratio was increased.
5. For a given *e/d* ratio, the strength and ductility decreased when the clear span between supports (*L/d* ratio) increased.

6. Number 8 bars displayed more ductility than #10 bars. This is attributed to the strain hardening behavior of #8 and #10 bars. The tension tests conducted illustrated that the f_{ut}/f_{yt} ratio for #8 bars was 1.67 and was 1.44 for #10 bars.
7. For cases where there is a high curvature ductility demand, tie spacing to longitudinal bar diameter ratios should be kept under 6. This is consistent with the relevant requirements (21.4.4.2) of ACI 318-02. It is important to note that for an L/d = 6, #8 bars displayed more ductility and stability than #10 bars or #6 bars. However, for design purposes it can be assumed that reinforcing bars with L/d = 6 will allow plastic hinge regions in columns to behave in a ductile manner.
8. For moderate curvature ductility demands, the spacing requirements discussed in item #7 can be relaxed, Based on the experimental evidence reported herein, for moderate levels of ductility an L/d ratio of 8 can be used as a limit.
9. For cases where longitudinal bars are expected to deform inelastically, L/d ratios greater than 8 should be avoided. Such large tie spacings (or unsupported bar lengths) should only be used in cases where no ductility is expected from a flexural member.

5.3 RECOMMENDATIONS FOR FURTHER RESEARCH

With the amount of data provided herein, it is possible to develop a unified constitutive model that predicts the stress-strain behavior of reinforcing bars under compression given the geometric and material properties of the bar. Then, buckling of reinforcing bars in concrete members can be incorporated in sectional

analyses. Hence, the development of a constitutive model for the compressive behavior of reinforcing bars should be performed next.

APPENDIX A

Actual eccentricities introduced at midspan of #8 and #10 reinforcing bars

Table A.1 Actual eccentricities introduced to #8 bars, d = 1.00-in

Specimen	*L/d*	*e/d*	*expected* e, in	*Actual e*, in	Specimen	*L/d*	*e/d*	*expected* e, in	*Actual e*, in	Specimen	*L/d*	*e/d*	*expected* e, in	*Actual e*, in
#1-8L4e0.0	4	0.0	0.0	0.0	#37-8L7e0.0	7	0.0	0.0	0.0	#73-8L10e0.0	10	0.0	0.0	0.0
#2-8L4e0.0	4	0.0	0.0	0.0	#38-8L7e0.0	7	0.0	0.0	0.0	#74-8L10e0.0	10	0.0	0.0	0.0
#3-8L4e0.1	4	0.1	0.1	0.101	#39-8L7e0.1	7	0.1	0.1	0.100	#75-8L10e0.1	10	0.1	0.1	0.101
#4-8L4e0.1	4	0.1	0.1	0.102	#40-8L7e0.1	7	0.1	0.1	0.102	#76-8L10e0.1	10	0.1	0.1	0.100
#5-8L4e0.2	4	0.2	0.2	0.200	#41-8L7e0.2	7	0.2	0.2	0.200	#77-8L10e0.2	10	0.2	0.2	0.200
#6-8L4e0.2	4	0.2	0.2	0.201	#42-8L7e0.2	7	0.2	0.2	0.201	#78-8L10e0.2	10	0.2	0.2	0.2005
#7-8L4e0.3	4	0.3	0.3	0.3005	#43-8L7e0.3	7	0.3	0.3	0.301	#79-8L10e0.3	10	0.3	0.3	0.301
#8-8L4e0.3	4	0.3	0.3	0.301	#44-8L7e0.3	7	0.3	0.3	0.301	#80-8L10e0.3	10	0.3	0.3	0.301
#9-8L4e0.4	4	0.4	0.4	0.400	#45-8L7e0.4	7	0.4	0.4	0.402	#81-8L10e0.4	10	0.4	0.4	0.401
#10-8L4e0.4	4	0.4	0.4	0.401	#46-8L7e0.4	7	0.4	0.4	0.4025	#82-8L10e0.4	10	0.4	0.4	0.401
#11-8L4e0.5	4	0.5	0.5	0.501	#47-8L7e0.5	7	0.5	0.5	0.501	#83-8L10e0.5	10	0.5	0.5	0.501
#12-8L4e0.5	4	0.5	0.5	0.502	#48-8L7e0.5	7	0.5	0.5	0.502	#84-8L10e0.5	10	0.5	0.5	0.502
#13-8L5e0.0	5	0.0	0.0	0.0	#49-8L8e0.0	8	0.0	0.0	0.0	#85-8L11e0.0	11	0.0	0.0	0.0
#14-8L5e0.0	5	0.0	0.0	0.0	#50-8L8e0.0	8	0.0	0.0	0.0	#86-8L11e0.0	11	0.0	0.0	0.0
#15-8L5e0.1	5	0.1	0.1	0.0995	#51-8L8e0.1	8	0.1	0.1	0.101	#87-8L11e0.1	11	0.1	0.1	0.101
#16-8L5e0.1	5	0.1	0.1	0.100	#52-8L8e0.1	8	0.1	0.1	0.101	#88-8L11e0.1	11	0.1	0.1	0.101
#17-8L5e0.2	5	0.2	0.2	0.2005	#53-8L8e0.2	8	0.2	0.2	0.2005	#89-8L11e0.2	11	0.2	0.2	0.199
#18-8L5e0.2	5	0.2	0.2	0.200	#54-8L8e0.2	8	0.2	0.2	0.200	#90-8L11e0.2	11	0.2	0.2	0.199
#19-8L5e0.3	5	0.3	0.3	0.3015	#55-8L8e0.3	8	0.3	0.3	0.301	#91-8L11e0.3	11	0.3	0.3	0.300
#20-8L5e0.3	5	0.3	0.3	0.300	#56-8L8e0.3	8	0.3	0.3	0.300	#92-8L11e0.3	11	0.3	0.3	0.3015
#21-8L5e0.4	5	0.4	0.4	0.401	#57-8L8e0.4	8	0.4	0.4	0.4015	#93-8L11e0.4	11	0.4	0.4	0.401
#22-8L5e0.4	5	0.4	0.4	0.403	#58-8L8e0.4	8	0.4	0.4	0.402	#94-8L11e0.4	11	0.4	0.4	0.400
#23-8L5e0.5	5	0.5	0.5	0.502	#59-8L8e0.5	8	0.5	0.5	0.502	#95-8L11e0.5	11	0.5	0.5	0.502
#24-8L5e0.5	5	0.5	0.5	0.502	#60-8L8e0.5	8	0.5	0.5	0.502	#96-8L11e0.5	11	0.5	0.5	0.504
#25-8L6e0.0	6	0.0	0.0	0.0	#61-8L9e0.0	9	0.0	0.0	0.0	#97-8L12e0.0	12	0.0	0.0	0.0
#26-8L6e0.0	6	0.0	0.0	0.0	#62-8L9e0.0	9	0.0	0.0	0.0	#98-8L12e0.0	12	0.0	0.0	0.0
#27-8L6e0.1	6	0.1	0.1	0.1015	#63-8L9e0.1	9	0.1	0.1	0.100	#99-8L12e0.1	12	0.1	0.1	0.0995
#28-8L6e0.1	6	0.1	0.1	0.100	#64-8L9e0.1	9	0.1	0.1	0.099	#100-8L12e0.1	12	0.1	0.1	0.099
#29-8L6e0.2	6	0.2	0.2	0.202	#65-8L9e0.2	9	0.2	0.2	0.201	#101-8L12e0.2	12	0.2	0.2	0.201
#30-8L6e0.2	6	0.2	0.2	0.201	#66-8L9e0.2	9	0.2	0.2	0.2005	#102-8L12e0.2	12	0.2	0.2	0.201
#31-8L6e0.3	6	0.3	0.3	0.303	#67-8L9e0.3	9	0.3	0.3	0.3005	#103-8L12e0.3	12	0.3	0.3	0.300
#32-8L6e0.3	6	0.3	0.3	0.303	#68-8L9e0.3	9	0.3	0.3	0.300	#104-8L12e0.3	12	0.3	0.3	0.302
#33-8L6e0.4	6	0.4	0.4	0.400	#69-8L9e0.4	9	0.4	0.4	0.4015	#105-8L12e0.4	12	0.4	0.4	0.4005
#34-8L6e0.4	6	0.4	0.4	0.4025	#70-8L9e0.4	9	0.4	0.4	0.400	#106-8L12e0.4	12	0.4	0.4	0.400
#35-8L6e0.5	6	0.5	0.5	0.504	#71-8L9e0.5	9	0.5	0.5	0.503	#107-8L12e0.5	12	0.5	0.5	0.501
#36-8L6e0.5	6	0.5	0.5	0.502	#72-8L9e0.5	9	0.5	0.5	0.501	#108-8L12e0.5	12	0.5	0.5	0.504

Table A.2 Actual eccentricities introduced to #10 bars, d = 1.27-in

Specimen	*L/d*	*e/d*	*expected* e, in	*Actual e*, in	Specimen	*L/d*	*e/d*	*expected* e, in	*Actual e*, in
#1-10L4e0.0	4	0.0	0.0	0.0	#28-10L8e0.3	8	0.3	0.381	0.382
#2-10L4e0.1	4	0.1	0.127	0.127	#29-10L8e0.4	8	0.4	0.508	0.5085
#3-10L4e0.2	4	0.2	0.254	0.254	#30-10L8e0.5	8	0.5	0.635	0.636
#4-10L4e0.3	4	0.3	0.381	0.383	#31-10L9e0.0	9	0.0	0.0	0.0
#5-10L4e0.4	4	0.4	0.508	0.506	#32-10L9e0.1	9	0.1	0.127	0.125
#6-10L4e0.5	4	0.5	0.635	0.634	#33-10L9e0.2	9	0.2	0.254	0.2545
#7-10L5e0.0	5	0.0	0.0	0.0	#34-10L9e0.3	9	0.3	0.381	0.382
#8-10L5e0.1	5	0.1	0.127	0.126	#35-10L9e0.4	9	0.4	0.508	0.510
#9-10L5e0.2	5	0.2	0.254	0.255	#36-10L9e0.5	9	0.5	0.635	0.637
#10-10L5e0.3	5	0.3	0.381	0.383	#37-10L10e0.0	10	0.0	0.0	0.0
#11-10L5e0.4	5	0.4	0.508	0.508	#38-10L10e0.1	10	0.1	0.127	0.127
#12-10L5e0.5	5	0.5	0.635	0.637	#39-10L10e0.2	10	0.2	0.254	0.255
#13-10L6e0.0	6	0.0	0.0	0.0	#40-10L10e0.3	10	0.3	0.381	0.384
#14-10L6e0.1	6	0.1	0.127	0.127	#41-10L10e0.4	10	0.4	0.508	0.509
#15-10L6e0.2	6	0.2	0.254	0.254	#42-10L10e0.5	10	0.5	0.635	0.639
#16-10L6e0.3	6	0.3	0.381	0.3815	#43-10L11e0.0	11	0.0	0.0	0.0
#17-10L6e0.4	6	0.4	0.508	0.508	#44-10L11e0.1	11	0.1	0.127	0.127
#18-10L6e0.5	6	0.5	0.635	0.636	#45-10L11e0.2	11	0.2	0.254	0.255
#19-10L7e0.0	7	0.0	0.0	0.0	#46-10L11e0.3	11	0.3	0.381	0.381
#20-10L7e0.1	7	0.1	0.127	0.126	#47-10L11e0.4	11	0.4	0.508	0.5085
#21-10L7e0.2	7	0.2	0.254	0.255	#48-10L11e0.5	11	0.5	0.635	0.6355
#22-10L7e0.3	7	0.3	0.381	0.382	#49-10L12e0.0	12	0.0	0.0	0.0
#23-10L7e0.4	7	0.4	0.508	0.510	#50-10L12e0.1	12	0.1	0.127	0.128
#24-10L7e0.5	7	0.5	0.635	0.637	#51-10L12e0.2	12	0.2	0.254	0.255
#25-10L8e0.0	8	0.0	0.0	0.0	#52-10L12e0.3	12	0.3	0.381	0.381
#26-10L8e0.1	8	0.1	0.127	0.127	#53-10L12e0.4	12	0.4	0.508	0.508
#27-10L8e0.2	8	0.2	0.254	0.254	#54-10L12e0.5	12	0.5	0.635	0.636

APPENDIX B
Interpolation Program

An interpolation program was used to calculate the average curve when two specimens were tested for the same *L/d-e/d* combination. The program was written in Microsoft Visual Basic 6.0 for application on Microsoft Excel 2000. The data was arranged in a spreadsheet and the interpolated output was brought into columns inside the same spreadsheet.

The variables were defined as follows:

Range 1	the maximum values of strains for which the stress will be interpolated corresponding to what the collected data allowed for in specimen 1
Range 2	the maximum values of strains for which the stress will be interpolated corresponding to what the collected data allowed for in specimen 2
e	the incremented strain value for which the stress was being interpolated
x1	the next value of strain that was lower than e
x2	the next value of strain that was larger than e
y1	the value of stress correspondent to x1
y2	the value of stress correspondent to x2
f	the interpolated value of stress corresponding to e
i	counter variable for the amount of strain values for which interpolation of stresses was performed

j, m	counter variables to change from cell to cell to the next strain value for which interpolation of stress was performed
k, n	counter variables to change from cell to cell to store the interpolated stress values

The program lines are as follows:

```
Public Range1, Range2, e, x1, x2, y1, y2, f As Double
Public i, j, k, l, m, n As Integer
```

```
Sub program()
   i = 1
   j = 0
   k = 1
   l = 1
   m = 0
   n = 1
   Range1 = Worksheets("AVERAGE").Range("L3")
   Range2 = Worksheets("AVERAGE").Range("M3")
   For i = 1 To Range1
      e = 0.00005
      e = e * i
      j = j + 1
      Worksheets("AVERAGE").Range("C4").Offset(j, 0) = e
      k = k - 1
10     k = k + 1
      x1 = Worksheets("AVERAGE").Range("A4").Offset(k, 0)
      x2 = Worksheets("AVERAGE").Range("A5").Offset(k, 0)
      y1 = Worksheets("AVERAGE").Range("B4").Offset(k, 0)
      y2 = Worksheets("AVERAGE").Range("B5").Offset(k, 0)
      If e < x1 Then
         GoTo 10
      End If
      If e > x1 Then
         If e < x2 Then
         f = y1 - (((x1 - e) / (x1 - x2)) * (y1 - y2))
         Worksheets("AVERAGE").Range("D4").Offset(j, 0) = f
         Else: GoTo 10
         End If
      End If
      If i = Range1 Then
      GoTo 20
      End If
```

```
    Next i
20  For l = 1 To Range2
      e = 0.00005
      e = e * l
      m = m + 1
      Worksheets("AVERAGE").Range("G4").Offset(m, 0) = e
      n = n - 1
30      n = n + 1
      x1 = Worksheets("AVERAGE").Range("E4").Offset(n, 0)
      x2 = Worksheets("AVERAGE").Range("E5").Offset(n, 0)
      y1 = Worksheets("AVERAGE").Range("F4").Offset(n, 0)
      y2 = Worksheets("AVERAGE").Range("F5").Offset(n, 0)
      If e < x1 Then
         GoTo 30
      End If
      If e > x1 Then
         If e < x2 Then
         f = y1 - (((x1 - e) / (x1 - x2)) * (y1 - y2))
         Worksheets("AVERAGE").Range("H4").Offset(l, 0) = f
         Else: GoTo 30
         End If
      End If
      If l = Range2 Then
      GoTo 40
      End If
    Next l
40 End Sub
```

A similar program was used to interpolate the results obtained for the load vs. lateral deformation curves where two specimens were tested (#8 reinforcing bars). The only change was that the increments of displacements for which the load was being interpolated was performed every 0.001″ and not 0.00005 like for the strains in the stresses interpolation.

APPENDIX C

Test Results

The figures presented in this appendix illustrate the results obtained for all *L/d-e/d* combinations for the #8 and #10 bars. Each figure contains three plots in which the axial load vs. axial deformation, the stress-strain curve under compression, and the load vs. lateral deformation relationships are presented.

The variables shown in the plot are defined as follows:

P	axial compressive load, kips
Δ_V	vertical deformation, inches
f_s	axial stress, ksi
ε_c	axial strain in compression, ksi
Δ_L	lateral deformation, inches
#x	test specimen number
#x LP1	axial load vs. vertical deformation curve from linear potentiometer #1 for specimen *#x*
#x LP2	axial load vs. vertical deformation curve from linear potentiometer #2 for specimen *#x*
#x AVERAGE	average axial load vs. vertical deformation curve of linear potentiometer #1 and #2 for specimen *#x*
AVERAGE	average stress-strain curve or average axial load vs. lateral deformation curve of two specimens (*#x*)

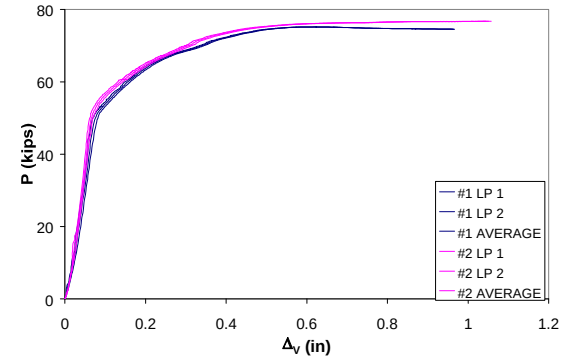

(a)

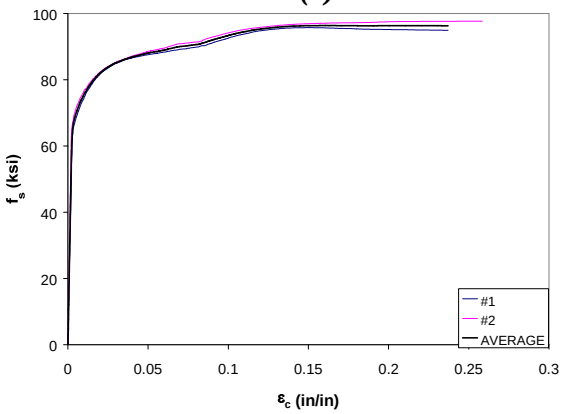

(b)

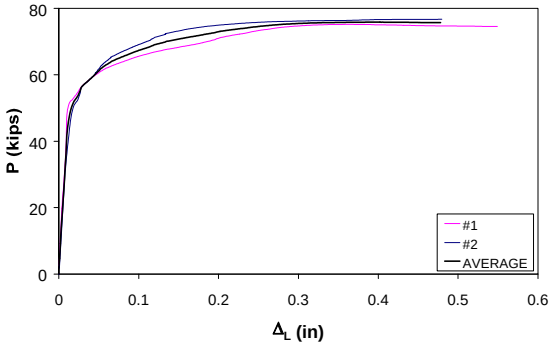

(c)

Figure C.1 Experimental load-deformation plots of #8 bars with L/d = 4 and e/d = 0.0

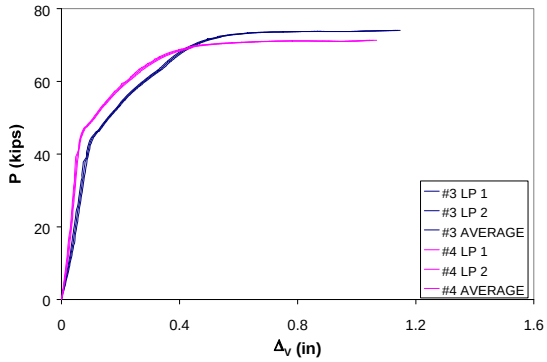

(a)

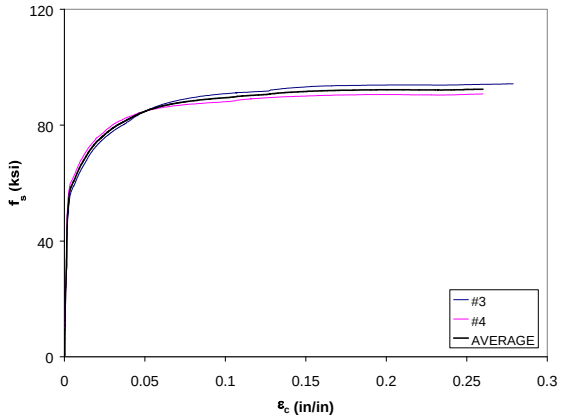

(b)

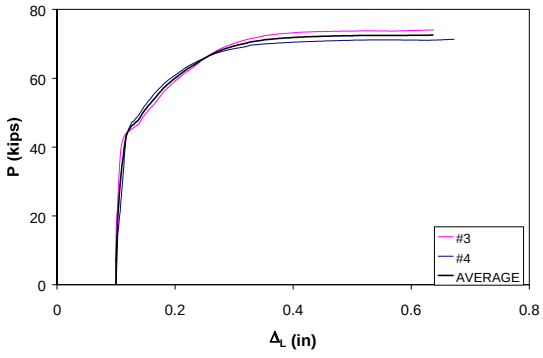

(c)

Figure C.2 Experimental load-deformation plots of #8 bars with L/d = 4 and e/d = 0.1

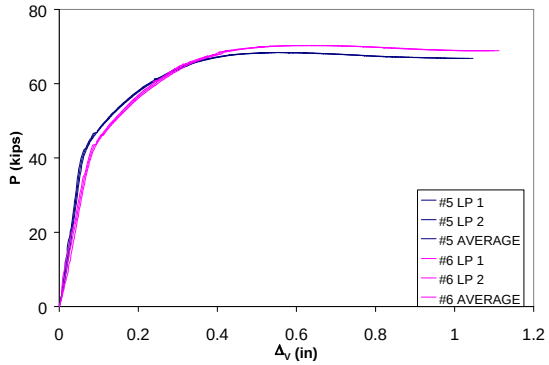

(a)

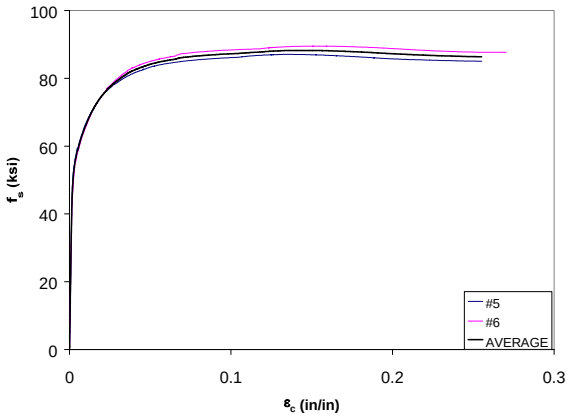

(b)

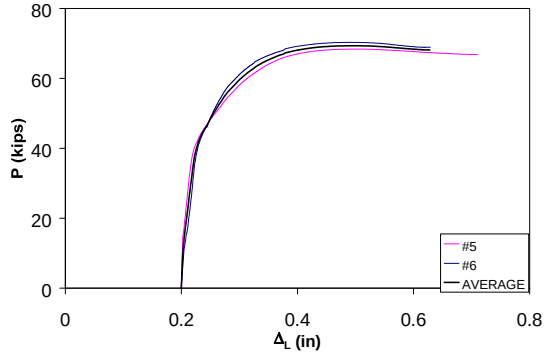

(c)

Figure C.3 Experimental load-deformation plots of #8 bars with L/d = 4 and e/d = 0.2

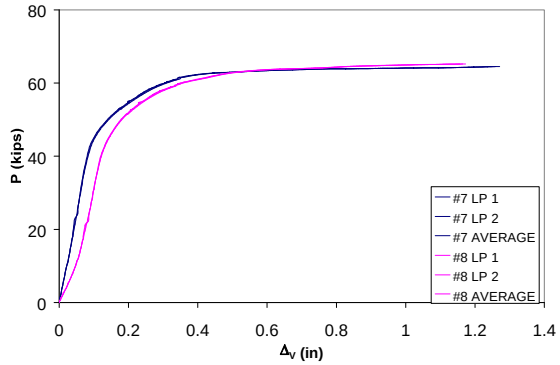

(a)

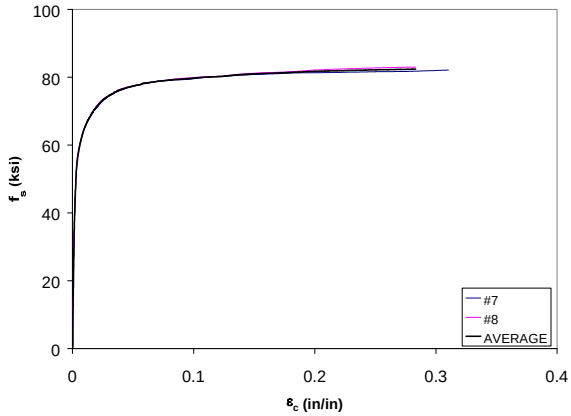

(b)

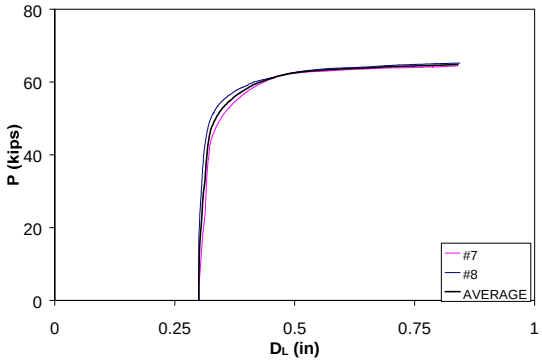

(c)

Figure C.4 Experimental load-deformation plots of #8 bars with L/d = 4 and e/d = 0.3

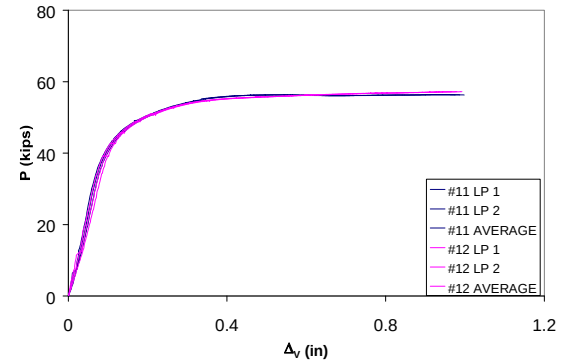

(a)

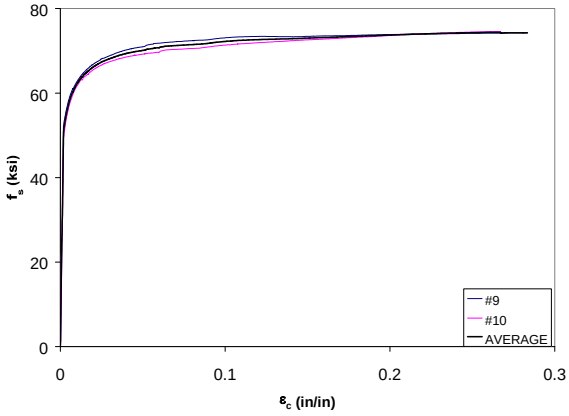

(b)

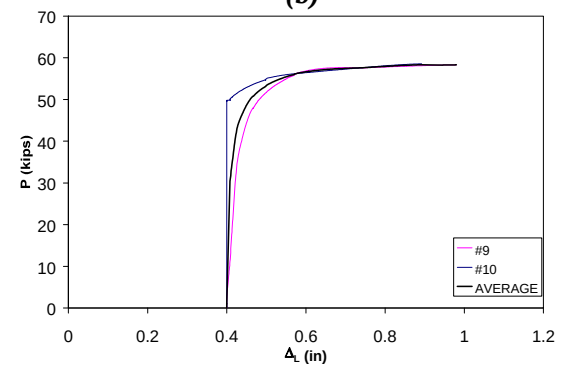

(c)

Figure C.5 Experimental load-deformation plots of #8 bars with L/d = 4 and e/d = 0.4

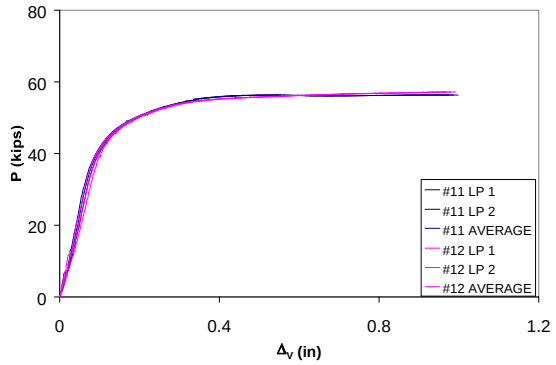

(a)

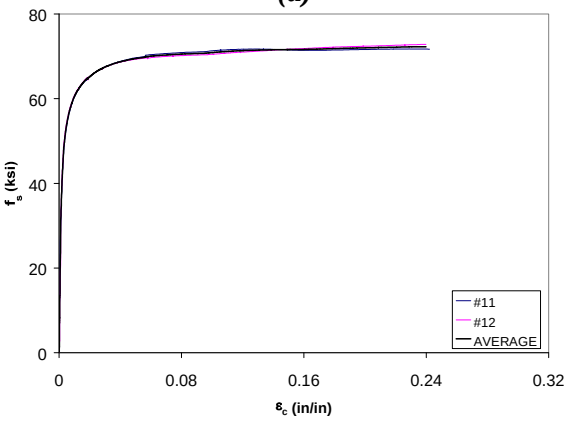

(b)

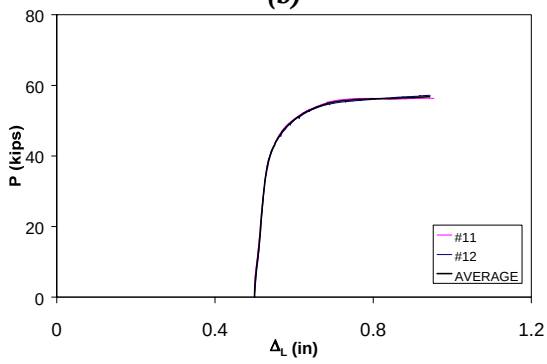

(c)

Figure C.6 Experimental load-deformation plots of #8 bars

with L/d = 4 and e/d = 0.5

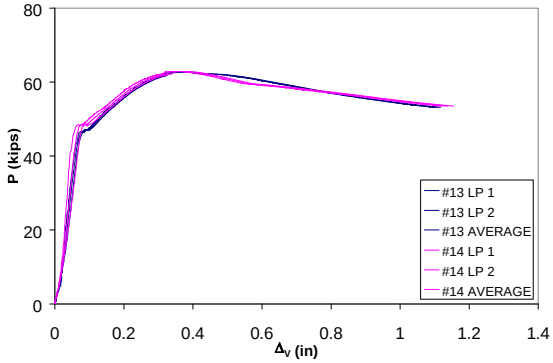

(a)

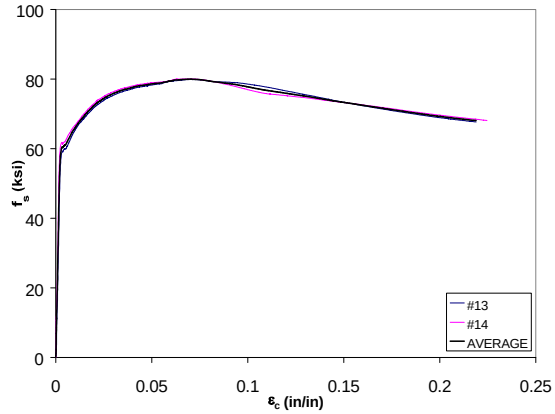

(b)

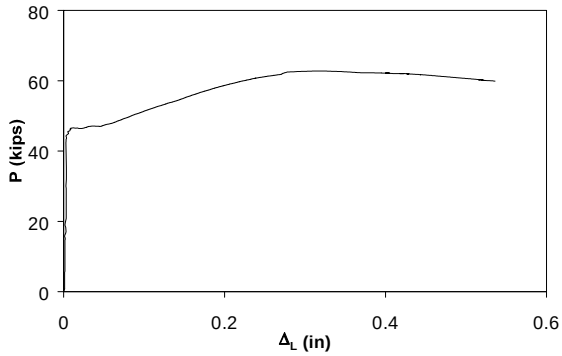

(c)

Figure C.7 Experimental load-deformation plots of #8 bars

with L/d = 5 and e/d = 0.0

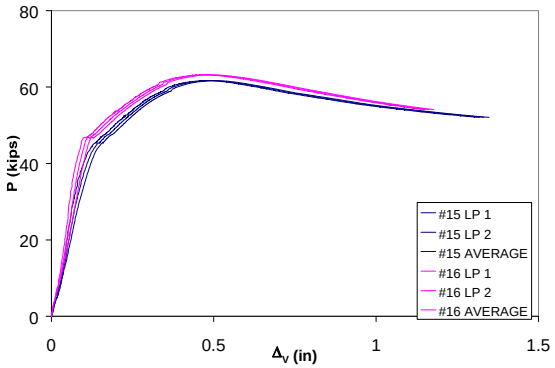

(a)

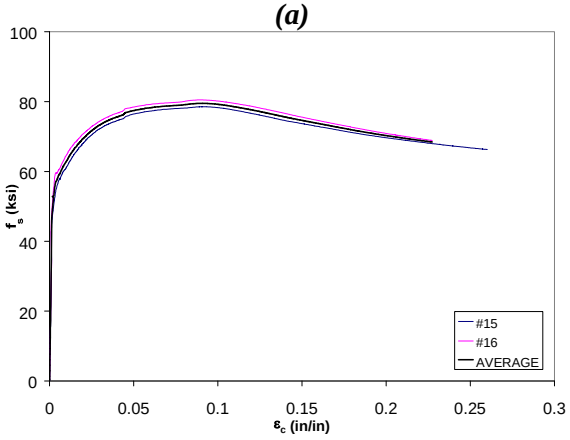

(b)

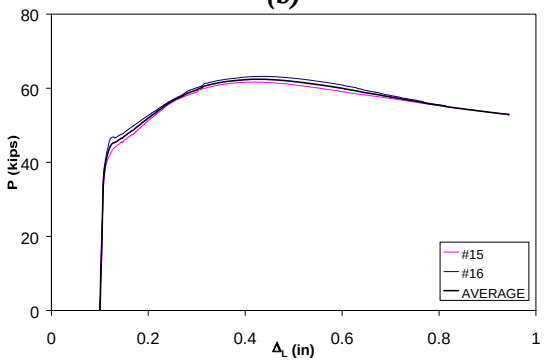

(c)

Figure C.8 Experimental load-deformation plots of #8 bars with L/d = 5 and e/d = 0.1

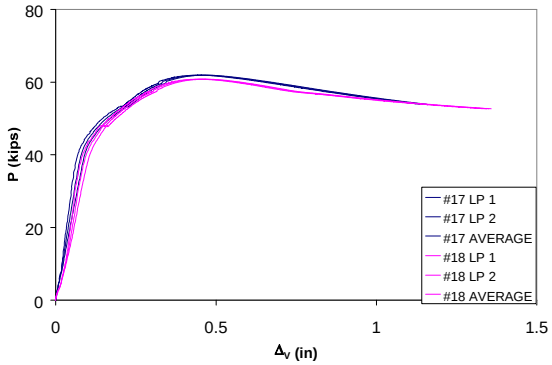

(a)

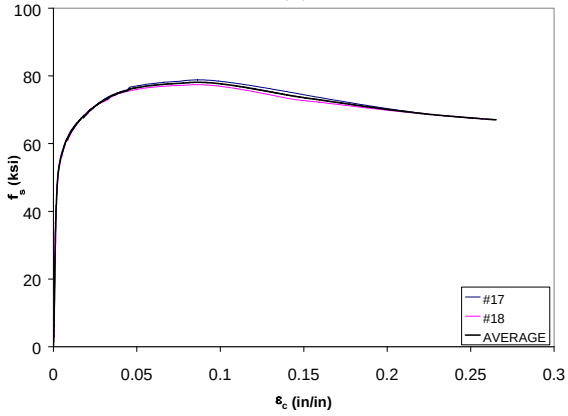

(b)

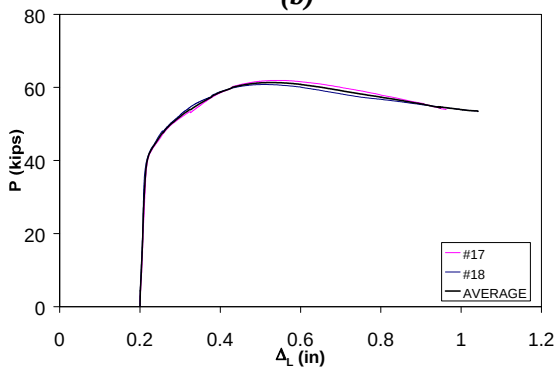

(c)

Figure C.9 Experimental load-deformation plots of #8 bars with L/d = 5 and e/d = 0.2

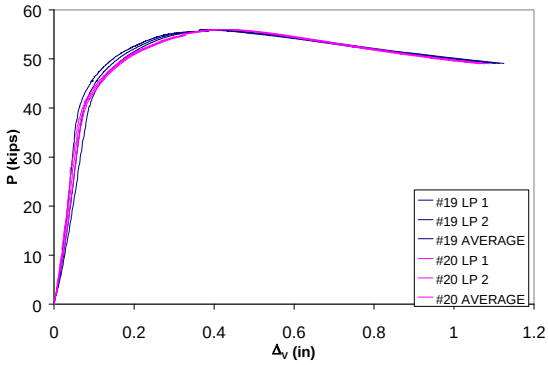

(a)

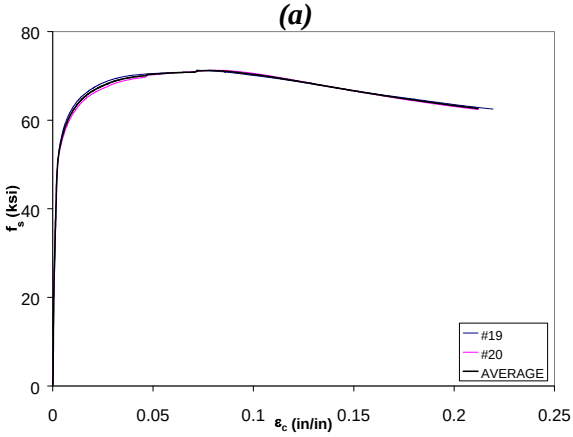

(b)

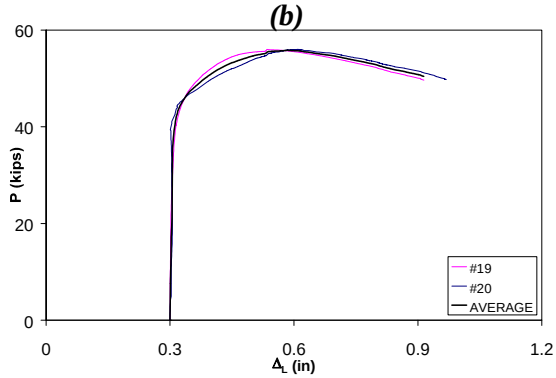

(c)

Figure C.10 Experimental load-deformation plots of #8 bars with L/d = 5 and e/d = 0.3

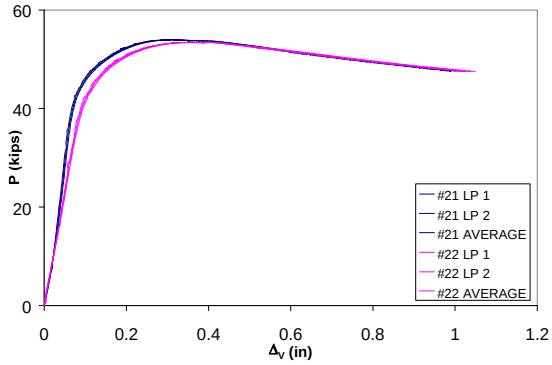

(a)

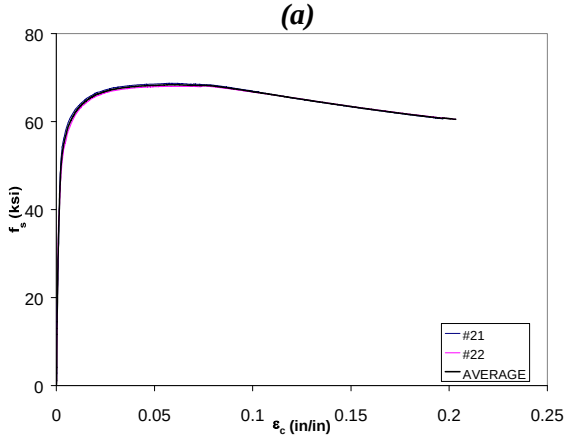

(b)

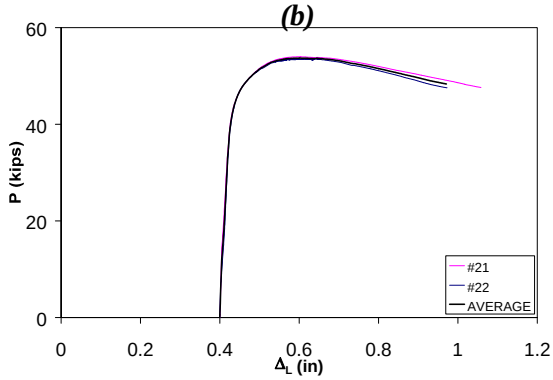

(c)

Figure C.11 Experimental load-deformation plots of #8 bars with L/d = 5 and e/d = 0.4

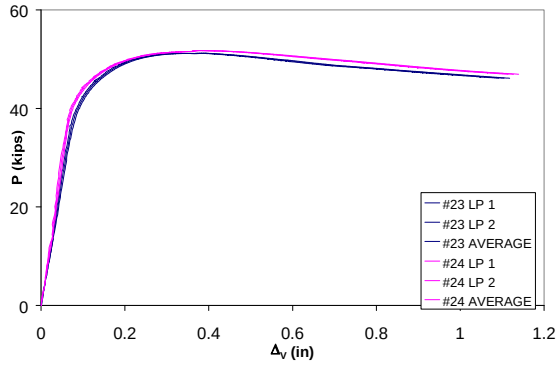

(a)

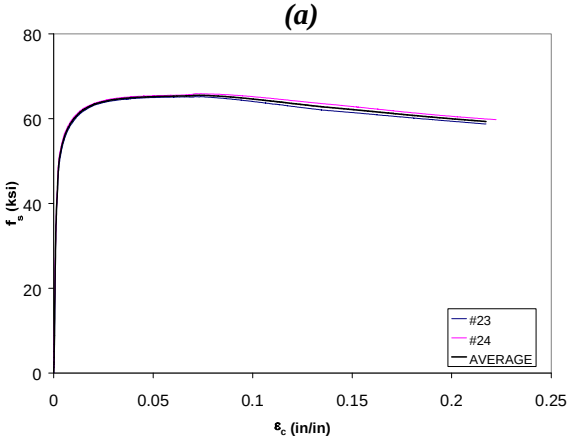

(b)

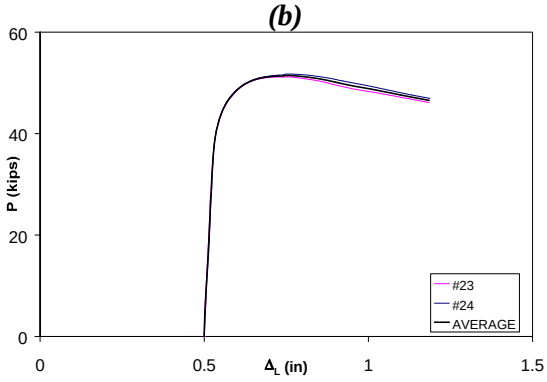

(c)

Figure C.12 Experimental load-deformation plots of #8 bars with L/d = 5 and e/d = 0.5

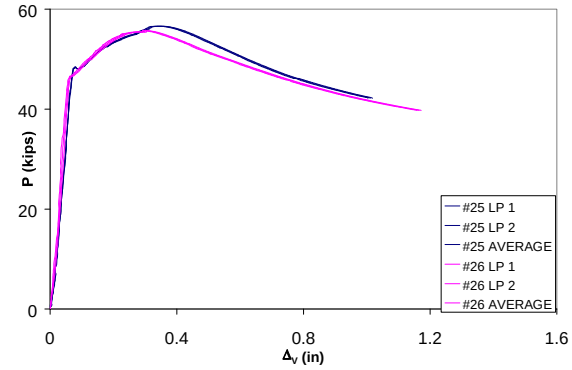

(a)

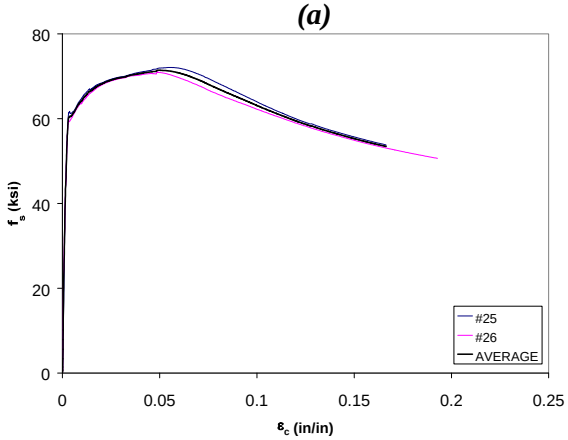

(b)

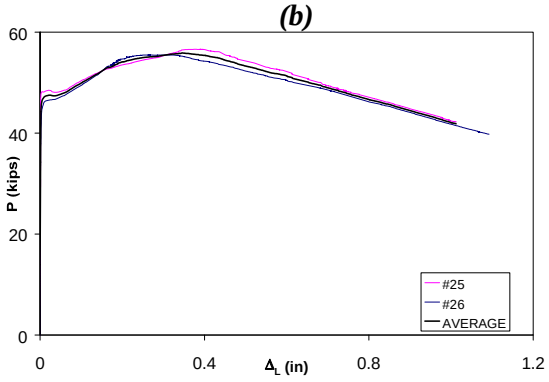

(c)

Figure C.13 Experimental load-deformation plots of #8 bars with L/d = 6 and e/d = 0.0

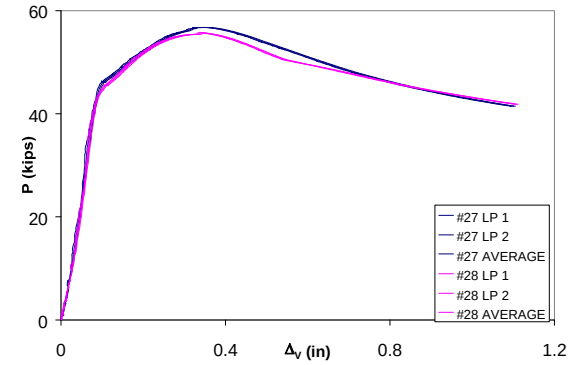

(a)

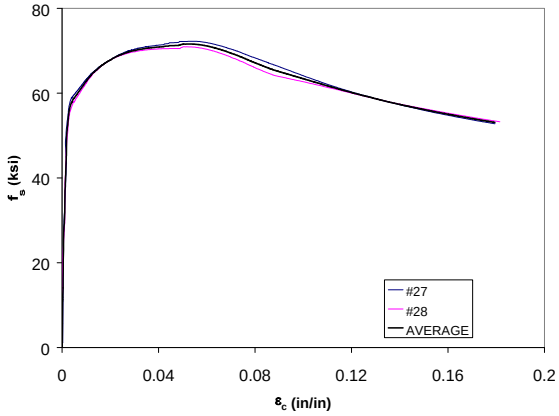

(b)

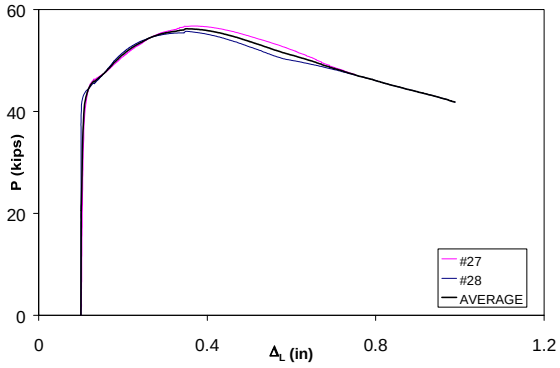

(c)

Figure C.14 Experimental load-deformation plots of #8 bars with L/d = 6 and e/d = 0.1

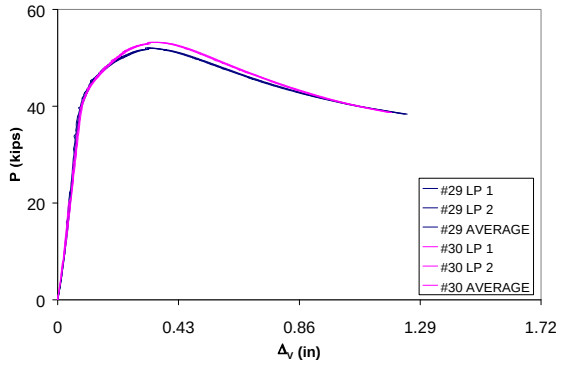

(a)

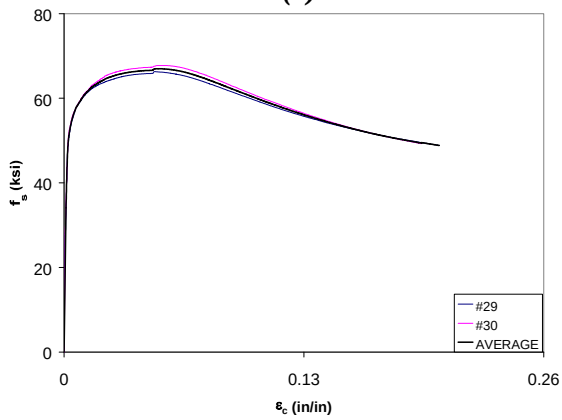

(b)

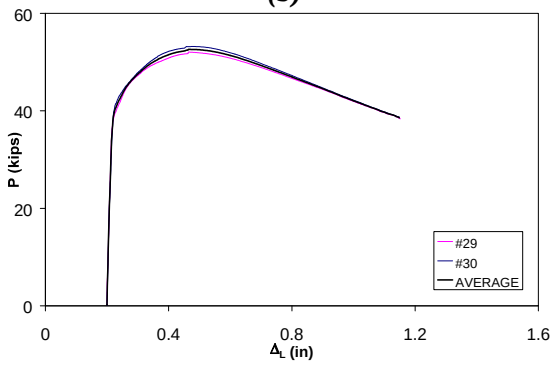

(c)

Figure C.15 Experimental load-deformation plots of #8 bars with L/d = 6 and e/d = 0.2

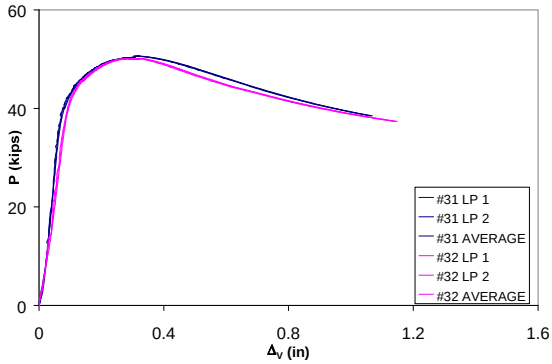

(a)

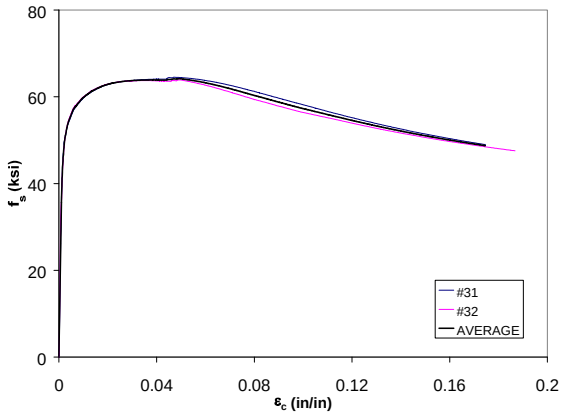

(b)

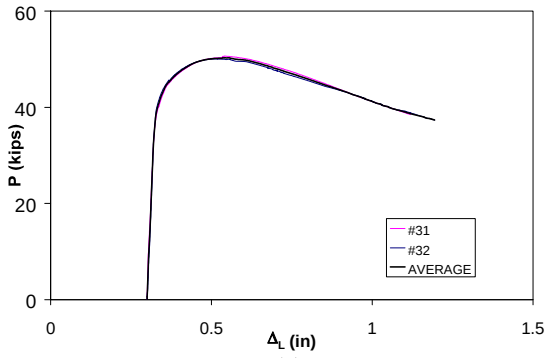

(c)

Figure C.16 Experimental load-deformation plots of #8 bars

with L/d = 6 and e/d = 0.3

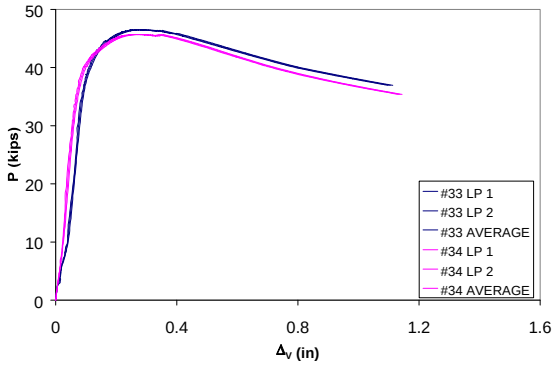

(a)

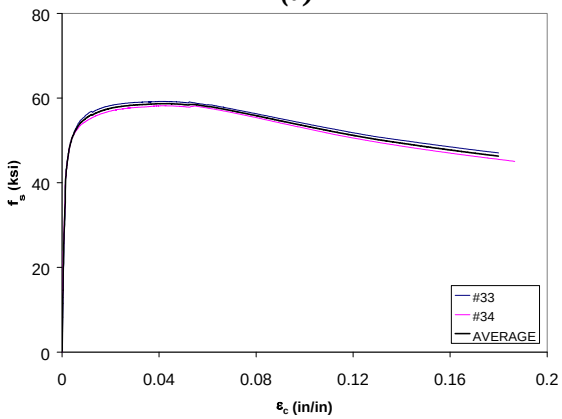

(b)

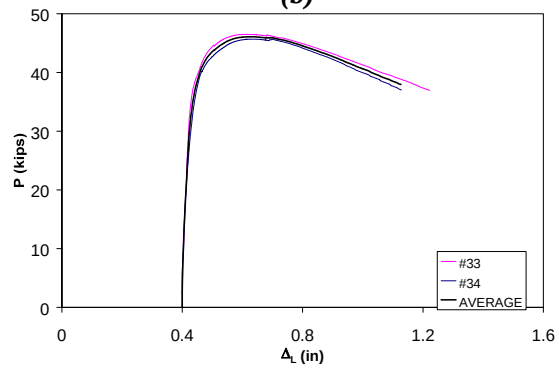

(c)

Figure C.17 Experimental load-deformation plots of #8 bars with L/d = 6 and e/d = 0.4

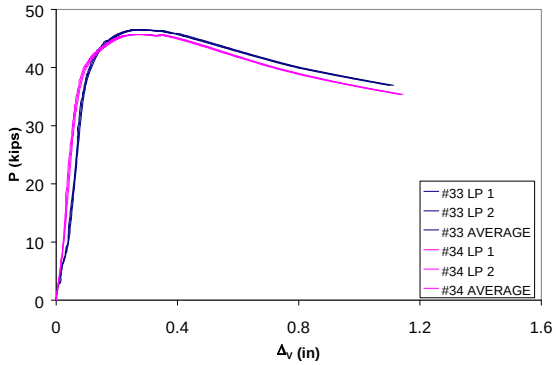

(a)

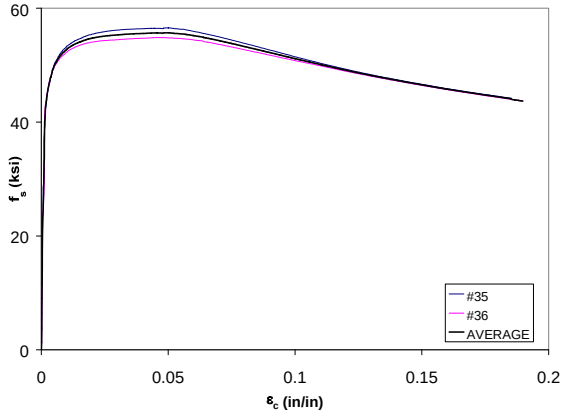

(b)

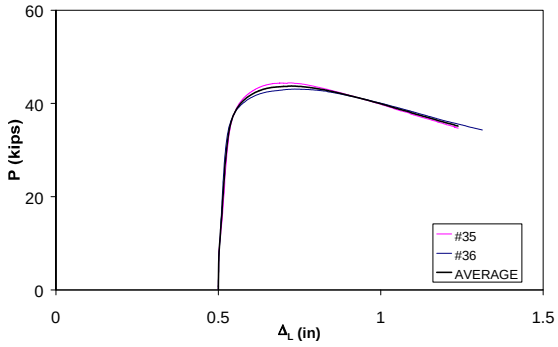

(c)

Figure C.18 Experimental load-deformation plots of #8 bars with L/d = 6 and e/d = 0.5

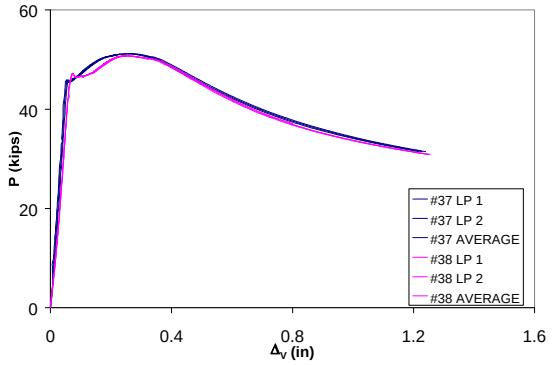

(a)

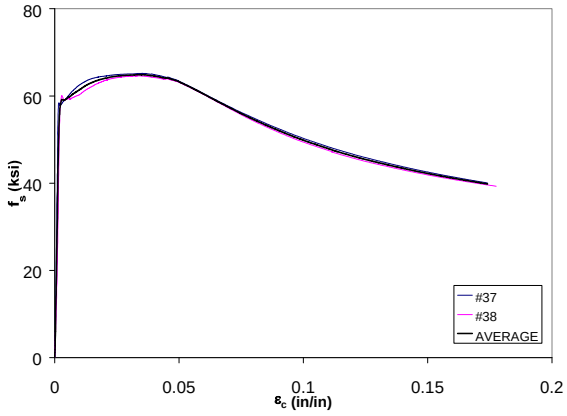

(b)

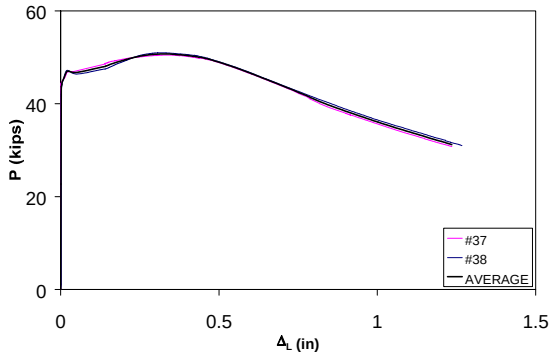

(c)

Figure C.19 Experimental load-deformation plots of #8 bars

with L/d = 7 and e/d = 0.0

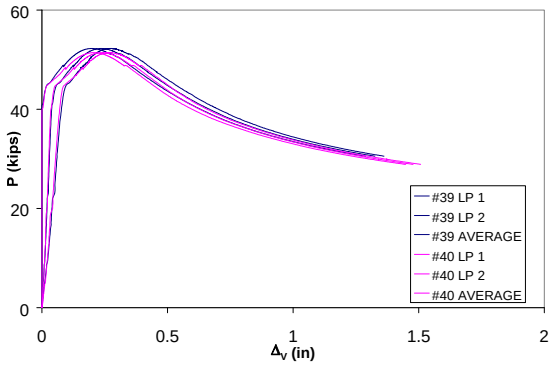

(a)

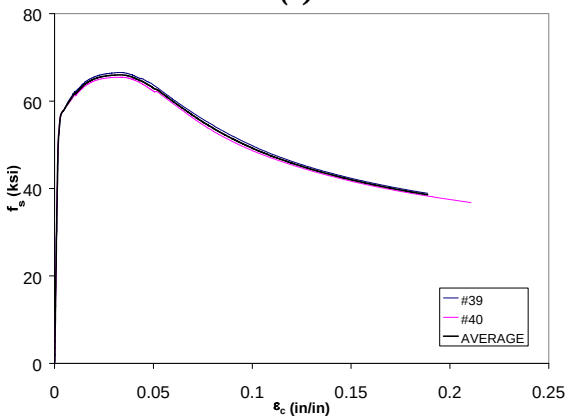

(b)

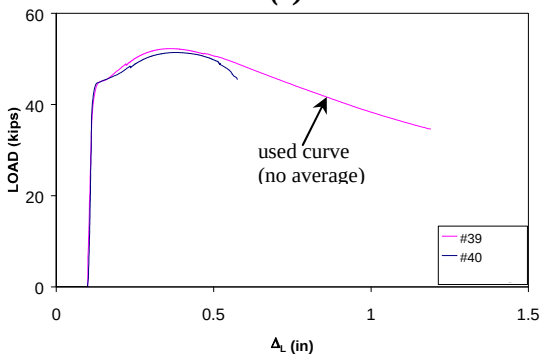

(c)

Figure C.20 Experimental load-deformation plots of #8 bars

with L/d = 7 and e/d = 0.1

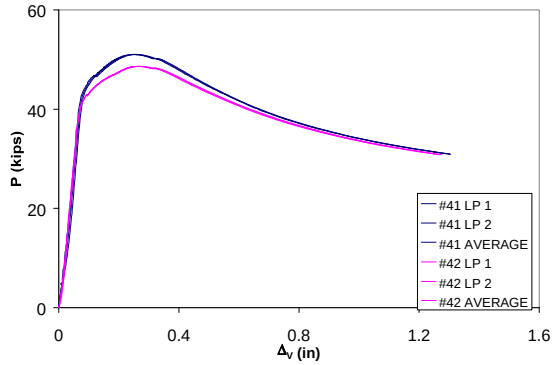

(a)

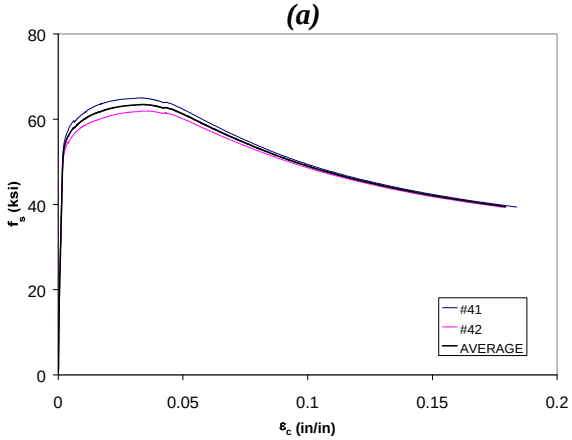

(b)

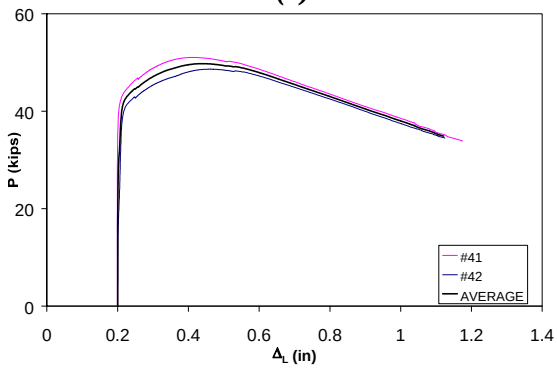

(c)

Figure C.21 Experimental load-deformation plots of #8 bars with L/d = 7 and e/d = 0.2

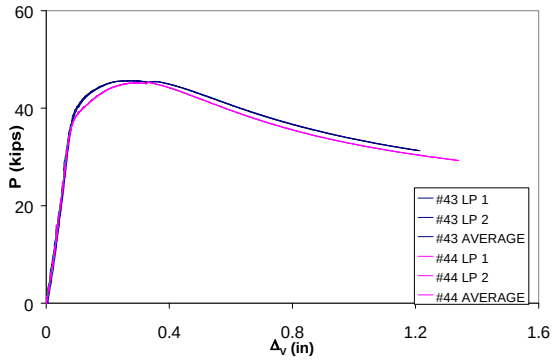

(a)

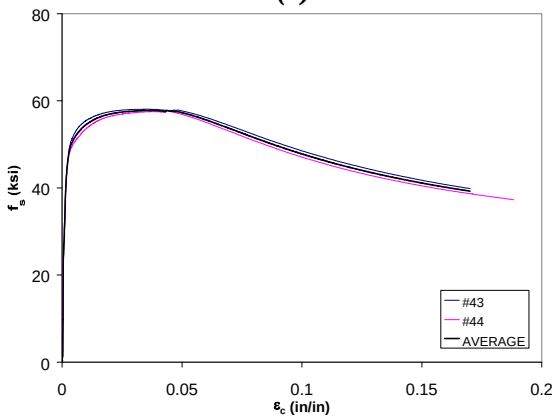

(b)

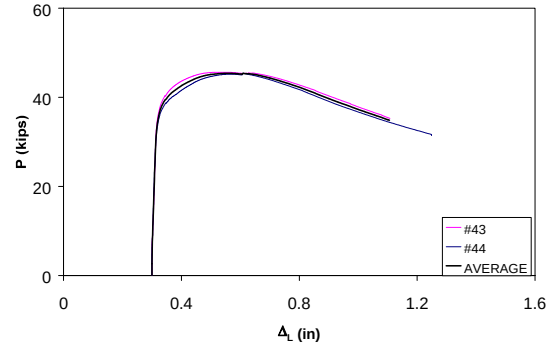

(c)

Figure C.22 Experimental load-deformation plots of #8 bars with L/d = 7 and e/d = 0.3

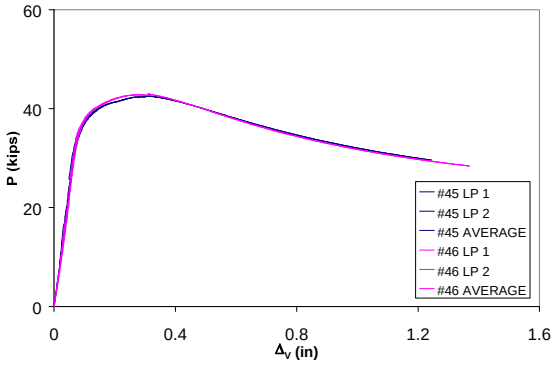

(a)

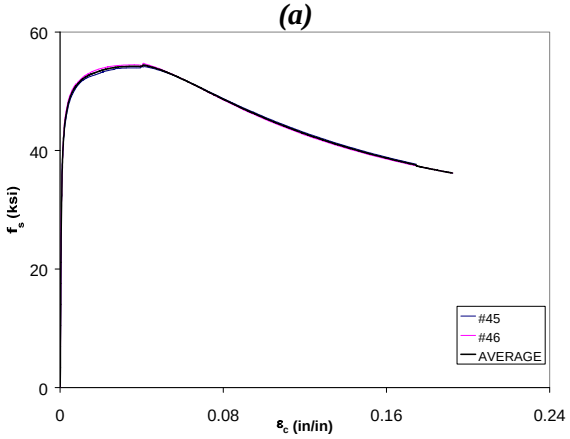

(b)

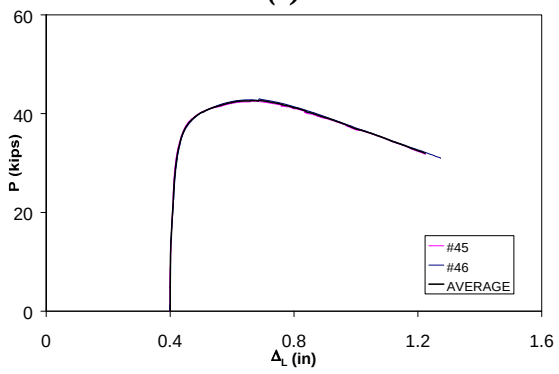

(c)

Figure C.23 Experimental load-deformation plots of #8 bars with L/d = 7 and e/d = 0.4

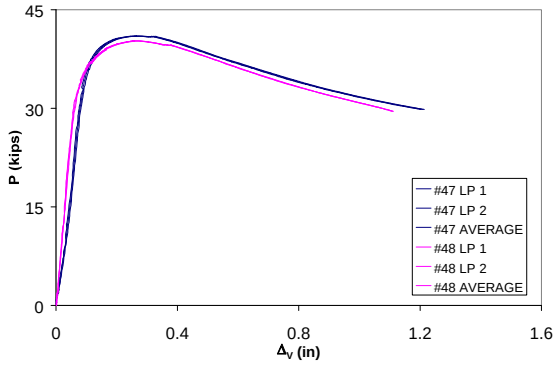

(a)

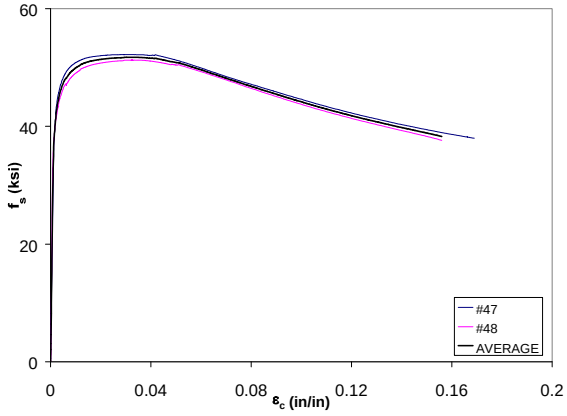

(b)

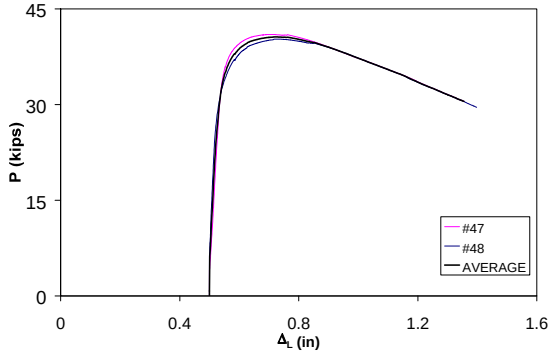

(c)

Figure C.24 Experimental load-deformation plots of #8 bars with L/d = 7 and e/d = 0.5

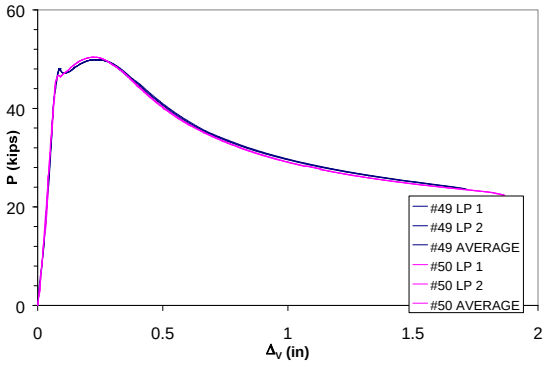

(a)

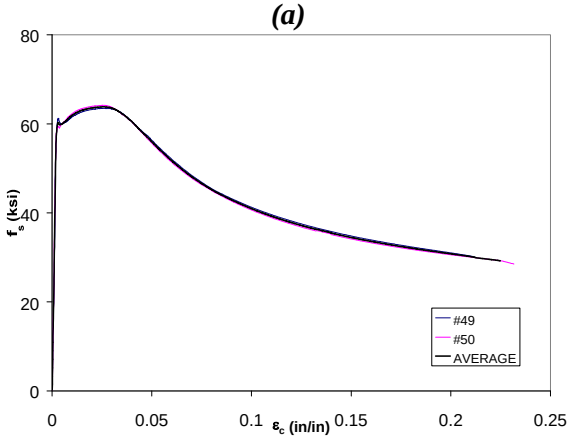

(b)

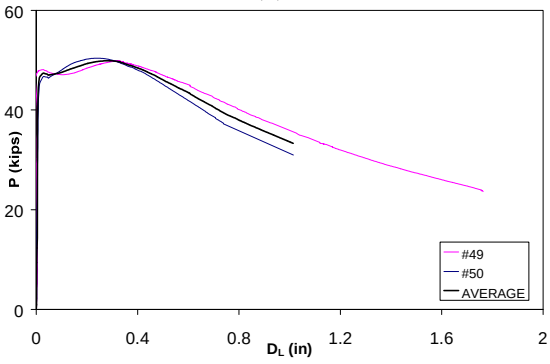

(c)

Figure C.25 Experimental load-deformation plots of #8 bars with L/d = 8 and e/d = 0.0

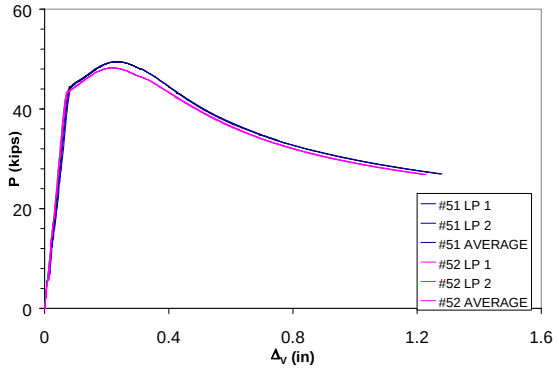

(a)

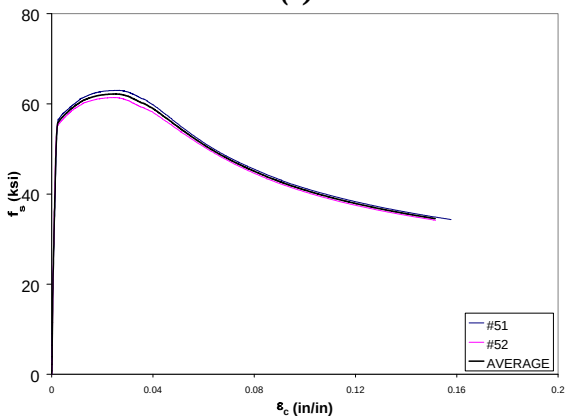

(b)

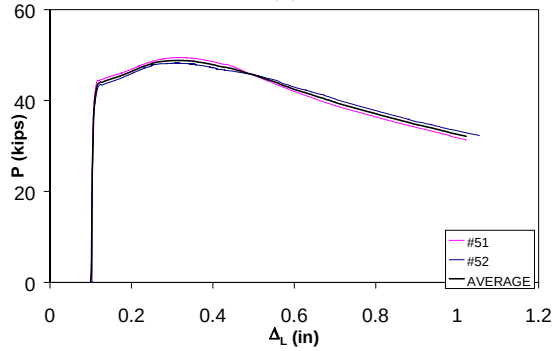

(c)

Figure C.26 Experimental load-deformation plots of #8 bars with L/d = 8 and e/d = 0.1

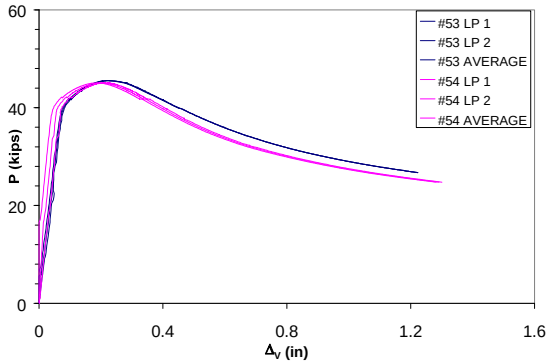

(a)

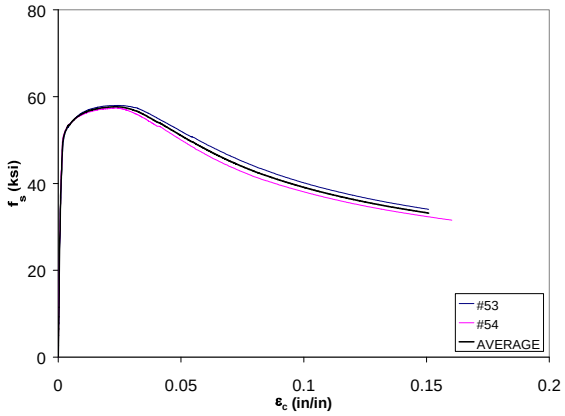

(b)

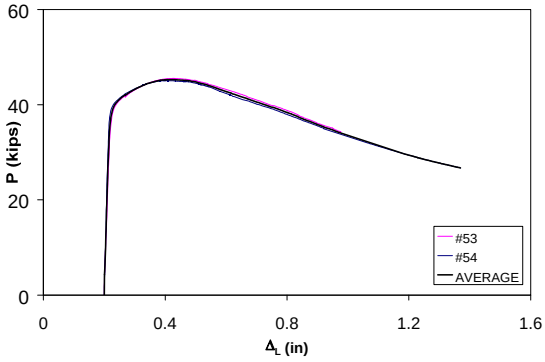

(c)

Figure C.27 Experimental load-deformation plots of #8 bars with L/d = 8 and e/d = 0.2

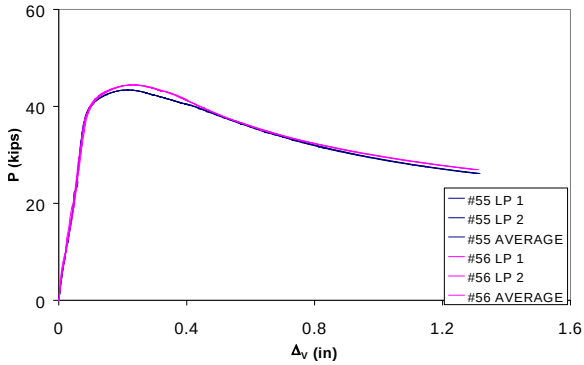

(a)

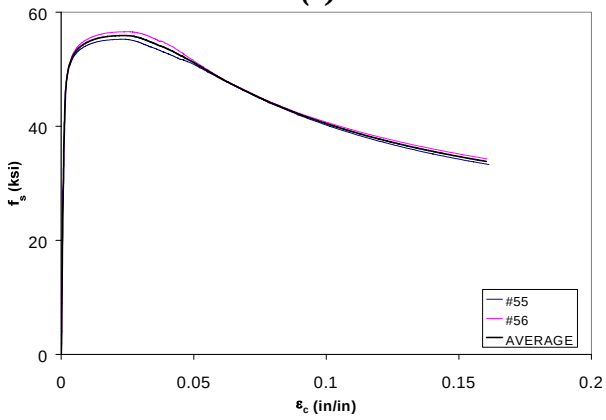

(b)

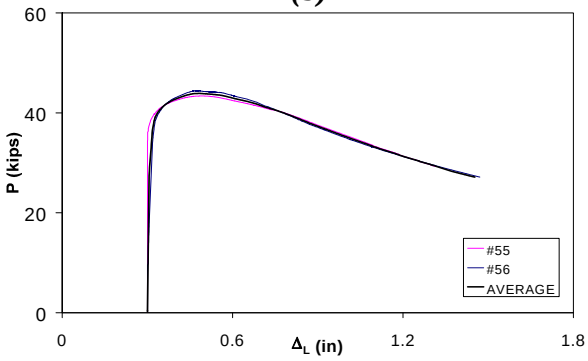

(c)

Figure C.28 Experimental load-deformation plots of #8 bars with L/d = 8 and e/d = 0.3

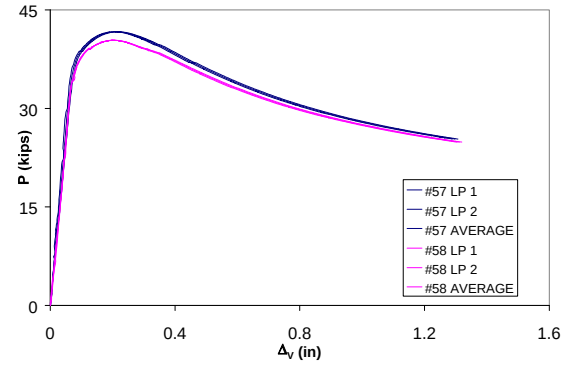

(a)

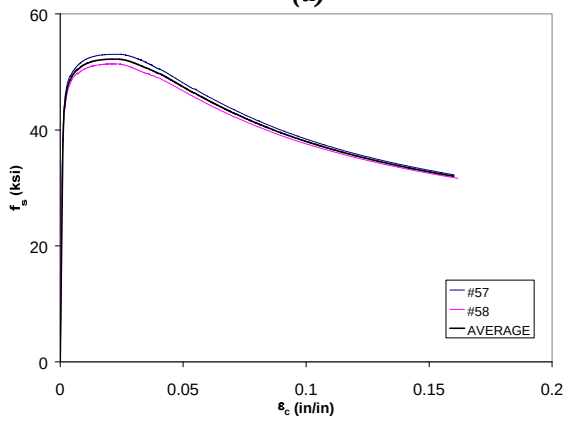

(b)

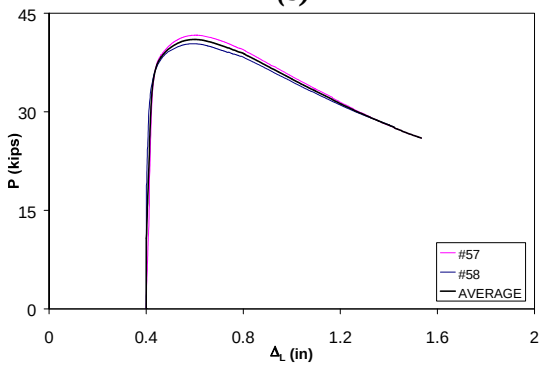

(c)

Figure C.29 Experimental load-deformation plots of #8 bars with L/d = 8 and e/d = 0.4

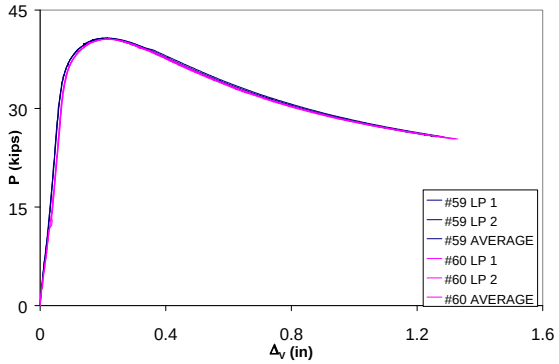

(a)

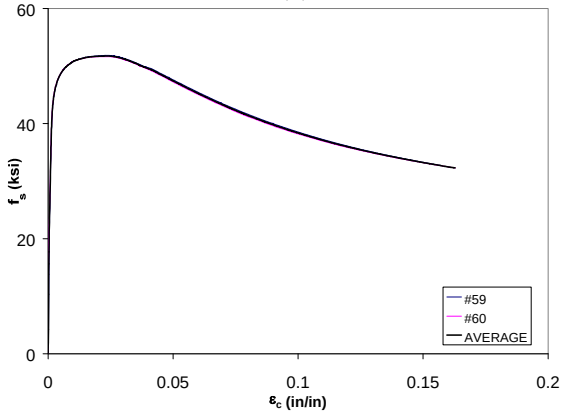

(b)

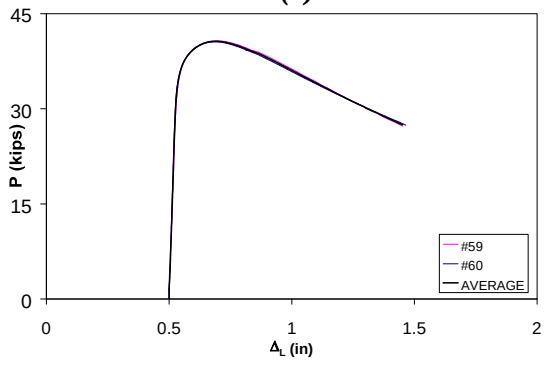

(c)

Figure C.30 Experimental load-deformation plots of #8 bars with L/d = 8 and e/d = 0.5

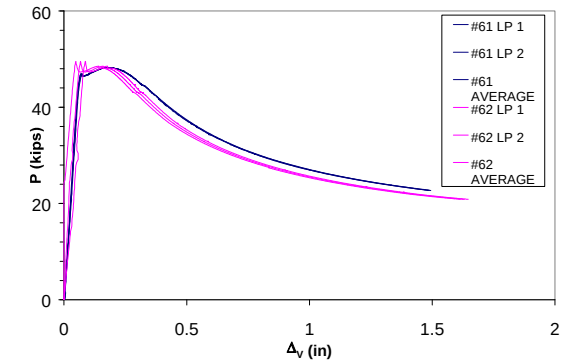

(a)

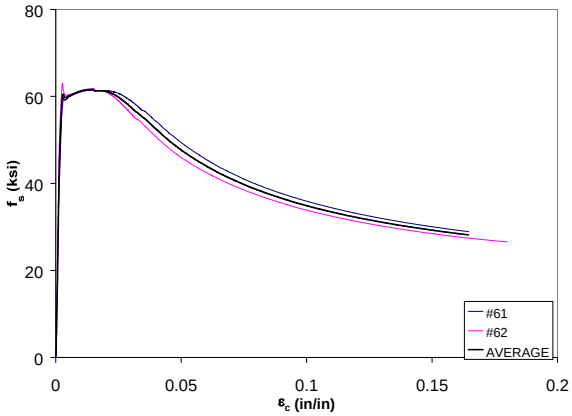

(b)

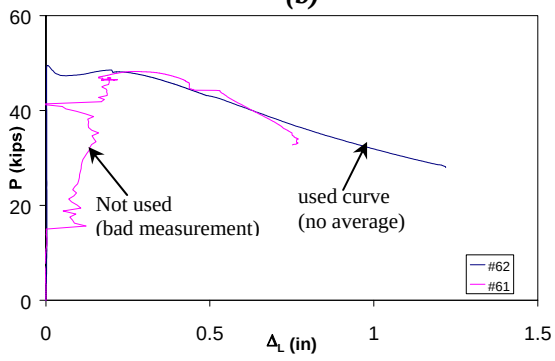

(c)

Figure C.31 Experimental load-deformation plots of #8 bars

with L/d = 9 and e/d = 0.0

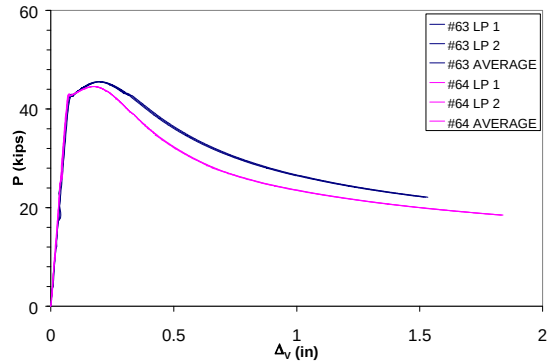

(a)

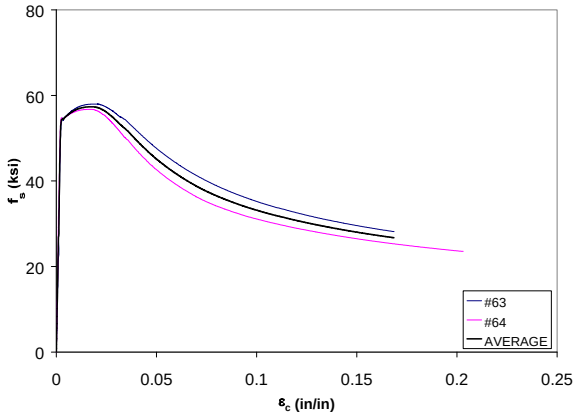

(b)

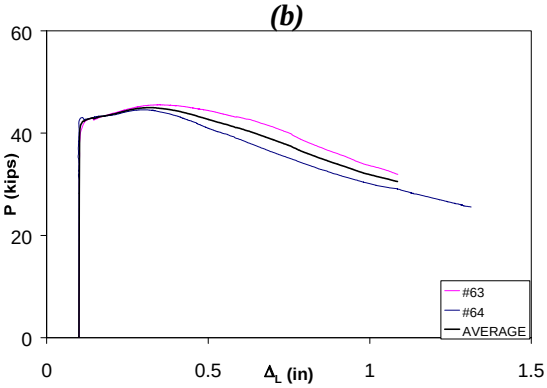

(c)

Figure C.32 Experimental load-deformation plots of #8 bars with L/d = 9 and e/d = 0.1

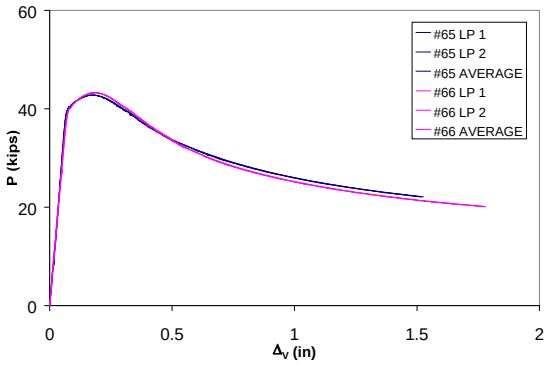

(a)

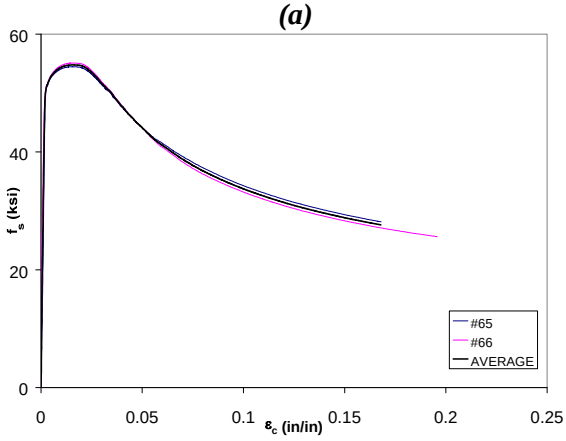

(b)

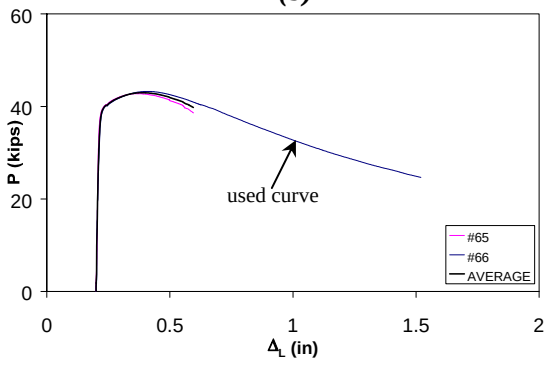

(c)

Figure C.33 Experimental load-deformation plots of #8 bars with L/d = 9 and e/d = 0.2

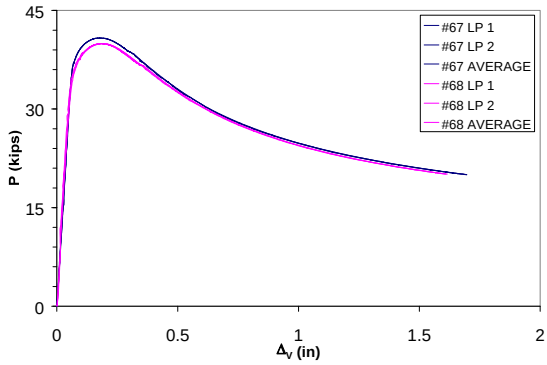

(a)

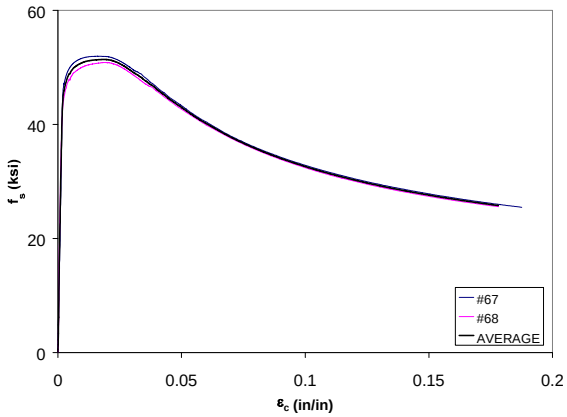

(b)

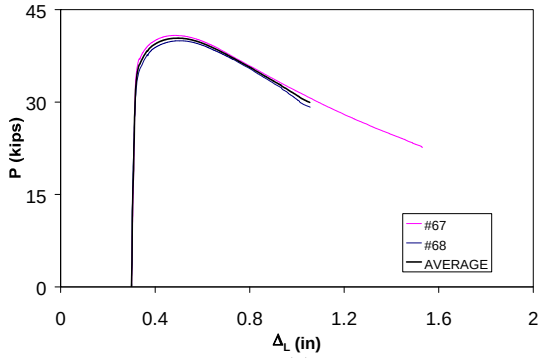

(c)

Figure C.34 Experimental load-deformation plots of #8 bars with L/d = 9 and e/d = 0.3

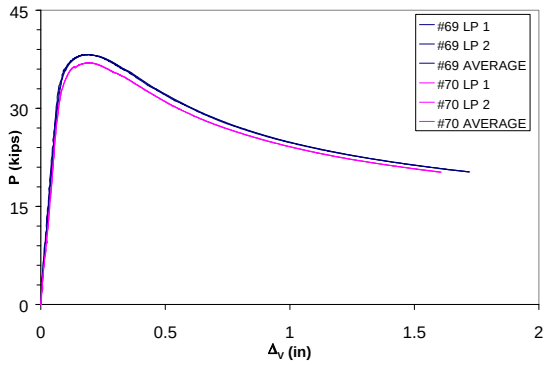

(a)

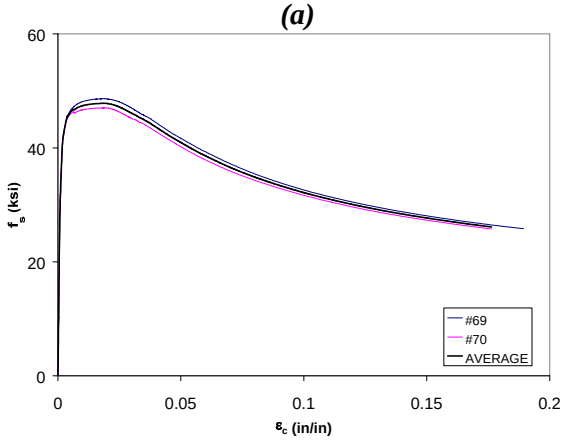

(b)

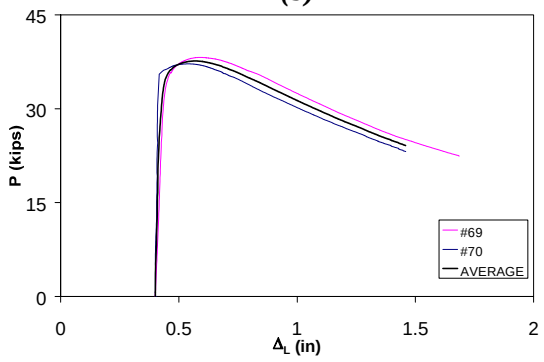

(c)

Figure C.35 Experimental load-deformation plots of #8 bars with L/d = 9 and e/d = 0.4

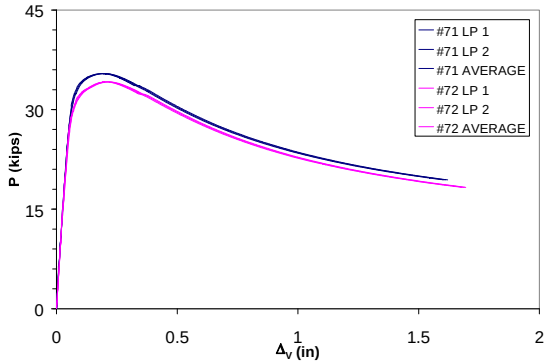

(a)

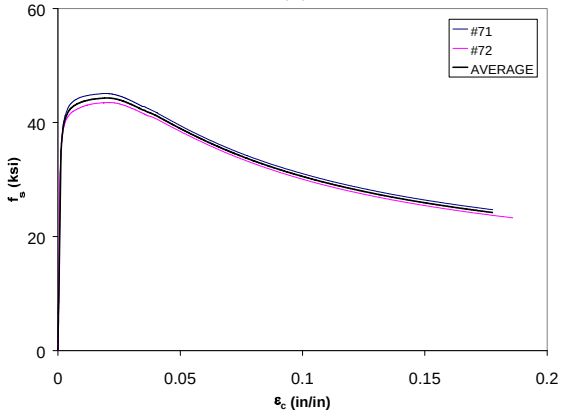

(b)

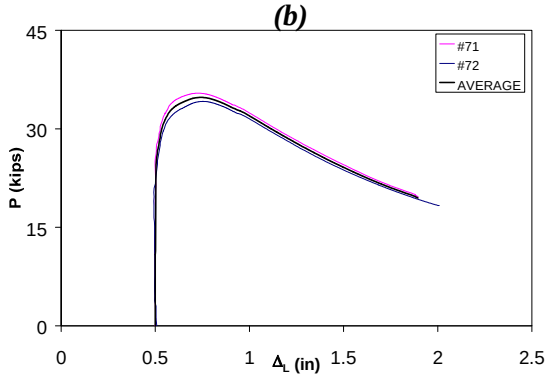

(c)

Figure C.36 Experimental load-deformation plots of #8 bars with L/d = 9 and e/d = 0.5

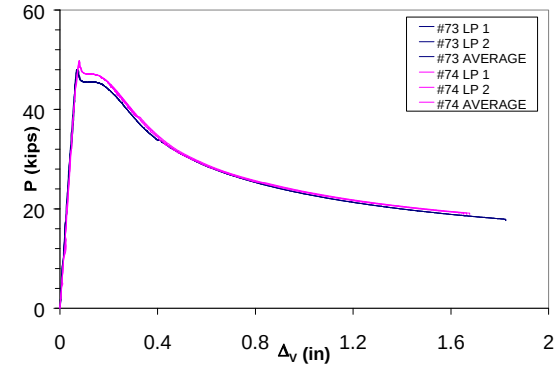

(a)

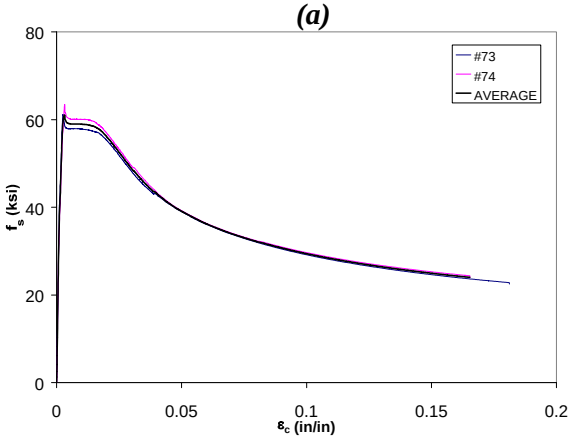

(b)

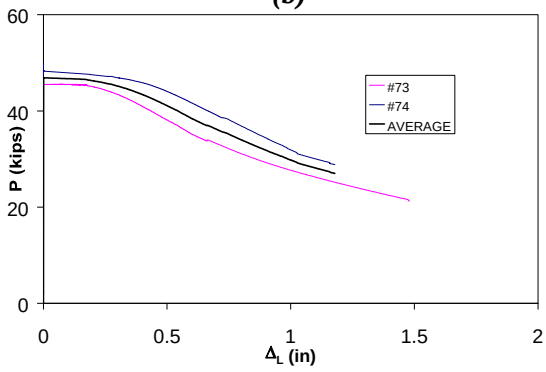

(c)

Figure C.37 Experimental load-deformation plots of #8 bars

with L/d = 10 and e/d = 0.0

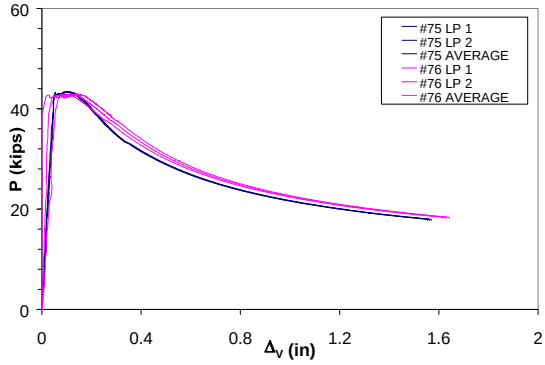

(a)

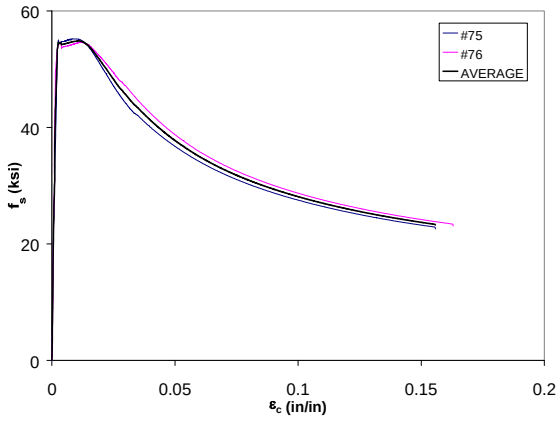

(b)

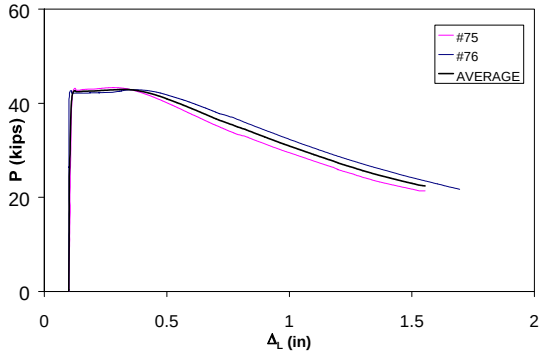

(c)

Figure C.38 Experimental load-deformation plots of #8 bars with L/d = 10 and e/d = 0.1

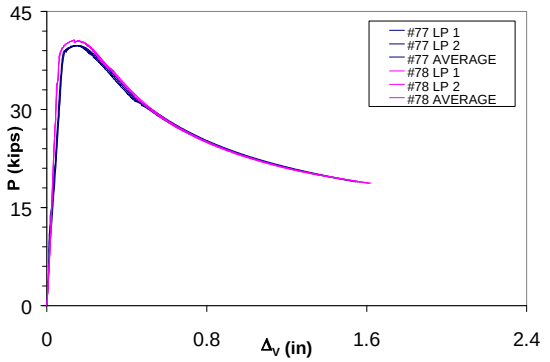

(a)

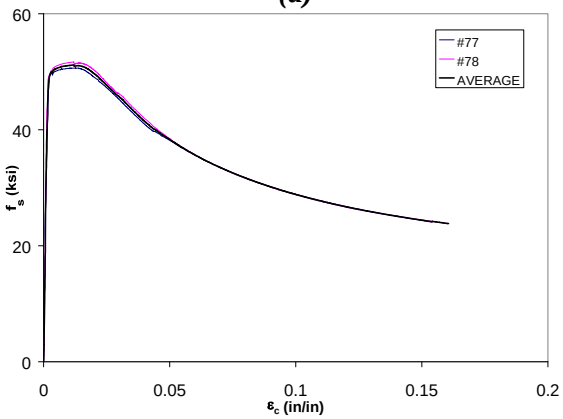

(b)

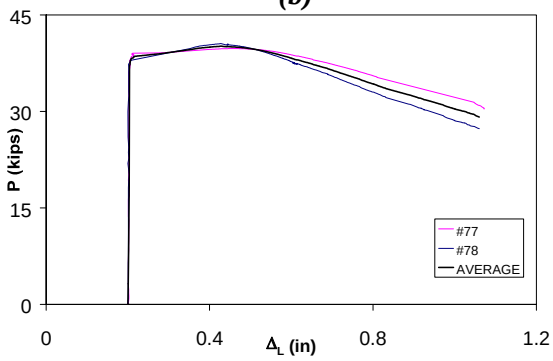

(c)

Figure C.39 Experimental load-deformation plots of #8 bars with L/d = 10 and e/d = 0.2

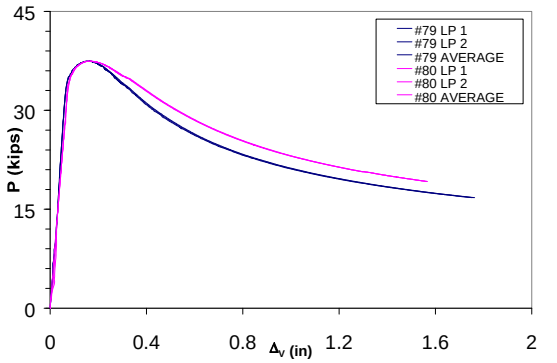

(a)

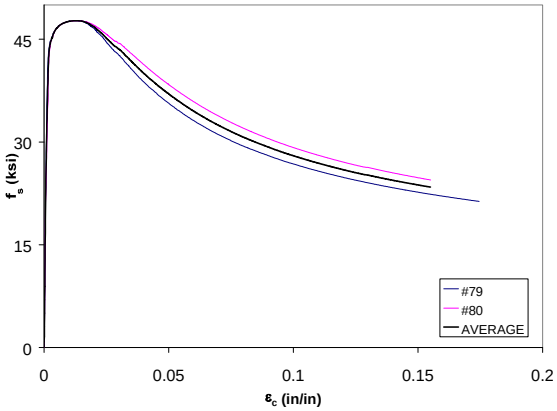

(b)

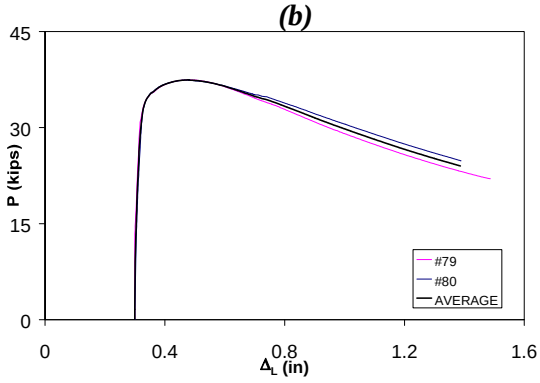

(c)

Figure C.40 Experimental load-deformation plots of #8 bars

with L/d = 10 and e/d = 0.3

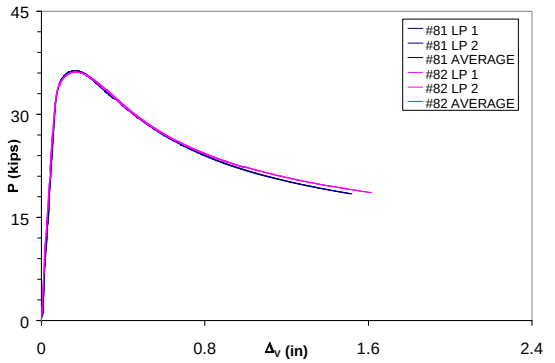

(a)

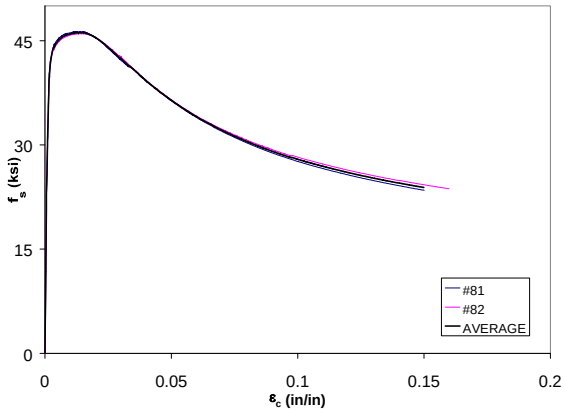

(b)

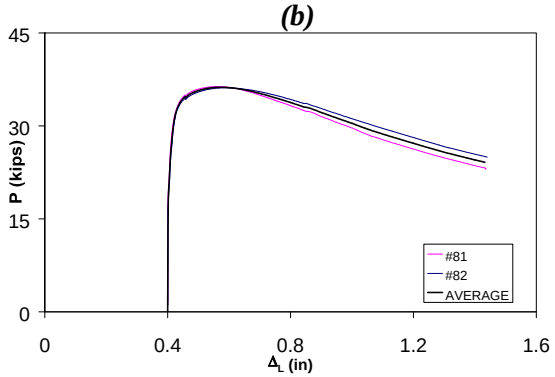

(c)

Figure C.41 Experimental load-deformation plots of #8 bars with L/d = 10 and e/d = 0.4

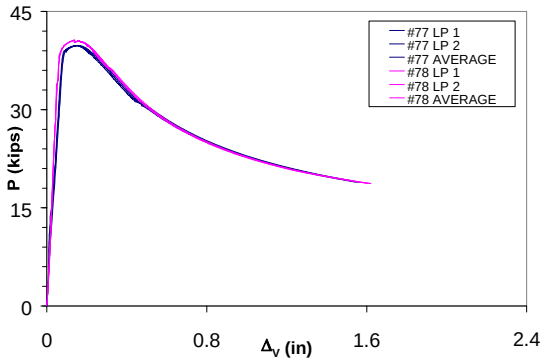

(a)

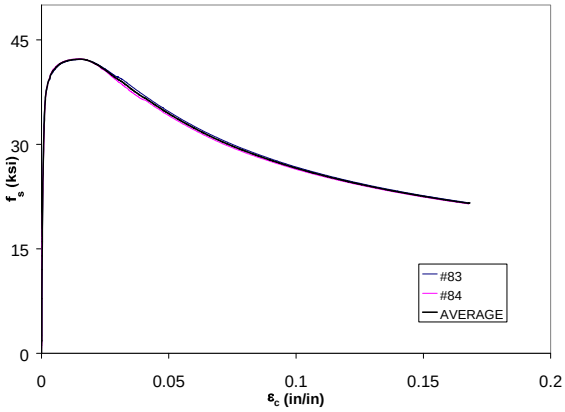

(b)

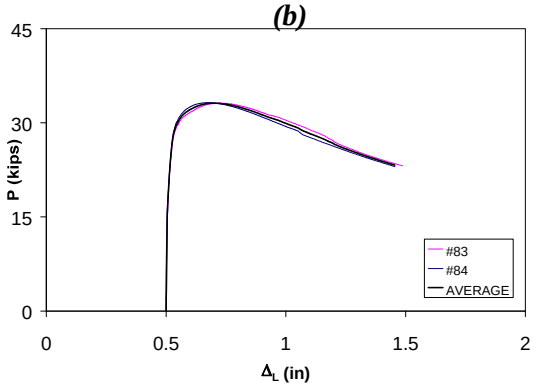

(c)

Figure C.42 Experimental load-deformation plots of #8 bars with L/d = 10 and e/d = 0.5

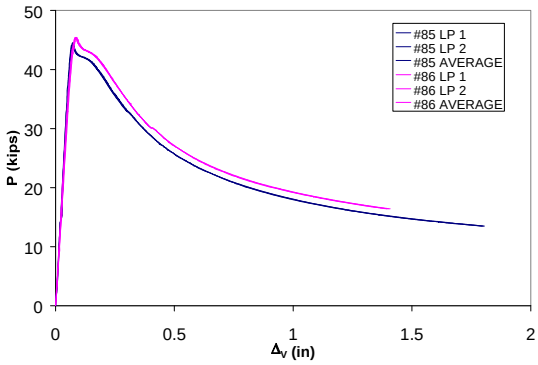

(a)

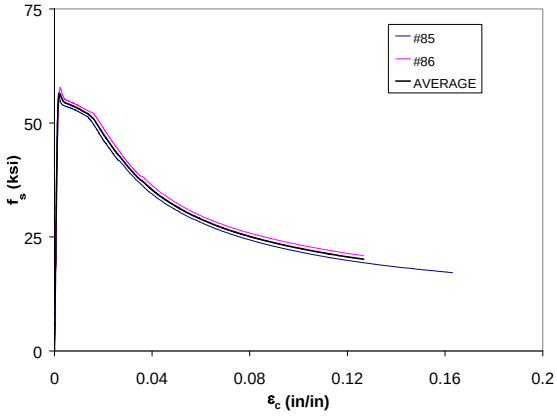

(b)

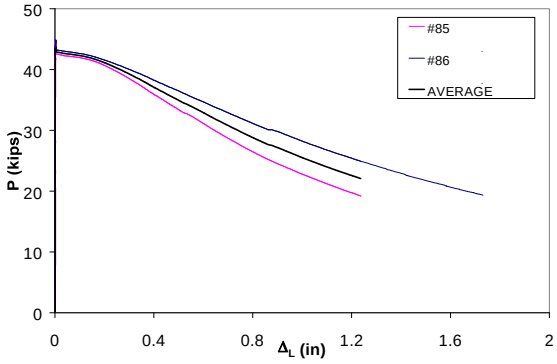

(c)

Figure C.43 Experimental load-deformation plots of #8 bars with L/d = 11 and e/d = 0.0

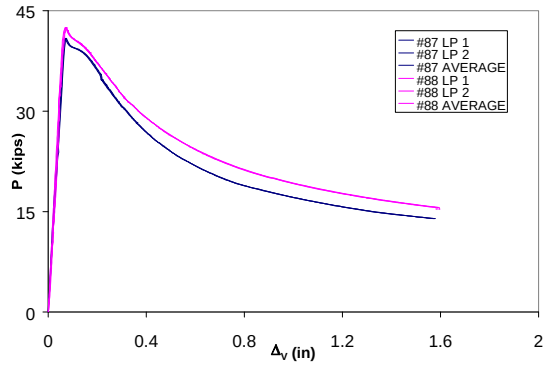

(a)

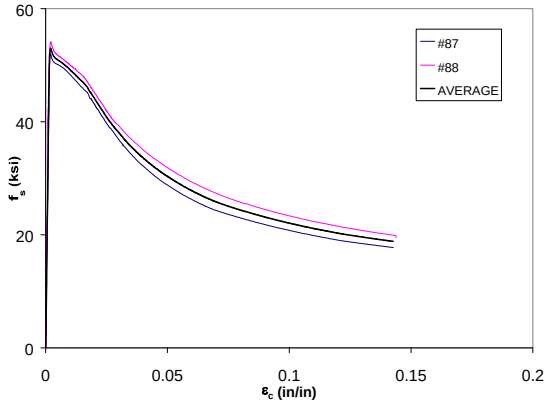

(b)

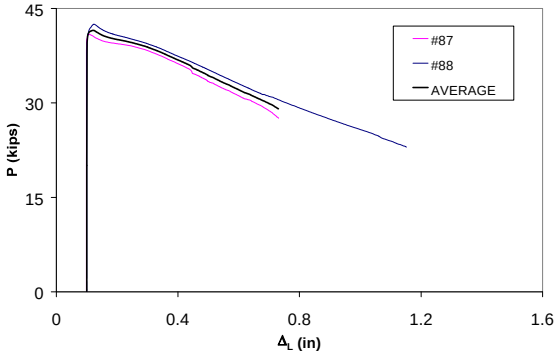

(c)

Figure C.44 Experimental load-deformation plots of #8 bars with L/d = 11 and e/d = 0.1

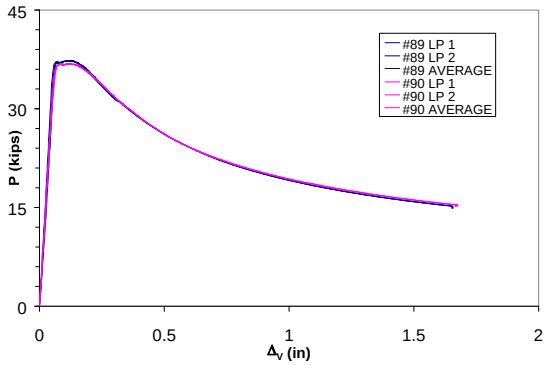

(a)

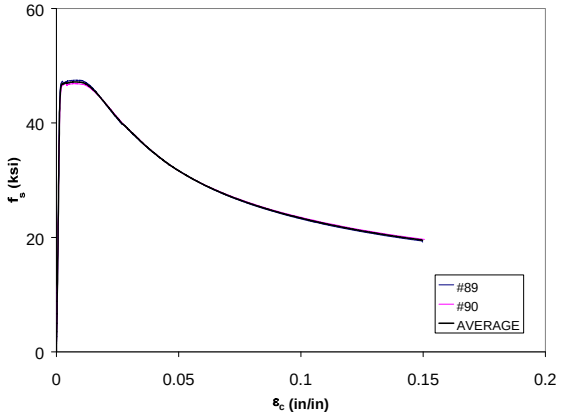

(b)

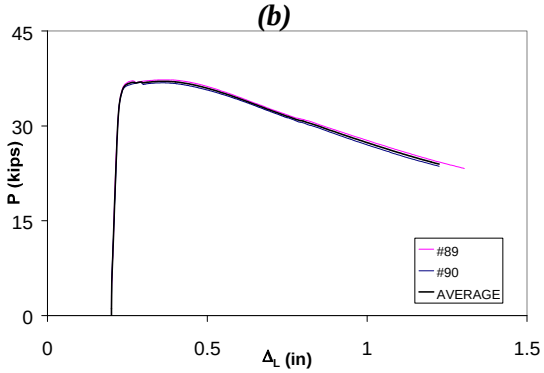

(c)

Figure C.45 Experimental load-deformation plots of #8 bars with L/d = 11 and e/d = 0.2

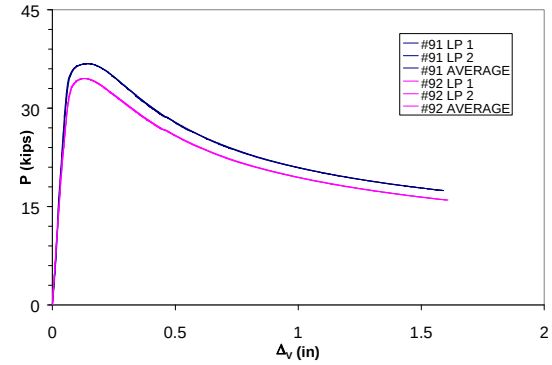

(a)

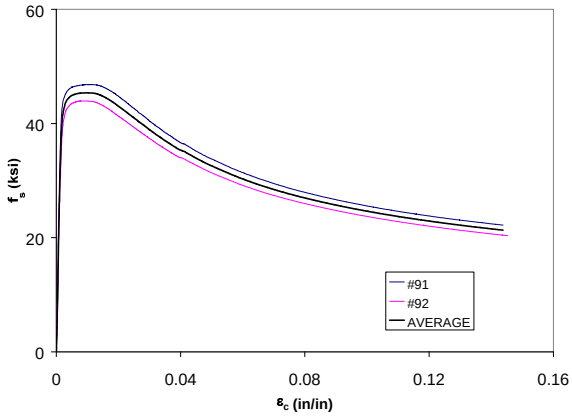

(b)

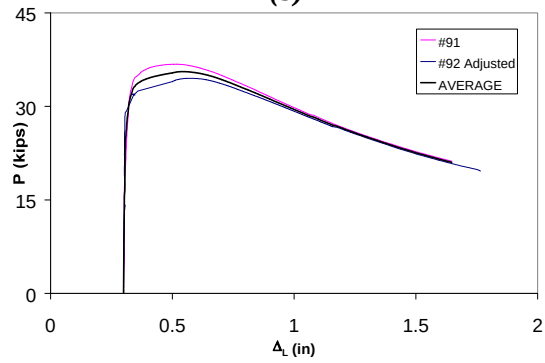

(c)

Figure C.46 Experimental load-deformation plots of #8 bars with L/d = 11 and e/d = 0.3

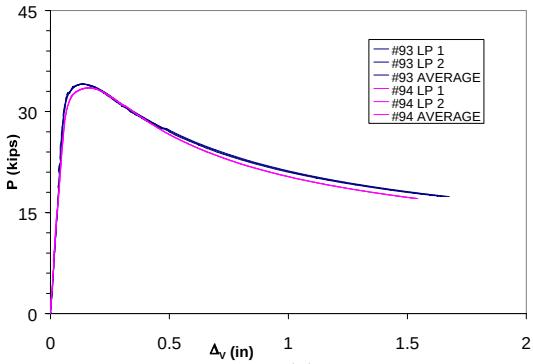

(a)

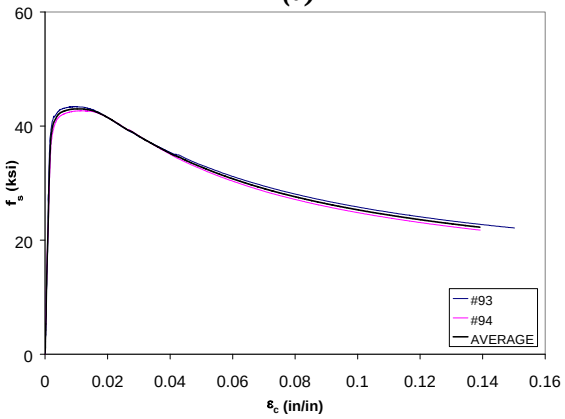

(b)

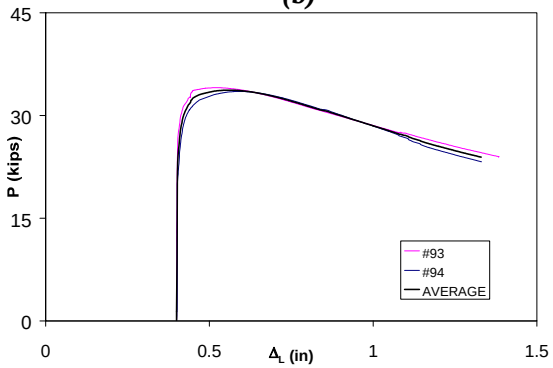

(c)

Figure C.47 Experimental load-deformation plots of #8 bars with L/d = 11 and e/d = 0.4

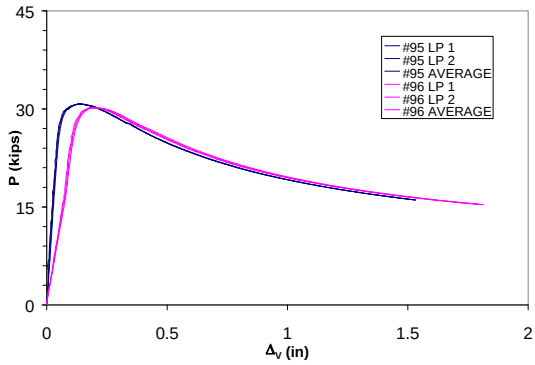

(a)

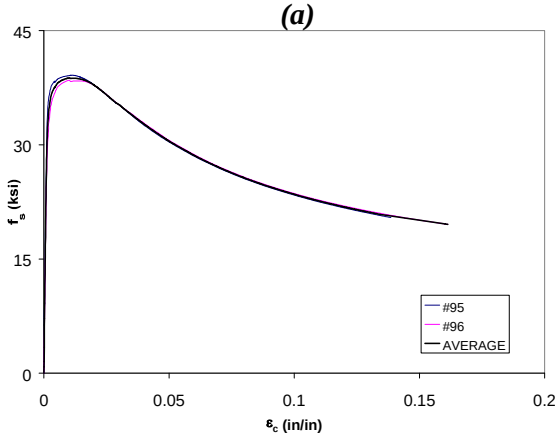

(b)

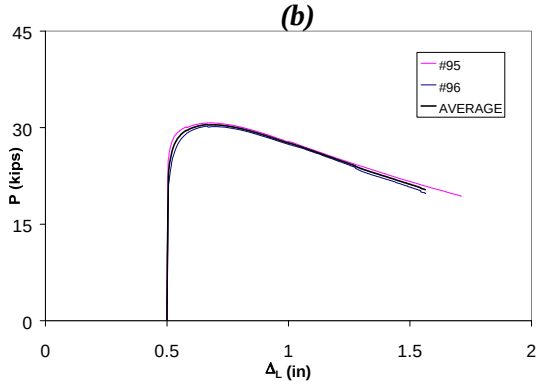

(c)

Figure C.48 Experimental load-deformation plots of #8 bars with L/d = 11 and e/d = 0.5

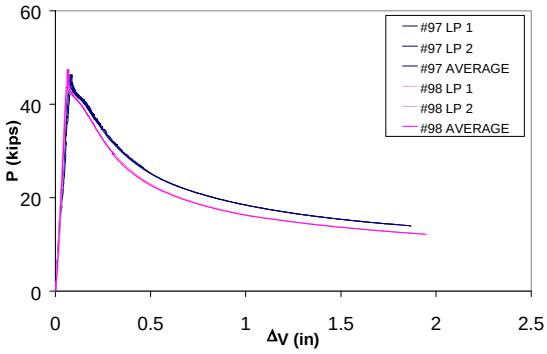

(a)

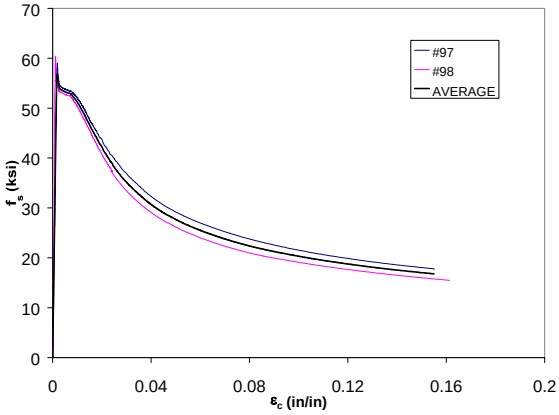

(b)

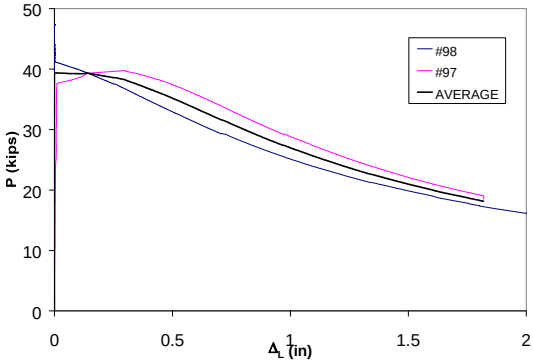

(c)

Figure C.49 Experimental load-deformation plots of #8 bars with L/d = 12 and e/d = 0.0

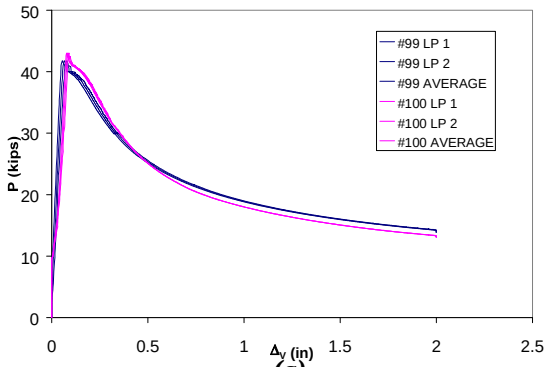

(a)

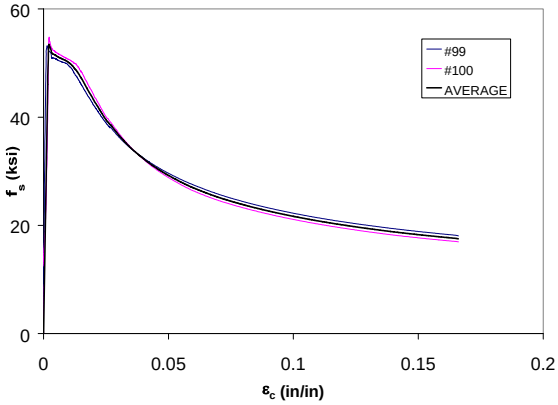

(b)

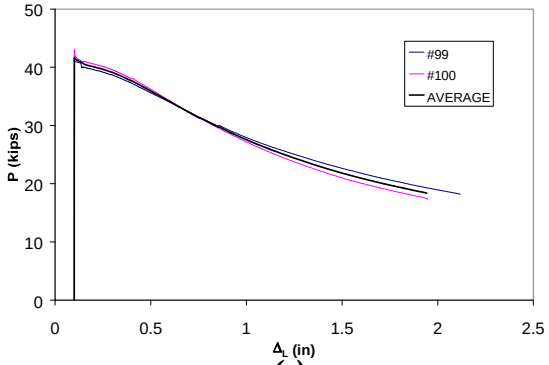

(c)

Figure C.50 Experimental load-deformation plots of #8 bars with L/d = 12 and e/d = 0.1

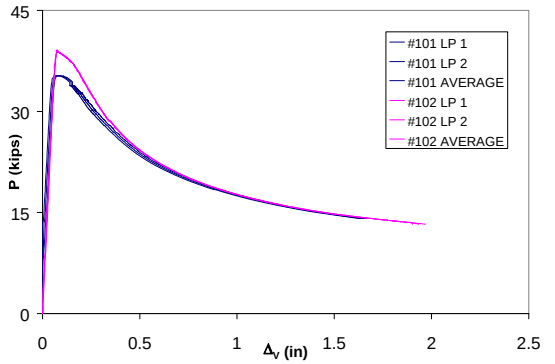

(a)

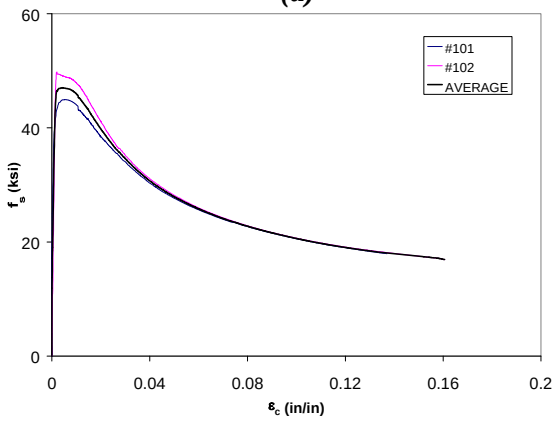

(b)

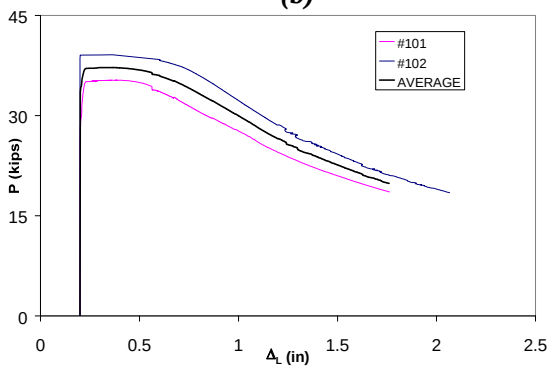

(c)

Figure C.51 Experimental load-deformation plots of #8 bars with L/d = 12 and e/d = 0.2

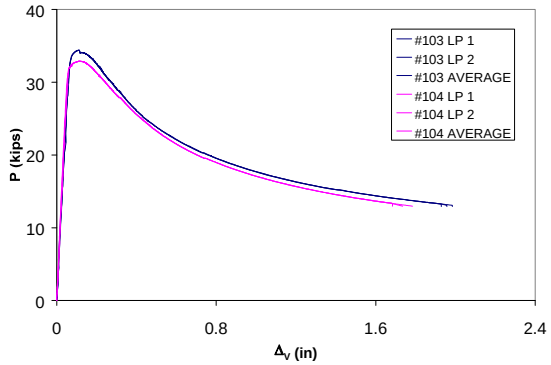

(a)

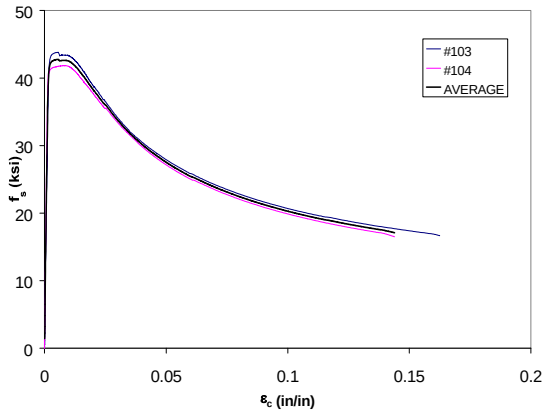

(b)

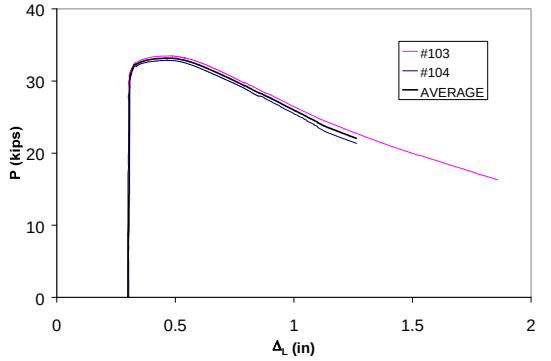

(c)

Figure C.52 Experimental load-deformation plots of #8 bars with L/d = 12 and e/d = 0.3

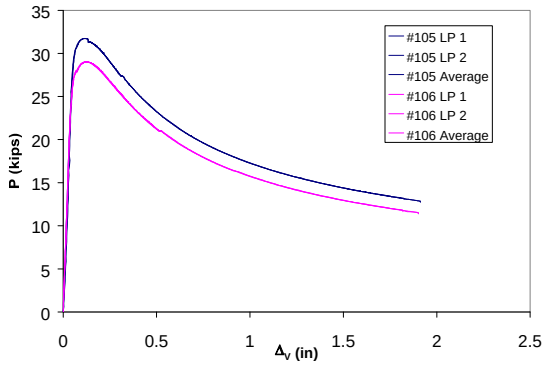

(a)

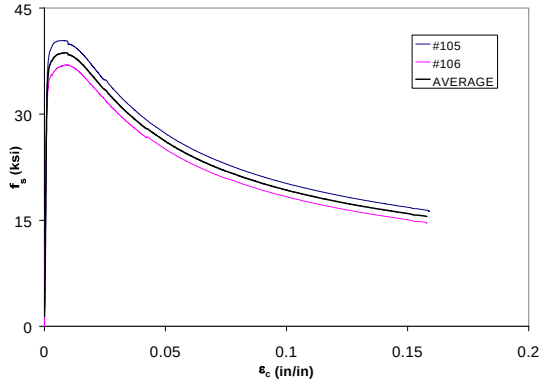

(b)

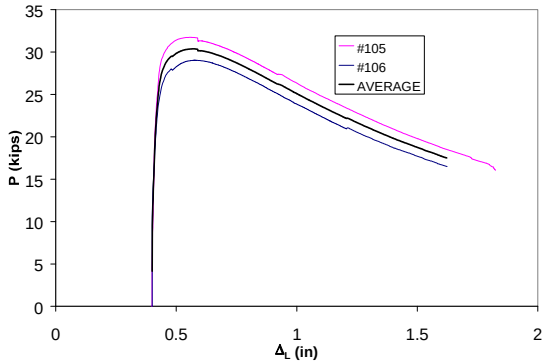

(c)

Figure C.53 Experimental load-deformation plots of #8 bars with L/d = 12 and e/d = 0.4

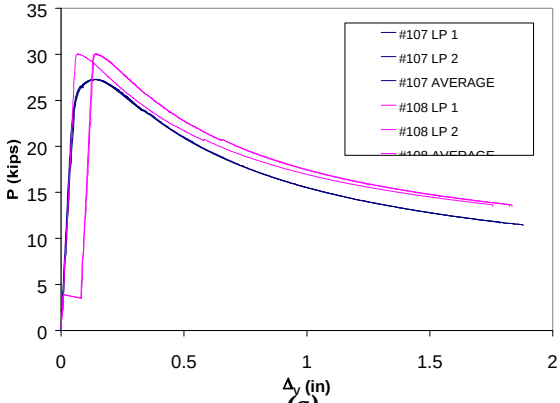

(a)

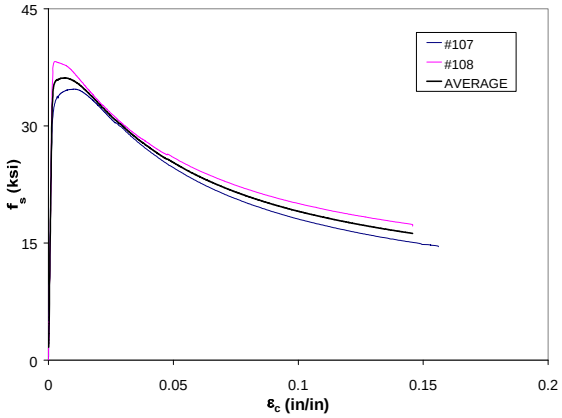

(b)

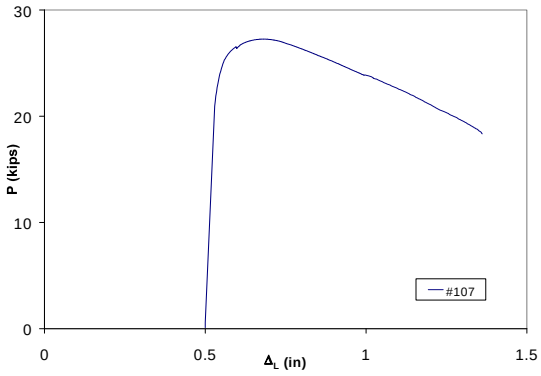

(c)

Figure C.54 Experimental load-deformation plots of #8 bars with L/d = 12 and e/d = 0.5

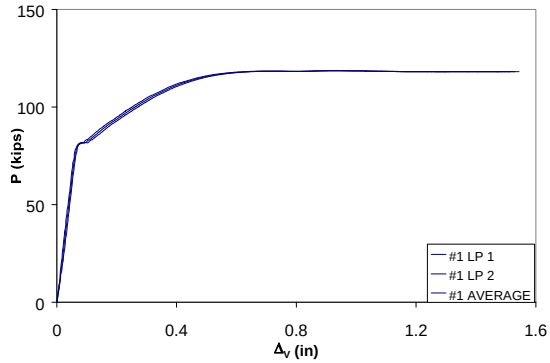

(a)

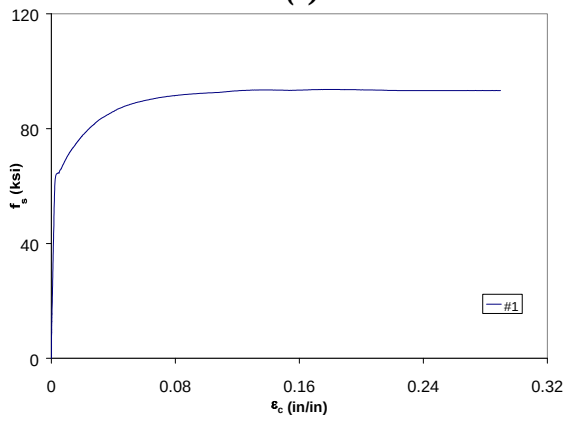

(b)

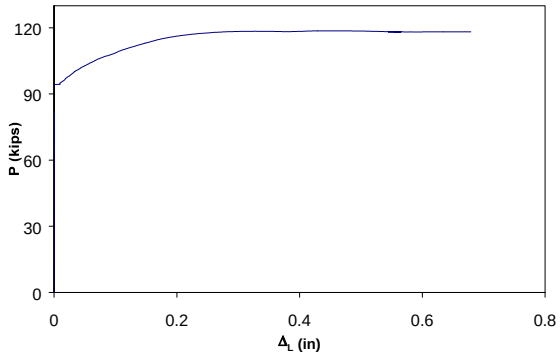

(c)

Figure C.55 Experimental load-deformation plots of #10 bar with L/d = 4 and e/d = 0.0

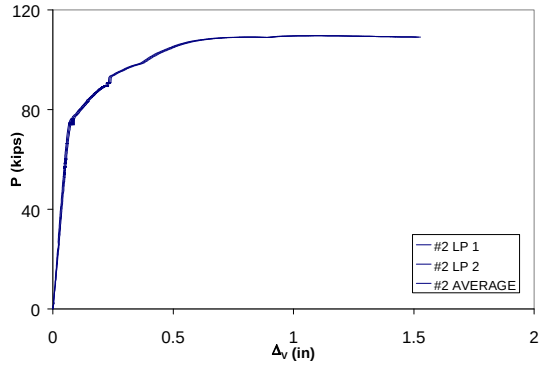

(a)

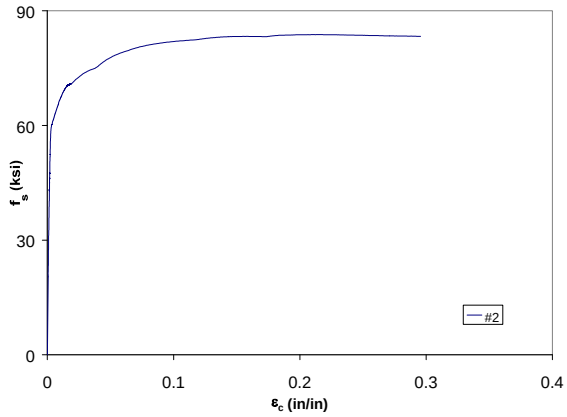

(b)

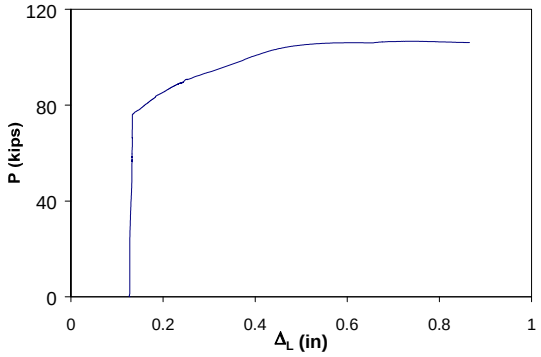

(c)

Figure C.56 Experimental load-deformation plots of #10 bar with L/d = 4 and e/d = 0.1

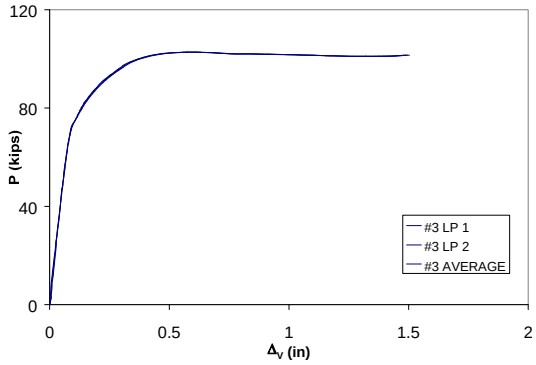

(a)

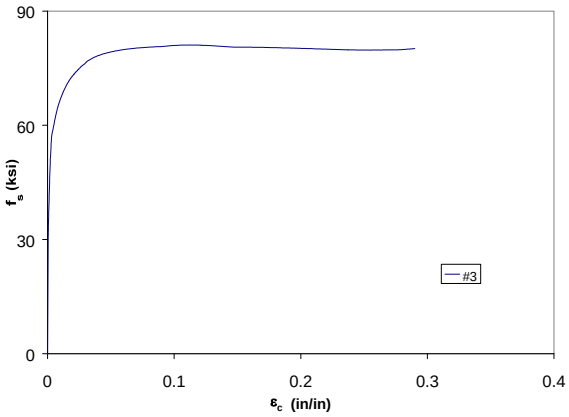

(b)

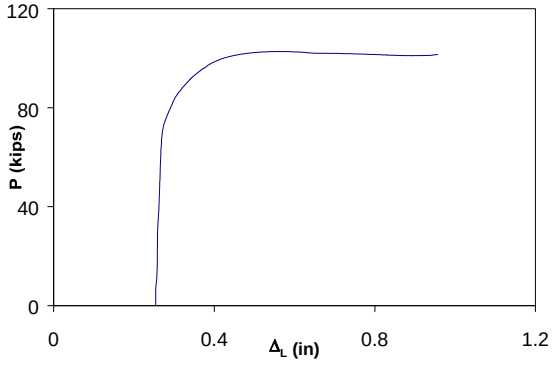

(c)

Figure C.57 Experimental load-deformation plots of #10 bar with L/d = 4 and e/d = 0.2

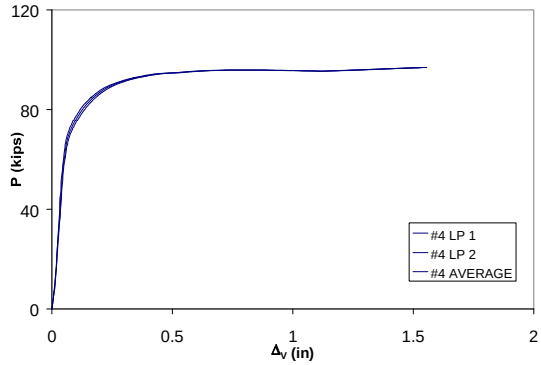

(a)

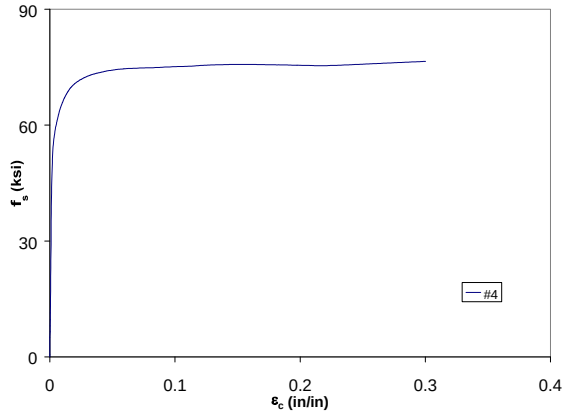

(b)

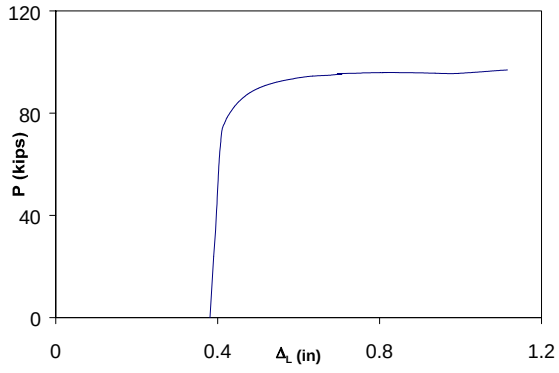

(c)

Figure C.58 Experimental load-deformation plots of #10 bar with L/d = 4 and e/d = 0.3

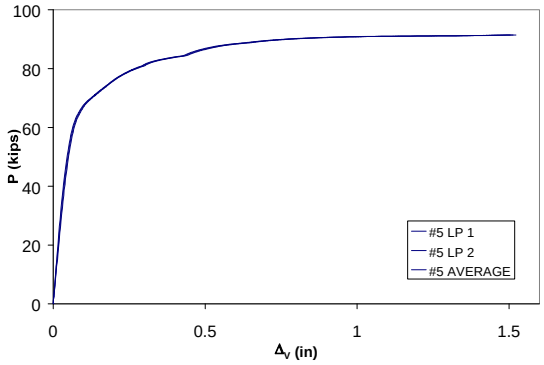

(a)

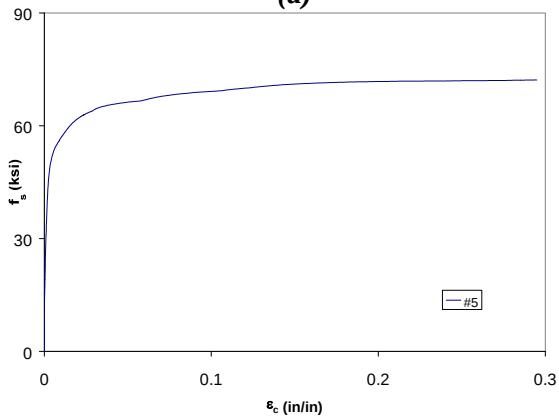

(b)

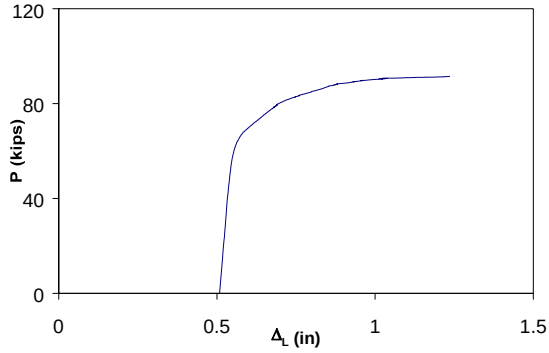

(c)

Figure C.59 Experimental load-deformation plots of #10 bar with L/d = 4 and e/d = 0.4

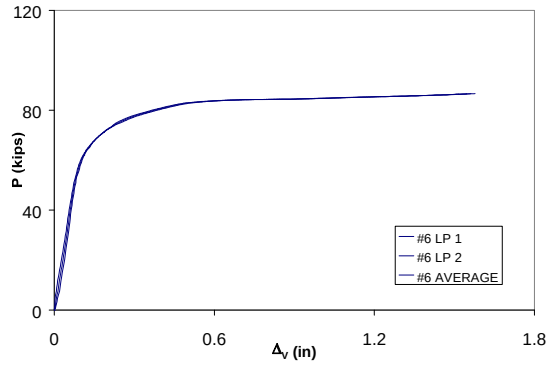

(a)

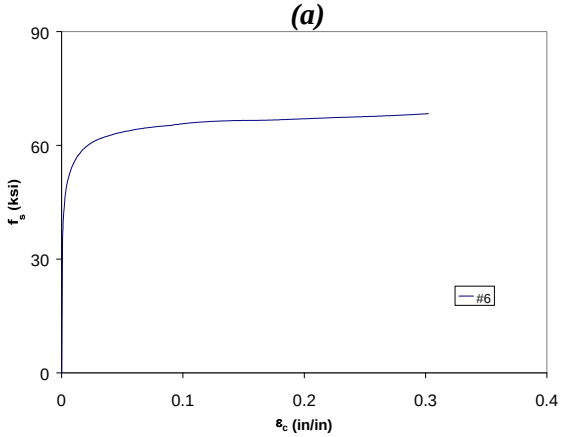

(b)

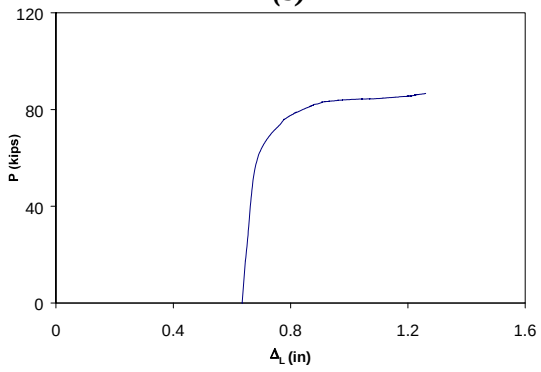

(c)

Figure C.60 Experimental load-deformation plots of #10 bar with L/d = 4 and e/d = 0.5

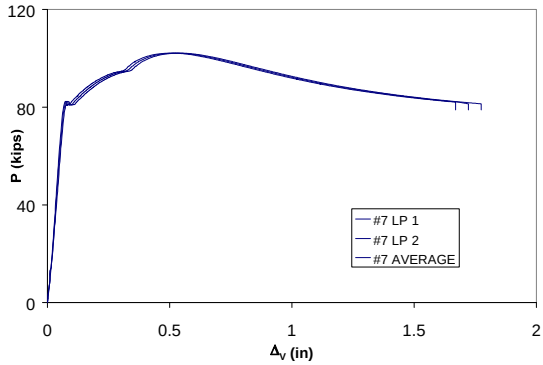

(a)

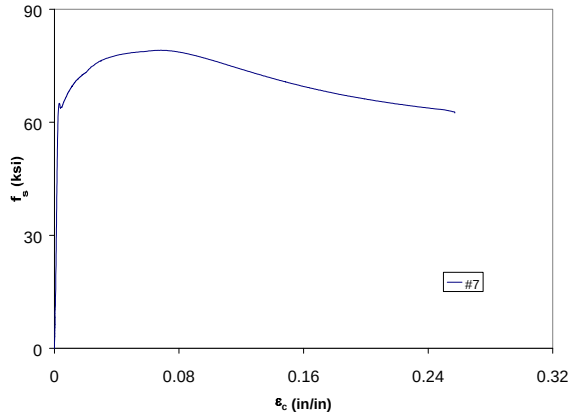

(b)

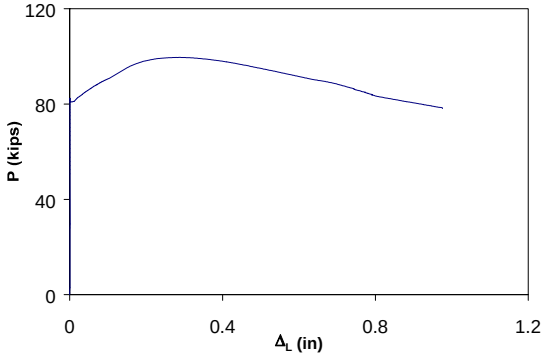

(c)

Figure C.61 Experimental load-deformation plots of #10 bar with L/d = 5 and e/d = 0.0

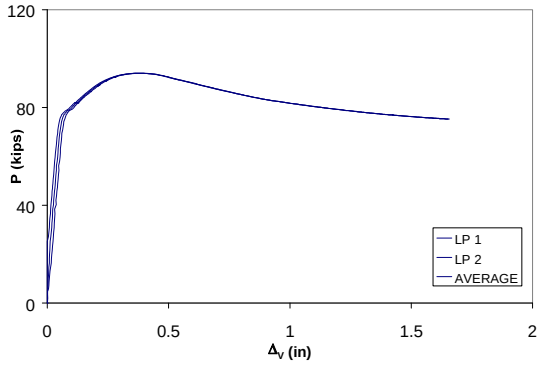

(a)

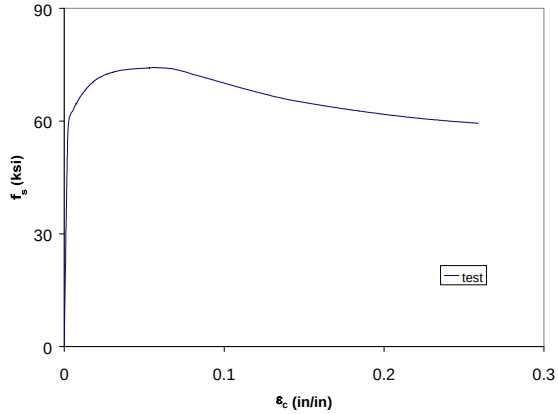

(b)

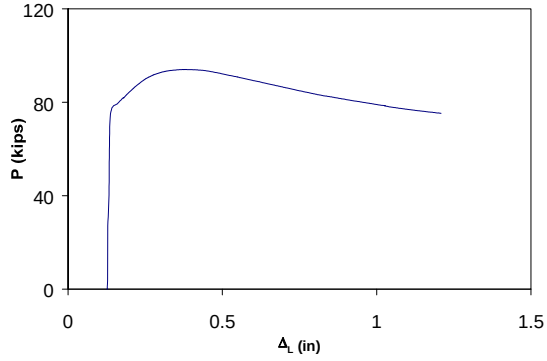

(c)

Figure C.62 Experimental load-deformation plots of #10 bar with L/d = 5 and e/d = 0.1

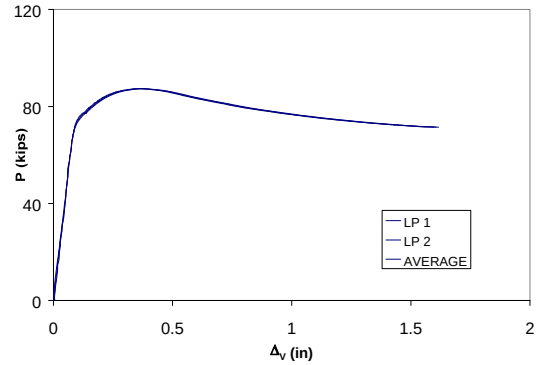

(a)

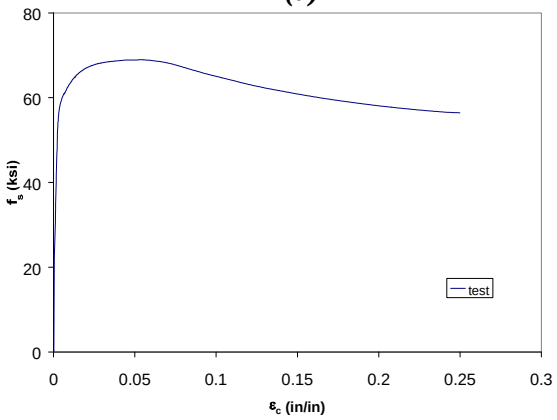

(b)

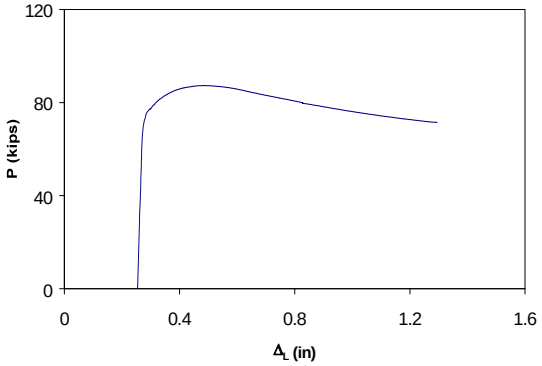

(c)

Figure C.63 Experimental load-deformation plots of #10 bar with L/d = 5 and e/d = 0.2

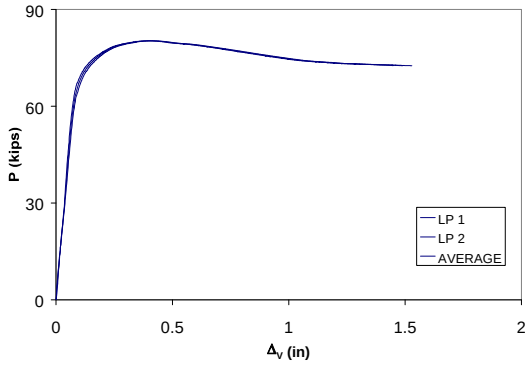

(a)

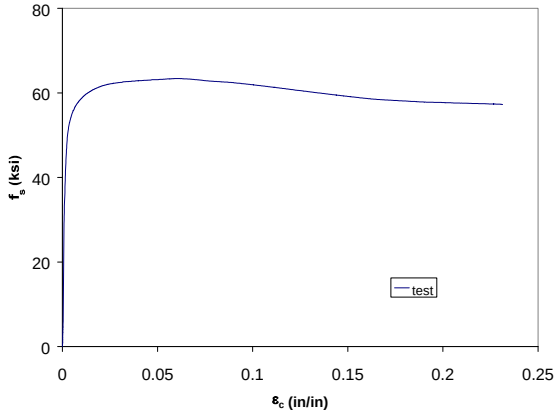

(b)

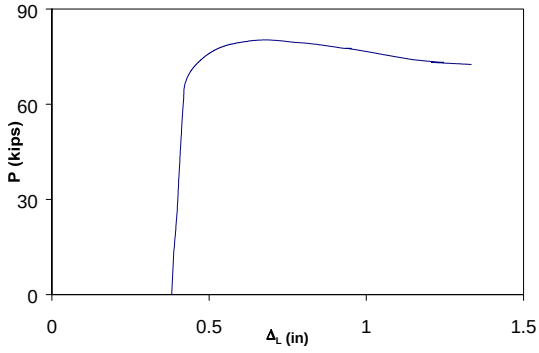

(c)

Figure C.64 Experimental load-deformation plots of #10 bar with L/d = 5 and e/d = 0.3

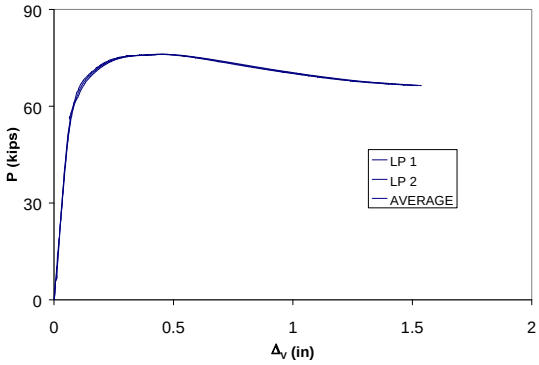

(a)

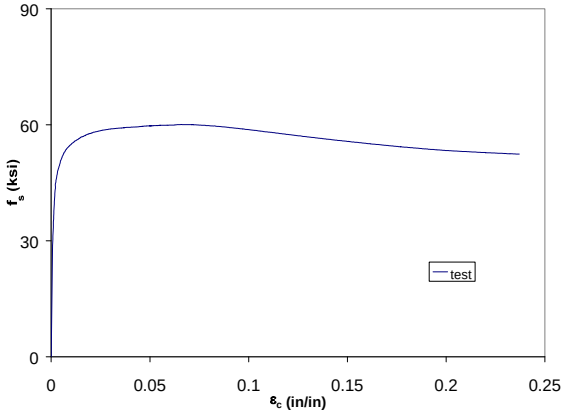

(b)

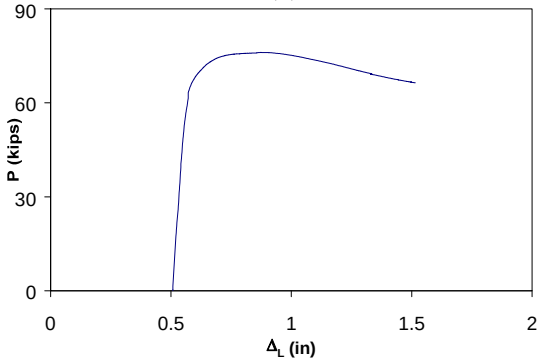

(c)

Figure C.65 Experimental load-deformation plots of #10 bar with L/d = 5 and e/d = 0.4

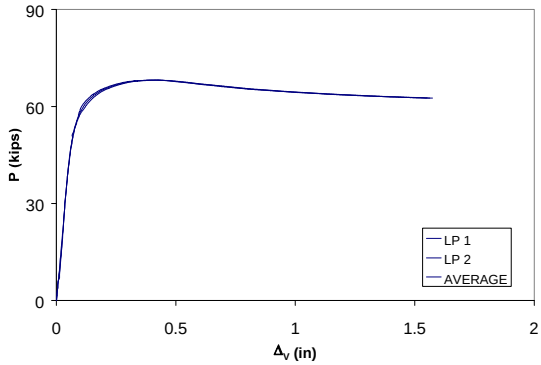

(a)

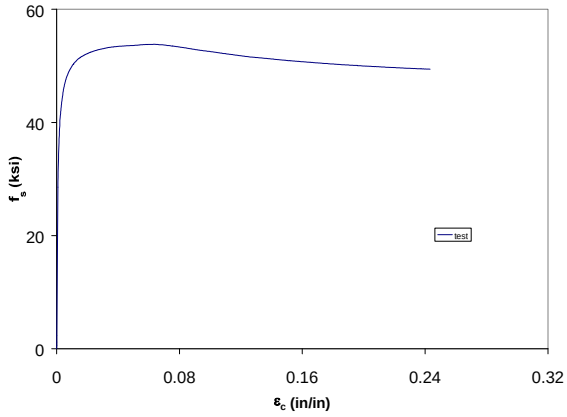

(b)

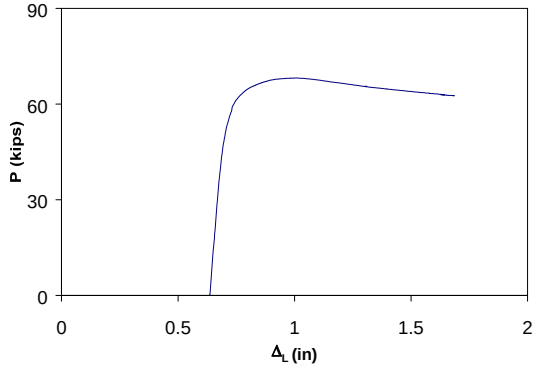

(c)

Figure C.66 Experimental load-deformation plots of #10 bar with L/d = 5 and e/d = 0.5

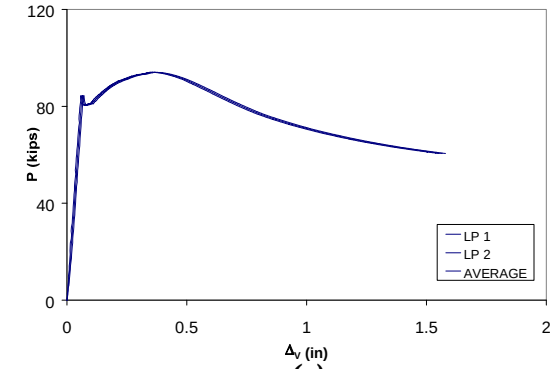

(a)

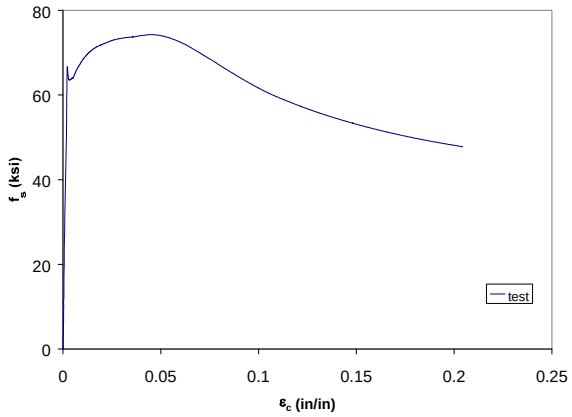

(b)

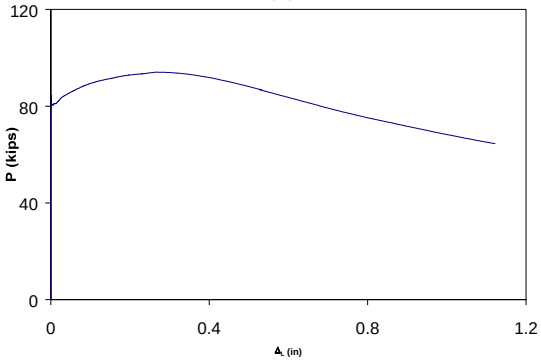

(c)

Figure C.67 Experimental load-deformation plots of #10 bar with L/d = 6 and e/d = 0.0

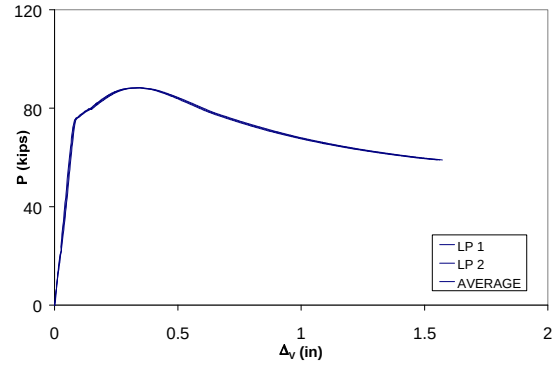

(a)

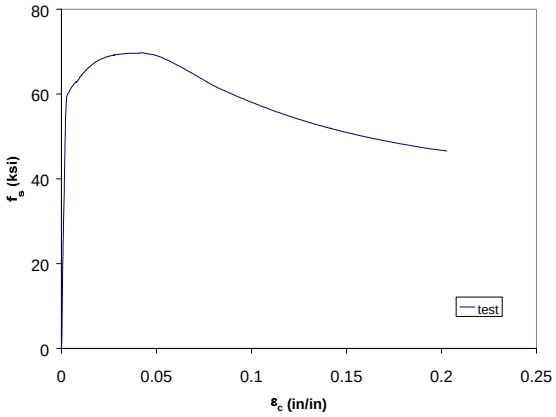

(b)

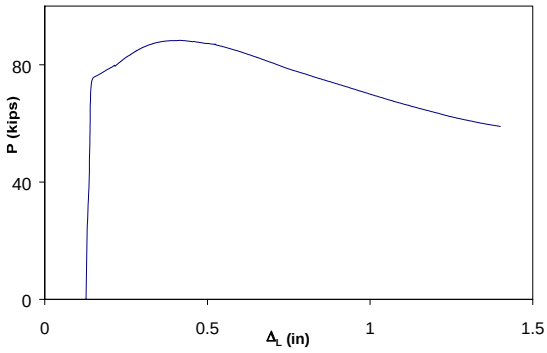

(c)

Figure C.68 Experimental load-deformation plots of #10 bar with L/d = 6 and e/d = 0.1

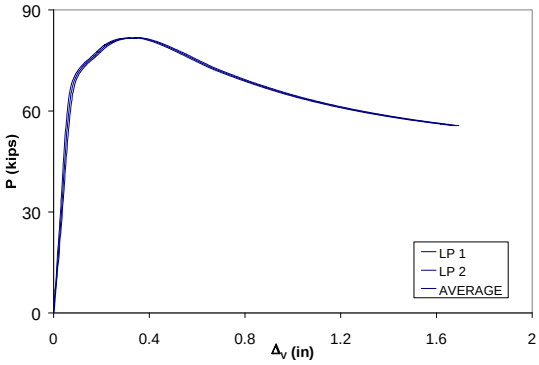

(a)

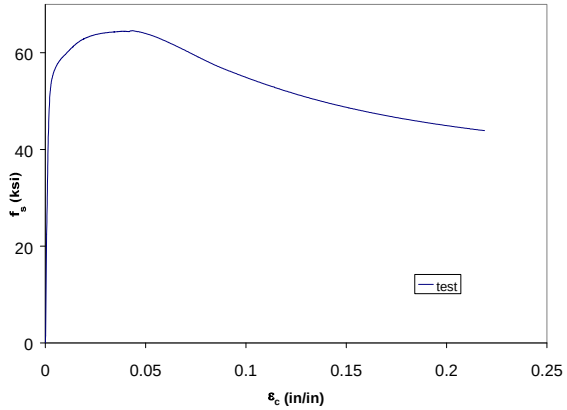

(b)

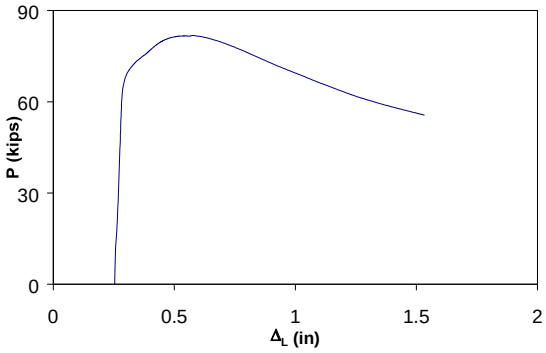

(c)

Figure C.69 Experimental load-deformation plots of #10 bar with L/d = 6 and e/d = 0.2

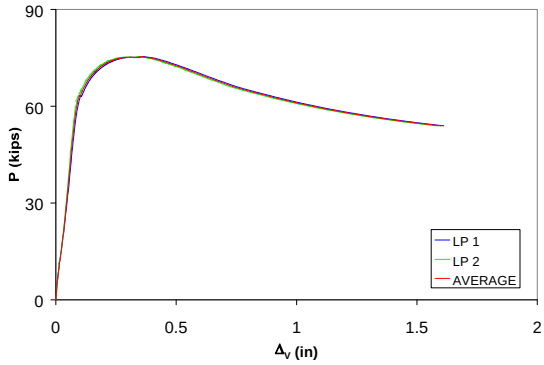

(a)

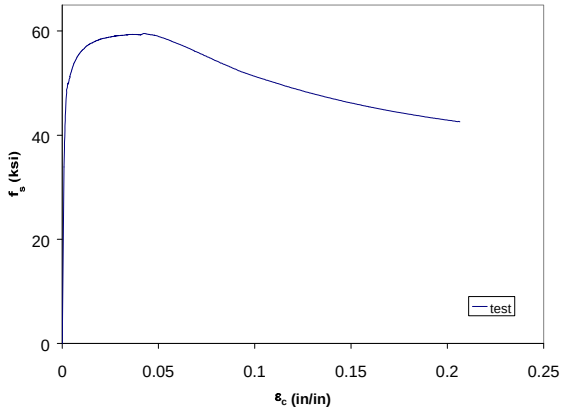

(b)

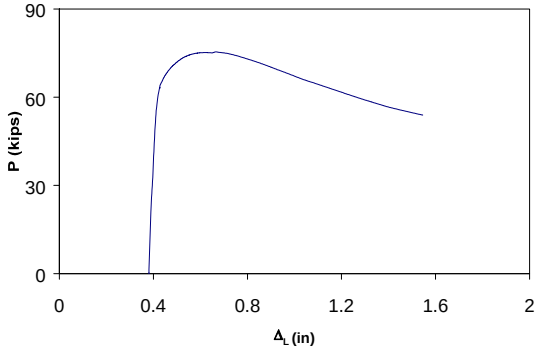

(c)

Figure C.70 Experimental load-deformation plots of #10 bar with L/d = 6 and e/d = 0.3

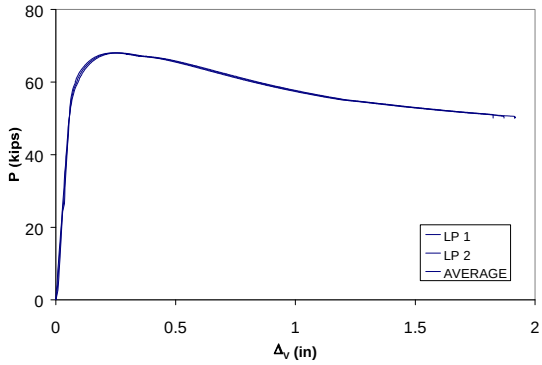

(a)

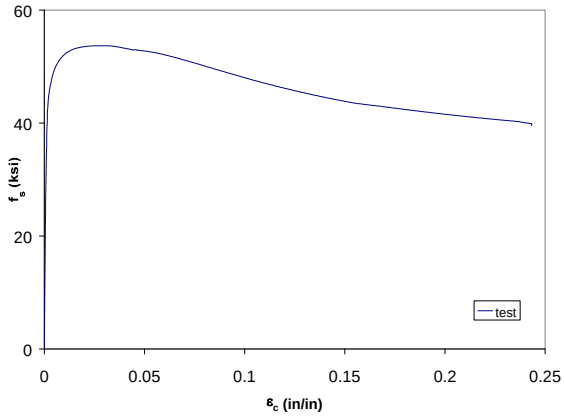

(b)

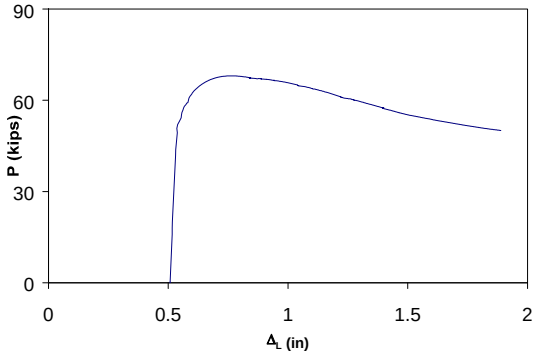

(c)

Figure C.71 Experimental load-deformation plots of #10 bar with L/d = 6 and e/d = 0.4

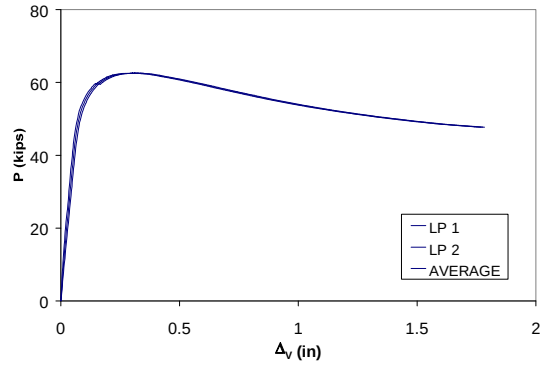

(a)

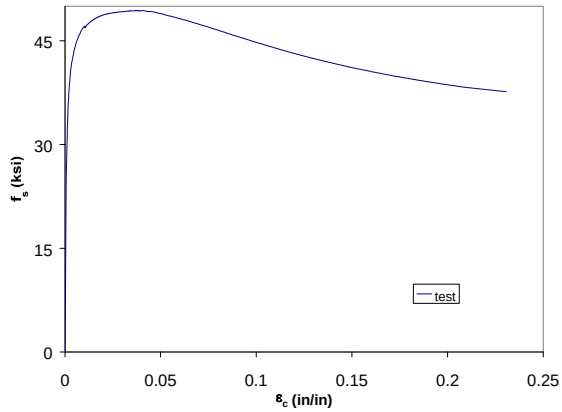

(b)

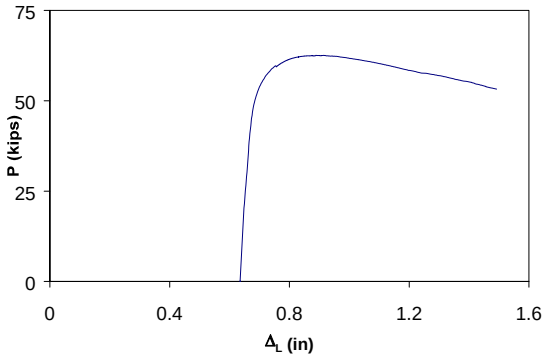

(c)

Figure C.72 Experimental load-deformation plots of #10 bar with L/d = 6 and e/d = 0.5

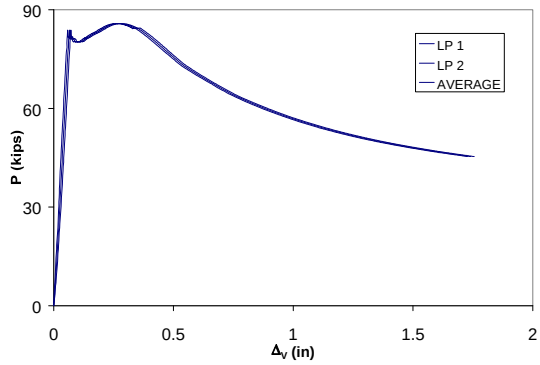

(a)

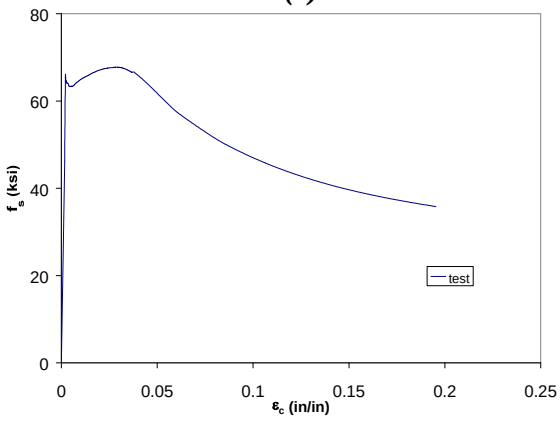

(b)

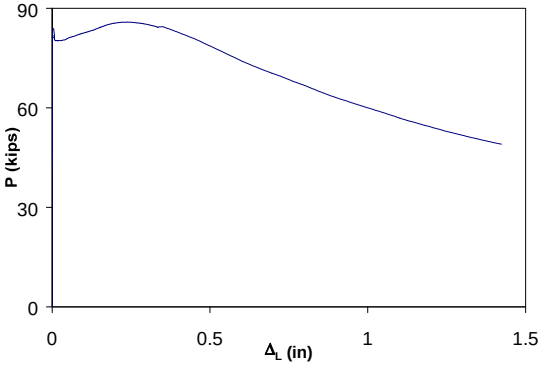

(c)

Figure C.73 Experimental load-deformation plots of #10 bar with L/d = 7 and e/d = 0.0

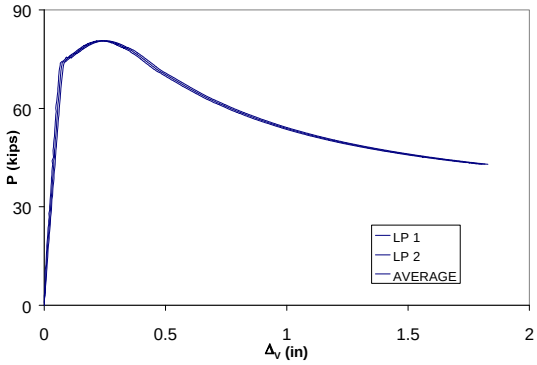

(a)

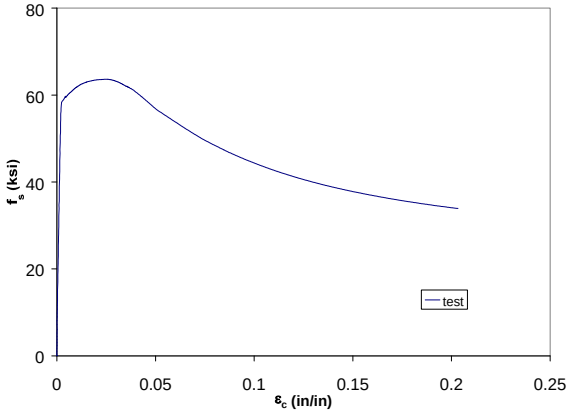

(b)

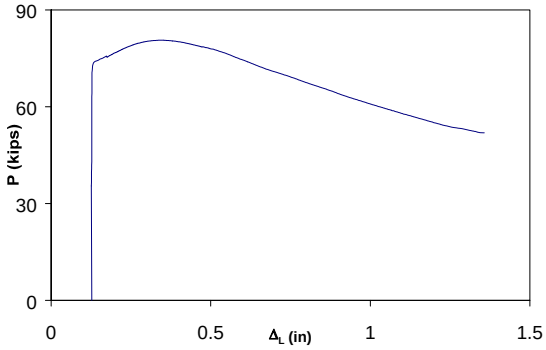

(c)

Figure C.74 Experimental load-deformation plots of #10 bar with L/d = 7 and e/d = 0.1

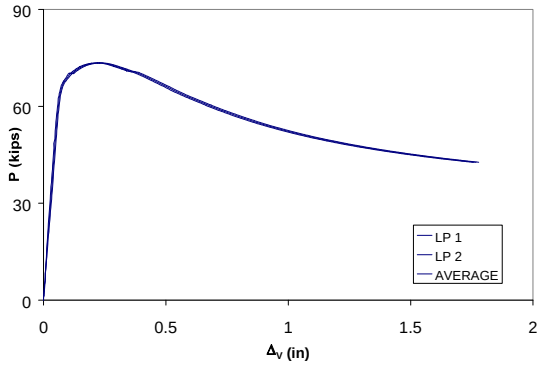

(a)

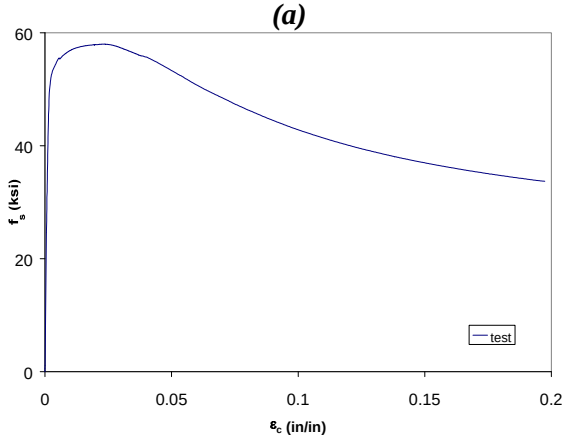

(b)

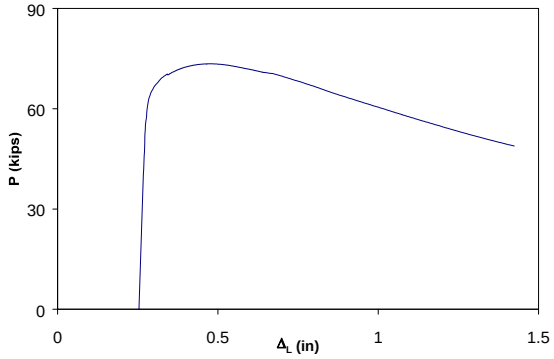

(c)

Figure C.75 Experimental load-deformation plots of #10 bar with L/d = 7 and e/d = 0.2

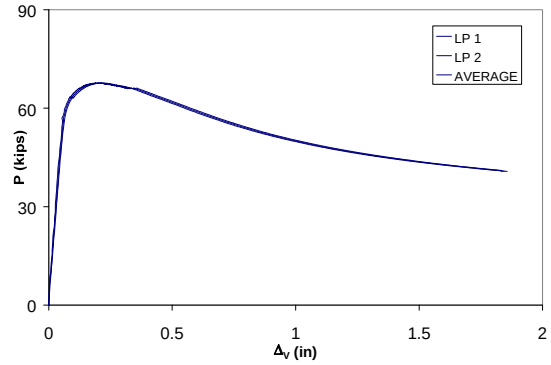

(a)

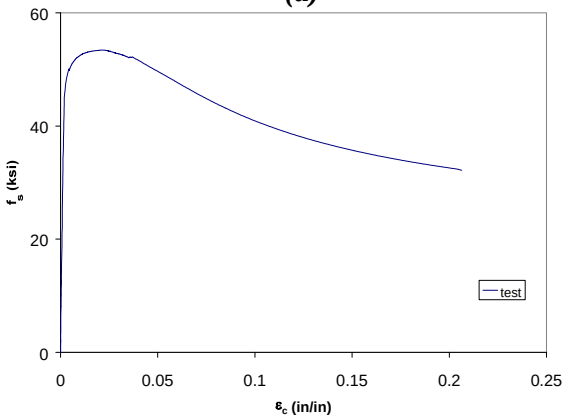

(b)

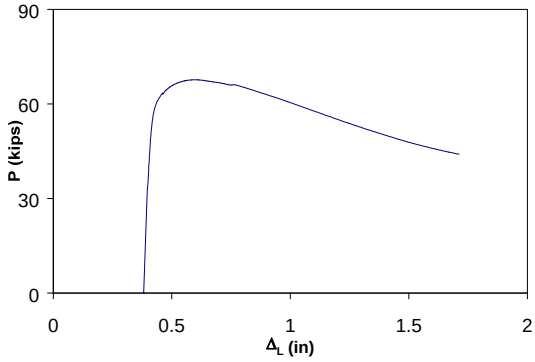

(c)

Figure C.76 Experimental load-deformation plots of #10 bar with L/d = 7 and e/d = 0.3

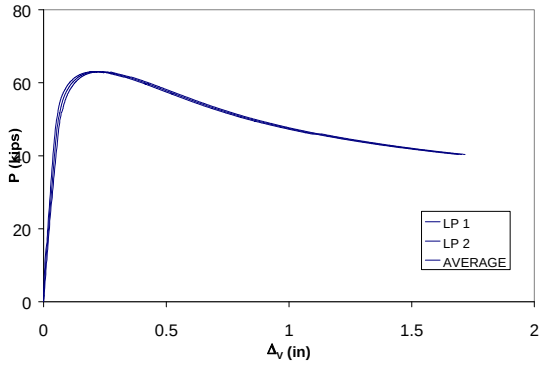

(a)

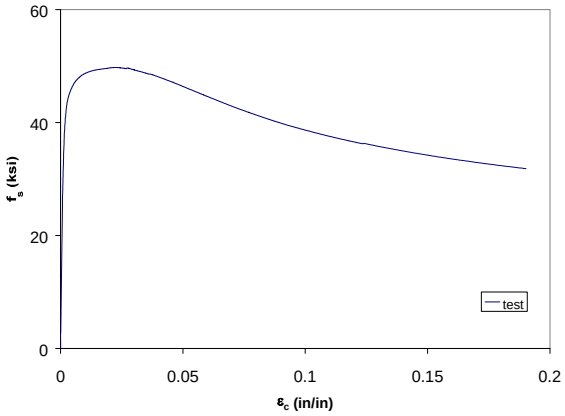

(b)

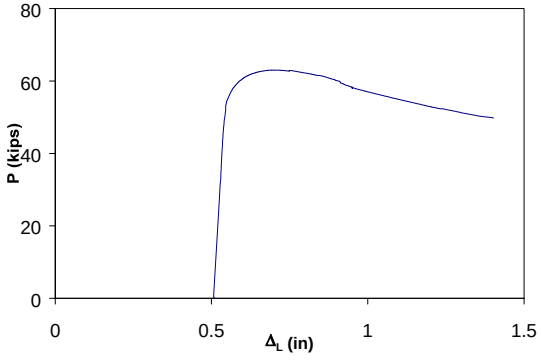

(c)

Figure C.77 Experimental load-deformation plots of #10 bar with L/d = 7 and e/d = 0.4

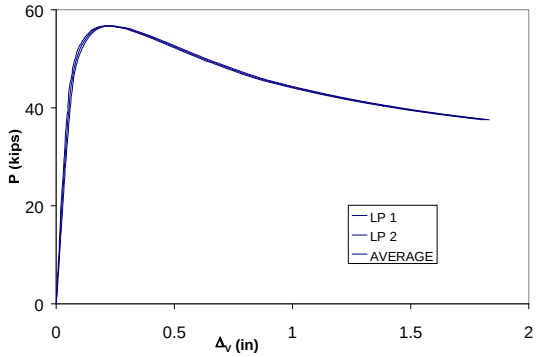

(a)

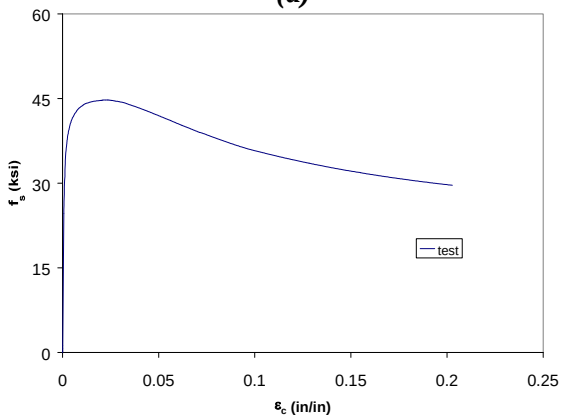

(b)

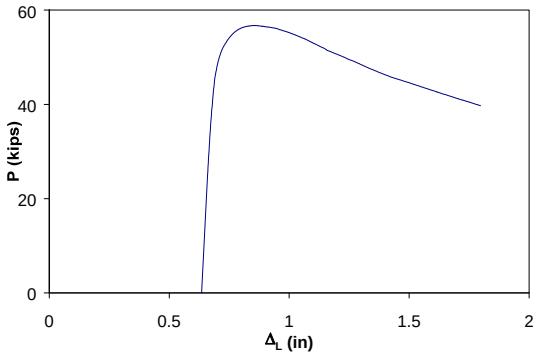

(c)

Figure C.78 Experimental load-deformation plots of #10 bar with L/d = 7 and e/d = 0.5

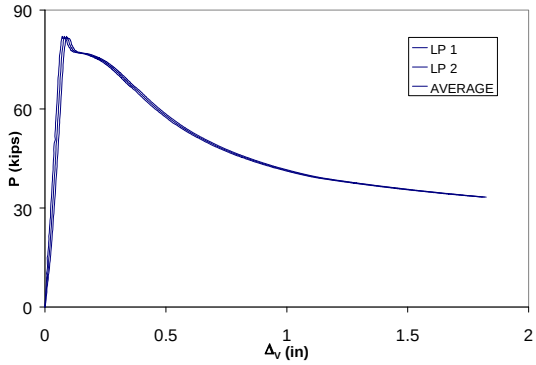

(a)

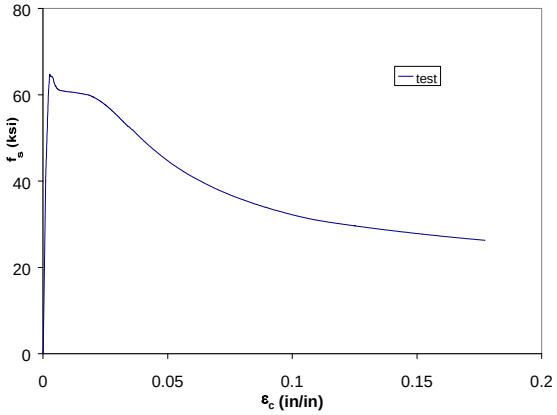

(b)

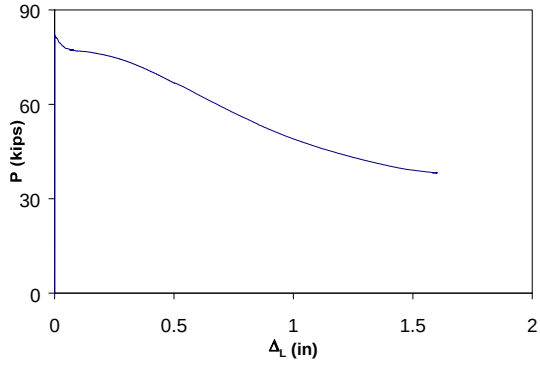

(c)

Figure C.79 Experimental load-deformation plots of #10 bar with L/d = 8 and e/d = 0.0

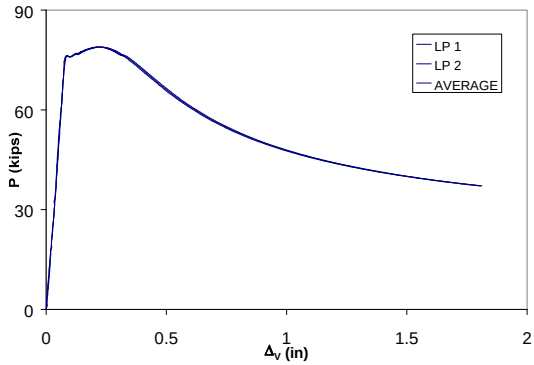

(a)

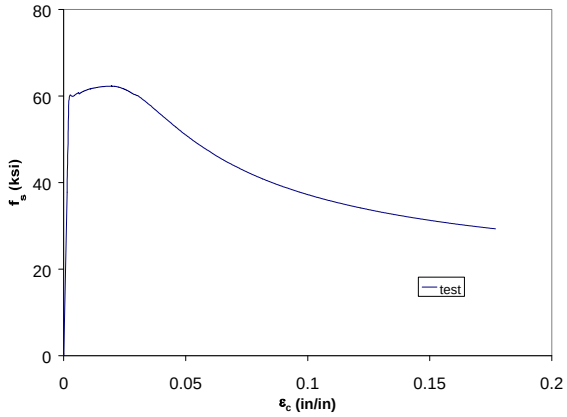

(b)

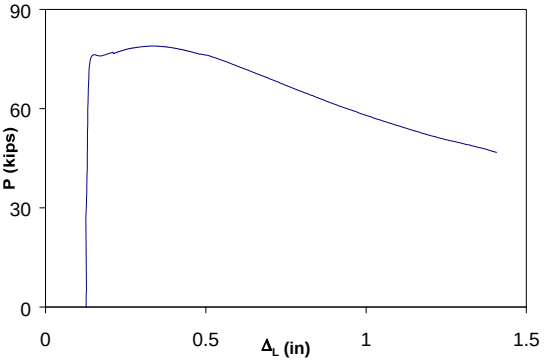

(c)

Figure C.80 Experimental load-deformation plots of #10 bar with L/d = 8 and e/d = 0.1

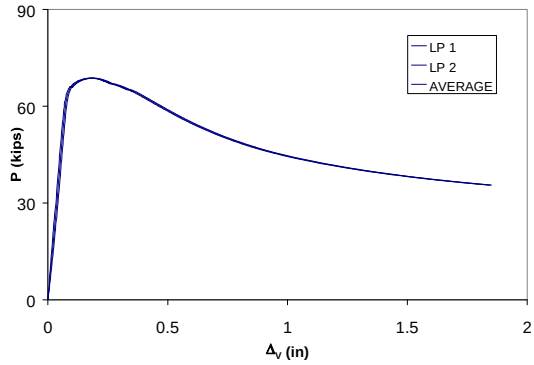

(a)

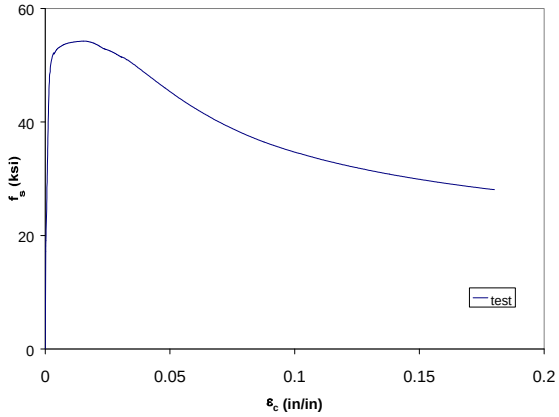

(b)

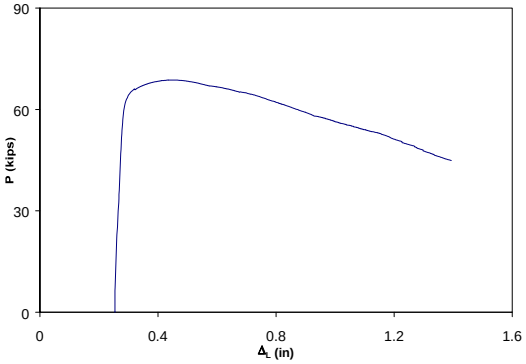

(c)

Figure C.81 Experimental load-deformation plots of #10 bar with L/d = 8 and e/d = 0.2

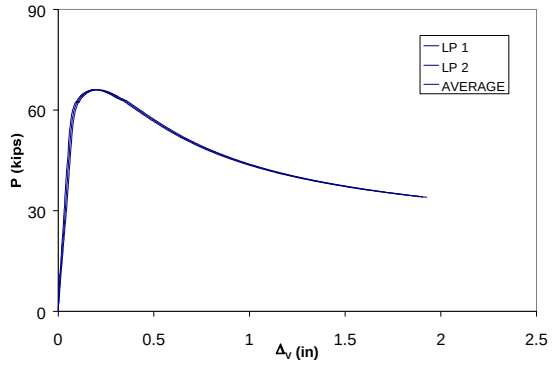

(a)

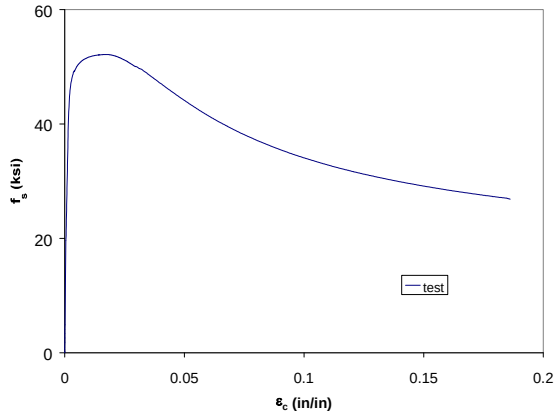

(b)

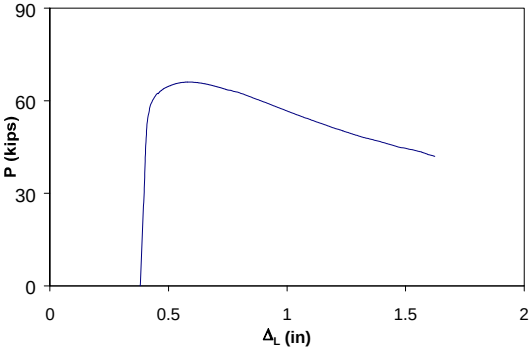

(c)

Figure C.82 Experimental load-deformation plots of #10 bar with L/d = 8 and e/d = 0.3

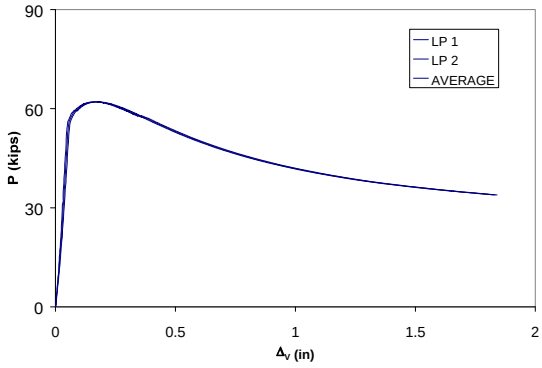

(a)

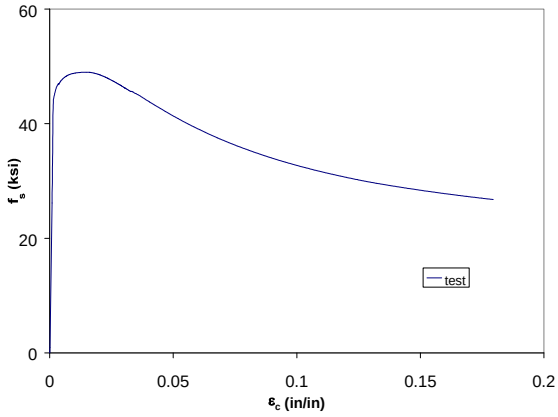

(b)

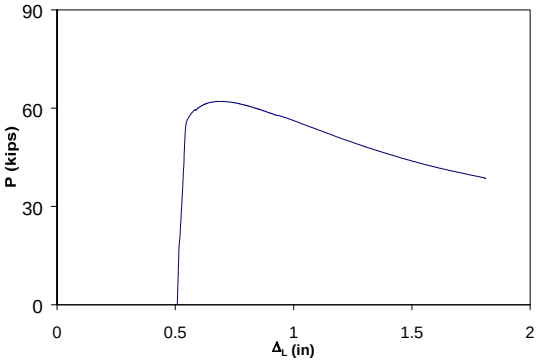

(c)

Figure C.83 Experimental load-deformation plots of #10 bar with L/d = 8 and e/d = 0.4

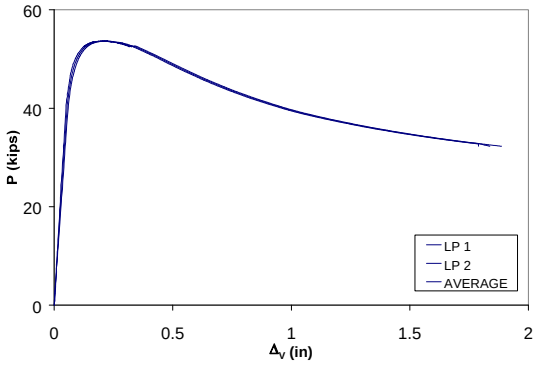

(a)

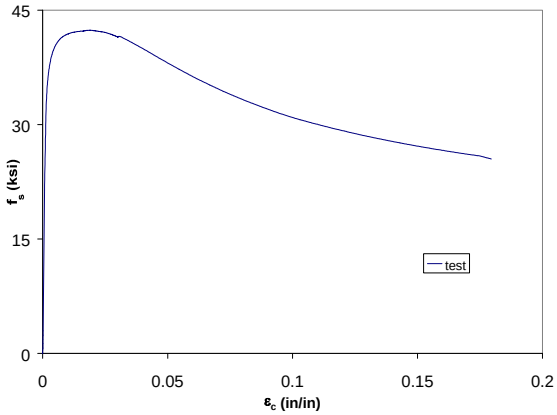

(b)

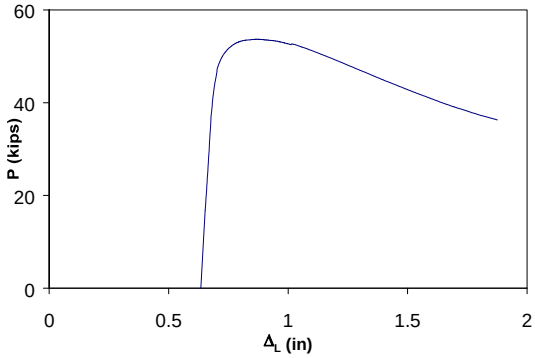

(c)

Figure C.84 Experimental load-deformation plots of #10 bar with L/d = 8 and e/d = 0.5

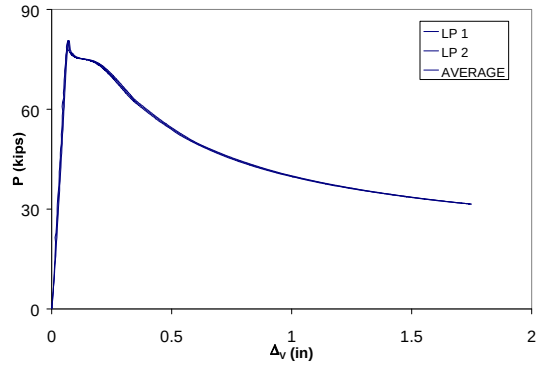

(a)

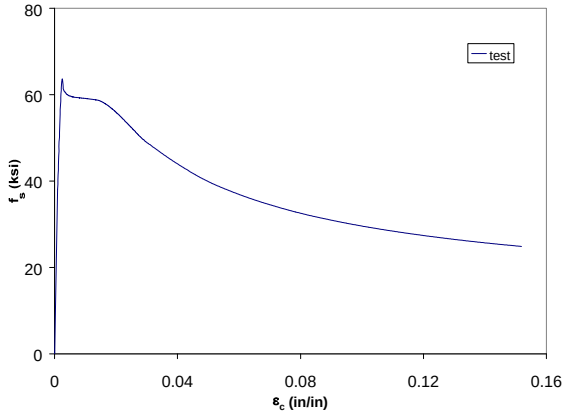

(b)

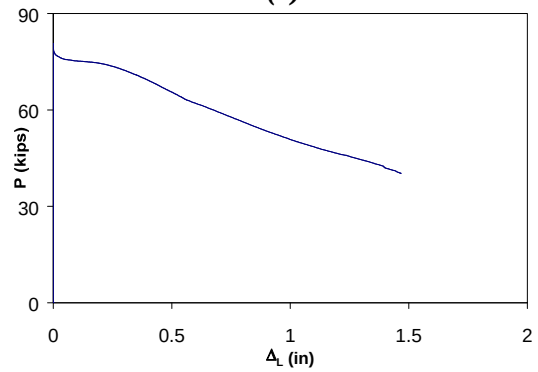

(c)

Figure C.85 Experimental load-deformation plots of #10 bar with L/d = 9 and e/d = 0.0

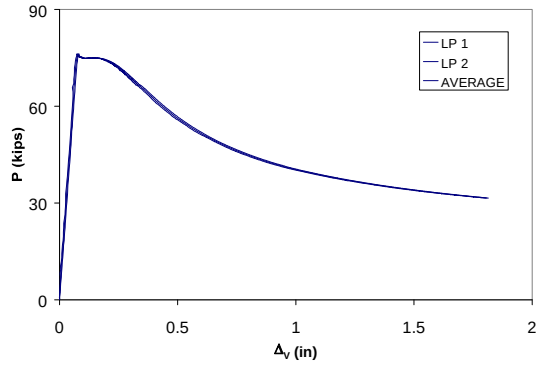

(a)

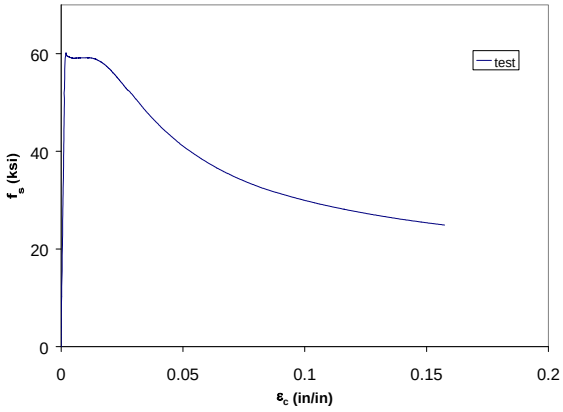

(b)

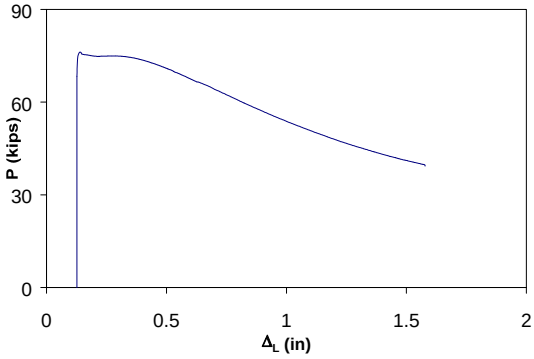

(c)

Figure C.86 Experimental load-deformation plots of #10 bar with L/d = 9 and e/d = 0.1

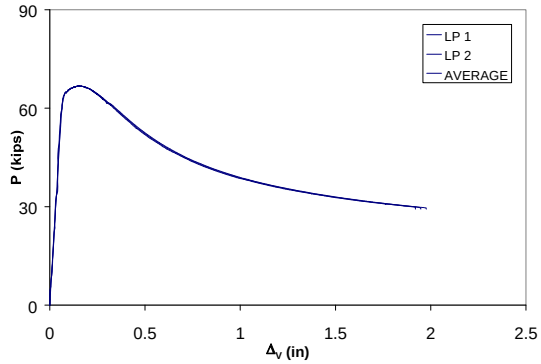

(a)

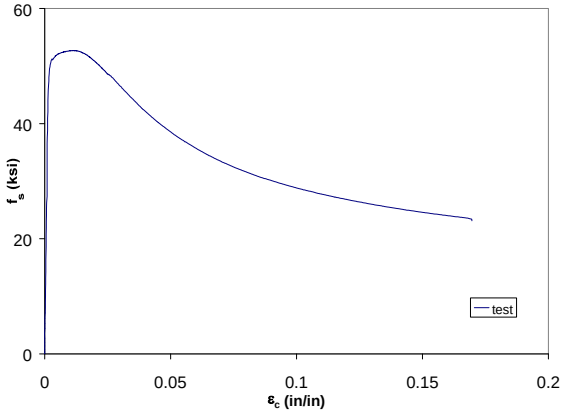

(b)

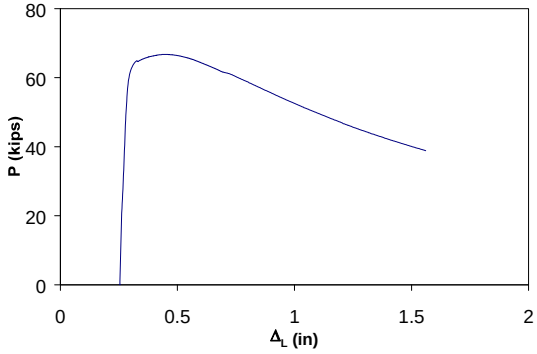

(c)

Figure C.87 Experimental load-deformation plots of #10 bar with L/d = 9 and e/d = 0.2

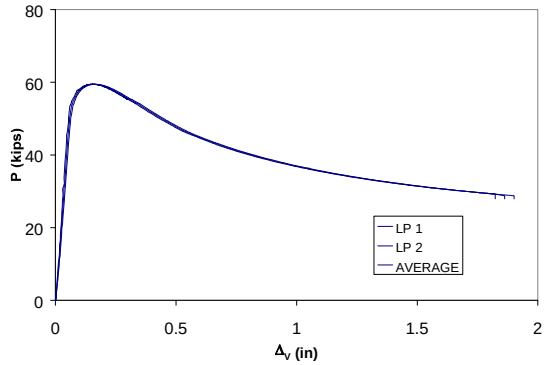

(a)

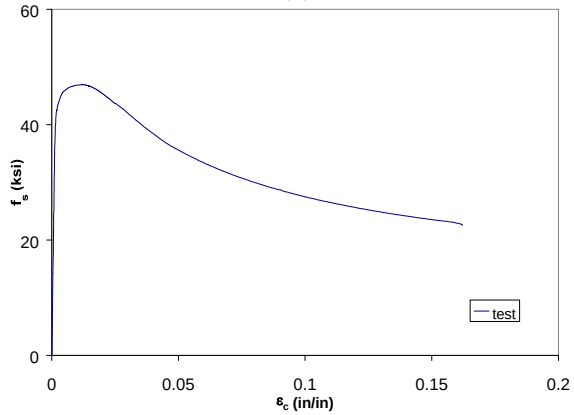

(b)

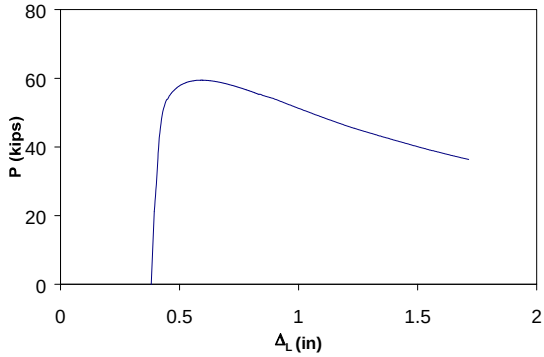

(c)

Figure C.88 Experimental load-deformation plots of #10 bar with L/d = 9 and e/d = 0.3

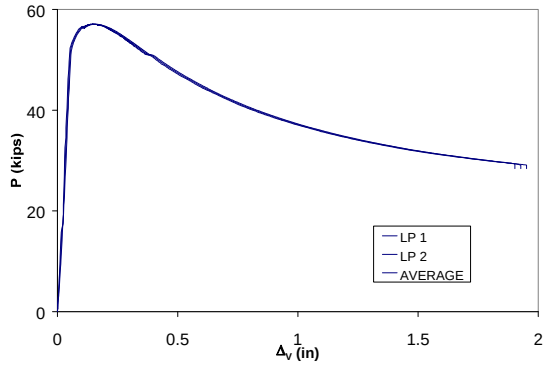

(a)

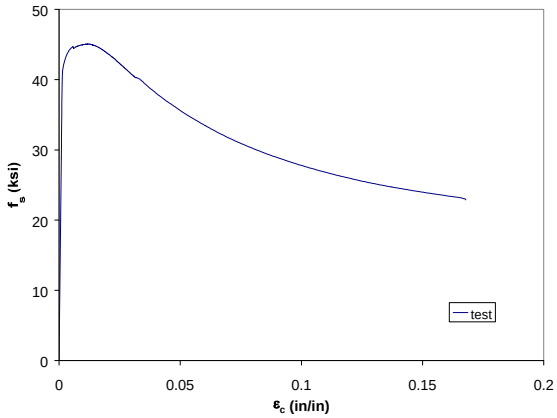

(b)

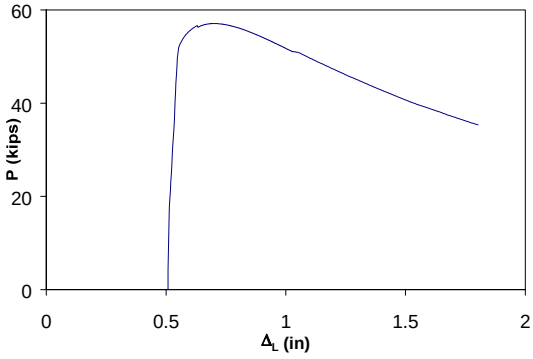

(c)

Figure C.89 Experimental load-deformation plots of #10 bar with L/d = 9 and e/d = 0.4

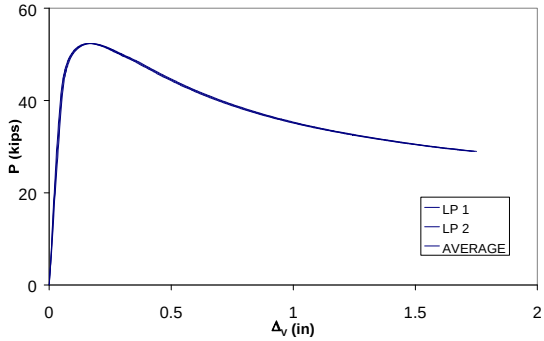

(a)

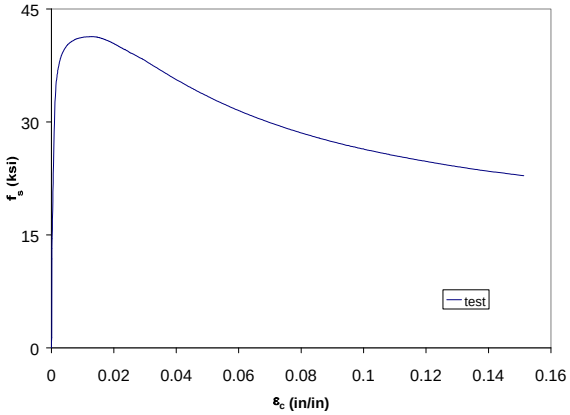

(b)

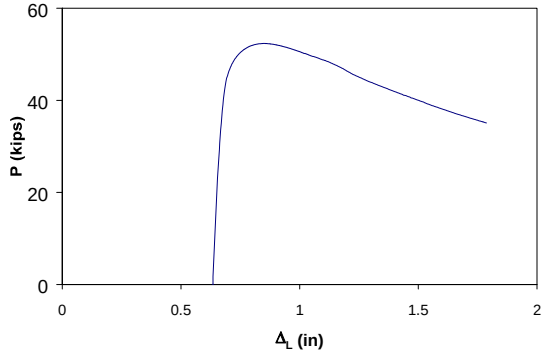

(c)

Figure C.90 Experimental load-deformation plots of #10 bar with L/d = 9 and e/d = 0.5

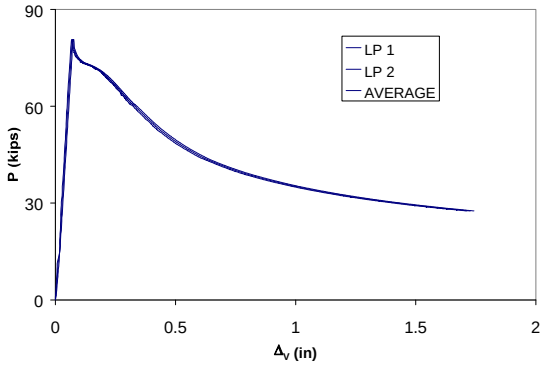

(a)

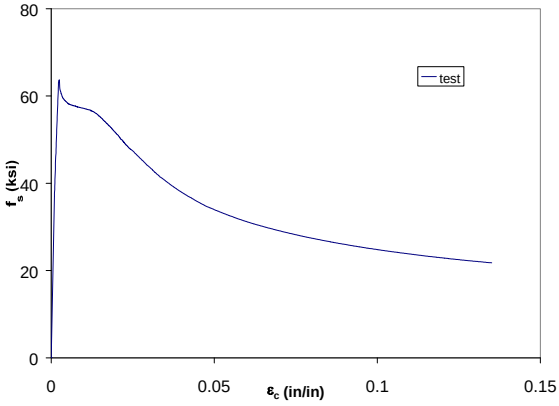

(b)

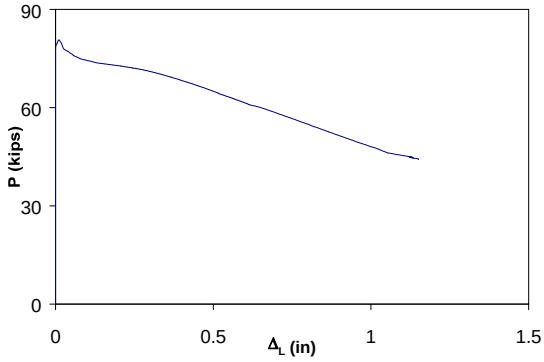

(c)

Figure C.91 Experimental load-deformation plots of #10 bar with L/d = 10 and e/d = 0.0

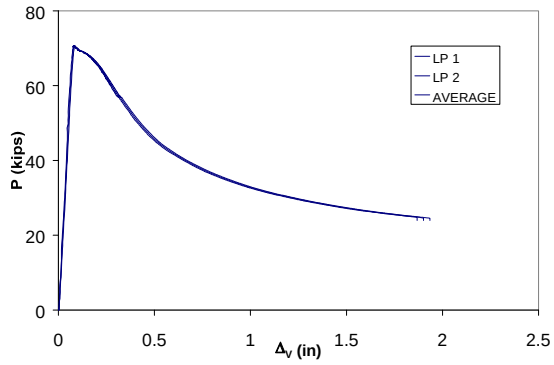

(a)

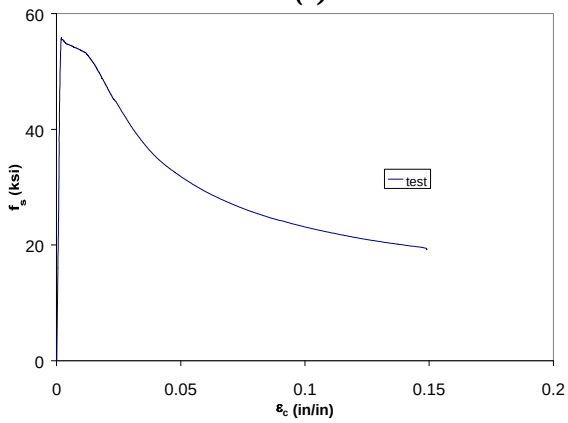

(b)

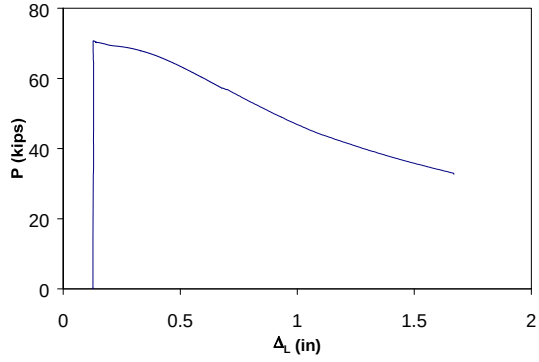

(c)

Figure C.92 Experimental load-deformation plots of #10 bar with L/d = 10 and e/d = 0.1

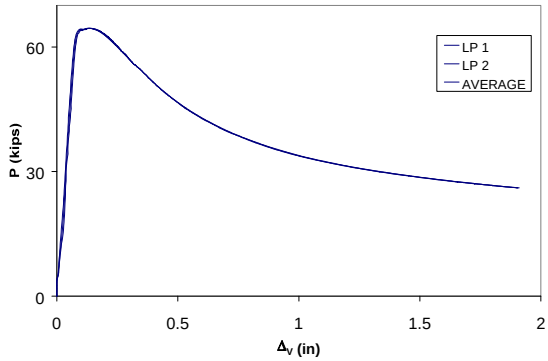

(a)

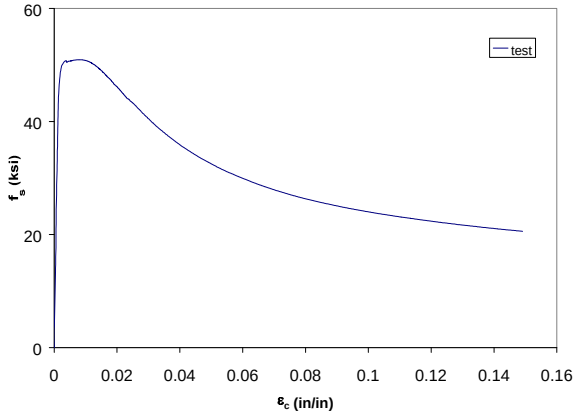

(b)

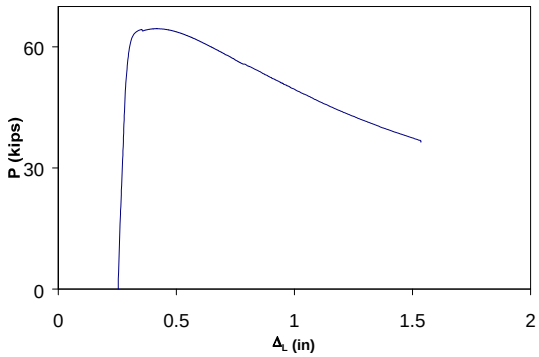

(c)

Figure C.93 Experimental load-deformation plots of #10 bar with L/d = 10 and e/d = 0.2

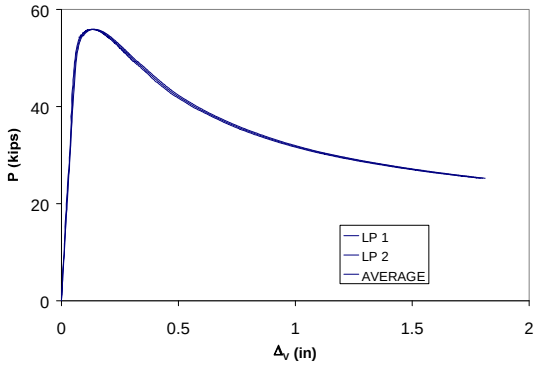

(a)

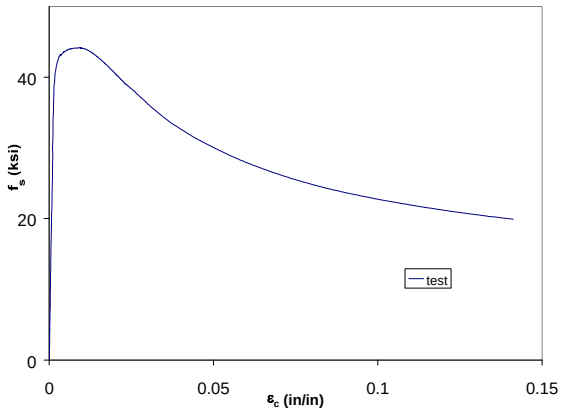

(b)

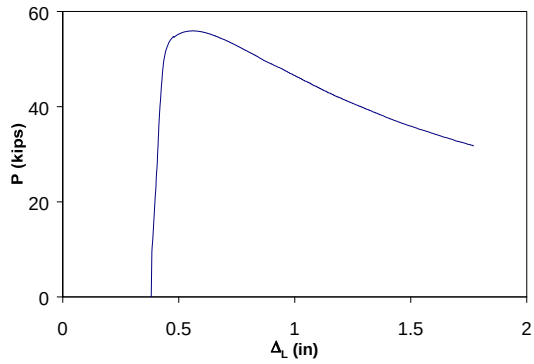

(c)

Figure C.94 Experimental load-deformation plots of #10 bar with L/d = 10 and e/d = 0.3

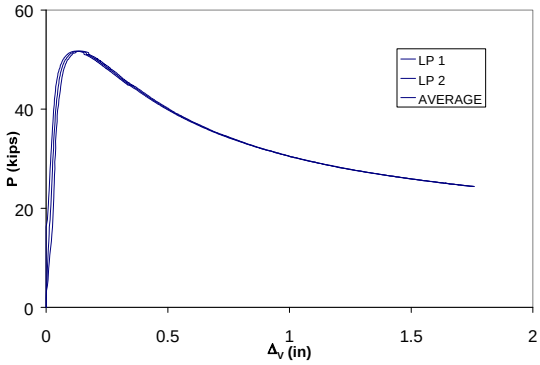

(a)

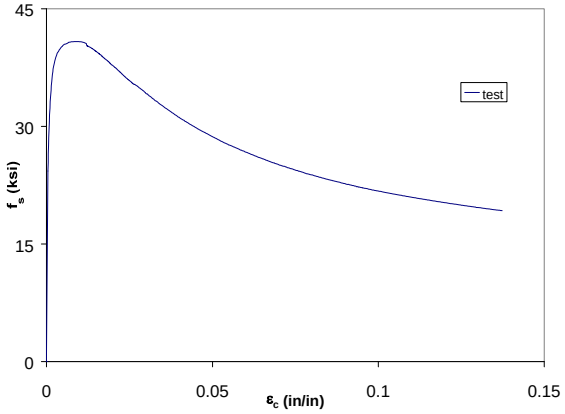

(b)

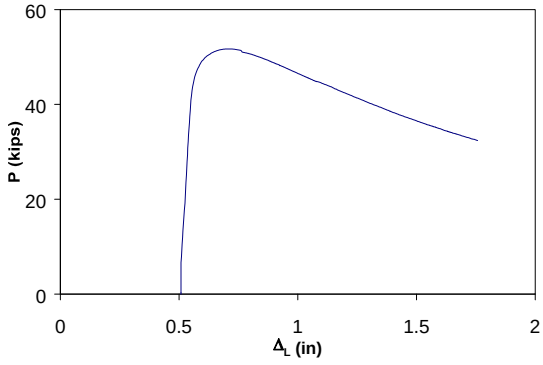

(c)

Figure C.95 Experimental load-deformation plots of #10 bar with L/d = 10 and e/d = 0.4

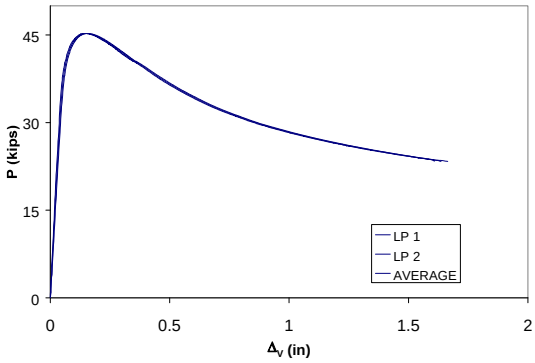

(a)

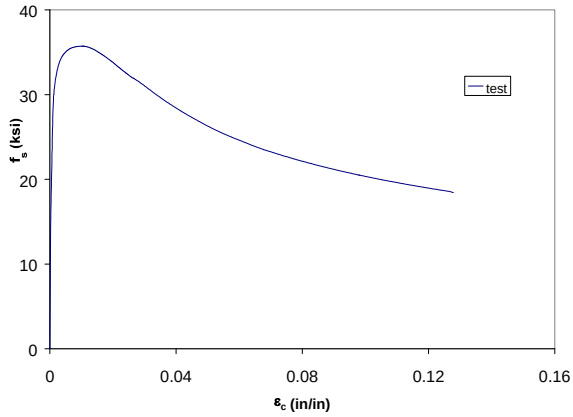

(b)

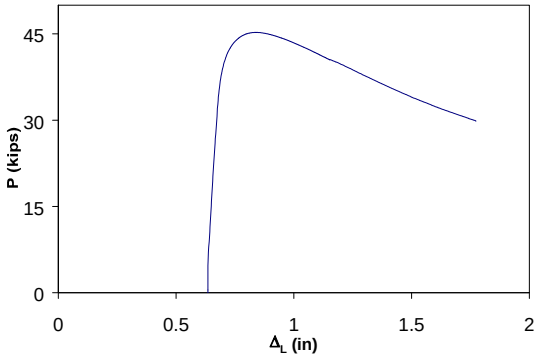

(c)

Figure C.96 Experimental load-deformation plots of #10 bar with L/d = 10 and e/d = 0.5

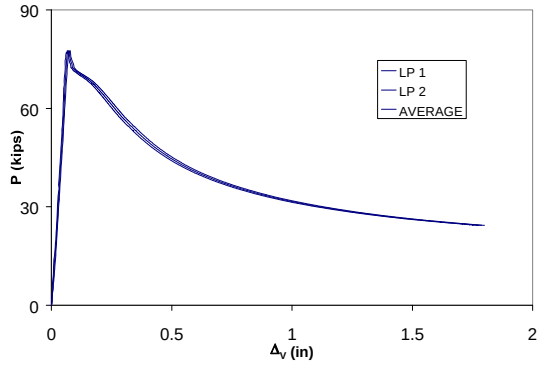

(a)

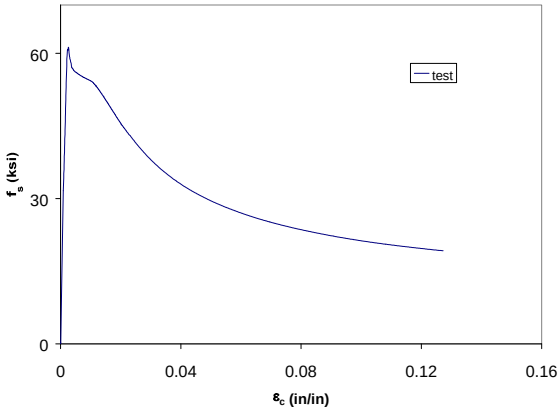

(b)

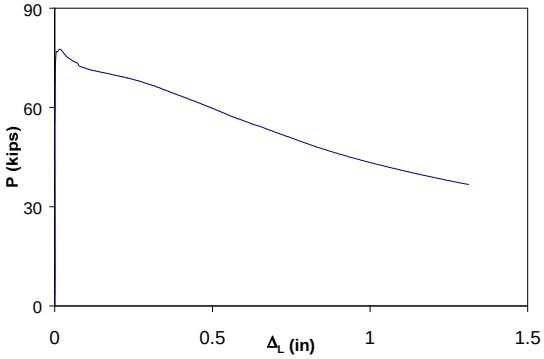

(c)

Figure C.97 Experimental load-deformation plots of #10 bar with L/d = 11 and e/d = 0.0

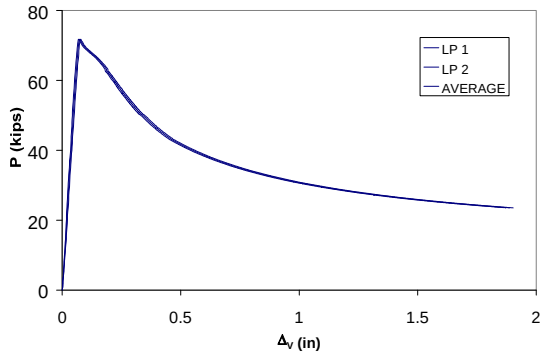

(a)

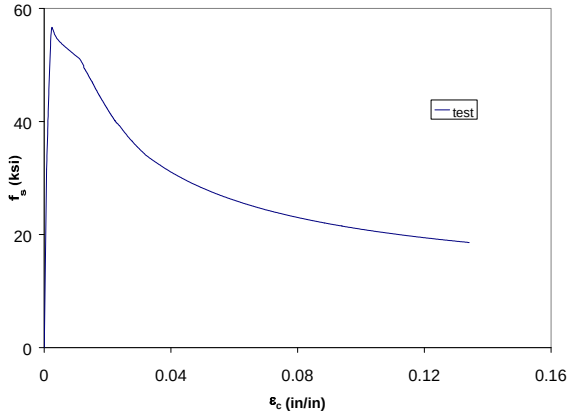

(b)

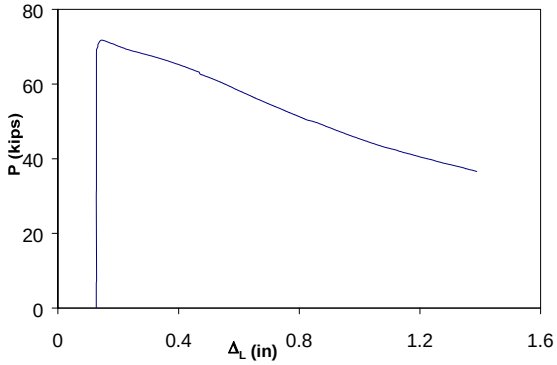

(c)

Figure C.98 Experimental load-deformation plots of #10 bar with L/d = 11 and e/d = 0.1

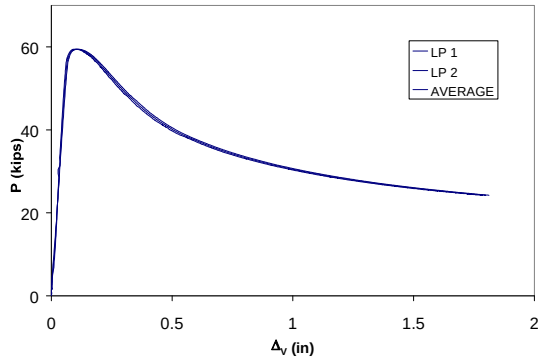

(a)

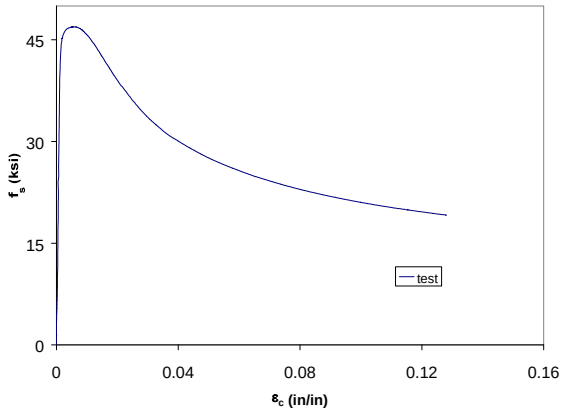

(b)

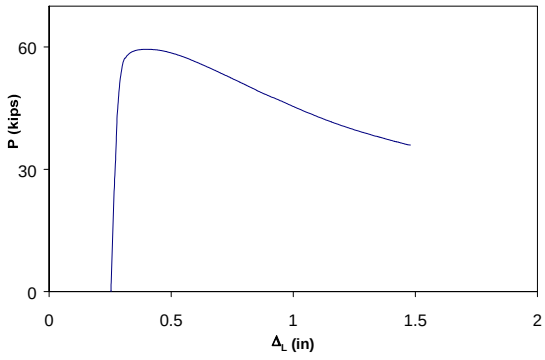

(c)

Figure C.99 Experimental load-deformation plots of #10 bar with L/d = 11 and e/d = 0.2

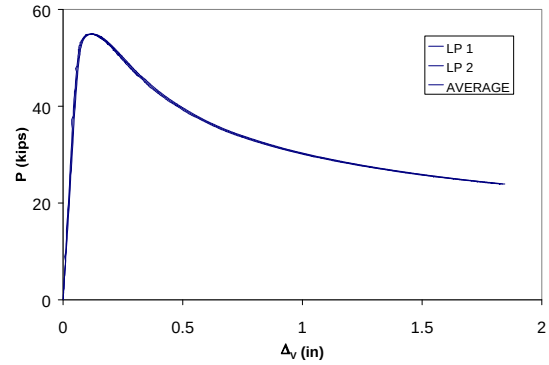

(a)

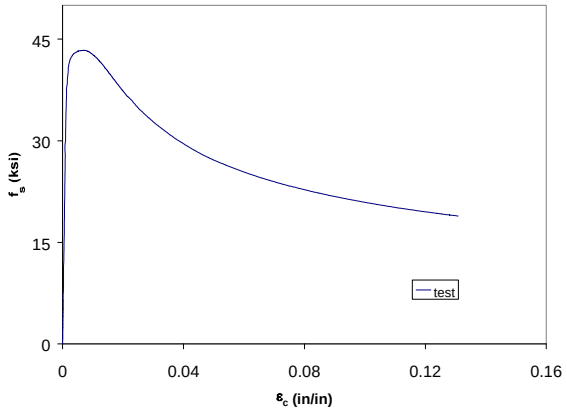

(b)

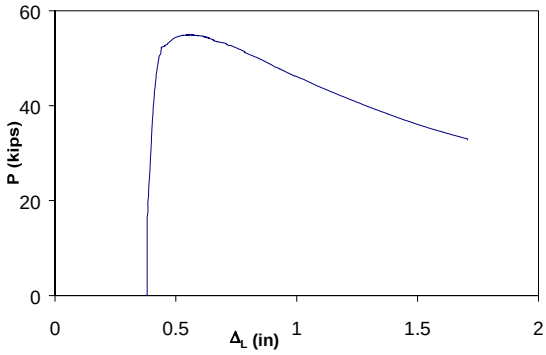

(c)

Figure C.100 Experimental load-deformation plots of #10 bar with L/d = 11 and e/d = 0.3

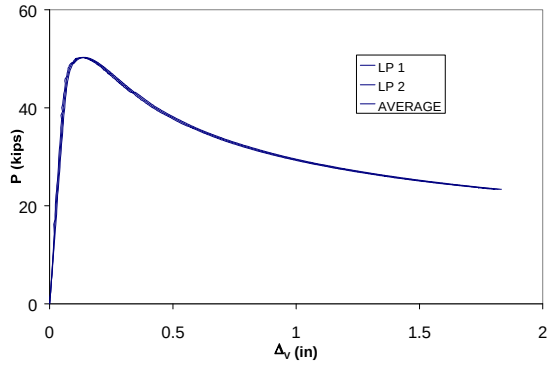

(a)

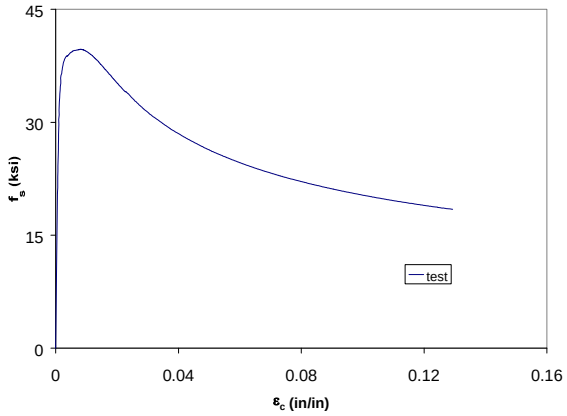

(b)

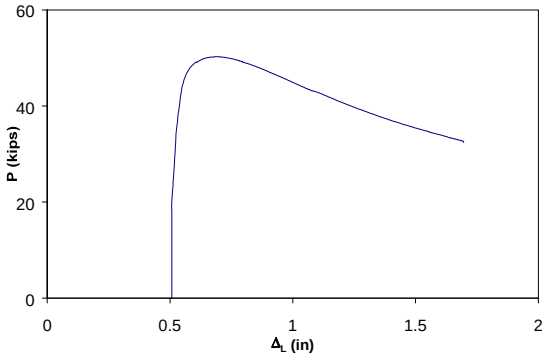

(c)

Figure C.101 Experimental load-deformation plots of #10 bar with L/d = 11 and e/d = 0.4

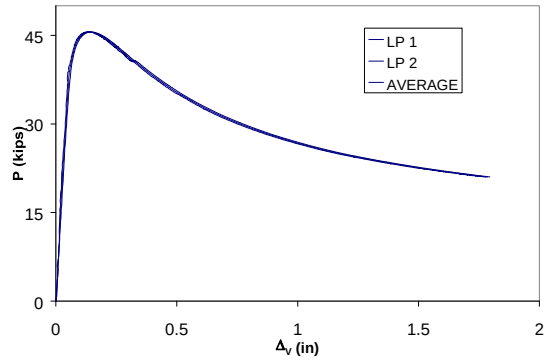

(a)

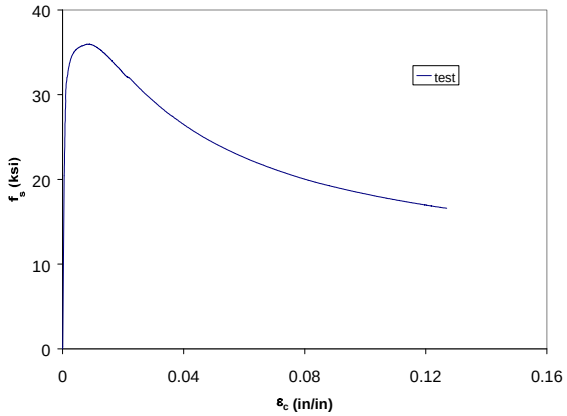

(b)

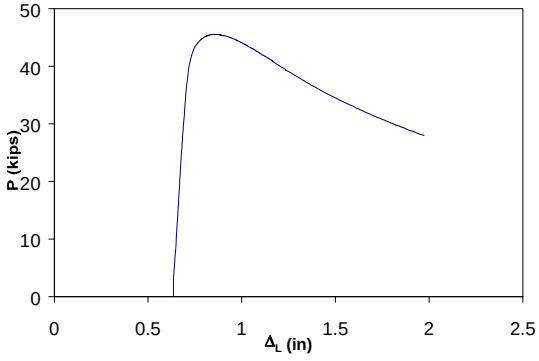

(c)

Figure C.102 Experimental load-deformation plots of #10 bar with L/d = 11 and e/d = 0.5

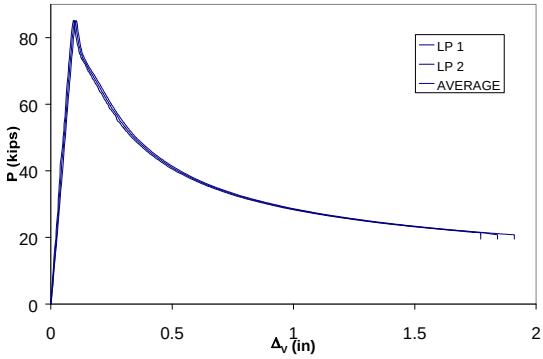

(a)

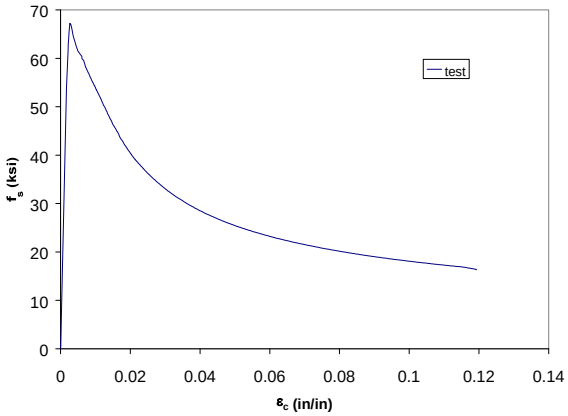

(b)

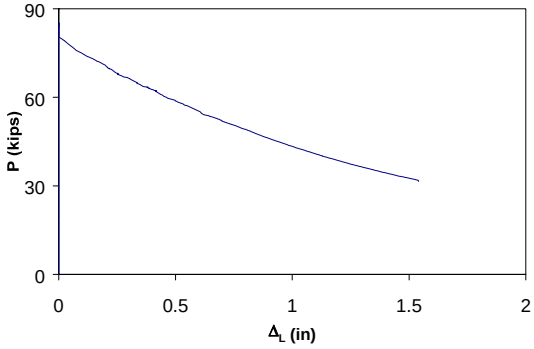

(c)

Figure C.103 Experimental load-deformation plots of #10 bar with L/d = 12 and e/d = 0.0

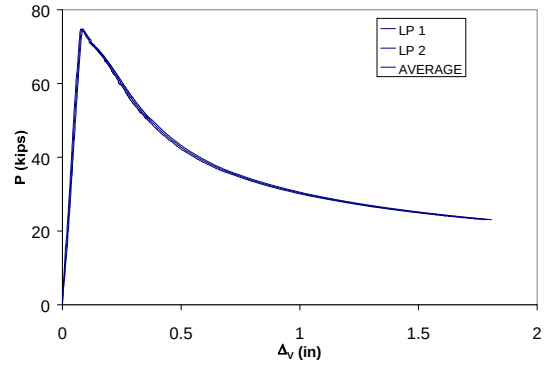

(a)

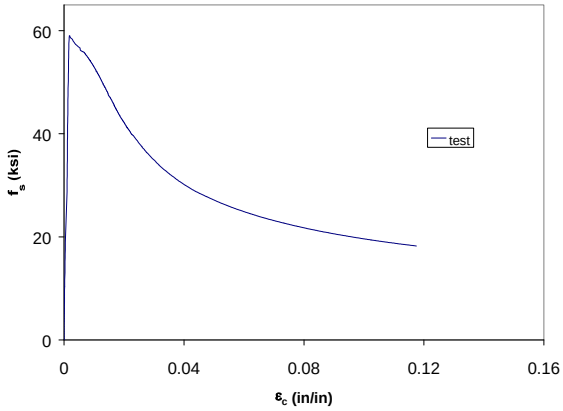

(b)

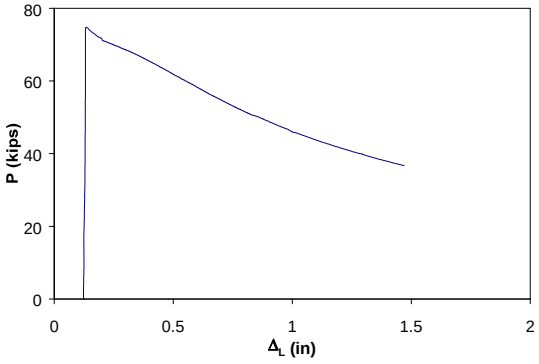

(c)

Figure C.104 Experimental load-deformation plots of #10 bar with L/d = 12 and e/d = 0.1

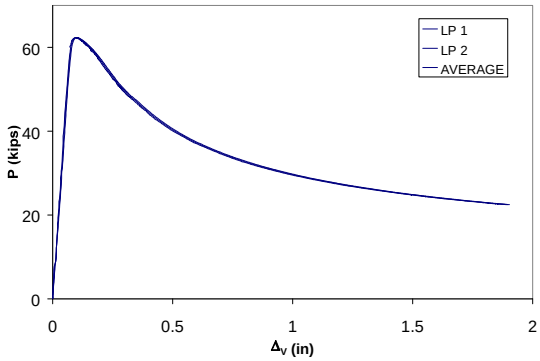

(a)

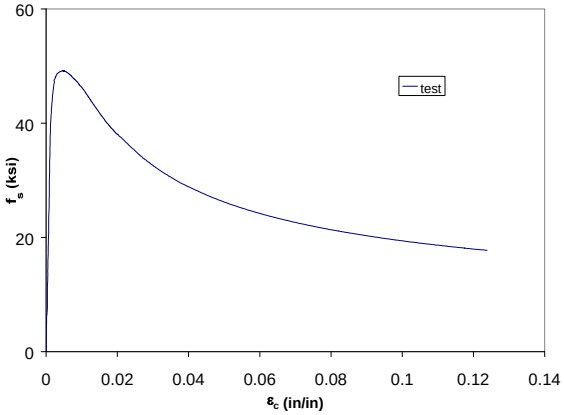

(b)

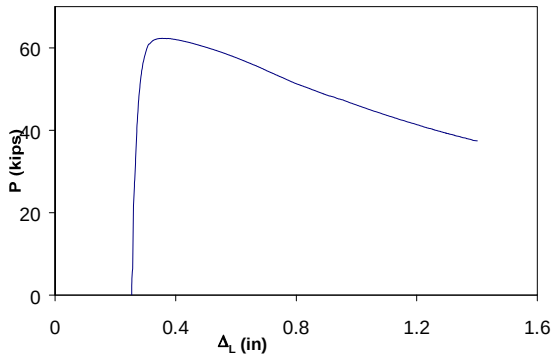

(c)

Figure C.105 Experimental load-deformation plots of #10 bar with L/d = 12 and e/d = 0.2

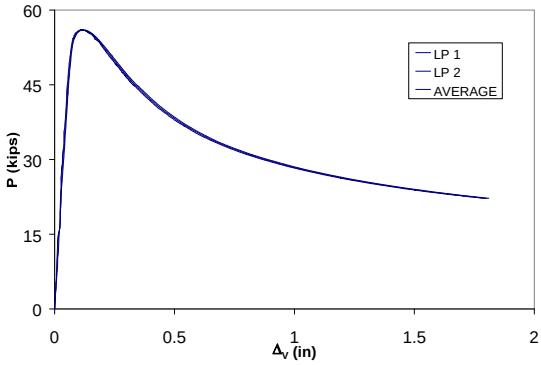

(a)

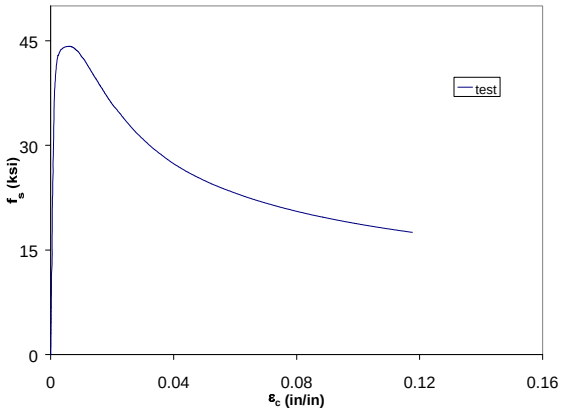

(b)

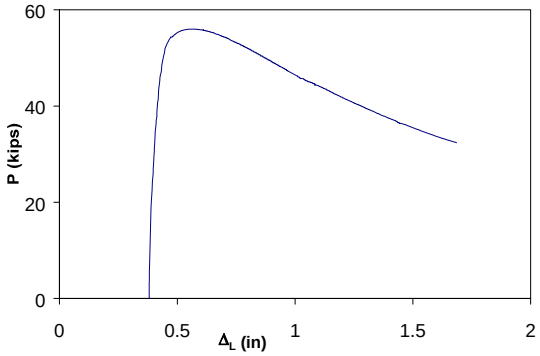

(c)

Figure C.106 Experimental load-deformation plots of #10 bar with L/d = 12 and e/d = 0.3

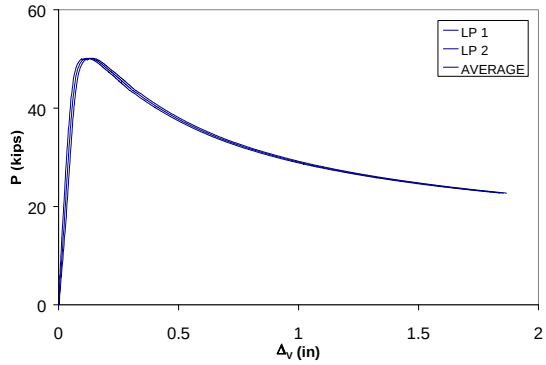

(a)

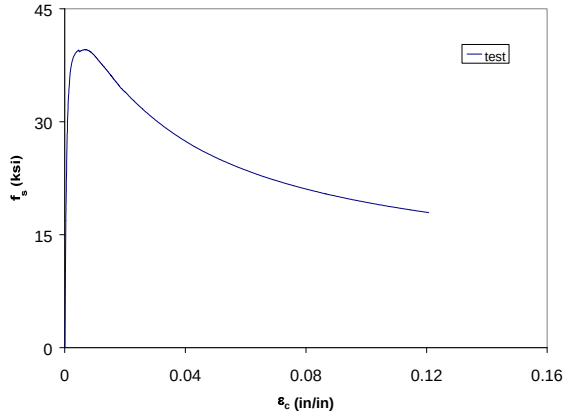

(b)

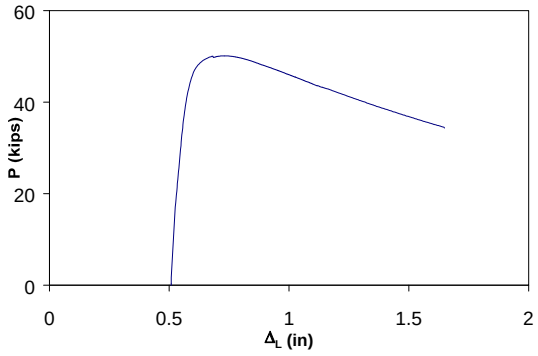

(c)

Figure C.107 Experimental load-deformation plots of #10 bar with L/d = 12 and e/d = 0.4

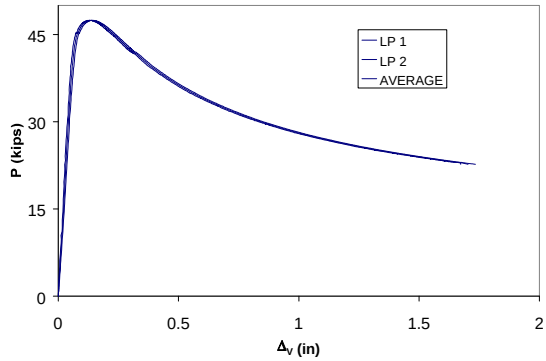

(a)

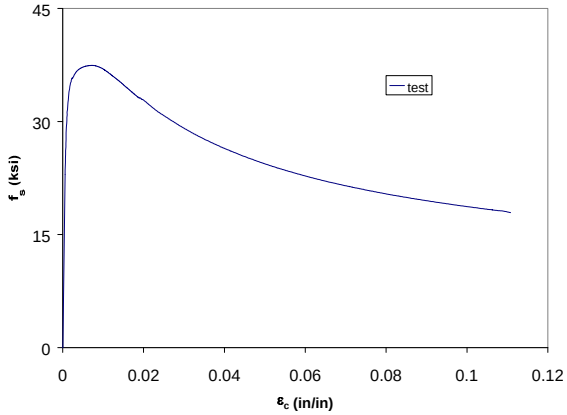

(b)

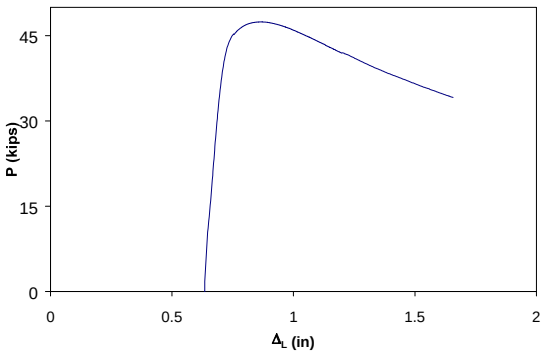

(c)

Figure C.108 Experimental load-deformation plots of #10 bar with L/d = 12 and e/d = 0.5

REFERENCES

1. ACI Committee 318, *Building Code Requirements for Reinforced Concrete* (ACI 318-02), American Concrete Institute, 2002

2. Bayrak, Oguzhan, *Seismic performance of rectilinearly confined high strength concrete columns*, PhD dissertation, University of Toronto, Toronto, 1999.

3. Bayrak, Oguzhan and Sheikh, Shamin A., "Plastic Hinge Analysis", *Journal of Structural Engineering* V. 127 No.9, September 2001.

4. Bresler, B. and Gilbert, P.H., "Tie requirements for reinforced concrete columns, *Journal of the American Concrete Institute* V. 58, 1961.

5. Filippou, F.C., Bertero, V.V., and Popov, E.P., "Effect of bond deterioration on hysteretic behavior of reinforced concrete joints", *Report No. UCB/EERC-83/19*, University of Berkley, California, 1983.

6. Kaar, P.H. and Corley, W.G., "Properties of confined concrete for design of earthquake resistant structures", *Proceeding 6th World Conference on Earthquake Engineering*, Indian Society of Earthquake Technology, Vol.1, 1977.

7. Mander, J.B., Priestley, M.J.N., and Park, R., "Seismic design of bridge piers", *Report No. 84-2*, Department of Civil Engineering, University of Canterbury, February 1984.

8. Mau, S.T. and El-Mabsout, Mounir, "Inelastic buckling of reinforcing bars", *Journal of Engineering Mechanics* V. 115 No.1, January 1989.

9. Mau, S.T., "Effect of tie spacing on inelastic buckling of reinforcing bars, *ACI Structural Journal* V. 87 No.6, November-December1990.

10. Menegotto, M., and Pinto, P.E., "Method of analysis of cyclically loaded R.C. frames including changes in geometry and non-elastic behavior of elements under combined normal force and bending moment", *IABSE Proceedings*, 1973.

11. Monti, Giorgio and Nuti, Camillo, “Nonlinear cyclic behavior of reinforcing bars including buckling”, *Journal of Structural Engineering* V. 118 No.12, December1992.

12. Papia, Maurizio and Russo, Gaetano, “Compressive concrete strain at buckling of longitudinal reinforcement”, *Journal of Structural Engineering* V. 115 No.2, February 1989.

13. Papia, Maurizio, Russo, Gaetano, and Zingone, Gaetano, “Instability of longitudinal bars in RC columns”, *Journal of Structural Engineering* V. 114 No.2, February 1988.

14. Park, R. and Paulay, T., *Reinforced concrete structures*, John Wiley and Sons, New York, NY, 1975.

15. Russo, Gaetano, “A buckling model for reinforcing bars”, *International Journal of Mechanical Sciences* V. 30 No.1, 1988.

16. Scott, B.D., Park, R., and Priestly, M.J.N., “Stress-strain behavior of concrete confined by overlapping hoops at low and high strain rates”, *Journal of American Concrete Institute*, V.79, January-February1982.

17. Scribner, Charles F., “Reinforcement buckling in reinforced concrete flexural members”, *ACI Journal* V. 84, November-December 1986.

18. Sheikh, Shamin A. and Uzumeri, S.M., “Strength and ductility of tied concrete columns”, *ASCE Journal Structural Division* 106, No. ST5, 1980.

19. Sheikh, Shamin A., and Khoury, S.S., “Confined concrete columns with stubs”, *ACI Structural Journal*, V. 90 No. 4, 1993.

20. Sheikh, Shamin A., *Effectiveness of rectangular ties as confinement steel in reinforcement concrete column*”, PhD dissertation, University of Toronto, Toronto, 1978.

21. Timoshenko, Stephen P. and Gere, James M., *Theory of Elastic Stability*, 2nd edition, McGraw-Hill Book Company, Inc., NY 1961.

22. Vallenas, J., Bertero, V.V., and Popov, E.P., “Concrete confined by rectangular hoops and subjected to axial loads”, *UCB/EERC-77/13 Report*, University of California, Berkley, 1977.